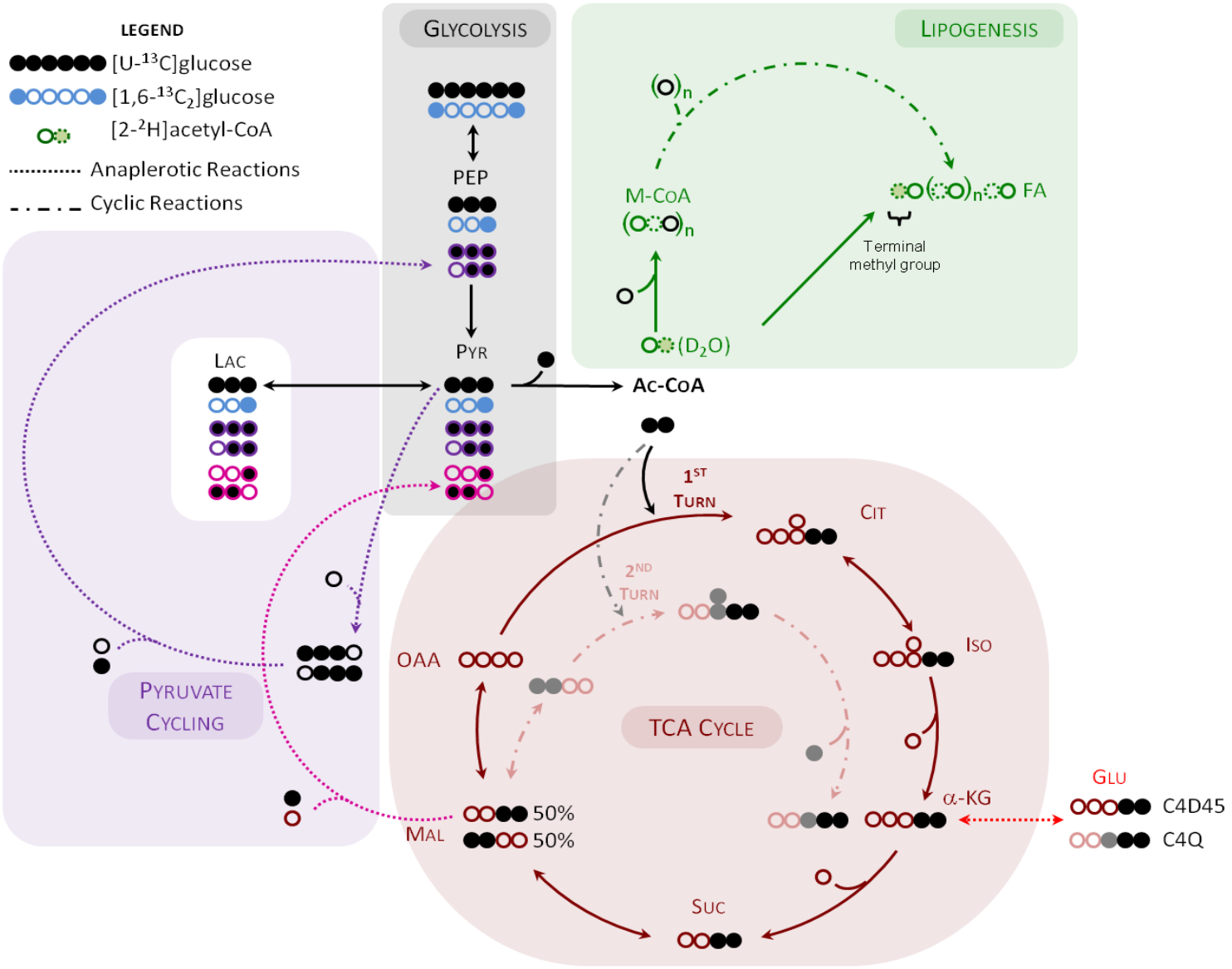

Ludgero Canário Tavares

UNRAVELING CANCER METABOLISM THROUGH FLUX ANALYSIS AND METABOLIC ENGINEERING

Tese de doutoramento em Biociências, Especialização em Bioquímica, orientada pelo Professor Doutor Rui A. Carvalho e co-orientada pelo Doutor Paulo J. Oliveira e apresentada ao Departamento de Ciências da Vida da Faculdade de Ciências e Tecnologia da Universidade de Coimbra

Fevereiro de 2015

· U C ·

UNIVERSIDADE DE COIMBRA

UNRAVELING CANCER METABOLISM THROUGH FLUX ANALYSIS AND METABOLIC ENGINEERING

UNIVERSIDADE DE COIMBRA

Ludgero C. Tavares, MSc

Faculty of Science and Technology

Department of Life Sciences

University of Coimbra

Coimbra, February 2015

Tese submetida para prestação de
provas conducentes ao grau de

Doutor em Biociências

Especialização em Bioquímica

Thesis submitted as a requirement

for the degree of

PhD in Biosciences

Specialization in Biochemistry

Front Cover: Schematics of ^{13}C and ^{2}H labelling patterns through different metabolic pathways (see p. 50)

This work was conducted at the Center for Neurosciences and Cell Biology (CNC), University of Coimbra and at the Department of Life Sciences, Faculty of Sciences and Technology, University of Coimbra, Portugal, under the supervision of Paulo J. Oliveira, PhD and Rui A. Carvalho, PhD.

The presented work was supported by a PhD fellowship from the Portuguese Foundation for Science and Technology (FCT) awarded to the author (SFRH/BD/66600/2009), by the CNC institutional grant supported by Compete/FEDER and National Funds (Pest-C/SAU/LA0001/2013-2014) and by a FCT research grant awarded to RA Carvalho (PTDC/EBB-EBI/115810/2009).

Published work

Part of the work included in this Thesis is already published in international peer-reviewed scientific journal, and is referred below:

Tavares, Ludgero C.; Jarak, Ivana; Nogueira, Fernando N.; Oliveira, Paulo J.; Carvalho, Rui A. Metabolic evaluations of cancer metabolism by NMR-based stable isotope tracer methodologies. European Journal of Clinical Investigation, v. 45, n. 1, p. 37-43, 2015.

The results exhibited in this Thesis were presented in national and international scientific meetings in the form of oral or poster communication.

Tavares, Ludgero C.; Oliveira, Paulo J.; Carvalho, Rui A. Metabolic coupling in lung cancer cell lines by ^{13}C NMR isotopomer analysis. In: Asia Pacific Lung Cancer Conference. Kuala Lumpur. Journal of Thoracic Oncology. 2014.

Tavares, Ludgero C.; Oliveira, Paulo J.; Carvalho, Rui A. Mitochondrial functioning in lung cancer cell lines. In: Asia Pacific Lung Cancer Conference. Kuala Lumpur. Journal of Thoracic Oncology. 2014.

Tavares, Ludgero C.; Oliveira, Paulo J.; Carvalho, Rui A. Lung cancer cell proliferation control by metabolic inhibitors and media composition. In: 48th Annual Scientific Meeting of European Society for Clinical Investigation. Utrecht. European Journal of Clinical Investigation. 2014.

Tavares, Ludgero C.; Oliveira, Paulo J.; Carvalho, Rui A. Substrate dependency on lung cancer cell proliferation. In: XVIII Congress of the Portuguese Biochemical Society. Coimbra. Sociedade Portuguesa de Bioquímica. 2014.

Tavares, Ludgero C.; Oliveira, Paulo J.; Carvalho, Rui A. Metabolic coupling in lung cancer cell lines by ^{13}C-NMR isotopomer analysis. In: 47th Annual Scientific Meeting of European Society for Clinical Investigation. Albufeira. European Journal of Clinical Investigation. 2013.

Acknowledgements / Agradecimentos

Apesar de este Tese de Doutoramento estar redigida em Inglês, para que os agradecimentos possam traduzir tudo o que quero agradecer terei de os escrever na minha língua materna.

Agradeço à Fundação para a Ciência e Tecnologia pelo suporte financeiro que me prestou na forma de bolsa de doutoramento e de projetos científicos.

Quero agradecer ao Professor Rui pela orientação. Reconheço-lhe uma infindável capacidade de trabalho e um enorme sentido de justiça. Obrigado por ter acreditado nas minhas capacidades, por me ter apoiado incondicionalmente e por todo o conhecimento que transmitiu ao longo destes anos. Espero ter sido um estudante à altura do desafio.

Ao Doutor Paulo, pela sua constante disponibilidade, amizade e apoio. Obrigado por toda a atenção e paciência que dispensaste comigo e pelos desafios constantes, e ainda, por todas as atividades desportivas.

Agradeço também ao Doutor John pelas suas sugestões e apoio ao longo de todo o doutoramento.

Agradeço a todos que com as suas sugestões, críticas e ideias me ajudaram e encorajaram na realização desta Tese.

Gostaria também de agradecer à minha família por terem sempre a porta aberta

Dedico esta Tese ao meu pai, por todo o apoio que sempre

me prestou e por todos os sacrifícios que suportou por mim

Para a Cristiana, por todos os momentos

em que não pude estar contigo

“And all the roads we have to walk are winding

And all the lights that lead us there are blinding

There are many things that I would like to say to you

But I don't know how

Because maybe

You're gonna be the one that saves me

And after all

You're my wonderwall”

Oasis – Wonderwall

(1995)

Contents

List of Figures

List of Tables

Abbreviations

2-DG 2-deoxyglucose

3-BrPA 3-bromopyruvate

AcCoA acetyl-coenzyme A

ACho acetylcholine

ACLY ATP citrate lyase

ACO aconitase

ACSS2 acetyl-CoA synthetase isoform 2

ADP adenosine diphosphate

AIF apoptosis-inducing factor

ALDA aldolase A

ALT alanine transaminase

AMP adenosine monophosphate

ANOVA analysis of variance

AOA aminooxyacetic acid

AST aspartate transaminase

ATP adenosine triphosphate

Bcl-2 B-cell lymphoma family

CAF cancer-associated fibroblast

ChoKα choline kinase α

c-Myc v-myc avian myelocytomatosis viral oncogene homolog

CoA coenzyme A

CS citrate synthase

CSC cancer stem cell

CT computerized tomography

Cyt C cytochrome C

DCA dichloroacetate

DHEA dehydroepiandrosterone

DMA dimethyl aspartate

DMK dimethyl α-ketoglutarate

DMSO dimethyl sulfoxide

DNA deoxyribonucleic acid

DNL *de novo* lipogenesis

DOC sodium deoxycholate

DTT dithiothreitol

EBV Epstein-Barr vírus

EGCG epigallocatechin gallate

EGF epidermal growth factor

ER endoplasmatic reticulum

ETC electron transport chain

$FADH_2$ flavin adenine nucleotide

FASN fatty acid synthase

FBS fetal bovine serum

FCCP carbonyl cyanide 4-(trifluoromethoxy)phenylhydrazone

FGF fibroblast growth factor

FH fumarate hydratase

G6PDH glucose-6-phosphate dehydrogenase

GAPDH glyceraldehyde-3-phosphate dehydrogenase

Glc glucose

GLDH glutamate dehydrogenase

Gln glutamine

GLS glutaminase

GLUT glucose transporter

GPCho glycerophosphocholine

GSH/GSSG glutathione

GSK3 glycogen synthase kinase-3

HIF hypoxia-inducible factor

HK hexokinase

HPLC high performance liquid chromatography

IA iodoacetic acid

IDH isocitrate dehydrogenase

KCN potassium cyanide

Lac lactate

LDH lactate dehydrogenase

Max myc-associated protein X

MCT monocarboxylate transporter

ME malic enzyme

miRNA micro ribonucleic acid

MMP matrix metalloproteinases

MRI nuclear resonance imaging

mRNA messenger ribonucleic acid

MS mass spectrometry

mtDNA mitochondrial DNA

NAD^+/NADH nicotinamide adenine dinucleotide

$NADP^+$/NADPH nicotinamide adenine dinucleotide phosphate

nDNA nuclear DNA

NK natural killer cells

NMR nuclear magnetic resonance

OAA oxaloacetate

p53 protein 53

PARP1 poly(ADP-ribose) polymerase 1

PBS phosphate buffered saline

PC pyruvate carboxylase

PCA principal component analysis

PCho phosphocholine

PDGF platelet-derived growth factor

PDH pyruvate dehydrogenase

PDK pyruvate dehydrogenase kinase

PDP pyruvate dehydrogenase phosphatase

PEPCK phosphoenolpyruvate carboxykinase

PET positron emission tomography

PFK phosphofructokinase

PHD prolyl hydroxylases

PI3K/Akt/mTOR phosphoinositide 3-kinase/ protein kinase B/ mammalian target of rapamycin pathway

PK pyruvate kinase

PKM pyruvate kinase muscle isozyme

PPP pentose phosphate pathway

PtdCho phosphatidylcholine

Pyr pyruvate

R-2HG (R)-enantiomer of 2-hydroxyglutarate

ROS reactive oxygen species

RPMI Roswell Park Memorial Institute 1640

SDH succinate dehydrogenase

SDS sodium dodecyl sulfate

siRNA small interfering ribonucleic acid

SOD superoxide dismutase

SPSS Statistical Package for Social Sciences 17.1

SRB sulphorhodamine b

TBS-T tris buffered saline, tween-20

TCA tricarboxylic acid cycle

TGFβ tumor growth factor β

TIGAR TP53-inducible glycolysis and apoptosis regulator

TKT transketolase

TMRM tetramethylrhodamine methyl ester

UK United Kingdom

US United States

VDAC voltage-dependent anion channel

VEGF vascular endothelial growth factor

WHO World Health Organization

Abstract

Cancer therapies have significantly improved over the last decades. However, some cancers, such as lung cancer, still have very poor outcomes and high mortality rates, even when proper treatment is applied. New treatment strategies must be adopted, which will require better understanding of cancer mechanisms. For that purpose, three human lung cell lines were used in this study, MRC-5, a human lung fibroblast cell line and A549, H1299, two human non-small lung cancer cells.

The metabolic remodeling occurring in carcinogenesis cells is firmly established. However, to understand the connection between the cellular metabolic profile and carcinogenesis, an accurate measurement of metabolic fluxes is required. In order to quantify the fluxes in these metabolic pathways, stable isotopes tracers and nuclear magnetic resonance techniques were employed. For the quantification of carbon intermediary metabolism cells were grown in ^{13}C labelled glucose while for *de novo* lipogenesis (DNL) assessment $^{2}H_2O$ was supplemented to the culture media. To better understand and characterize cellular bioenergetics, mitochondrial membrane potential, oxygen consumption, and energy charge were also assessed. Also, recent reports describe a reductive carboxylation operated by isocitrate dehydrogenase (IDH), which may provide acetyl-coenzyme A to DNL, favoring carcinogenesis. To evaluate the impact of this reaction in the overall metabolism, IDH isoforms 1 and 2 were genetically silenced and metabolism was assessed by stable isotopes tracers. Finally, to establish a bridge between metabolic fluxes and cancer proliferation, substrate dependency studies were performed. Several metabolic inhibitors were also tested, targeting glycolysis, TCA cycle, pentose phosphate pathway (PPP) and transaminases.

In this work we were able to quantify the glycolytic, TCA cycle and DNL fluxes. All cell lines exhibited heterogeneous metabolic profiles, with two distinct cancer cell lines. A549 cell line exhibited a more glycolytic phenotype while the H1299 cell line showed relatively active TCA cycle. However, both cell lines exhibited an increased DNL rate relatively to MRC-5 cell line. The overall mitochondrial bioenergetic parameters were in agreement with the metabolic profiles. The mitochondrial network was polarized and

active in all cell lines, although H1299 cell line exhibited higher basal oxygen consumption and spare respiratory capacity. The reductive carboxylation operated by IDH did not contributed significantly to DNL. However, IDH silencing altered the redox homeostasis and IDH1 silencing in the A549 cell line increased the ^{13}C enrichment of glutamine pools. Relatively to substrate dependency, all cell lines exhibited a reduced proliferation under glutamine deprivation. Finally, metabolic inhibition studies revealed an increased sensitivity in cancer cell lines to the inhibition of glucose-6-phosphate dehydrogenase, glyceraldehyde-3-phosphate dehydrogenase and transaminases, all reactions able to supply anabolic precursors or reducing equivalents.

This work revealed that A549 and H1299 cancer cell lines exhibited different metabolic profiles even though they are both derived from non-small lung cancer. Both cancer cell lines have increased DNL but the reductive carboxylation by IDH did not contributed significantly to DNL. Nevertheless, IDH is involved in redox homeostasis and IDH1 may have a regulatory effect on glutamine pools. We were able to establish a connection between the metabolic profile and potential therapeutic targets, such as DNL or PPP.

Keywords: cancer; NMR; stable isotopes; metabolism; isocitrate dehydrogenase.

Resumo

As terapias anticancerígenas evoluíram significativamente nas últimas décadas. No entanto, os tratamentos nalguns tipos de cancros, como o do pulmão, continuam a ter baixas taxas de sucesso e elevadas taxas de mortalidade. Novas estratégias de tratamento terão de ser adotadas, as quais irão requerer uma aprofundada investigação acerca dos mecanismos do cancro. Para esse propósito, utilizámos neste estudo três linhas humanas de pulmão, MRC-5, uma linha celular de fibroblastos de pulmão e a A549 e H1299, ambas de adenocarcinoma de pulmão.

A reestruturação metabólica que ocorre durante o processo carcinogénico está firmemente estabelecida. No entanto, para entender a conexão entre o perfil metabólico celular e a carcinogénese, é necessária uma quantificação precisa dos fluxos metabólicos. De forma a quantificar esses fluxos, utilizámos marcação por isótopos estáveis e técnicas de ressonância magnética nuclear. Para a quantificação e caracterização do metabolismo intermediário de carbono, as células foram cultivadas em meio de cultura contendo glucose marcada com ^{13}C enquanto para a quantificação da lipogénese o meio de cultura foi suplementado com $^{2}H_2O$. De forma a compreender melhor o metabolismo destas células, foram também avaliados parâmetros bioenergéticos, nomeadamente o potencial de membrana mitocondrial, o consumo de oxigénio e a carga energética. Descobertas recentes descrevem uma carboxilação redutiva operada pela isocitrato desidrogenase (IDH), a qual poderá abastecer acetil-coenzima A para a síntese lipídica, favorecendo o processo cancerígeno. Para avaliar o impacto desta reação no metabolismo, as isoformas 1 e 2 da IDH foram geneticamente silenciadas e o metabolismo foi analisado através de marcação por isótopos estáveis. Finalmente, para estabelecer uma ponte entre os fluxos metabólicos e a proliferação celular, realizaram-se estudos de dependência de substratos. Foram ainda utilizados vários inibidores metabólicos, dirigidos à glicólise, ciclo de Krebs, via das pentoses fosfato e transaminases.

Neste estudo conseguimos quantificar os fluxos da glicólise, do ciclo de Krebs e da lipogénese. Todas as linhas celulares exibiram perfis metabólicos heterogéneos,

sendo as duas linhas de cancro distintas. A linha celular A549 exibiu um fenótipo mais glicolítico enquanto a linha celular H1299 demonstrou uma atividade razoável do ciclo de Krebs. Contudo, ambas as linhas celulares de cancro exibiram uma elevada lipogénese relativamente à linha celular MRC-5. Os parâmetros bioenergéticos demostraram estar de acordo com os perfis metabólicos. A rede mitocondrial estava ativa e polarizada em todas as linhas celulares, mas no entanto, a linha H1299 exibiu um consumo basal de oxigénio e uma reserva respiratória máxima mais elevados. A carboxilação redutiva realizada pela IDH não contribuiu de forma significativa para a lipogénese. No entanto, o silenciamento da IDH causou distúrbios no redox intracelular e o silenciamento da IDH1 na linha celular A549 aumentou o enriquecimento de ^{13}C na *pool* de glutamina. Relativamente à dependência de substrato, todas as linhas celulares revelaram uma redução da proliferação em condições de privação de glutamina. As linhas celulares cancerígenas exibiram uma sensibilidade aumentada relativamente à linha MRC-5, na inibição da glucose-6-fostato desidrogenase, gliceraldeído-3-fosfato desidrogenase e transaminases.

Este trabalho revelou que as linhas celulares A549 e H1299 possuem diferentes perfis metabólicos apesar de serem ambas derivadas de adenocarcinoma do pulmão. As duas linhas cancerígenas possuem uma lipogénese aumentada mas a carboxilação redutiva através da IDH não contribui de forma significativa. No entanto, a IDH está envolvida no redox intracelular e a IDH1 poderá estar a exercer funções regulatórias nas *pools* de glutamina. Conseguimos ainda estabelecer uma relação entre o perfil metabólico e potenciais alvos terapêuticos, nomeadamente a lipogénese ou a via das pentoses fosfato.

Palavras-Chave: cancro; RMN; isótopos estáveis; metabolismo; isocitrato desidrogenase.

Part I

General Introduction

Chapter 1
Cancer

1.1 History of Cancer and Epidemiology

> "*Cancer is a generic term for a large group of diseases that can affect any part of the body. Other terms used are malignant tumours and neoplasms. One defining feature of cancer is the rapid creation of abnormal cells that grow beyond their usual boundaries, and which can then invade adjoining parts of the body and spread to other organs, the latter process is referred to as metastasizing.*" In World Health Organization (WHO), Fact sheet n. 297, November 2014.

The proper definition of cancer cannot be expressed as a single disease, but rather as a broad group of diseases with certain common characteristics. If left untreated, cancer can ultimately result in death. This work will focus on the characterization of some common features, at the cellular level, mainly related with cancerous metabolism.

1.1.1 A brief historical timeline

The word cancer was introduced by Hippocrates (460-375 BC), considered the father of modern medicine, who described and diagnosed several types of cancer such as cervical, rectal, skin mouth, stomach and breast cancer. Some of these cancerous growths reminded Hippocrates of a moving crab, which he named as *karkinos* (Greek for

crab) that was later translated for the Latin word *cancer* (Hajdu 2011a). However, the first written description of cancer is far much older, dating back to circa 1600 BC, on the Edwin Smith Papyrus, where was described a breast cancer (Wyld et al. 2014). Albeit written records, paleopathological findings suggested that tumors were present in prehistorical fauna, long before humans.

Cancer is an ancient disease, older than us as Humans, but our current knowledge still struggles to find efficient treatments. For centuries the treatment remained similar, with the use of cauterization or excision, use of lotions, salts and herbal remedies when possible or simply palliative care when the cancer was diagnosed as untreatable. However, treatment options were not always available due to superstitions, taboos, religious beliefs or social restrictions and surgical treatments remained rare and were extremely hazardous (Hajdu 2011a). Only when the Renaissance begun on the 14th century and Gutenberg introduced the movable printer on the 15th century, the ideas start spreading and medicine and surgery bloomed. The *post-mortem* dissections became accepted and anatomic data expanded. Early 'chemotherapeutic' remedies appeared for the treatment of several disorders, including arsenic, mercury, lead, sulfur, iron, zinc, copper, iodine and potassium (Hajdu 2011b). Lung cancer was described as occupational hazard in metal ore miners. In 1620, more than a century after tobacco was introduced in Europe, Thomas Venner warned about the immoderate use of tobacco leading to hurt on the eyes, brain and heart, trembling limbs and recommends its use only for medicinal purposes, not recreational. On the Early Modern period, the invention of microscope was a major breakthrough that led to the cell theory, published by Theodor Schwann in 1838, where the cell, with its ultra-structure, was the building block of all living organisms (Wolpert 1995). This was essential for describing abnormal cancer cells and the development of histology and pathophysiology led to better cancer classifications (Hajdu 2012a). In the late 19th century/early 20th century cell biologists and physicians focused on the elemental origins of cancer cells and postulate some theories related with embryonic characteristics (genetic predisposition), irritation (chronic inflammation), hormonal secretions and infections (Hajdu 2012a). Until then, treatment was mainly focused on surgery or cauterization with very poor results. Advances in anesthesia by William Morton, antiseptic techniques by Joseph Lister, blood

transfusion as well new and bolder operative procedures allowed brighter outcomes (Wyld et al. 2014). Remarkably, some of the surgical procedures developed at this time are still applied in certain cases today, more than a century later, just with minor improvements. Only with the discovery of X-rays and ionizing radiation, new therapies were developed. X-rays became a useful diagnostic tool and after realizing both carcinogenic and tumor-suppressive properties of ionizing radiation, it was successfully applied for treating inoperable tumors, forging the radiation therapy. Major progresses were also achieved in the field of virology and cancer chemotherapeutics (Hajdu 2012b; Moore et al. 2010). Due to variable outcomes, cancer began to be regarded as a mixture of chemically sensitive and resistant cells. At the beginning of the 20th century the use of animals for research purposes increased and the first *in vitro* cancer tissue culture was established, leading the path to today's immense long-term tissue culture inventory. The inevitably Warburg effect was described by Otto Warburg (Warburg et al. 1927; Warburg 1956), stating that even in the adequate presence of oxygen concentrations, cancerous cells consume glucose at higher rates than normal tissues, through lactic fermentation. This concept is still valid today and it is the cornerstone of Positron Emission Tomography (PET). By this time, several carcinogens were identified, including petroleum and oils constituents, radium, asbestos, hormones and certain infections. Smoking was definitely established as causative of lip, jaw, cheek and tongue cancer in 1928. Several preexisting conditions and even hereditary predisposition were associated with probable cancerous outcomes (Hajdu et al. 2013a). These advances in cancer characterization and classification, cytology, clinical laboratorial analysis and histological grading led to far much better diagnosis and predicted outcomes, but survival rates did not improved significantly. Amazingly, only in 1928, a classical work by Frederick Griffith (Griffith 1928) implied bacterial transformation through genetic information transfer. For the next decades an intense research was developed around genetic information and nucleotides were suggested as probable carriers of such genetic information in the Avery-MacLeod-McCarty experiment, instead of the widely believed proteins. Research took a significant step in 1953 with the Watson-Crick deoxyribonucleic acid (DNA) double helix molecular model (Watson et al. 1953). From here on, the genetic code rules were unraveled with postulation of three base codons, translation and transcription mechanisms with the birth of molecular biology. Cancer and genetic mutations became

a major focus of interest and the term 'oncogene' was introduced, conveying the idea of cancer-related genes (Huebner et al. 1969). Due to the previous advances in the field, the new generations of surgeons, pathologists, radiologists and overall medicine professionals had increasing specific formation, including oncology. New and groundbreaking tests emerged and mass screening programs for early detection were launched, such as mammography for breast cancer or Papanicolau smear for the uterus cancer. Also new technology such as angiography, optic fiber endoscopy, ultrasonic echography, flow citometry, nuclear imaging and computerized tomography (CT) scan became increasingly available and greatly aided in the detection of primary and metastatic tumors (Hajdu et al. 2013b). Chemotherapeutics research increased significantly entering into the modern era. After the experimentalism with urethane and nitrogen mustard, promising anticancer compounds emerge such as cortisone, methotrexate, cisplatin, adriamycin, 5-fluorouacil and many others. Radiation therapy also evolved, either as an adjuvant therapy for chemotherapy or surgery in several types of cancer or as first-line treatment for certain cancers such as the Hodgkin's lymphomas (Hajdu et al. 2013b). These improvements were due to enhanced expertise and technology that allowed powerful radiation yet precise focusing without damaging other tissues or skin. Until mid-20th century, surgery was the defining treatment for cancer and, as the sole solution, several radical procedures were developed and were accepted as standard procedures. This paradigm gradually changed over time into more conservative surgeries with adjuvant therapies (Wyld et al. 2014). Several research associations, institutes and periodic scientific journals were created, and the TNM staging system was introduced for uniform classification of malignant tumors, presently revised and still in use by the WHO. All these contributions pushed cancer treatment to modern standards and granted earlier detection, improved diagnosis and treatments, and consonant better outcomes and rates of survival (Hajdu et al. 2013b). The rates of survival greatly improved in the last decades with the expansion of cell biology, pharmacology, immunology and overall cancer research. Introduction of state-of-the-art imagiological tools, namely Nuclear Resonance Imaging (MRI) and PET. The human genome sequencing and next-generation sequencing techniques allowed performing individual genetic analysis for cancer risk assessment due to several cancer-associated mutations, single nucleotide polymorphisms and even epigenetic modifications (Wyld et

al. 2014). Immunotherapy advances, personalized treatments as well minimal invasive surgery techniques and medical oncologic multi-disciplinary teams granted actual standards of low morbidity and increasing rates of survival in several cancers.

1.1.2 Cancer epidemiology

Although effective cancer diagnosis and treatment as greatly evolved, especially in the last decades, cancer remains a burden throughout the world, either in developing or developed countries. Several associations and organizations publish, on a regular basis, epidemiologic studies and several cancer statistics, and the numbers are quite staggering. The WHO states that in 2012 alone, there were 14.1 million new cancer cases with 8.2 million cancer related deaths. Africa, Asia and Central and South America account for 60% of the new cases and about 70% of the 8.2 million deaths (Bender 2014a). The 5-year prevalence is about 32.5 million people. For the year 2030 the worldwide projected incidence of all cancers is 23.6 million people, an increment of approximately 68% (9.5 million new cases). This increase is expected to be higher in countries with low and medium Human Development Index (Cancer Research UK 2014). The most common cancers diagnosed in 2012 were lung, breast, colorectal, prostate and stomach. In men, prostate cancer is the most prevalent (mainly in developed countries) while in women is, by far, the breast cancer. However, worldwide, lung cancer is the most common cancer-related death, with an astonishing toll of 1.59 million deaths per year, followed by liver, stomach, colorectal and breast cancer, each with less than half the cases of lung cancer (Cancer Research UK 2014).

Despite the availability of effective treatments for several types of cancer in developed countries (with trending decreased rates of mortality), the number of new cases and deaths are increasing. Cancer screening and early detection may improve the chances of survival but in order to fight the increasing incidence we must look for prevention. As history as shown, several cancers are associated with an exposure to certain environments or chemicals. The International Agency for Research on Cancer published several monographs, revised in 2012, containing an extensive list of described and potential carcinogens. Contact with these carcinogens can arise from to

occupational activities, environmental exposure or even dietary habits, which should be tightly regulated and restricted by legal mechanisms. Cancers caused by alcohol abuse and longtime tobacco consumption are two well known examples of preventable cancers (Nelson et al. 2013; WHO 2008). Tobacco smoking is single-handedly responsible for approximately 30% of all human cancers. Apart direct contact with carcinogens, behavioral habits and 'western' lifestyle are associated cancerous risks, including excessive sunlight exposure, poor and unbalanced diet, physical inactivity and overweight, reproductive and hormonal factors, among others (American Cancer Society 2014; Siegel et al. 2014; Cogliano et al. 2011). Up to 20% of worldwide cancer cases can be attributed to chronic infections such as human hepatitis B/C virus, human papillomavirus, Epstein-Barr virus (EBV) or *Helicobacter pylori* (WHO 2008; Moore et al. 2010). This risk can be managed with prophylactic vaccination for human hepatitis B virus and human papillomavirus or antibiotic therapy for Helicobacter pylori. Unfortunately, not all cancers can be prevented; genetic predisposition and longer life expectancy are risk factors for developing cancer (White et al. 2014). Nevertheless, adopting healthy lifestyles and avoiding exposure to carcinogens can effectively prevent the majority.

A major health concern for the next decades will rise on the developing world. These countries' populations are expected to grow, live longer and adopt a developed world lifestyle together with their risks. Age alone is a major risk factor for cancer progress, but unlike developed countries, these countries seldom have a capable healthcare system, trained professionals or sufficient funding to cope with the costs (White et al. 2014; Bender 2014a). In developing countries, infections-driven cancers are responsible for 26% of all cases, three times higher than developed countries (WHO 2008). Besides, fears and cultural settings difficult public awareness regarding cancer, prevention and screening campaigns are scarce and even palliative care is hard to implement with several countries imposing legal restrictions for morphine access.

1.2 Lung cancer, the assassin

1.2.1 Lung Function

The lungs are a part of the respiratory system and its main purpose is to promote gaseous exchanges, delivering oxygen (O_2) to the bloodstream and releasing carbon dioxide (CO_2) into the atmosphere. The two lungs are located in the thorax, behind the rib cage, enclosed by the pleurae and surrounding the heart. This organ possesses an expandable spongiform texture with internal honeycomb-like structures called alveoli, dramatically increasing the surface area, allowing an extremely efficient gaseous exchange. In fact, it is so effective that a human can live with only one functional lung (Cerfolio et al. 2013). At the inspiration, the diaphragm contracts and the rib cage expand, causing a pressure drop inside the lung. Air enters through the nose or mouth, flows through the pharynx, larynx, trachea and branches for both right and left lungs at the bronchi. From here, bronchi ramifies into smaller bronchi and bronchioles and end at the alveolar sacs. The alveolar sacs are clusters of individual alveoli, formed by highly vascularized epithelial cells and it is in these structures that gaseous exchanges occur. The pulmonary artery delivers deoxygenated blood to the lungs, hemoglobin present in the erythrocytes binds the atmospheric O_2 and the dissolved CO_2 (mostly in the form of HCO_3^-) is released into the alveolar sacs. The oxygenated blood returns to the heart by the pulmonary vein and is pumped throughout the body. The diaphragm and intercostals muscles relax, compressing the lungs and forcing the exhalation of the CO_2-rich air, completing the cycle (Seeley et al. 2001).

1.2.2 Tobacco and lung cancer

Tobacco was introduced by the 16th century in Europe by Portuguese and Spanish, brought from America. Initially presented with ‘medicinal properties’ tobacco could be chewed, smoked or inhaled. Over centuries it became generally accepted and increasingly popular, particularly after the cigarette-rolling machine invention. However

only in mid-20th century tobacco was undoubtedly linked to cancer (Dani et al. 2011; Proctor 2012).

Tobacco smoking can cause 13 different cancers, namely: oral cavity, nasal cavity and nasal sinuses, pharynx, larynx, esophagus, stomach, pancreas, liver, urinary bladder, kidney, uterine cervix, myeloid leukemia and the most common, lung (WHO 2008). Several other chronic disorders are result of smoking, namely cardio- and cerebro-vascular disorders and chronic obstructive pulmonary diseases (Mainali et al. 2014; Dani et al. 2011). Passive smoke can also cause lung cancer and smokeless tobacco has been associated with oral cancers. Tobacco smoke contains more than 70 described carcinogens, including aldehydes, nitrosamines and polycyclic aromatic hydrocarbons (Sobus et al. 2014). Besides tobacco smoke, a rather long list of carcinogens contribute to lung cancer, namely asbestos, coal, heavy metals and radiation (Cogliano et al. 2011). Lung cancer can be classified in non-small cell cancer or small cell cancer (85% and 15% of all cases, respectively), the latter usually caused by smoking and is the most aggressive. The non-small cell cancer can be classified in further subtypes: adenocarcinoma (40%), the most prevalent form, occurs in the alveoli and is regularly present in non smokers; squamous cell carcinoma (30%), arises commonly near the bronchi, grows slower and is more frequent in men; and large cell carcinoma (15%), which grows and spreads rapidly (Bender 2014b).

Lung cancer alone is responsible for one fifth of total cancer-related deaths. Tobacco and cigarette smoking are major risk factors for developing cancer and more than 80% of the lung cancer cases are attributable to smoking (WHO 2008). Duration of smoking is the main determinant for lung cancer risk assessment, in nearly half the cases, patients smoked more than 40 years. The risk also increases proportionally with the amount of tobacco consumed and it has been shown that smoking cessation, at any time of adulthood is beneficial and reduces the risk, especially if cessation occurs before midlife (WHO 2008). Awareness and prevention campaigns will be the best way to fight the increasing incidence. Different tactics have already proven successful, from the implementation of warnings and pictures on the cigarette packs to tax increases and even prohibitions (Bender 2014b). Unfortunately, aggressive tobacco marketing in developing countries is expected to increase the number of smokers, including a large

number of new adolescent consumers (Proctor 2012; WHO 2008). In China, the most populous country in the world, more than half of the male population smokes cigarettes, to a total of 365 million active smokers and 677 million passive smokers. The Chinese government is the world's largest tobacco producer and China alone consumes one third of the cigarettes smoked worldwide, leading to an estimated 3000 kills per day due to lung cancer (He et al. 2013; Bender 2014b). Inversely, in the United States (US) the number of smokers and incidence is slowly falling, but despite relatively good health care conditions, the expected 5-year survival rate is of 17% (DeSantis et al. 2014). In the last three decades, prostate or breast cancer treatment, when properly attended, went from a 70% 5-year survival rate to over 90% at the present day. However, lung cancer treatment did not improve as significantly in the same time frame, 5-year survival rate did not grow more than 10%, and mortality closely follows incidence rates (May 2014). It has one of the worst predicted outcomes when compared to other types of cancer. There is still too much information to unravel about cellular functioning and specific cancer alterations, with new potential therapeutic targets and solutions to better treat this disease. Throughout this work we will use human lung cancer cell lines and will focus on their metabolic specificities, hoping to enlighten the mechanisms and pathways behind such a gruesome disease.

1.3 Cancer biochemistry

The proper definition of cancer points out to a large group of diseases. More than hundred different types of cancers, most of them organ-specific, can affect the human body. Cancer can even metastasize and spread cancerous cells throughout the entire body, either by invasion of adjacent tissues or bloodstream and lymphatic transport, forming new tumors. Each type of cancer has its own characteristics and particularities, conferring different susceptibilities to different therapeutics. But the defining hallmark, the abnormal and uncontrolled growth of cells, is present in all cancer types.

1.3.1 Hallmarks

The transformation from a normal to a cancerous cell is not completely understood. However, with substantial amount of cancer research published in the course of the years, a subset of acquired capabilities (cancer hallmarks) seem to be present in several types of cancers and are related or promote the tumorigenic process (Hanahan et al. 2011). It is also clear that it is a progressive and multi-stage process, usually requiring more than one modification, sometimes present in the form of a lesion. Enabling characteristics such as genomic instability (sometimes minimal mutations) or tumor-promoting inflammation are recurrently the foundation for these acquired modifications. Several proteins related with maintenance and repair of DNA are usually defective and genome becomes increasingly unstable, leading to an increased mutation incidence rate on cancers. When those modifications translate into novel malignant capabilities, transformed cells might avoid anticancer mechanisms and begin the development of a tumor.

Self-sufficiency in growth signaling

One of the first hallmarks to be described was self-sufficiency in growth signaling due to oncogene modulation. Extracellular growth signals bind to transmembrane receptors, initiating and regulating the cell cycle and division in normal cells. However, in cancer cells this mechanism can be impaired due to alterations on the intracellular response to growth factors, on the growth factors or receptors. Several oncogenes can command the cell to produce their own growth factors or express altered membrane receptors (Roy et al. 2013; Hanahan et al. 2000). Mutations on *RAS* genes are present in more than 20% of all cancers and these altered proteins may deregulate downstream cell growth signaling pathways, independently of growth factor stimuli (Downward 2009; Hanahan et al. 2000). However, this self-sufficiency is more complex, several of these pathways are intertwined with other processes, namely paracrine (cell-to-cell) signaling or inflammatory processes from neighboring cells.

Insensitivity to antigrowth signaling

The second hallmark is tightly related with the previous and is the acquisition of antigrowth signaling insensitivity. Antigrowth signaling can modulate the cell cycle by inducing cells into resting (G_0) or irreversibly into post-mitotic phases. Tumor growth factor β (TGFβ) activates retinoblastoma protein pathways, which in turn impede the progression from G_1 to S by controlling transcription factors. Cell-to-cell contact inhibition and other important oncogenes, such as *MYC* may also interfere (Soucek et al. 2008). Downregulation and dysfunction of receptors and retinoblastoma protein pathway enzymes or transcription factors promotion render the cells insensitive to antigrowth factors. Unbalances between on growth/antigrowth factors homeostasis can trigger the cell to enter mitosis, supporting carcinogenesis (Hanahan et al. 2000).

Evading apoptosis

When a normal cell stops receiving survival signaling or develops a severe anomaly, internal mechanisms of self-destruction are usually implemented, apoptosis, a smooth programmed cell death (Fuchs et al. 2011). Apoptosis can be triggered from external or internal stimuli, including viral infection, inflammatory signaling, lack of survival factors, appropriate signaling for death or even extensive DNA damage. Through an intricate transduction cascade, several pro-apoptotic or anti-apoptotic proteins (B-cell lymphoma family, Bcl-2) are activated. Bcl-2-associated X protein and Bcl-2 antagonist, two main proapoptotic proteins disrupt the outer mitochondrial membrane, releasing several proapoptotic signaling, namely cytochrome C (Cyt C). In turn, Cyt C will activate several effector proteins called caspases that begin the orchestrated cell lysis. This mechanism is critical for the early destruction of cancer cells, but alterations in receptors or proteins, increasing anti-apoptotic signaling and/or reducing pro-apoptotic pathways, confer the third hallmark, evading apoptosis (Hanahan et al. 2000). In more than 50% of all cancers, one of the major tumor suppressive proteins, tumor protein 53 (p53) is dysfunctional or inactivated, being unable to detect DNA mutations or oncogenene overexpression. Other mechanisms such as autophagy and necrosis can also impact the tumorigenesis, especially necrosis, where the cell death releases

proinflammatory signals, initiating an immune inflammatory response and favoring the microenvironment for cancer proliferation (Hanahan et al. 2011).

Limitless replicative potential

If cancer cells become insensitive from external growth/antigrowth signaling and avoid apoptosis, uncontrolled proliferation is in sight. Luckily, cells have another internal maintenance mechanism that limits the replicative potential, referred as cellular senescence. Ageing, in mammals, is characterized by an increase risk of associated diseases (such as cancer), dilapidated cellular functions and impaired stress response. Cells have a limited number of replications, cannot divide infinitely, but cancer cells dodged this mechanism, acquiring the fourth hallmark, limitless replicative potential or 'biological immortality' (Hanahan et al. 2000). Telomeres, thousands short repeats of 6 base pairs (6 bp, TTAGGG) at the end of the chromosome, are considered the main gate-keepers of these processes. At each cell cycle, these extensions are shortened until a threshold is reached, where DNA polymerases can no longer attach efficiently to the 3' chromosomal ends during S phase, impeding the cell cycle on a G_1/G_0-like state. Basically, the telomeres act as a counting mechanism, and when the count ends, chromosomal disarrangements consequently lead cells to their death. However, in the majority of cancers, telomerase is usually overexpressed. This enzyme adds 6 bp repeats on the telomeric DNA, maintaining telomeres above a critical threshold thus allowing unlimited replication (Holohan et al. 2014).

Sustained angiogenesis

Once a cell acquires tumorigenic capabilities, it proliferates and develops a tumor, with a cluster of disordered cells. This cluster cannot grow further from capillary blood vessels, since nutrients that are required for maintaining cellular functions do not diffuse through distances larger than 100 μm. In order to develop macroscopic structures, cancer must be able to promote blood vessel irrigation, acquiring angiogenic capacity, the fifth hallmark (Hanahan et al. 2000). Surprisingly, mutated cells usually cannot perform this ability on early stages but it is often acquired throughout the development of cancer. However, these new vessels are not similar to normal

circulatory systems they lack hierarchy between vessel calibers, circuits are tortuous with irregular blood flow and prone to leaking and microhemorrhages. Pro- and anti-angiogenic and cell adhesion signaling interfere with this process. Some of the major proangiogenic growth factors are the vascular endothelial growth factor (VEGF), the fibroblast growth factor (FGF) and matrix metalloproteinases (MMP) (Araújo Jr et al. 2014). Overexpression of these factors and downregulation of anti-angiogenic factors such as thrombospondin-1 or angiostatin drive a homeostatic imbalance, favoring the synthesis of new blood vessels (Sharma et al. 2013; Lieser et al. 2013). Previously mentioned oncogenes like *RAS* can upregulate VEGF expression and tumor suppressor genes like *TP53* fail to upregulate thrombospondin-1. Actually, VEGF inhibitors treatments have shown to impair angiogenesis but recent studies show a deleterious side-effect, by increasing the invasiveness and metastatic potential, introducing the sixth hallmark (Pàez-Ribes et al. 2009).

Invasion and metastasis

Invasiveness and metastasis are responsible for very poor treatment outcomes, generally resulting in death. Primary tumor cancer cells can grow and invade adjacent tissues or organs, hampering their function, and detach, being transported to further locations by blood or lymphatic system, establishing new colonies in different parts of the body. These processes are complex, since there are changes in cellular adhesion molecules, extracellular proteases to promote the detachment and alteration of coupling enzymes to allow the adhesion in other environments. The most common alteration is relative to E-cadherin, a calcium (Ca^{2+}) dependent adhesion transmembrane protein involved in cell-to-cell contact. E-cadherin is dysfunctional in most epithelial cancers whether by mutation, downregulation or extracellular domain proteolysis. Immunoglobulin super-family adhesion proteins may also be downregulated or mutated into highly or poorly adhesive isoforms (Vestweber 2014). Cancerous integrins, which bind to extracellular matrix, may have an increased amount of isoforms, allowing the metastases to adhere on different environments (Li et al. 2011; Hanahan et al. 2000). Extracellular proteolytic activity upregulation and protease inhibitor downregulation help to destroy the extracellular matrix, favoring the invasion and detachment of cancer

cells. Protease expression can even be heightened due to signaling from neighboring stromal and inflammatory cells (Hanahan et al. 2000).

Evading immune destruction

More recently, two more hallmarks were introduced, starting with the evading of immune destruction. Inflammatory response can have antithetical effects; by fostering carcinogenesis with the secretion of growth and angiogenic signaling and extracellular matrix remodeling enzymes; or by promoting the destruction of tumoral or pretumoral tissue with the recruitment of immune system cells. Hypothesis arose from cancers in immunocompromised patients, where virus-related cancers have higher incidence rates, and from donor-derived cancers in transplanted patients (Hanahan et al. 2011). However, epidemiological data also shows that chronically immunosuppressed patients do not have higher incidence rates of non-viral cancers. Deficiencies on either innate and adaptive immune system or cancerous immune evading mechanisms may lie as the basis of this hallmark. Cancer may be modulating cytotoxic T lymphocytes and natural killer cells (NK) action by secreting TGFβ (or other immunosuppressive factors) or by recruiting additional immunosuppressive inflammatory cells such as regulatory T cells (Hanahan et al. 2011). Although evidences are present, it is still an emerging hallmark and needs further research.

Reprogramming energy metabolism

At last, the hallmark that will be the main focus on this work, the deregulation of cellular energetics. Under normal nutrient and oxygen availability, cells perform glycolysis, producing pyruvate that is driven to mitochondria and tricarboxylic acid cycle (TCA cycle). TCA cycle-derived reducing equivalents can be directed for adenosine triphosphate (ATP) production at the electron transport chain (ETC) with the consumption of O_2. Generally, under anaerobic conditions, cells favor glycolysis and pyruvate is converted to lactate by lactate dehydrogenase (LDH), avoiding mitochondrial O_2 consumption. However, cancerous phenotype is characterized by an aerobic glycolysis state, where the cell relies mostly on glycolysis and lactic fermentation even in the adequate presence of oxygen, the Warburg effect (Warburg 1956; Warburg et al.

1927). Even though mitochondrial oxidative phosphorylation is much more efficient than glycolysis in terms of energy per glucose molecule oxidized, glycolysis is a faster process. Increased glycolysis also favors several biosynthetic pathways such as nucleotides and aminoacid anabolism. Several oncogenes like *RAS* or *MYC* and upregulation of glucose transporters (GLUT) have been associated with glycolytic phenotypes. Moreover, inefficient oxygenation on the tumor tissue stimulate hypoxia-inducible factors (HIFs) that also upregulate glycolysis (Hanahan et al. 2011).

These eight hallmarks are commonly present in all types of cancers. The acquisition of each capability does not need to follow a preset sequence or timeline. They can be acquired at any time of the tumorigenic process. Also, these are suggested theories and mechanisms to achieve the hallmark capability, but there may be several other unknown mechanisms to reach the same endpoint.

1.3.2 Tumor microenvironment

Throughout tumor progression, several subpopulations of cells start to emerge, with diverse degrees of differentiation, inflammation and invasiveness. The tumor microenvironment is regarded as a heterogeneous pool of cells, from stromal cells, to cancer stem cells and immune inflammatory cells. These mixtures of specialized cells and subpopulations with interdependent functions can be providing cancer fostering conditions.

Cancer stem cells

Cancer stem cells (CSCs) are a relatively newly described and overlooked subclass of cancerous cells. These CSC may be responsible for the development of new tumors and therapy resistance as they possess similarities with normal stem cells, sharing common transcriptional markers and metabolic characteristics (Vega-Naredo et al. 2014). Even though rare, they have been found in different cancers and their origin is still not clear: normal stem cells may transform onto CSCs; progenitor cells may acquire

certain malignant characteristics, inducing stem-like properties; or even plasticity between CSC and non-CSCs is conceivable. Once the stem cell likeness is acquired, these cells can self-renewal, originate differentiated cancer cells and present a completely altered radio- and chemotherapy resistance and are possibly responsible for cancer recurrence after treatments (Vega-Naredo et al. 2014).

Immune inflammatory cells

As discussed previously, evading immune destruction is a cancer hallmark and cancer has long been associated with a chronic inflammation status. Cancer progression, as an insult, initiates an inflammatory process, recruiting several leukocytes to vicinity of cancer cells. These leukocytes like cytotoxic T lymphocytes and NKs are responsible for the destruction of malignant cells that possess anomalous structures or signaling. Cancer only develops when these malignant cells evade or overcome the immune system. These inflammatory responses should be transitory and not permanent. However, chronic inflammatory state is associated with several pathologies, being cancer one of them. Macrophages, mastocytes, neutrophils and T/B lymphocytes are related with tumor promotion due to the secretion of several growth factors, namely epidermal growth factor (EGF), VEGF, FGF, MMPs and pro-inflammatory cytokines. Such signaling stimulate cancer progression, remodel extracellular matrix facilitating invasion and metastasis and support angiogenesis (Hanahan et al. 2011). Inflammation can have antagonizing results, with tumor destruction or tumor promoting outcomes, in a complex and delicate balance.

Stromal tissue

Wound healing requires the growth of connective tissue around the insulted area, in a process known as desmoplasia. As solid tumors proliferate, a desmoplastic reaction occurs, similar to wound healing, recruiting and producing connective tissue to support the tumor. These stromal cells also play a role in carcinogenic process. Pericytes (mesenchymal cells) provide support for endothelial cells of bloodstream vessels and send homeostatic paracrine signaling. However, tumor pericytes have their function impaired, destabilizing vasculature (Hanahan et al. 2011). Fibroblasts are also present in

large numbers in carcinomas (cancers that develop from epithelial tissue). Some subpopulations of fibroblasts have a procarcinogenic phenotype and are referred to as cancer-associated fibroblasts (CAFs). These CAFs are mesenchymal cells with smooth muscle characteristics, usually present in wound healing, termed myofibroblasts. However, on chronic inflammation they cause excessive fibrosis such as in lung or liver. Expression of α-smooth muscle actin allows the differentiation of myofibroblasts from normal fibroblasts. The origin of these fibroblasts is not clear, possibly arising from normal fibroblasts, vascular smooth muscle, pericytes or even from bone marrow-derived stem cells (Micke et al. 2004). This transformation is related with several factors but particularly TGFβ and platelet-derived growth factor (PDGF). CAFs show tumor growth stimulation effects by modulating extracellular matrix, angiogenesis and paracrine signaling, in a crosstalk with tumor microenvironment. Secretion of several growth factors have already been identified, such as insulin-like growth factor, EGF, MMPs, VEGF and PDGF (Micke et al. 2004; Navab et al. 2011). Moreover, the metabolism of these CAFs is altered, expressing a glycolytic phenotype and secreting lactate and pyruvate for the extracellular media, supplying epithelial cancer cells with energy-rich metabolites that can undergo oxidative phosphorylation, in a phenomenon named reverse Warburg effect. These secretions also acidify the extracellular microenvironment, promoting invasion and metastasis (Bonuccelli et al. 2010). The cancer stromal dynamics are quite complex and heterogeneous and sometimes disregarded but further research may explore potential therapeutic targets.

1.4 Metabolic malignancy

Cancer metabolism is severely altered due to genetic and epigenetic mutations affecting several cofactors, signaling, transporters, proteins and enzymes, interfering with metabolic pathways. Oncogene research shed some light on these alterations by associating cancer development with several point mutations, translocations, deletions and amplifications in metabolic-related pathways (Stratton et al. 2009). These mutations may shift nutrient uptake of aminoacids, lipids or nucleotides, improving their incorporation in anabolic processes.

1.4.1 Warburg effect

The first steps towards unraveling cancer metabolism were taken more than 80 years ago, when Otto Warburg described low ATP levels notwithstanding the excessive uptake of glucose by tumors (Warburg 1956; Warburg et al. 1927). Even in the presence of adequate O_2 concentrations, the cancer cells buildup substantial amounts of lactate, promoting lactic fermentation instead of the much more energetically efficient oxidation by the TCA cycle and coupled oxidative phosphorylation. This aerobic glycolysis named Warburg effect is still not fully understood but it is a common feature in many fast growing cancers. However, some studies have shown that mitochondria in these "Warburg-like" cancer cells are not completely inactive or even in some specific cases can supply most of the ATP (Rodríguez-Enríquez et al. 2010; Phelan et al. 2014). In fact, mitochondria can have a regular oxidative phosphorylation but carcinogenesis promotes a reprogramming of biosynthetic pathways towards glucose consumption. There are even cancers, such as prostate cancer, that have low rates of glucose consumption and increased fatty acid uptake, depending on the mitochondrial β-oxidation for the generation of ATP (Liu et al. 2006).

Aerobic glycolysis is not an efficient method to generate energy in the form of ATP; glycolysis can only generate 2 net molecules of ATP per glucose molecule whereas the full oxidation to CO_2 by the TCA cycle followed by oxidative phosphorylation can achieve 30-32 ATPs, a process seemingly 15 times more efficient. Additionally, at the end of glycolysis, two molecules of pyruvate are produced, with the reduction of two coenzyme molecules of nicotinamide adenine dinucleotide (NAD^+) into NADH. Since large amounts of pyruvate are being produced, for regeneration purposes, NADH must be converted back to NAD^+. This occurs mainly by reducing pyruvate to lactate through the LDH (Locasale et al. 2010). Overexpression of monocarboxylate transporters (MCT) promote lactate extrusion, maintaining intracellular pH and exerting a positive feedback loop on glycolytic enzymes such as phosphofructokinase (PFK), the rate-limiting enzyme of glycolysis (Mogi et al. 2013; Leite et al. 2011). However, as long as glucose is available, glycolysis is a much faster process than oxidative phosphorylation and may be preferred under rapid proliferating requirements while cancerous overexpression of GLUTs

nourish these glucose needs (Pfeiffer et al. 2001; Mogi et al. 2013). Also, microenvironmental factors such as hypoxia may induce a glycolytic metabolism, since the O_2 availability as an electron acceptor for the oxidative phosphorylation is diminished and hypoxia-inducible factor 1 (HIF-1) signaling pathway is activated. This uncoupling of mitochondrial metabolism from glycolysis seems to be crucial for cancer cell survival, since a reversal from glycolytic to oxidative phosphorylation phenotype induces cellular death and promotes apoptosis (Bonnet et al. 2007; Vega-Naredo et al. 2014). However, mitochondrial dysfunction can be due to mitochondrial DNA (mtDNA)/nuclear DNA (nDNA) mutations affecting, among others, TCA cycle or ETC enzymes (Gaude et al. 2014). Overexpression or alterations on glycolytic enzymes such as pyruvate kinase muscle isozyme 2 (PKM2) or LDH heighten the glycolytic phenotype and may operate different functions that ultimately favor tumorigenesis (Ganapathy-Kanniappan et al. 2013).

Nevertheless, proliferating cells have an increased requirement of anabolic precursors and ATP availability is not the limiting factor. In fact, cell cycle regulates the cellular division and several macromolecules are needed to perform mitosis, from lipids and phospholipids for cellular membranes and organelles, to constitutive proteins and nucleotides to perform DNA replication (Locasale et al. 2010). The Warburg effect may be responsible for supplying most of these central carbon precursors through the form of metabolic intermediates. Pentose phosphate pathway (PPP) is a parallel pathway to glycolysis that oxidizes glucose mainly for anabolic processes and redox homeostasis. In several cancers this pathway has an higher flux and may be providing pentoses for nucleotide biosynthesis and reducing equivalents in the form of nicotinamide adenine dinucleotide phosphate (NADPH) (Jiang et al. 2014). These reducing equivalents are extremely useful and need constant regeneration, since they are cofactors in lipid biosynthesis and help to maintain the reduced levels of glutathione (GSH), a powerful non-enzymatic antioxidant defense. Actually, glutathione (GSH/GSSG) is responsible for counteracting chemotherapeutics and evading apoptosis by successfully maintaining homeostatic redox levels (Traverso et al. 2013). Glycolytic intermediates or end-products can also generate anabolic precursors. Dihydroxyacetone phosphate can be converted into glycerol and acetyl coenzyme A (AcCoA) can enter lipid biosynthesis.

Aminoacids such as serine, glycine and cysteine can be produced from 3-phosphoglicerate alanine from pyruvate, aspartate from oxaloacetate, among many other conversions, providing non-essential aminoacids for protein synthesis (Vander Heiden et al. 2011; Dang et al. 2011). Nevertheless, glucose is constituted only by carbon, oxygen and hydrogen and cannot provide other elements such as nitrogen, phosphorus and sulfur. However, other substrates are incorporated in cancer cells to reprise the needs, and one particular aminoacid is avidly consumed by cancer cells, glutamine, providing both carbon and nitrogen substrates (DeBerardinis et al. 2007).

The 'reverse Warburg effect'

The reverse Warburg effect is a relatively recent theory stating that Warburg effect is compartmentalized between cancer and stromal cells. Cancer cells may be inducing a shift towards glycolytic phenotype on the stromal tissue, on fibroblasts presumably. The energy-rich end-products released by these stromal cells are then secreted to the extracellular medium and absorbed by cancer cells. Inside cancer cells these metabolites such as lactate, pyruvate and β-hydroxybutyrate, can undergo mitochondrial metabolism and oxidative phosphorylation for energy purposes, while glycolysis is mainly employed for anabolic precursor synthesis. Some remodeling in terms of mitochondrial bioenergetics and transmembrane transporters support this mechanism (Bonuccelli et al. 2010; Sotgia et al. 2012). It is not an outrageous theory considering that similar physiological processes occur in the human body. In the Cori cycle, under long term exercise and low O_2 concentrations, lactate is release by the muscles and in the liver is converted to pyruvate and back to glucose through gluconeogenesis. The brain, a glucose-dependent organ, has an interesting cross-talk between astrocytes and neurons. Astrocytes are glial cells that accumulate glycogen and perform aerobic glycolysis exporting lactate. The lactate is imported by neurons, converted into pyruvate and oxidized through mitochondrial metabolism for ATP production. Inversely, neurons import glutamine and convert it to glutamate to act as neurotransmitter. Once released by neurons, astrocytes import the extracellular glutamate and recycle it back to glutamine, a circuit relevant in neurotransmitter homeostasis and neurodegenerative diseases (Dang et al. 2011; Mason et al. 2004). It is a more complex mechanism than the classic Warburg effect but it may help explain the

relatively high rates of oxidative phosphorylation occurring in certain cancers, usually slow growing cancers (Zu et al. 2004).

Cancerous growth has definitely a high energetic and biosynthetic demand to cope with the elevated proliferation rate. However, nutrient availability on the tumor microenvironment is neither steadily supplied nor homogeneous, with transient hypoxic conditions, mainly due to a poor neo-vascularization and irregular growth. Under these particular circumstances, aerobic glycolysis seems to be an advantageous phenotype. Glycolysis is a central metabolic pathway that interplays with several other pathways, conferring some metabolic plasticity. Considering the irregular supply of O_2 on tumors, the dissociation of O_2 levels from ATP production may be advantageous. The Warburg effect allows a regular supply of energy, independently of O_2 levels in the extracellular medium. Moreover, mitochondria with less active metabolism produce lower reactive oxygen species (ROS) levels at the ETC, which provides survival advantages by avoiding apoptosis. However, the Warburg effect, is not energetically efficient and the buildup of toxic byproducts can be deleterious to the cell (Hsu and Sabatini 2008). Even though the Warburg effect it is still far from completely understood, several mechanisms have already been elucidated and will be analyzed in further detail.

1.4.2 Oncogenic transcription factors

Gene expression patterns and overall signaling pathways are altered in cancer cells. The expression of oncogenes or lack of tumor suppressor genes develops metabolic responses critical for the establishment of the Warburg effect. Some of these oncogenes are transcription factors that promote a downstream expression or activation of a series of enzymes and pathways.

Hypoxia-inducible factor

A reduction in O_2 tension either by excessive consumption or deficient delivery is considered a hypoxic condition. These conditions trigger a response by HIF transcription

factors, causing the cells to adapt their metabolism and survival strategies. HIFs are heterodimeric transcription factors composed by one α and one β subunits and the α subunit contains highly preserved proline residues that can undergo hydroxylation (Semenza 2000). Expression of HIF-1α is ubiquitous while HIF-2α is only expressed on endothelial, lung, renal and hepatic tissue. Under normoxic conditions, prolyl hydroxylases (PHD) perform an oxygen-dependent hydroxylation of the α subunit, targeting it for ubiquitination and consequent degradation. These PHD have an absolute requirement for oxygen but also iron (Fe^{2+}) and α-ketoglutarate (Unwith et al. 2014). Under hypoxic conditions these PHD are inhibited, allowing the stabilization of α subunits (namely HIF-1α) and dimerization of the transcription factor with subsequent target gene expression. The target genes expressed range from GLUTs, hexokinase (HK), PFK, aldolase A (ALDA), glyceraldehyde-3-phosphate dehydrogenase (GAPDH), phosphoglycerate kinase, enolase 1, PKM2, LDHA to transketolase (TKT) and pyruvate dehydrogenase kinase 1 (PDK), among others tightly related with the glycolysis, PPP and TCA cycle (Soga 2013). Additionally, HIF mediates the upregulation of several proangiogenic growth factors such as VEGF and PDGF (Unwith et al. 2014).

Given the fact that tumors exhibit transient or chronic states of hypoxia, HIF activation has been firmly established as an important player in tumorigenesis and metastasis, by enhancing glycolysis while limiting oxidative phosphorylation and promoting angiogenesis and chemotherapy resistance (Samanta et al. 2014; Abrantes et al. 2014). PDK phosphorylates and inactivates pyruvate dehydrogenase (PDH), a crucial mitochondrial enzymatic complex that converts pyruvate into AcCoA prompting its entry into the TCA cycle and an increased expression of PDK may limit the TCA cycle turnover (Kroemer et al. 2008).

However, cancer cells have developed oxygen-independent regulation mechanisms due to alterations in diverse pathways, promoting HIF-1α stabilization. Receptor tyrosine kinases are high-affinity receptors for several growth factors and activate the phosphoinositide 3-kinase/protein kinase B/mammalian target of rapamycin (PI3K/Akt/mTOR) pathway, which can promote HIF-1α stabilization through a signaling cascade while promoting survival and proliferation (Semenza 2010). Upregulation or

mutations on the tyrosine kinases, stimulation of PI3K/Akt/mTOR pathway by other oncogenes such as *RAS* or antagonist malfunction such as glycogen synthase kinase-3 (GSK3) may led to an increase on HIF signaling (Flügel, et al. 2012; Semenza 2010). Moreover, certain mutations in seemingly unrelated metabolic proteins could affect the HIF signaling. Cancerous mutations on TCA cycle proteins such as succinate dehydrogenase (SDH) or fumarate hydratase (FH) can generate a buildup of succinate or fumarate. Given that PHD require the decarboxylation of α-ketoglutarate to succinate, a buildup of succinate (or interconvertible fumarate) will inhibit PHD function (Isaacs et al. 2005; Kaelin 2009).

HIF-1α is an intricate pathway with many agonists and antagonists but it is a promising therapeutic target currently under research and definitely one of the major players is the Warburg effect, considering the extensive upregulation of pro-glycolytic enzymes (Unwith et al. 2014).

c-Myc

c-Myc is a transcription factor encoded by the proto-oncogene *MYC*. This transcription factor heterodimerizes with the myc-associated protein X (Max) and bind on consensus sequences (CACGTG) of DNA (E-boxes). c-Myc regulates several cellular mechanisms, including cell cycle progression and proliferation, regulation of micro ribonucleic acid (miRNA) transcription, intermediary metabolism, adhesion and mobility. Due to a wide regulatory function, c-Myc is tightly controlled. However, dysfunction or overexpression of this mechanism, causing signaling independent activation, is related with cancer development and as an estimated occurrence in more than 70% of the cases (Soga 2013; Maya-Mendoza et al. 2014).

This transcription factor is involved in glucose and glutamine metabolism and ribosomal and mitochondrial biogenesis. Considering the metabolic effects of c-Myc, there are very similar effects to those operated by HIF, by upregulating energetic and anabolic pathways. Several glycolytic enzymes such as HK, PKM, LDH, and even PDK and fatty acid synthase (FASN) are upregulated (Fogal et al. 2014; Hu et al. 2011; Soga 2013). HIF and c-Myc actually have a somewhat complex negative and positive feedback mechanisms, but in cancer they may have a symbiotic effect with HIF-2α stabilizing the

c-Myc-Max complex, further favoring the Warburg effect (Yeung et al. 2008). However, one of main features of c-Myc deregulation in cancer is the modulation of the glutamine metabolism. The degradation of glutamine, in a process named glutaminolysis, can originate glutamate and α-ketoglutarate, and nitrogen can be recruited for DNA synthesis, needed during fast cell proliferation. Glutaminase (GLS) is the enzyme that converts glutamine into glutamate and ammonia and c-Myc overexpression was shown to increase the levels of GLS and stimulate glutamine transporters expression (Knox et al. 1969; Gao et al. 2009; Wise et al. 2008). c-Myc acts in parallel with the Warburg effect and while glutamine dependency is a common characteristic in cancer development, c-Myc inhibition or glutamine shortage have been shown to induce apoptosis and tumor regression (Yuneva et al. 2007; Soucek et al. 2008; Le et al. 2012)

p53

Tumor protein 53 or p53 is a transcription factor encoded by the *TP53* gene, a widely studied tumor suppressor gene, conserved in many species. It is activated by a myriad of signals, from increased oxidative stress, DNA damage, hypoxia, nutrient depletion, oncogenes, among others. p53 is also involved in several processes, including apoptosis and senescence, DNA damage repair and maintenance, cell cycle arrest and proliferation (Bieging et al. 2014). Although the mostly associated function is DNA repair and maintenance, p53 also plays an important role in metabolic remodeling and oxidative phosphorylation. GLUT expression is repressed and GLS expression is increased during p53 activation (Soga 2013). *TP53* regulates cytochrome C oxidase (complex IV) assembly, therefore stimulating oxidative phosphorylation since complex IV is the major site of O_2 utilization in the ETC. Besides, p53 inhibits glycolysis through the activation of a relatively recent discovered enzyme, TP53-inducible glycolysis and apoptosis regulator (TIGAR) (Bensaad et al. 2006). Fructose-2,6-biphosphate is an allosteric regulator of glycolysis, binding to PFK and stimulating the conversion of fructose-6-phosphate to fructose-1,6-biphosphate, the third and rate-limiting step of glycolysis. TIGAR has a biphosphatase domain which degrades fructose-2,6-biphoshate into fructose-6-phosphate, reducing fructose-2,6-biphosphate levels and consequently declining glycolytic fluxes, redirecting glucose for the PPP and NADPH production (Green et al. 2006). This p53 remodeling can either promote ROS levels by increasing complex IV

assembly or ROS scavenging by blocking glycolysis and promoting NADPH production through PPP and GSH regeneration. This balance of ROS orchestrated by p53 under normal circumstances can promote apoptosis and autophagy or improve DNA damage repair, depending on the severity of the insult. This transcription factor is also activated by HIF signaling, counteracting their effects. High levels of p53 degrade HIF-1α but increase the levels of mouse double minute 2 homolog protein. Double minute 2 homolog protein decreases p53 levels in a negative feedback loop but may induce HIF-1α stabilization (Nieminen et al. 2005). There are also common regulatory points with c-Myc, where c-Myc can induce ubiquitination and consequent destruction of p53 or suppresses double minute 2 homolog protein, stimulating p53 (Chen et al. 2012; Yeung et al. 2008).

However, in cancer, p53 is frequently dysfunctional, mutated or suppressed, ceasing these functions of metabolic regulation, favoring glycolytic flux to oxidative phosphorylation (Bensaad et al. 2006). It is a complex interplay between several signaling pathways, with positive and negative feedback loops, but this triad of transcription factors, HIF, c-Myc and p53 are quite relevant in the metabolic shift leading to the Warburg effect.

1.4.3 Tumorigenic glycolysis

Aerobic glycolysis is a common feature in many cancers and oncogenes or lack of tumor suppressor genes are responsible for heightening this characteristic, but glycolysis enzymes can also be altered or mutated, assisting this phenotype. High glycolytic rates confer selective advantage by promoting uncontrolled growth and resistance to chemotherapy, so glycolytic key-enzymes will be discussed in further detail (Zhao et al. 2013; Tavares-Valente et al. 2013; Ganapathy-Kanniappan et al. 2013).

Hexokinase

Blood glucose enters the cells through several GLUTs, which are usually overexpressed in cancer as previously discussed. HK performs the first and irreversible reaction of glycolysis, phosphorylating glucose (or other hexoses) into glucose-6-

phosphate, with the consumption of one ATP molecule. This negatively charged phosphoryl group will hinder the glucose transport back to the extracellular medium, rendering the molecule available for glycolysis, PPP or glycogenesis (Nelson et al. 2005).

There are 4 mammalian isozymes, with HKI, II and III showing high affinity for glucose and allosteric inhibition by glucose-6-phosphate, and a IV isozyme known as glucokinase, which has low affinity for glucose and is not inhibited by the end-product of the reaction. HKI is ubiquitously expressed in all organs and is quite insensitive to hormonal regulation, and even though glycolysis is a cytosolic pathway, this enzyme is predominantly associated with the outer membrane of the mitochondria (Wilson 2003). On the other hand, HKII is located mainly in insulin-sensitive tissue such as muscle and adipose tissue. This isoform is located either on cytosol or bound to mitochondria. HKIII have lower expression rates and HKIV is present mainly in the liver and pancreas (Nederlof et al. 2014). HKI has been generally linked to catabolism and HKII and IV to anabolism. However, the cytosolic or mitochondrial location of the HK is not static and it has been implied with compartmentalization and metabolic fate of glucose. By being bound to the mitochondria, HKs use preferentially intramitochondrial pools of ATP for catabolic functions while cytosolic location may provide glucose-6-phosphate for PPP or glycogen (Wilson 2003). This transportation to mitochondria is not clear and may be regulated by glucose-6-phosphate and kinases such as the PI3K/Akt pathway or GSK3 (John et al. 2011).

In cancer cells, HK expression is dramatically increased due to overexpression or transcriptional upregulation (HIF, c-Myc), especially the HKII isoform, with over 70% of the protein bound to mitochondria (Pastorino et al. 2002). HKII binds to the voltage-dependent anion channel (VDAC) in the outer mitochondrial membrane and causes a sensitivity loss to the allosteric inhibitor glucose-6-phosphate (Pedersen 2007). VDAC is a channel that allows the transport of many solutes and metabolites between the cytosol and mitochondrial intermembranar space, such as ATP, and has a major role in the mitochondrial permeability transition pore and apoptosis (Sun et al. 2008). So, the attachment of HKII (and I) to VDAC allows the efficient recruitment of oxidative phosphorylation-derived ATP to perform the reaction and prevents apoptosis by inhibiting the Bax-induced Cyt C release (Pastorino et al. 2002; Cerella et al. 2014).

HKII bound to mitochondria promotes the Warburg effect and hallmark capabilities and is currently a chemotherapeutic target for co-adjuvant therapy, where metabolic inhibitors show synergistic effects with common chemotherapeutics. Some glycolytic inhibitor compounds are under pre-clinical and early phase clinical trials, the 2-deoxyglucose (2-DG), 3-bromopyruvate (3-BrPA) and lonidamide (Zhao et al. 2013). 2-DG is a glucose analog that undergoes phosphorylation and cannot be recognized and metabolized by the next enzyme, phosphoglucose isomerase, acting as a competitive inhibitor of HKs. 2-DG-P becomes trapped inside the cell and the buildup will cause a depletion of ATP production and proapoptotic activation (Zagorodna et al. 2012). It shows good anticancer effects as a co-adjuvant therapy but has some concerns about toxicity (Minor et al. 2010; Sullivan et al. 2014; Levesley et al. 2013). 3-BrPA is a halogenated pyruvate analog with alkylating properties, highly reactive to thiol (-SH) side groups. This molecule is likely to be transported to the cell by MCTs (overexpressed in cancer cells) and is a potent inhibitor of HKII by reacting with the thiol residues present on this enzyme. In fact, it is more efficient than 2-DG and can act solely as a chemotherapeutic drug (Ko et al. 2001; Galina 2014; Ihrlund et al. 2008). Moreover, it has been shown to promote the HKII release from the outer mitochondrial membrane (Chen et al. 2009). The HKII inhibition of cancer cell glycolytic phenotype causes a severe ATP depletion and suppresses multidrug transporter activity, which in turn may improve chemotherapeutic activity (Xu et al. 2005; Pedersen 2012; Ko et al. 2004) Interactions with the mitochondria are also described, promoting ROS generation, apoptosis, autophagy and interaction (alkylation) with TCA cycle enzymes or other glycolytic enzymes (Zhang et al. 2014; Galina 2014).

Glyceraldehyde-3-phosphate dehydrogenase

This enzyme is a multifunctional enzyme, displaying glycolysis unrelated activities. GAPDH is the sixth step of glycolysis, converting glyceraldehyde-3-phosphate into 1,3-biphosphoglicerate, requiring a reduction of NAD^+ into NADH. Besides glycolytic activity, this housekeeping protein is involved in the regulation of gene expression, membrane trafficking/fusion and cytoskeletal dynamics, DNA maintenance, redox homeostasis and cell signaling (Cerella et al. 2014; Tristan et al. 2011). Similarly to HK, GAPDH has different functions in different subcellular localizations and is subject of

several posttranslational modifications or oligomerization into homotetrameric structures. In the cytosol this enzyme can regulate endoplasmatic reticulum (ER) calcium (Ca^{2+}) signaling by binding to a Ca^{2+} channel. Under oxidative stress, GAPDH is inactivated by posttranslational modifications, redirecting metabolism towards PPP, to maintain the redox homeostasis and GSH/GSSG levels (Ralser et al. 2007). This is a reversible modification that allows this enzyme to regulate metabolism or redox, acting as a sensor of oxidative stress. GAPDH also interacts with microtubular structures, promoting tubulin and actin polymerization and vesicular tubular clusters trafficking between the ER and Golgi complex (Tristan et al. 2011). Mitochondrial associated GAPDH may have opposite effects upon stress, yet poorly understood. Due to loss of mitochondrial membrane potential and matrix swelling, it may promote survival by promoting ATP production and mitophagy for clearance of damaged mitochondria; or may induce pro-apoptotic signaling by binding to VDAC and releasing Cyt C and apoptosis-inducing factor (AIF) (Tristan et al. 2011; Colell et al. 2007). Nitric oxide stress will lead to translocation of GAPDH to the nucleus with irreversible sulphonation, causing cell dysfunction and p53-mediated death. Severe DNA damage activates a DNA repair enzyme poly(ADP-ribose) polymerase 1 (PARP1) that can inhibit GAPDH glycolytic function, lowering ATP production and accelerating cell death. Inside the nucleus, GAPDH can also promote DNA repair and transcription, regulate cell cycle and protects telomeres (Tristan et al. 2011).

This enzyme expression is increased in several types of cancer and can actually be used for prognostic estimation once it is correlated with increased aggressiveness, drug resistance and poor prognosis scenarios (Cuezva et al. 2004; Guo et al. 2013). With so many interactions with cellular mechanisms, it may favor carcinogenesis through several ways. As discussed previously, the switch from glycolysis to PPP is beneficial for redox homeostasis and nucleotide synthesis. Other interesting cancer enabling characteristics are the regulation of DNA transcription and repair. GAPDH may bind to telomeric DNA, protecting from degradation and promoting the limitless replicative potential hallmark and evading senescence. But this is still controversial, since negative regulation of telomerases by GAPDH has been shown to promote senescence (Demarse et al. 2009; Nicholls et al. 2012). Also, GAPDH overexpression has been shown to promote cyclin B

activity, increasing mitosis and accelerating cell cycle (Tristan et al. 2011). Also, upon glycolytic stimulation, GAPDH releases a small guanosine triphosphatase, member of the Ras superfamily, which upregulates mTOR pathway and stimulates cell survival and proliferation (Lincet et al. 2014).

This enzyme is a putative therapeutic target given its multifunctional nature, but it is a ubiquitously expressed protein, hampering the therapeutic efficiency and widening the range of side effects. Nevertheless, it is a concomitant target of 3-BrPA therapy and HKII inhibition (Ehrke et al. 2014; Ganapathy-Kanniappan et al. 2012). Iodoacetic acid (IA), also an alkylating reagent, has shown specific and irreversible inhibition of GAPDH (Schmidt et al. 2009). The mechanism of inhibition of 3-BrPA and IA appears to be alkylation of reactive thiol groups of cysteines in the enzyme's active center and inhibition induces apoptosis, blocks tumor progression and compromises GSH homeostasis, but it is still a poorly understood mechanism.

Pyruvate kinase

Pyruvate kinase performs the last and irreversible step of glycolysis, converting phosphoenolpyruvate into pyruvate with a formation of an ATP molecule. There are two muscle isozymes, M1 and M2, which derive from the same messenger ribonucleic acid (mRNA) but with different splicing, differing in 21 aminoacids. PKM1 is a constitutive homotetrameric isoform, found in normal adult cells; PKM2 is an embryonic isoform, capable of oligomerization in highly active homotretrameric or less active homodimeric complexes (Mazurek et al. 2005).

However, several types of cancer express higher levels of the embryonic isoforms PKM2, predominantly the dimer, and this is considered an important alteration towards aerobic glycolysis (Christofk et al. 2008; Wong et al. 2014). High concentrations of the upstream fructose-1,6-biphosphate metabolite causes two inactive dimmers to associate and form the highly active PKM2 tetramer. When fructose-1,6-biphosphate drop, the tetramer dissociate again into two less active dimers (Mazurek et al. 2005; Hitosugi et al. 2009). The presence of an inactive form of a glycolytic enzyme in cancer cells seems inconsistent with the Warburg effect. Though, by generating a blockade at the end of the glycolysis, upstream metabolites will accumulate and may be redirected

for anabolic processes, such as nucleotide, phospholipids and aminoacids synthesis. The switch between highly active tetramer and inactive dimer may act as a sensor for heterogeneous nutrient and oxygen conditions. This enzyme is upregulated and is a coactivator of c-Myc and HIF, in a positive feedback loop (Filipp 2013; Wu et al. 2014). Also, increased or decreased affinity to phosphoenolpyruvate can be promoted by aminoacids, serine and alanine, respectively (Mazurek et al. 2005). Also, this enzyme has glycolytic unrelated functions, such as histone phosphorylation and nuclear signaling (Wu et al. 2014; Yang et al. 2013a).

Studies have shown that reverting PKM2 to PKM1 or inhibition of PKM2 results in a tumor growth inhibition, thereby proving its significance in altered cancer metabolism (Guo et al. 2011; Christofk et al. 2008; Zhao et al. 2013).

Lactate dehydrogenase

On cancer cells exhibiting the Warburg effect, the pyruvate generated in the PK will most likely undergo lactic fermentation performed by the LDH. This enzyme does not belong to glycolysis, which ends at the previous discussed step, pyruvate. LDH catalyzes the conversion of pyruvate into lactate with an oxidation of NADH into NAD^+. This step is necessary to regenerate NAD^+ in order to maintain the glycolytic flux. There are two major isoforms, A and B rearranged in homo or heterotetrameric complexes. LDHA kinetically favors the reaction towards lactate production while LDHB converts mainly lactate back to pyruvate for further oxidation (Shi et al. 2014; Le et al. 2010).

As discussed previously, overexpression of LDH, and LDHA more specifically, is a characteristic of the cancer cells exhibiting the Warburg effect and is correlated with poor prognosis in cancer (Le et al. 2010; Zhao et al. 2013; Girgis et al. 2014). Given the increased glycolytic flux in cancer cells, overexpression of LDHA allows the regeneration of NAD^+ and MCTs export the excess lactate. This acidification of extracellular medium promotes further invasiveness of cancer cells. LDHA expression is also upregulated by low oxygen concentrations and HIF as well as c-Myc transcription factor (Fantin et al. 2006).

The inhibition or knockdown of LDHA results in cancer growth inhibition and stimulation of mitochondrial metabolism, exhibiting a role for cancer therapy (Fantin et al. 2006; Girgis et al. 2014). Some LDH inhibitors have already been applied, namely FX11 and oxamate, with early positive outcomes (Le et al. 2010; Zhou et al. 2010). Oxamate promotes an ATP depletion, increased mitochondrial function and ROS production, resulting in a cell cycle arrest and apoptosis and autophagy (Yang et al. 2014a). These inhibitors interfere with cancer development but still have low potency, requiring high doses and increasing the risk of producing unwanted side-effects (Miao et al. 2013).

1.4.4 TCA cycle dysfunctions

Glycolysis alteration and upregulation is not the only player in malignancy onset. Mitochondrial malfunction and deregulation is also a major intervenient on the rewiring of metabolic pathways in the Warburg effect. Mitochondria encase a myriad of important cellular functions, including energy and ROS production, Ca^{2+} level modulation and apoptosis regulation. In fact, it is an organelle so relevant that their malfunction is associated with several pathological conditions, including cardiovascular disorders, muscular- and neuro-degeneration, and evidently, cancer (Gaude et al. 2014). Regarding ETC, several oncogenes, such as *TP53* or *RAS*, modulate respiratory complexes expression and activity, impairing normal function and ATP and ROS production (Jose et al. 2011). Depending on the type of tumor and nutrient availability, cancer cells display varying degrees of mitochondrial utilization, either for ATP synthesis from oxidative phosphorylation or anabolism of aminoacids, lipids or nucleotides. Concerning metabolic pathways and TCA cycle, a complex rearrangement may occur, from altered anaplerotic sources to inhibition or mutation of key enzymes (Obre et al. 2014).

Pyruvate dehydrogenase

Once finished the glycolysis, pyruvate can be directed to several fates. The most common are fermentation into lactate by LDH, transamination into alanine, by alanine transaminase (ALT), or TCA cycle oxidation. Pyruvate dehydrogenase (PDH) complex is

the mitochondrial enzyme that catalyzes the shuttling of pyruvate into TCA cycle in the form of AcCoA. The function of this complex is tightly regulated by pyruvate dehydrogenase kinases (PDK) and pyruvate dehydrogenase phosphatases (PDP). PDK phosphorylates three specific serine residues in the PDH, rendering the enzyme inactive while PDP operates the reverse process restoring catalytic activity. Humans possess four different PDK isoforms with tissue-specific expression, with ADP, NAD^+, CoA, pyruvate and alanine as allosteric inhibitors (Chen et al. 2012; Jha et al. 2013). A recent report described the translocation of the entire PDH complex from the mitochondria to the nucleus, as a response to stress or cell cycle, implying unknown broader physiological effects driven by this enzymatic complex (Sutendra et al. 2014). The conversion of pyruvate into AcCoA involves a decarboxylation step and requires a molecule of CoA. Coupled to this reaction there is a reduction of NAD^+ to NADH. So this complex is the main gateway responsible for coupling glycolysis and TCA cycle/oxidative phosphorylation.

In cancer cells, PDK is usually overexpressed or upregulated by HIF, repressing PDH function and limiting TCA cycle turnover and ROS formation while promoting fermentation (Kim et al. 2006; Wigfield et al. 2008). This lower ROS production prevents apoptosis and increased lactate levels are correlated with poor prognosis (Jha et al. 2013).

Since it is a key regulator of mitochondrial metabolism it is a promising therapeutic target. Dichloroacetate (DCA) is a pyruvate analog drug imported intracellularly through MCTs. The drug binds to the regulatory pyruvate binding site of PDK, inhibiting PDK, especially the PDK2 isoform. This unblocks PDH allowing the pyruvate to be oxidized by the mitochondria, elevating ROS levels and promoting apoptosis (Bonnet et al. 2007). This drug has shown promising results in cancer *in vitro* and *in vivo* as a sole or co-adjuvant treatment, with low toxicity, fast acting mechanism and low cost of production (Kankotia et al. 2014).

Isocitrate dehydrogenase

IDH is a nuclear encoded protein expressed in three isoforms with different cellular localizations. IDH1 and IDH2 are homodimers dependent of nicotinamide

adenine dinucleotide phosphate ($NADP^+$) cofactor and IDH3 is heterotetrameric NAD^+ dependent enzyme. IDH1 is located at the cytoplasm and peroxisomes while IDH2 and IDH3 are located only in mitochondria. IDH3 isoform is mostly related with TCA cycle oxidation and IDH1/2 are mainly focused for NADPH production and redox homeostasis (Cohen, et al. 2013). Nonetheless, all isoforms promote a decarboxylation, converting isocitrate into α-ketoglutarate with a reduction of $NAD(P)^+$ molecule (Cardaci et al. 2012). The reverse reaction, referred as reductive carboxylation, converting α-ketoglutarate back to isocitrate has been described in certain tissues such as heart, liver and adipose tissue (Adamo et al. 1965; Yoo et al. 2008).

This enzyme revealed to be frequently mutated in several types of cancers, including glioma, leukemia, lymphoma, thyroid, prostate and colorectal. These mutations are usually somatic (heterozygous missense) mutations occurring in one aminoacid residue located in the active site of the enzyme that is vital for isocitrate binding. The residue is the arginine-132 in IDH1 and the arginine-172 or -140 on IDH2 (Dang et al. 2009). This mutation acts as a gain-of-function, where normal and reverse activity are abolished and starts converting α-ketoglutarate into the (R)-enantiomer 2-hidroxyglutarate (R-2HG) with consumption of a NADPH molecule (Leonardi et al. 2012). The mutated enzymes will consume the α-ketoglutarate pools and buildup higher concentrations of R-2HG (up to several mM), initiating tumorigenic stimuli given the structural similarity between α-ketoglutarate and R-2HG. This mutation may act as a competitive inhibitor of α-ketoglutarate dependent dioxygenases, namely ten-eleven translocation enzymes, jumonji histone demethylases and PHD. Ten-eleven translocation enzymes and histone demethylases control demethylation processes in DNA and their inhibition will lead to hypermethylated DNA and anomalous epigenetic regulation of DNA (Rakheja et al. 2012; Xu et al. 2011). PHD inhibition lead to the stabilization of HIF, promoting tumorigenesis but this is still a controversial point, whether R-2HG inhibits or promotes PHD activity (Koivunen et al. 2012). Even though IDH3 is not a target for these specific mutations, an aberrant isoform has been recently shown to be an upstream activator of HIF (Zeng et al. 2014). Furthermore, the reverse function of wild-type IDH is also an interesting metabolic bypass in cancer cells under hypoxia or with defective mitochondria (Mullen et al. 2012; Metallo et al. 2012; Ward et

al. 2010). In cancer, TCA cycle may provide carbon skeletons for lipid, aminoacid and nucleotide synthesis despite of uncoupled ATP production. As discussed previously, c-Myc is usually upregulated in cancer promoting glutamine metabolism while p53 is downregulated, inducing GLS expression. Glutamine can be converted to glutamate by GLS and consequently to α-ketoglutarate by glutamate dehydrogenase (GLDH) or transaminases, feeding the TCA cycle and replenishing the intermediary pools (Obre and Rossignol 2014). The reductive carboxylation operated by IDH will generate isocitrate that can be converted back to citrate through aconitase (ACO). Citrate is then exported to the cytosol, converted to AcCoA by ATP citrate lyase (ACLY) and may be directed for *de novo* lipogenesis (DNL) (Mullen et al. 2012; Metallo et al. 2012). This metabolically advantageous pathway provides anabolic precursors for rapid cell proliferation, allowing a versatile utilization of different substrates.

Specific treatments for the mutated enzymes are still under research and only a few inhibitors have been discovered (Popovici-Muller et al. 2012; Rohle et al. 2013). However, since large α-ketoglutarate pools are necessary for the neomorphic activity of IDH, some studies targeting glutamine metabolism have successfully decreased the levels of R-2HG, by inhibiting GLS. In fact, treatment of certain leukemias resort to modulation of plasma levels of asparagine and glutamine with rather efficient results (Emadi et al. 2014; Elhammali et al. 2014).

Succinate dehydrogenase

SDH is the only TCA cycle enzyme encoded by mtDNA and is embedded in the inner mitochondrial membrane, towards the matrix. All other TCA cycle enzymes are enconded by nDNA. This enzyme is also a known as succinate-ubiquinone oxyreductase or complex II, establishing a bridge between TCA cycle and ETC. It is a heterotetrameric complex with two catalytic subunits (A and B) and two hydrophobic subunits (C and D) which anchor the enzyme and provide the binding site for ubiquinone (Nelson et al. 2005). A recent report discovered a new assembly factor (SDH5) (Hao et al. 2009). This enzyme catalyzes the oxidation of succinate to fumarate with a coupled reduction of ubiquinone to ubiquinol.

SDH was the first metabolic gene discovered to be mutated in hereditary cancers (Baysal et al. 2000). Further studies showed that mutations in all subunits are related with some type of cancer, causing an enzymatic loss-of-function (Oermann et al. 2012). Besides somatic mutations, some hereditary cases (such as paranglioma and phaechromocytoma) are heterozygous germline mutations which result in a loss of heterozigosity and function (Cardaci et al. 2012). The accumulation of succinate, will inhibit PHD leading to HIF stabilization and induce an overexpression (Pollard et al. 2005; Selak et al. 2005). Similarly with IDH mutations, succinate also seems to play a role in epigenetic modifications (Yang et al. 2013b). Given that SDH is a part of the ETC, the loss-of-function will impair the oxidative phosphorylation, promoting Warburg effect characteristics.

Due to the ubiquitous nature of SDH it is a problematic chemotherapeutic target. Actual treatments focus on a reversion of the effects caused by succinate buildup, by promoting α-ketoglutarate dependent dioxygenases, diminishing pseudo-hypoxia angiogenesis and promoting demethylating agents (Morin et al. 2014).

Fumarate hydratase

The next step in the TCA cycle is catalyzed by FH (or fumarase) in a reversible hydration/dehydration reaction, converting fumarate into malate and vice-versa. This enzyme is a homotetramer and may be located in the mitochondria, participating in the TCA cycle or in the cytosol, being involved in the urea cycle, purine synthesis and DNA damage response. Furthermore, the cytosolic conversion of fumarate to malate may help regulate redox levels, since malate can be converted to pyruvate by the malic enzyme (ME), with generation of NADPH (Adam et al. 2013; Yogev et al. 2010).

Recessive mutations of this enzyme cause severe encephalopaties and early death while dominant mutations predispose to benign and malign tumors, namely hereditary leiomyomas and renal cancer (Tomlinson et al. 2002). The inactivation of FH leads to a buildup of fumarate, which also causes the inhibition of α-ketoglutarate dependent dioxygenases and stabilization of HIF transcription factor (Pollard et al. 2005). Additionally, excess fumarate may posttranslationally modify cysteine residues generating 2-succinocysteine, a process referred as succination. The activity of TCA cycle

enzyme ACO, catalyzer of the reversible isomerization of citrate, may be impaired due to succination in a dose-dependent manner (Ternette et al. 2013). Interestingly, cancer cells with mutated and inactive FH develop a way to bypass the blockade imposed on the TCA cycle, through the glutamine metabolism. Glutamine-derived carbons prompted at the α-ketoglutarate are rerouted to heme biosynthesis, from succinyl-CoA by the aminolevulinic acid synthase. This pathway also produces NADH at the α-ketoglutarate dehydrogenase, which can be converted to ATP by the ETC (Frezza et al. 2011).

The main effects of mutated IDH, SDH and FH are very similar, with the inhibition of α-ketoglutarate dependent dioxygenases. Given analogous consequences of hypermethylation and HIF stabilization, the three cases present roughly the same treatment strategies (Morin et al. 2014).

The enzymes described above emerged as the major players in cancerous TCA cycle remodeling but there is evidence of alterations in different enzymes, in some cases still poorly elucidated. However, to avoid elongation these will not be focused. Furthermore, concerning mitochondrial bioenergetics, ETC is also subject to mutations and modulation by oncogenes and cancerous signaling. Only SDH (complex II) was analyzed in terms of metabolic compromising aspects, all other complexes will not be discussed in detail but their relevance in terms of ATP synthesis, regulation of mitochondrial membrane potential and cellular signaling must be acknowledged. For a more detailed analysis consult this recent and interesting review of mitochondrial metabolic defects in cancer (Gaude et al. 2014).

1.4.5 Cooperative pentose phosphate pathway

PPP is a glycolysis parallel pathway, sharing common intermediates, occurring entirely in the cytosol. The PPP has two branches: initiated at glucose-6-phosphate, the oxidative branch with three irreversible reactions that generates NADPH and ribonucleotides; and the non-oxidative branch, composed of reversible reactions that may recruit or deliver fructose-6-phosphate and glyceraldehyde-3-phosphate,

depending on the metabolic needs. Cells requiring NADPH for redox homeostasis promote the oxidative branch for NADPH production and redirect the non-oxidative pathway to fructose-6-phosphate, which can be converted back to glucose-6-phosphate, replenishing the oxidative branch (Patra et al. 2014). PPP is highly active in red blood cells for maintenance of reduced GSH given their exposure to ROS (Delgado et al. 2004). In rapidly dividing cells, PPP is directed towards ribonucleotides synthesis, consuming glucose-6-phosphate, fructose-6-phosphate and glyceraldehyde-3-phosphate. This is crucial in cancer since they possess a heightened requirement for nucleotides and NADPH, useful for cell survival, redox homeostasis and fatty acid synthesis (Patra et al. 2014).

Glucose-6-phosphate dehydrogenase

The most studied enzyme of PPP is the first and classical rate-limiting step, glucose-6-phosphate dehydrogenase (G6PDH). This enzyme catalyzes the oxidation of glucose-6-phosphate into 6-phosphogluconolactone with a concomitant production of NADPH. This expression and activity are tightly regulated, with an inactive monomer or active dimer, regulated by NADP+/NADPH ratio, where NADPH acts as an allosteric inhibitor (Patra et al. 2014). G6PDH is the most common hereditary enzyme deficiency in humans, prevalent in 400 million people, responsible for chronic hemolytic anemia. This deficiency causes an activity reduction, which may be a protective mechanism against malaria, since most of the cases are from endemic malaria regions and PPP is the main NADPH source in red blood cells (Stincone et al. 2014).

In cancer, G6PDH is usually overexpressed and presents increased activity (Jonas et al. 1992; Wang et al. 2012). Given that the G6PDH is the rate-limiting step, all PPP modulation has an impact at this bottleneck. Transcription factor p53 may act as a direct inhibitor of G6PDH, but since it is usually suppressed in cancer, PPP remains uninhibited. Furthermore, p53 activates TIGAR, which promotes the PPP by converting fructose-2,6-biphosphate to fructose-6-phosphate, reducing the PFK activity. However, TIGAR expression has been shown to be deregulated in cancers, independently of p53 and associated with mitochondrial HKII, supporting ROS protection and cell survival (Cheung et al. 2012). As discussed previously HIF and c-Myc signaling result in upregulation of

GLUTs, HK, PFK, ALDA and PKM2, among others. This modeling promotes glycolysis but also PPP, delivering large amounts of substrates and allowing the utilization of such as anabolic precursors. GLUTs and HK promote the synthesis of glucose-6-phosphate, substrate for G6PDH while PKM2 blocks glycolysis, creating a buildup of all glycolytic substrates upstream of phosphoenolpyruvate. Moreover, activation of mTOR pathway, which is upregulated in several cancers, promote G6PDH expression (Tsouko et al. 2014).

Considering the tumorigenic performance of active PPP in cancer, inhibition of G6PDH poses as an interesting target. In fact there are several sugar phosphates and nucleotides that compete for substrates or cofactor (Pelicano et al. 2006). A powerful uncompetitive inhibitor of G6PDH is dehydroepiandrosterone (DHEA), a naturally synthesized steroid that may even have tumor preventive characteristics. However, treatment requires high oral dosage and produces active androgens. The inhibition of PPP leads to an increase in oxidative stress and present anti-proliferative effects, but the mechanism of action is still not consensual (Preuss et al. 2013; Yoshida et al. 2003; Boros et al. 1997).

Transketolase

While G6PDH initiates the oxidative branch, transketolase (TKT) catalyzes two reactions in the non-oxidative branch. These non-oxidative reactions are reversible and TKT may redirect the flux of PPP depending on the needs. TKT reversibly converts ribose-5-posphate and xylulose-5-phosphate into sedoheptulose-7-phosphate and glyceraldehyde-3-phosphate; xylulose-5-phosphate and erythrose-4-phosphate into fructose-6-phosphate and glyceraldehyde-3-phosphate (Patra et al. 2014).

Cancer cells require large amounts of riboses for nucleotide synthesis and in fact up to 80% of the ribonucleotides may be provided by the non-oxidative branch of PPP (Boros et al. 1997). Unsurprisingly, TKT is overexpressed in several cancers, promoting cancerous growth and allowing the utilization of different substrates such as riboses or fructose to cope with the elevated biosynthetic demands of cancer proliferation (Kayser et al. 2011; Liu et al. 2010).

Inhibition of TKT is a plausible target for specific cancer treatment (Semilia et al. 2015). Oxythiamine is a thiamine antagonist known to inhibit TKT, strongly competing with the cofactor required for the reaction, thiamine pyrophosphate (TPP). The treatment with oxythiamine suppresses nucleotide synthesis and induce cell apoptosis (Wang et al. 2013; Boros et al. 1997).

1.4.6 Cancerous *de novo* lipogenesis

Misconceptions and generalizations regarding mitochondrial metabolism and TCA cycle pushed the research towards the Warburg effect and increased glycolytic flux. Aided by compelling data and well described enzymatic mechanisms, it attracted the main focus of metabolic research on cancer. In recent years, researches in alternative pathways, such as PPP or DNL, show increasingly intertwined relationships and provide a better understanding of cancer metabolism. Even though these parallel metabolic pathways were described long time ago, their contribution to cancerous processes has been overlooked.

Lipids and fatty acids are quite versatile molecules with anabolic and catabolic properties. Lipids can be stored, produce energy through β- and TCA cycle oxidation and serve as precursors for steroids, vitamins and hormones. Fatty acids may derive from stored/dietary lipid degradation or synthesis through DNL. In a postprandial state with an overflow of circulating carbohydrates, DNL is upregulated, producing fatty acids from the carbohydrate-derived AcCoA, occurring mainly in the liver and adipose tissue. These fatty acids may be esterified with a glycerol molecule and stored as triglycerides for posterior use. Glucose will undergo glycolysis and produce pyruvate that enters mitochondria through PDH in the form of AcCoA. AcCoA reacts with oxaloacetate to generate citrate through citrate synthase (CS) in the TCA cycle. Contrarily to β-oxidation which occurs in the mitochondria, DNL is a cytosolic pathway, so citrate is exported to cytosol and converted back to AcCoA through ACLY, becoming available for initiating fatty acid synthesis and elongation, mevalonate synthesis or acetylation reactions (Nelson et al. 2005). However, DNL have a limited capability of synthesizing polyunsaturated fatty acids, therefore enriching the cells with saturated (mainly

palmitate, stearate and other smaller fatty acids) or monounsaturated fatty acids (Rysman et al. 2010). Dysregulation of this pathway is associated with several pathologies, including cancer, insulin resistance and type 2 diabetes, non-alcoholic fatty liver disease and even viral infections (Ameer et al. 2014).

Cytosolic supply of acetyl-coenzyme A

DNL is increased in cancer cells where there is a large requirement of fatty acids for assembly of the new membrane phospholipids and may be a marker for aggressive cancers (Menendez et al. 2007). CS expression was found increased in some types of cancer, which can be advantageous for DNL upregulation by providing larger pools of citrate (Chen et al. 2014). Citrate is then exported to cytosol by a tricarboxylate transporter and converted back to AcCoA and oxaloacetate by the ACLY, which is coupled to ATP hydrolysis. The withdrawal of citrate pools for DNL also impairs the regular TCA function unless anaplerotic oxaloacetate is introduced to regenerate citrate. Oxaloacetate formed by ACLY in the cytosol may return to the mitochondria through the malate/aspartate shuttle. However, as discussed previously, cytosolic oxaloacetate is likely to undergo decarboxylation by the ME, producing NADPH and pyruvate that may reenter mitochondria and TCA cycle through PDH (Icard et al. 2012). Nonetheless, glutaminolysis may also provide oxaloacetate through transamination, oxidation at the TCA cycle or supply directly citrate through reductive carboxylation by IDH (Metallo et al. 2012). ACLY overexpression has been detected in several types of cancer and is upregulated by the PI3K/Akt pathway. AcCoA will feed the building blocks necessary for fatty acid synthesis, but first must undergo a carboxylation by acetyl-CoA carboxylase, producing malonyl-CoA and initiating DNL.

Fatty acid synthase

FASN is an intricate multi-enzymatic complex that produces saturated fatty acids. The synthesis involves the repetitive addition of two AcCoA-derived carbons at each cycle, in the form of malonyl-CoA. Each cycle performs a condensation, reduction, dehydration and another reduction, oxidizing 2 NADPH molecules. Considering, palmitate with a 16 carbons skeleton, it requires 14 NADPH molecules in 7 cycles,

consuming a sizeable amount of reducing equivalents. With exception for the liver and adipose tissue, expression of FASN is low in normal cells. However, in several types of cancer FASN is highly expressed, providing not only lipids necessary for proliferation but may also provide ATP through β-oxidation, such as in cancers with metabolomics diverging from the Warburg effect (Flavin et al. 2010; Liu 2006). FASN may be upregulated by growth factors and PI3K/Akt pathway, usually altered in cancer cells. Moreover, this pathway provides oxidizing power in the form of $NADP^+$, which may support aerobic glycolysis given that large pools of NAD^+ are required for maintaining a steady glycolytic flux (Gameiro et al. 2013a).

Additionally, synthesized fatty acids are mostly saturated, which allows denser membrane packing, causing significant changes in membrane fluidity, transport dynamics and signal transduction. In fact, this altered membrane properties turn cells less sensitive to peroxidation and may impair chemotherapeutic uptake (Rysman et al. 2010). Inhibition or silencing of each enzyme involved in DNL (ACLY, ACC and FASN) induces generally the same effects, namely growth arrest, apoptosis and DNL decreased flux (Ameer et al. 2014). FASN is the most studied of the three and several small molecule inhibitors have already been found targeting different enzymes in the complex that can act as sensitizers for chemotherapy (Menendez et al. 2007).

1.4.7 Aminoacid metabolism

Aminoacids may derive from dietary sources or protein degradation and can perform a vast array of functions. In the human body, these molecules can be oxidized for ATP production, participate in biosynthesis of nucleotides, amines and proteins, transport ammonia through the alanine cycle and participate in ammonia secretion by the urea cycle. Regarding catabolism, aminoacids can be classified as glucogenic, by generating pyruvate or TCA cycle intermediates, or ketogenic, by generating acetoacetyl-CoA or AcCoA. There are also aminoacids that may provide both glucogenic and ketogenic substrates such as tryptophan, phenylalanine, tyrosine, threonine and isoleucine. Even though aminoacid oxidation for ATP synthesis is usually low, under severe starving conditions it is upregulated as a survival mechanism (Nelson et al. 2005).

Central role of glutamine

In a healthy individual, glutamine is produced mainly at the skeletal muscle and lungs and absorbed at the intestine, liver and kidneys. However, the whole balance is altered upon tumorigenesis or inflammatory processes where lungs and skeletal muscle increase their glutamine production, liver and kidneys may change their net flux and the tumor becomes the most avid glutamine consumer (Hensley et al. 2013; Hulsewé et al. 2003).

Glutamine pools are converted to glutamate via glutaminase, releasing the amide nitrogen as ammonia. Glutamate can also be used to produce several other non-essential aminoacids through the action of transaminases, which transfer the glutamate amino group to the α-ketoacid thus generating α-ketoglutarate in quickly reversible reactions. Besides transaminases, glutamate can additionally generate α-ketoglutarate through GLDH, prompting the entry of carbon in the TCA cycle as an anaplerotic route or even as respiratory substrate. Glutamine-derived α-ketoglutarate can then be oxidized to malate or oxaloacetate and form pyruvate (via pyruvate cycling), accompanied by the formation of reducing equivalents both in the TCA cycle and at the ME, that can feed several processes, such as ATP production, lipid synthesis or redox homeostasis. Glutamate and glutamine are generally present in higher concentrations than any other aminoacid, sometimes an order of magnitude higher, and even though glutamate is not an abundant extracellular nutrient, glutamine pools can be converted to glutamate in order to maintain its intracellular levels (DeBerardinis et al. 2010).

Carcinogenic tissue displays an altered metabolic profile and frequently an increase in glutamine uptake, namely c-Myc with increased expression of GLS and glutamine transporters as discussed previously (Wise et al. 2008). Nucleotide biosynthesis of purines and pyrimidines has a specific requirement for the γ amido group of glutamine and aspartate. Also, reductive carboxylation by IDH may provide citrate and AcCoA for lipid synthesis (Mullen et al. 2012; Metallo et al. 2012). Therefore an increased uptake of glutamine and glutaminolysis supports some of these carcinogenic needs. In fact, glutamine deprivation promotes apoptosis and enhances

chemotherapeutic treatments by sensitizing the cells (Obre et al. 2014; Yuneva et al. 2007; Drogat et al. 2007).

Transaminase bypass

Transaminases allow the conversion of non-essential aminoacids pools in a simple reaction but with broad consequences. The mechanism requires the transfer of the amino group to an α-ketoacid, generating the corresponding α-ketoacid and aminoacid in quickly reversible reactions. Two main studied transaminases are aspartate and alanine transaminase (AST, ALT), which are widely used as biomarkers for hepatic function assessment (Nelson et al. 2005).

ALT converts glutamate and pyruvate into α-ketoglutarate and alanine. This mechanism is critical in the alanine cycle, where alanine acts as circulatory transporter of pyruvate and nitrogen from the muscles to the liver where it is converted back to pyruvate that can be directed for gluconeogenesis and ammonia for the urea cycle. This enzyme establishes a connection between glycolysis and glutaminolysis. Pyruvate may undergo reduction into lactate or transamination into alanine and both reactions are reversible, allowing flexible access to large pools of metabolites buildup by the Warburg effect. Alanine is a glucogenic aminoacid and by providing pyruvate, it can be converted to AcCoA for TCA cycle oxidation or DNL, while the reverse reaction may provide anaplerotic substrate in the form of α-ketoglutarate, consuming pyruvate from the aerobic glycolysis and glutamate derived from glutaminolysis. Since alanine is easily exported, it allows cancer cells to export excess glutamate (and therefore excess nitrogen) and pyruvate (as lactate precursor) in the form of alanine while retaining the carbon skeleton as α-ketoglutarate. Inhibition of this enzyme as shown to impair growth and promote mitochondrial metabolism (Beuster et al. 2011).

AST has a more complex interaction with metabolism has it converts glutamate and oxaloacetate into α-ketoglutarate and aspartate. This enzyme may work in parallel with ALT, since they share common substrates. Furthermore, it introduces a bypass across the TCA cycle by converting two intermediates, α-ketoglutarate into oxaloacetate. As discussed previously, citrate pools may be recruited for DNL and AST

may provide replenishment of oxaloacetate pools, sustaining both TCA cycle and biosynthetic processes (Nelson et al. 2005).

Excessive ammonia from aminoacid degradation is toxic but it is converted and excreted in the form of urea, an energy consuming cycle occurring mainly in the liver. Aspartate is an intermediate of the urea cycle and together with argininosuccinate establishes a link between the TCA and urea cycles. Similarly to ALT, by consuming oxaloacetate and glutamate, the carbon skeleton of α-ketoglutarate remains in the TCA cycle while the aspartate (as nitrogen donor) is transferred for urea synthesis in the cytosol, generating argininosuccinate. This molecule is then cleaved in arginine (the precursor of urea) and fumarate that may return to the TCA cycle. Aspartate presents here another important function in mitochondrial substrate transportation. Cytosolic fumarate from urea cycle is converted by ME into malate and through the malate/aspartate shuttle it is retrieved at the TCA cycle, regenerating oxaloacetate. AST may be a target for cancer therapies since it is involved in redox maintenance and inhibition with aminooxyacetic acid (AOA) decreases breast cancer proliferation (Lyssiotis et al. 2013; Thornburg et al. 2008).

Other aminoacids such as serine or asparagine are also relevant for the carcinogenic process, as substrates for oxidation, biosynthesis and signaling (Ye et al. 2014; Zhang et al. 2014). However, to avoid further elongation and lose focus, it will not be discussed in further detail.

Chapter 2
Metabolism

2.1 Metabolic tracers

Alterations in cancer cell metabolism have long been known, and many researchers have pursued the goal of better defining the metabolic remodeling that accompanies carcinogenesis. Existing nuclear magnetic resonance (NMR) stable tracers methodologies can be adapted to the metabolic study of cancer cells and tumors. These stable isotope tracer methodologies were developed for the study of particular organs (Chance et al. 1983; Malloy et al. 1988) or metabolic conditions (Cline et al. 1999; Shulman et al. 2001; Dusick et al. 2007) but can easily be adapted and implemented to the study of cancer metabolism (Fan et al. 2009; Metallo et al. 2012; Zhang et al. 2014).

Figure 2.1 shows a schematic representation of central metabolic pathways that can be addressed by stable isotope tracer (^{2}H and ^{13}C) methodologies. Several tracers can provide unique information concerning specific metabolic pathways and some approaches involving multiple tracers can help identifying the intricate interplay between metabolic pathways.

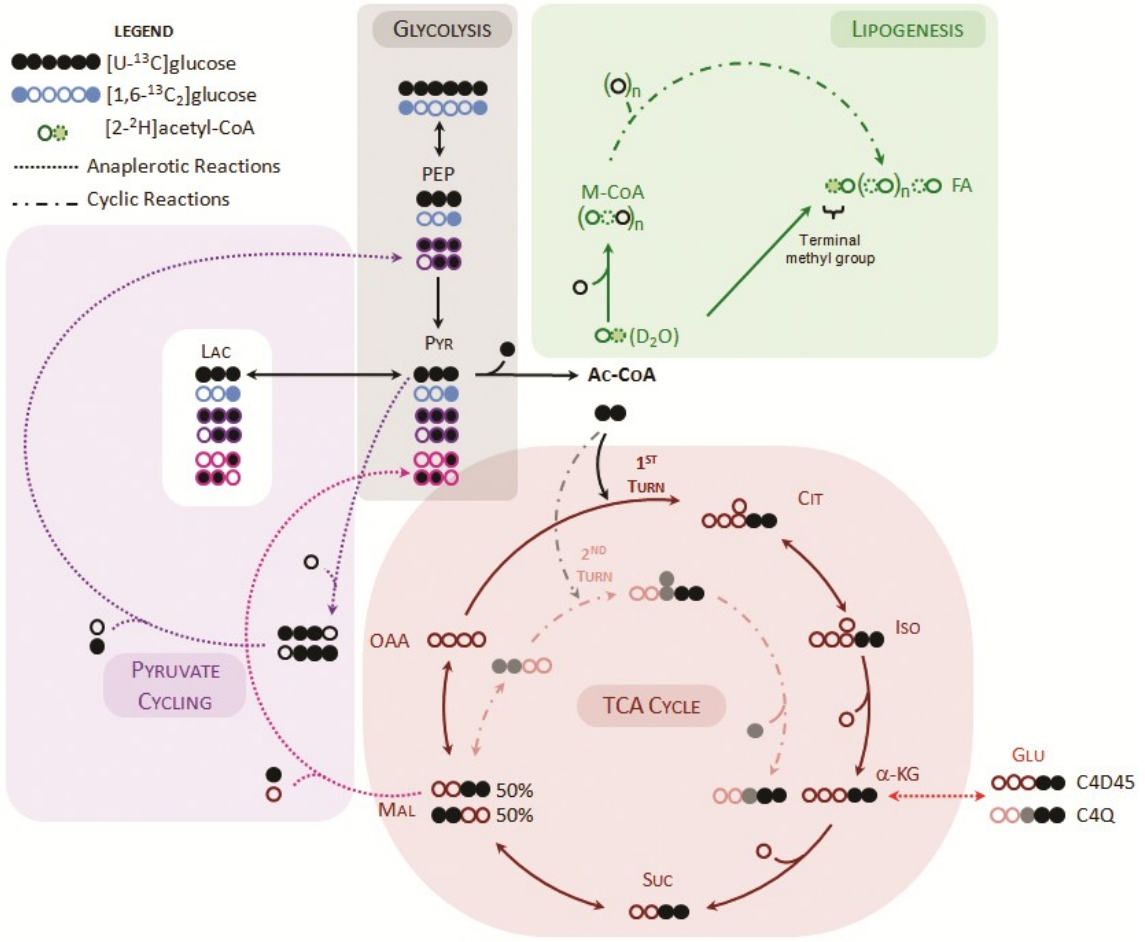

Figure 2.1 - Schematics of ^{13}C and ^{2}H labelling patterns through different metabolic pathways. Molecules are represented by their skeletal carbons, depicted as circles. Empty circles represent ^{12}C and filled circles ^{13}C. Colored circles illustrate the different metabolic pathways, where black represents glycolysis; brown is the TCA cycle; green is the lipogenesis pathway and purple is the pyruvate cycling. Glycolysis and TCA cycle function can be assessed by [U-^{13}C]glucose (black) or [1,6-$^{13}C_2$]glucose (blue). [U-^{13}C]glucose will originate two molecules of [U-^{13}C]pyruvate, which can undergo lactic fermentation by lactate dehydrogenase (LDH) and form [U-^{13}C]lactate (black) or can enter mitochondria and form [1,2-$^{13}C_2$]AcCoA (black) through pyruvate dehydrogenase (PDH). When [1,2-$^{13}C_2$]AcCoA enters TCA cycle it will label [4,5-$^{13}C_2$]α-ketoglutarate (αKG), and consequently give rise to [4,5-$^{13}C_2$]glutamate. If this αKG isotopomer stays in the cycle (faded black) it will originate multi-labeled glutamate isotopomers, such as [3,4,5-$^{13}C_3$]glutamate (2nd turn) and eventually [U-^{13}C]glutamate (multiple turns), which are distinguishable from [4,5-$^{13}C_2$]glutamate originated in the 1st turn. Ratios between multiple and double labeled glutamate isotopomers are frequently used as a measure of oxidative capacity and glycolysis/TCA cycle metabolic coupling. Lipogenesis can be determined by ^{2}H experiments, through administration of heavy water ($^{2}H_2O$), due to several hydration reactions that can label metabolic tracers. When AcCoA is labeled with ^{2}H (dotted green), it may be directed to *de novo* fatty acid synthesis and label fatty acids. By measuring the $^{2}H/^{1}H$ enrichment of the terminal methyl group from the fatty acids we can attain lipogenic activity. Pyruvate cycling is an anaplerotic pathway represented in dotted arrows. Through pyruvate carboxylase (PC) a $^{12}CO_2$ molecule is added to pyruvate, leading to a 50% loss of enrichment at C1 (purple) due to "backward scrambling" of the oxaloacetate molecule before being subject to decarboxylation. (PEP) Phosphoenolpyruvate; (Pyr) Pyruvate; (Lac) Lactate; (Ac-CoA) Acetyl-Coenzyme A; (Cit) Citrate; (Iso) Isocitrate; (α-KG) α-ketoglutarate; (Suc) Succinate; (Mal) Malate; (OAA) Oxaloacetate; (Glu) Glutamate; (M-CoA) Malonyl-CoA; (FA) Fatty Acid.

2.2 Glycolysis and lactic fermentation

The Warburg effect is a major metabolic change in many cancer cells, with an increased glycolytic flux without concomitant oxidation of pyruvate in the TCA cycle. This results in the production of considerable amounts of lactate even under aerobic conditions. Nevertheless, this metabolic phenotype is not unique to cancer cells. In fact, significant glycolytic activity can also be measured in non-tumorigenic fast-dividing cells and in tissues known to possess a high biosynthetic activity (Oliveira et al. 2012). In cancer, the pivotal role of the glycolytic pathway has been widely accepted. Furthermore, the mutations and deregulation occurring in several glycolytic enzymes discussed in the previous chapter demonstrates unequivocally that the unique metabolism of tumor cells is critical for tumorigenesis.

Glycolysis is divided in two phases, preparatory and payoff phase. The preparatory phase phosphorylates glucose and converts it into two trioses, glyceraldehydes-3-phosphate, with a consumption of 2 ATP molecules. The payoff phase, oxidizes the two trioses into pyruvate and, has the name suggests, produces 4 molecules of ATP and 2 NADH. Initiated with HK, glucose is phosphorylated at C6 into glucose-6-phosphate with a hydrolysis of ATP. This undergoes an isomerization to fructose-6-phosphate and PFK1 transfers another phosphoryl group from ATP to the C1, generating fructose-1,6-biphosphate. ALDA cleaves the glucose between the C3 and C4 into glyceraldehyde-3-phosphate and dihydroxyacetone-3-phosphate (these molecules can be interconverted). This reaction causes a change in the carbon labelling order, whereas glucose C1 and C6 are now glyceraldehyde-3-phosphate C3, remaining throughout the rest of glycolysis. The payoff phase starts with GAPDH, oxidizing glyceraldehyde-3-phosphate into 1,3-biphosphoglycerate with a reduction of NAD^+ to NADH. Phosphoglycerate kinase transfers the phosphoryl group of C1 to ADP and generates 3-phosphoglycerate and ATP. Phosphoglycerate mutase produces 2-phosphoglycerate and ENO operates dehydration to phosphoenolpyruvate, in two reversible reactions. At last, phosphoenolpyruvate is converted to pyruvate by PK with a production of ATP, finishing the glycolysis.

Glycolysis can be easily monitored using a glucose ^{13}C-tracer, since newly produced ^{13}C-enriched pyruvate exchanges with lactate and leads to the formation of ^{13}C-enriched lactate, distinguishable from the non-enriched counterpart. This distinction is possible by means of ^{1}H-NMR spectroscopy due to direct ($^{1}J_{HC}$) and long-range ($^{2}J_{HC}$, $^{3}J_{HC}$) ^{1}H-^{13}C scalar-scalar coupling. ^{13}C-lactate buildup in cell culture media is thus frequently used as a measure of glycolysis and combined with the assessment of the disappearance of provided tracers (e.g., [1-^{13}C]-, [U-^{13}C]- or [1,6-$^{13}C_2$]glucose), indirectly provides information concerning the contributions of TCA cycle oxidative flux and glycolysis to overall cellular metabolism. The use of [1,6-$^{13}C_2$]glucose has considerable advantages relative to other carbon tracers mostly associated with improved sensitivity: i) both three carbon units are ^{13}C enriched, avoiding the 50% dilution associated with tracers labelled in only one of the trioses (e.g., [1-^{13}C]- [2-^{13}C]glucose); ii) generated ^{13}C-satellites in the ^{1}H-methyl resonance of lactate are doublets, instead of doublets of triplets, found when using [U-^{13}C]glucose; iii) ^{13}C multiplets of intermediary metabolites have as well fewer resonances; all these warrant considerably higher signal to noise in NMR spectra – a major limitation in the application of stable tracer methodologies.

2.3 TCA cycle

Concerning the TCA cycle, several enzyme mutations have been associated with tumorigenesis, namely succinate SDH, FH and IDH (Cardaci et al. 2012). Mutations at IDH may disable the regular function of this enzyme and convert α-ketoglutarate to R-2HG. Also, reductive carboxylation operated by IDH consumes NADPH and α-ketoglutarate, boosting glutamate consumption and removing reducing equivalents, both useful for GSH recycling. Even though this reductive carboxylation is a regular physiological process under hypoxia conditions, it is highly advantageous when active in cancerous cells since it can be converted back to citrate and directed DNL (Metallo et al. 2012). The full oxidation of glucose and other nutrients in the TCA cycle coupled with mitochondrial oxidative phosphorylation constitutes an efficient mechanism of ATP production. This ATP is required for many thermodynamically unfavorable processes occurring in the cell, including ionic homeostasis, metabolite transport across intracellular compartments and

overall biosynthesis. While only a net production of 2 ATPs per glucose molecule occurs through glycolysis, its full oxidation to CO_2 in the TCA cycle holds the possibility of generating a total of 32 ATPs. However, highly proliferating cancer cells seldom exploit such catabolic procedure to derive the required ATP for all biosynthetic processes developed towards cellular division. Instead, cancer cells rely mostly on glycolysis-derived ATP and employ the TCA cycle as a metabolic pathway for metabolite inter-conversion. Highly abundant metabolites, namely aminoacids and ketoacids, are easily transformed into less abundant but equally needed species for protein synthesis or directed towards DNL to account for the higher demand of lipids during cell proliferation and division. ^{13}C-enriched anaplerotic metabolites, upon entrance in the TCA cycle, suffer several carbon rearrangements that are very informative concerning the interplay between TCA cycle and other major metabolic pathways like glycolysis, pyruvate cycling and DNL.

TCA cycle is initiated at the PDH complex, where pyruvate suffers a decarboxylation of the carboxyl group (C1), generating AcCoA. By losing C1 in the form of CO_2, pyruvate C2 and C3 are converted to AcCoA C1 and C2, respectively. Coupled to this reaction there is a reduction of NAD^+ to NADH. Through CS, oxaloacetate C2 reacts with AcCoA C2 in a condensation, forming citrate. ACO in a reversible two-step process generates isocitrate. Interestingly, citrate is a symmetric molecule but it reacts asymmetrically (prochiral), preserving the carbon skeleton of oxaloacetate and AcCoA and avoiding possible labeling scrambling. Through the already discussed IDH, isocitrate is converted to α-ketoglutarate with the production of NADH and a coupled decarboxylation. The CO_2 released in this step was derived from the C1 of oxaloacetate. α-ketoglutarate suffers another oxidative decarboxylation by the α-ketoglutarate dehydrogenase with a NADH production, generating succinyl-CoA. The CO2 released in this enzyme was derived from the C4 oxaloacetate. Thioester bond of succinyl-CoA is cleaved by succinyl-CoA synthetase, generating succinate and GTP, which can be subsequently converted to ATP. SDH operates the oxidation to fumarate with production of flavin adenine nucleotide ($FADH_2$). Fumarate is a symmetrical molecule and unlike citrate, it may react at both ends, allowing a labeling scrambling of the carbon skeleton, where C1 can be converted to C4 and vice-versa. Fumarase, also a reversible

enzyme, generates a non-symmetrical molecule, malate and malate dehydrogenase finishes the cycle by replenishing the pools of oxaloacetate, with a coupled production of NADH. On a first turn of the cycle the two carbons that are oxidized as CO_2 are in fact derived from oxaloacetate, meaning that none of the AcCoA derived carbons abandons the cycle.

2.3.1 TCA cycle turnover:

TCA cycle rates can be measured by ^{13}C NMR isotopomer analysis providing ^{13}C of enriched precursors are efficiently incorporated into TCA cycle intermediates. Thus, AcCoA should preferentially be labeled in C2 of the acetyl moiety or in both C1 and C2 (Figure 2.1). The reason for such is the fact that labelling in C2 of AcCoA produces labelling in various carbons of TCA cycle intermediates and the levels of incorporation are sensitive to the amount of TCA cycle turns (Chance et al. 1983; Malloy et al. 1988; Malloy et al. 1990; Carvalho et al. 2001). As an example, following the production of [U-^{13}C]pyruvate, [1,2-$^{13}C_2$]AcCoA is originated through PDH. On a first turn of the cycle, [1,2-$^{13}C_2$]- or [3,4-$^{13}C_2$]-oxaloacetate become enriched and its subsequent condensation with another molecule of [1,2-$^{13}C_2$]AcCoA prompts the formation of multiply labeled intermediates, namely [3,4,5-$^{13}C_3$]- and [1,2,4,5-$^{13}C_4$]α-ketoglutarate (Figure 2.1). The enrichment pattern is further complicated in subsequent turns, until an isotopic steady-state is reached. The glutamate pool, due to exchange with the α-ketoglutarate pool, becomes as well ^{13}C-enriched. The ^{13}C-multiplets, quartet (Q) versus doublet 45 (D45), in glutamate C4 provide a measure of TCA cycle turnover due to the distinctive value of the direct scalar-scalar coupling between C4 and C5 ($^1J_{C4C5}$=52 Hz) and C3 and C4 ($^1J_{C3C4}$=34 Hz). Particular attention must however be taken in some tissues and/or metabolic conditions where the exchange between metabolite pools might be compromised. If glutamate is not in fast exchange with the α-ketoglutarate pool, its labelling pattern will not fully reflect the TCA cycle dynamics and metabolic and isotopic steady state must be attained before metabolic conclusions can be drawn from the derived isotopic data (Carvalho et al. 2001; Weiss et al. 1995).

2.4 Pyruvate cycling

Instead of entering the TCA cycle through PDH, pyruvate can be carboxylated by the action of pyruvate carboxylase (PC) producing oxaloacetate. This oxaloacetate can follow the TCA cycle or be converted back to pyruvate through the combined actions of phosphoenolpyruvate carboxykinase (PEPCK) and PK or through the action of the ME. Carbon scrambling in these pathways alters the labelling patterns of TCA cycle intermediates and that way ^{13}C tracers can be utilized for monitoring their preponderance. If we consider the carboxylation of [U-^{13}C]pyruvate, two types of oxaloacetate isotopomers are formed due to backward scrambling, [1,2,3-$^{13}C_3$]- and [2,3,4-$^{13}C_3$]-oxaloacetate. This leads to a dilution in the ^{13}C-enrichment of pyruvate and the [2,3-$^{13}C_2$]pyruvate isotopomer reflects activity of pyruvate cycling (Figure 2.1, showed in purple). If instead the generated oxaloacetate isotopomers follow the TCA cycle and combine with unenriched AcCoA, further ^{13}C dilution occurs, leading to the appearance of [1,2-$^{13}C_2$]- and [3-^{13}C]pyruvate through pyruvate cycling (Figure 2.1, shown in pink).Cancer cells have increased biosynthetic activity and one would expect the involvement of this pyruvate-cycling pathway. The monitoring of this pathway is thus, in our perspective, very important for a better definition of the metabolic switch that occurs in tumorigenesis.

2.5 *De novo* lipogenesis

Considering that the majority of the lipids produced by DNL are palmitate, we will focus on the mechanism of FASN. The first AcCoA and malonyl-CoA bind to FASN by a thioester bound and losing the CoA. The acetyl from AcCoA, will be the methyl group at the end of the fatty acid acyl chain. More specifically, in terms of carbon labelling, the C2 of the first AcCoA will be the methyl group of palmitate. As discussed previously, even though citrate is a symmetrical molecule, citrate-derived AcCoA preserves the carbon order, avoiding labeling scrambling.

The first reaction occurring at FASN is a condensation between the acetyl group and the malonyl with the elimination of the CO_2 that was added previously by ACC. This reaction elongates the acyl chain by two carbons. The next reactions are a reduction, dehydration and another reduction, and at each reduction, one NADPH is oxidized. These series of reactions reduce the ketone group, remove the oxygen in the form of water and reduce the double bond, generating the saturated acyl chain. At the end of this cycle of four reactions, a new malonyl-CoA molecule binds to FASN and the elongation process continues, adding two more carbons in each cycle (Nelson et al. 2005).

In cancer cells, DNL is increased in order to assemble membranes for the dividing cells and organelles (Zaidi et al. 2013). The monitoring of the lipogenic sources is possible using stable isotope tracers, namely $^{2}H_2O$ (Silva et al. 2011; Murphy 2006), and ^{13}C enriched glucose and/or glutamine (Metallo et al. 2012; Gameiro et al. 2013b). By the $^{2}H_2O$ method it is possible to derive absolute rates of DNL, providing that accurate measures of the ^{2}H enrichment of the precursor [2-^{2}H]AcCoA are made (Silva et al. 2011). The relative contributions of the main lipogenic sources and pathways can simultaneously be derived providing the adequate ^{13}C-labelling patterns of the precursors are chosen. One possibility is the use of [1,6-$^{13}C_2$]glucose, that provides [2-^{13}C]AcCoA, plus [U-^{13}C]glutamine, that can generate [1,2-$^{13}C_2$]AcCoA by reductive carboxylation through IDH. These two ^{13}C tracers would be easily distinguishable in a ^{13}C NMR spectrum of lipids, since the first gives origin to a singlet in the lipidic methyl resonance, while the second would provide a doublet. The remaining contributions, due to unenriched lipogenic substrates, could be derived from the subtraction of the contribution of these two main substrates from the total DNL derived from the ^{2}H NMR analysis.

Chapter 3
Hypothesis and Aim of the Work

As described in the previous chapters, the development of specific metabolic remodeling in cancer cells is firmly established. However, due to the organ-specific nature of cancer and composite tumor microenvironment, the metabolic phenotype of tumor cells should be regarded as heterogeneous. The link between metabolic profile and tumorigenesis can only be rationally elucidated by the accurate determination of metabolic fluxes, namely the ones that are involved in the oxidative metabolism. To gain insight into this problematic and elucidate a comprehensive picture of cancer metabolism, a strong approach has to be developed to quantify metabolic fluxes and interpret them at the carbon level.

In this proposal, we aim to determine and modify metabolic fluxes involved in core catabolic and biosynthetic pathways, namely glycolysis, TCA cycle activity and *de novo* synthesis of fatty acids. We will quantitatively characterize individual metabolic fluxes of two non-small cell human lung carcinoma lines that show metabolic features required for proliferation, A549 and H1299 cell lines and a non-cancerous human lung fibroblast cell line, MRC-5.

The first strategy adopted, explored in the Chapter 5 will involve the quantitative determination of glycolytic, TCA cycle fluxes and anaplerotic reactions by isotopomer analysis. ^{13}C labeled glucose will be provided to the cell cultures and the incorporation of isotopes will be measured by NMR in metabolic intermediates considered relevant for

the metabolic pathways under analysis. For DNL evaluation, culture media reconstituted with 20% of $^{2}H_2O$ will be supplied to the cells in order to obtain fatty acid ^{2}H enrichment. The labeling pattern of each metabolite, obtained at isotopic steady-state, will be fitted and quantified to accurately estimate and interpret metabolic fluxes. This strategy will allow evaluating the level of mitochondrial and lipogenic activity of the cell lines through isotopomer analysis.

In Chapter 6, gene silencing studies will be performed to understand this switch in tumor cells. Elucidation of the IDH activity mechanism for the lipogenic pathway and assess its importance in the metabolism of aerobic glycolytic tumor cells via small interfering RNA (siRNA) silencing of IDH1 and IDH2. The effects of the perturbed metabolism on the overall network will be assessed by isotopomer analysis. Also, characterization of cellular bioenergetics parameters and other metabolic related enzymes will be correlated with data from isotopomer analysis.

The Chapter 7 will focus on the functional plasticity of carbon metabolism in aerobic glycolytic tumor cells at the level of mitochondrial function: given the conventional understanding of the Warburg effect, a provocative approach will be attempted to decipher the connection between metabolic fluxes and cell proliferation in tumor cells. This will be approached by using glycolysis and TCA cycle key-enzyme inhibitors and glucose/glutamine-deprived media and its influence on the cell proliferation.

Part II
Experimental Results

Chapter 4
Materials and Methods

4.1 Reagents

All reagents employed, unless otherwise expressed, were always of the highest purity grade available, analytical grade or superior. Aqueous solutions were prepared in ultrapure water (MilliQ Biocel A10 with pre-treatment via Elix 5, Millipore). Other common solvents utilized were dimethyl sulfoxide (DMSO), methanol, ethanol and chloroform (Sigma-Aldrich).

4.2 Cell culture

Three cell lines were acquired for the study, two human non-small lung cancer cell lines A549 and H1299 and a human lung fibroblast cell line, MRC-5 (ATCC, Barcelona, Spain).

Cells were grown in Roswell Park Memorial Institute (RPMI-1640) culture media (R6504, Sigma-Aldrich) supplemented with 10% fetal bovine serum (FBS)(10270, Gibco, Invitrogen), 1.5 g/L sodium bicarbonate (S5761, Sigma-Aldrich) and 1% antibiotic/antimycotic penicillin/streptomycin (A5955, Sigma-Aldrich), in a humidified atmosphere with 5% CO_2 at 37ºC (NU-4750E CO_2 incubator, Nuaire). Culture media was

reconstituted, pH was adjusted to 7.3, filtered with 0.22 μm sterilized filtration units and stored at 4ºC.

Standard protocol procedures were applied for cell manipulation. Cells were manipulated under a sterile environment in a Class II, Type A1 Biological Safety Cabinet (NU-425-400E Flow chamber, Nuaire) with sterile glass pipettes and cell culture tested disposable containers, mainly 10 mm petri dishes (83.1802, Sarstedt). For subculture, cells were washed with phosphate buffer saline (PBS; 137 mM NaCl; 2.7 mM KCl; 1.4 mM KH_2PO_4; 10 mM Na_2HPO_4), treated with Trypsin-EDTA 0.05% (25300 Gibco, Invitrogen) for 3 min at 37ºC and centrifuged at low relative centrifugal force (RCF) for 3 min (Rotofix 32A centrifuge, Hettich). Subculture ratios were usually 1:2 (but never exceeding 1:4) for the MRC-5 cell line and 1:5 (never exceeding 1:10) for cancer cells. Cell passages were kept low for all cell lines, with a maximum of 15 passages for MRC-5 and 25 passages for cancerous cell lines. Cell counting was assessed with trypan blue (T8554, Sigma-Aldrich) assay. Manual counting was performed with a hemocytometer under an inverted microscope while automated counting was performed with a TC-20 Automated Cell Counter (BioRad). Cells with low viability were discarded. All cultures were tested for *mycoplasma*, with negative results.

4.2.1 Specific media formulations

Substrate preference

For cell proliferation studies (see Section 4.6) to assess substrate preferences, different media formulations were reconstituted. Besides the regular RPMI medium, five variations of RPMI were reconstituted. All media were purchased from Sigma-Aldrich and supplemented with 10% FBS, 1% antibiotic/antimycotic and 1.5 g/L sodium bicarbonate.

The media without glucose (-Glc +Gln) was reconstituted from RPMI R1383 (with L-glutamine, without glucose and sodium bicarbonate). The media with galactose (-Glc +Gal +Gln) was reconstituted from the same RPMI R1383 but supplemented with 10 mM galactose (G0750, Sigma-Aldrich). Media without glutamine (+Glc -Gln) was purchased

already prepared and sterile-filtered, RPMI R7509 (with sodium bicarbonate, without L-glutamine and phenol red). For glutamine substitution experiments, replacement substrates were added at the same concentration of the removed glutamine (1.85 mM). Therefore, media without glutamine (+Glc -Gln) were supplemented with 1.85 mM asparagine or 1.85 mM ammonium chloride (A0884, A9434, Sigma-Aldrich).

^{2}H and ^{13}C labelled media

For NMR experiments three different media formulation were used. For carbon labelling experiments on Chapter 5, RPMI R1383 (with L-glutamine, without glucose and sodium bicarbonate) media was reconstituted with 10 mM 99% [U-^{13}C]glucose (CLM-1396; Euriso-top). For ^{2}H NMR experiments, regular RPMI media (R6504) was reconstituted with 20% $^{2}H_2O$ (A2521, Euriso-top).

The transfection experiments performed on Chapter 6 used R1383 media (with L-glutamine, without glucose and sodium bicarbonate), reconstituted with 10 mM 99% [1,6-$^{13}C_2$]glucose (453196, Sigma-Aldrich) and 20% $^{2}H_2O$.

4.3 Cell extraction

Depending on the experiment and purposes, extraction protocols were adjusted. The three main procedures applied in this work are described below. Whenever possible, all procedures hereby described were performed on ice.

4.3.1 Western blot extractions

For Western blotting experiments, extraction focused on intact and solubilized protein content. Cells were washed twice with ice-cold PBS and scraped (831830, Sarstedt) in 1.5 mL PBS. Cells were transferred to identified microtubes, centrifuged for 3 min, at 4ºC, 3000 rpm (5415R centrifuge, Eppendorf) and the supernatant was discarded. To the cellular pellet was added RIPA buffer (150 mM NaCl, 1% IGEPAL (CA-630), 1% sodium deoxycholate (DOC), 0.1% sodium dodecyl sulfate (SDS), 25 mM Tris-

HCl, pH 7.6), supplemented with 2 mM dithiothreitol (DTT), 100 mM phenylmethylsulfonyl fluoride, protease inhibitor cocktail (P8340, Sigma-Aldrich) and phosphatase inhibitor cocktail (P5726, Sigma-Aldrich) at 10μL/mL. Cells were resuspended, kept 30 min in ice, vortex mixed and a final ultra-sound sonication was applied with three 5 s pulses at 40 kHz. Extracts were stored at -80ºC until analysis.

4.3.2 Aqueous and organic phase extractions for NMR

For NMR experiments a specific protocol was optimized for cell culture. These extractions would require a fast lysis method to avoid stress and metabolic alterations during extraction. For the acquisition of good signal-to-noise ratio in NMR spectra, extract losses should be kept to a minimum and a good solubilization of aqueous and organic metabolites must be achieved. Additionally, the salt content in the extracts should be low, to avoid resonance broadening. An adaptation from described protocols was performed, allowing consecutive aqueous and organic extractions (Dettmer et al. 2011).

Aqueous extraction

For NMR experiments cells were grown in Petri dishes and after 48h incubation with tracers, at near confluency, cells were extracted. Cells were washed twice with ice-cold PBS and 1mL of ice-cold solution of methanol/water 80:20 (containing NaN_3) was directly added. This solution was spread manually throughout the petri dish to swiftly lyse cells. Cells were scraped and collected into 2 mL microtubes. Another 750 μL were added to the Petri dish to properly remove remnant cells and collected to the microtube. Extracts were centrifuged 5 min at 4ºC, 5000 ×g. The supernatant (aqueous phase) was transferred to another microtube, lyophilized and stored until NMR experiments. The pellet can undergo an organic phase extraction (see below), if necessary, and its protein content quantified for normalization purposes (see Section 4.4).

Organic extraction

To the pellet from the previous extraction, 1 mL of a chloroform/methanol/water 1:1:0.1 (containing NaN_3) solution was added. The solution was kept 1 h on ice, with 3 or 4 vortex mixes. Extract was centrifuged at 5 min at 4ºC, 5000 ×g and supernatant (organic phase) transferred to another microtube. After lyophilization, extracts were stored until NMR experiments acquisition. The denatured protein pellet was kept for protein quantitation and normalization purposes.

4.3.3 Adenine nucleotide extraction

Adenine nucleotide measurements were performed by High Performance Liquid Chromatography (HPLC) techniques. Due to the sensitive nature of adenine nucleotides homeostasis under stress, it is crucial to perform all protocol steps in ice.

First, cells were washed twice with ice-cold PBS and placed over ice. To the cells was directly added 1 mL of a 0.6 M perchloric acid ($HClO_4$) on a 5 mM EDTA solution. Cells were scraped and transferred to a 2 mL microtube. More 750 μL were added to the Petri dish to properly remove the remnant cells and collected into the same microtube. The extract was centrifuged 5 min, at 4ºC, 14000 ×g and the supernatant transferred to another microtube. The pellet was neutralized with 50 μL of a 1 M NaOH solution and stored at -80ºC for protein quantification. The supernatant was neutralized at pH≈7.5 with a 1.5 M Tris buffer, 3 M KOH solution. The neutralization forms a precipitate ($KClO_4$) that has to be discarded after centrifugation (5 min, at 4ºC, 14000 ×g). The supernatant is stored at -80ºC until HPLC experiments.

4.4 Protein quantification

All protein quantifications were performed with a bicinchoninic acid assay kit (BCA-1, Sigma-Aldrich), according to instructions. This spectrophotometric assay is based on the reduction of Cu^{2+} to Cu^{1+} by peptide bonds in an alkaline medium. Two bicinchoninic acid molecules form a purple complex with Cu^{1+}, with absorbance at 562

nm, in a temperature dependent reaction (Smith et al. 1985). This reaction is directly proportional to the amount of protein content and is compatible with several detergent concentrations present in RIPA buffer.

The assays were prepared on clear flat bottom 96 multiwell microplates, with 10 μL of sample and 90 μL of bicinchoninic acid reagent, and incubated at 60ºC for 1 h. A standard curve with bovine serum albumin (BSA) ranging from 0 to 2 mg/mL was calculated for all experiments. Both standards and samples were run in duplicate. Measurements were performed at 25ºC using a VictorX3 Multilabel Plate Reader (PerkinElmer), at 560 nm.

For protein quantitation of Western blot samples, cell extracts were thawed and a dilution was performed with water, usually ranging from 1:10 to 1:20 to fit the values on the standard curve. A diluted RIPA buffer was used for baseline correction.

Extraction procedures for preparation of both NMR and adenine nucleotide extracts denature protein in an insoluble pellet, that is difficult to solubilize with RIPA buffer alone. Prior to quantitation, a protocol for solubilization of protein content was required. A near saturated solution of 8 M urea was prepared. To each protein pellet were added 100 μL of this urea buffer and left at room temperature overnight to completely solubilize protein. The microtubes were kept closed to avoid evaporation and crystal formation. The samples were sonicated to destroy any remaining protein aggregates. The final solution should be translucid and homogeneous. To avoid salinity problems caused by urea on bicinchoninic acid quantitation performance (tolerates up to 3 M urea), samples were diluted with 200 μL of RIPA buffer.

4.5 Western blotting

4.5.1 General protocol

For Western blotting experiments, cells were extracted as previously described (see Section 4.3). After quantitation, all samples were diluted to a concentration of

3.125 μg/μL. Samples were denatured (usually in the day of each experiment) by adding a 5x Laemmli buffer (final concentration of 32 mM Tris-HCl, pH 6.8, 10% glycerol, 1% β-mercaptoethanol 2% SDS, 0.01, 0.005% bromophenol blue) and boiled for 5 min at 95ºC in a dry bath. The final protein concentration was 2.5 μg/μL and 25 μg of total protein extract were loaded in SDS-polyacrylamide electrophoresis gels (SDS-PAGE).

The acrylamide concentration of resolving gel was usually between 9% and 12% (depending on the size of the studied protein), mounted on 1.5 mm spaced glasses. Electrophoresis was performed with running buffer (190 mM glycine, 25 mM Tris-base, 3.5 mM SDS, pH=8.3) at room temperature, with 100 V during 2 h. Proteins were electrophoretically transferred from the gel to polyvinylidene difluoride membranes. Transfer was performed in transfer buffer (190 mM glycine, 25 mM Tris-base, 20% methanol) at 4ºC, 100 V during 90 min (all electrophoresis equipment was from BioRad; reagents were from BioRad or NZYtech) (Gallagher 2012).

Membranes were properly identified and blocked with 5% non-fat milk in Tris buffered saline with Tween-20 (TBS-T)(137 mM NaCl, 0.27 mM KCl, 25 mM Tris, 0.1% Tween-20) during at least 2 h, at room temperature, under agitation in a roller mixer. Membranes were washed 3 times during 5 min to remove the blocking solution. Primary antibodies were incubated overnight at 4ºC or 3 h at room temperature, always under constant mixing. Membranes were washed 3 times during 5 min with TBS-T and incubated with the respective secondary antibodies 1 h at room temperature. Membranes were washed again 3 times during 5 min with TBS-T. Under low luminance conditions, membranes were incubated with 150 μL ECF substrate (45-000-947, GE Healthcare) during a maximum of 5 min, excess was removed gently with filter paper. Detection and quantification was performed using a Biospectrum 500 Imaging System equipped with a VisionWorksLS Image Acquisition and Analysis Software (UVP). ECF reaction was stopped with methanol and membranes were bathed in Ponceau S dye (0.1% in 5% acetic acid solution) for 5 min. Excess was removed in water and Ponceau S staining was quantified for normalization purposes (Gallagher et al. 2008).

4.5.2 Antibodies

Antibodies were employed according to manufacturer's instructions and incubated with the respective secondary antibody, usually at a dilution of 1:5000. The Table 4.1 exhibits all primary antibodies and their respective dilution.

Table 4.1 - List of primary antibodies used throughout this work with the respective reference, dilution and molecular weight of target protein (kDa). Oxphos and Integrity are two cocktails of antibodies.

Primary Antibodies	Company / Code	Dilution	Molecular weight
HKI	Cell Signaling 2024	1:1000	102 kDa
HKII	Cell Signaling 2867	1:1000	102 kDa
GAPDH	Cell Signaling 5174	1:1000	37 kDa
PKM1/2	Cell Signaling 3190	1:1000	60 kDa
PKM2	Cell Signaling 4053	1:1000	60 kDa
LDHA	Cell Signaling 3582	1:500	37 kDa
PDH	Cell Signaling 3205	1:1000	43 kDa
PDK	Cell Signaling 3820	1:750	47 kDa
SOD1	Abcam ab13533	1:750	25 kDa
SOD2	Abcam ab13533	1:750	25 kDa
Oxphos	MitoScience MS604		
CI			20kDa
CII			30kDa
CIII		1:1000	47kDa
CIV			39kDa
CV			53kDa
Integrity	MitoScience MS620		
CV			55kDa
CIII			49kDa
Porin I/2		1:1000	29kDa
CypD			21kDa
Cyt C			12kDa

4.6 Cell proliferation assay

4.6.1 General protocol

Cell proliferation assays were performed with the sulforhodamine B (SRB) colorimetric assay (Vichai et al. 2006). SRB is a bright pink dye that stoichiometrically binds deprotonated aminoacid residues under mild acidic conditions and dissociates under basic conditions. By binding on basic residues of fixed cells, SRB cannot distinguish between viable and dead cells, but the amount of staining is proportional to the cell mass. Absorbance may be measured at 490-530 nm or fluorometrically at 488 nm (excitation) and 585 nm (emission).

Cells were seeded 12h before experiment at 5×10^4 cell/well, in 48 multiwell microplates with a working volume of 500 μL. Cells were seeded with a repetition pipette with disposable tips (Electronic HandyStep, Brand) for a faster and precise seeding. This was performed in regular RPMI medium to allow the cells to adhere. After a 12h period, the medium was removed, cells were washed with PBS, new medium was added and treatments were performed.

At selected time-points (0h, 8h, 24h and 24h intervals up to 168h, depending on the experiment) media was removed from the corresponding well and cells were washed with PBS. The microplate was placed back into the incubator and the process was repeated until the final time-point was collected and allowed to dry. Cells were fixed for at least 1h in a 1% acetic acid solution in methanol at -20ºC. Fixation solution was discarded and microplates were allowed to dry in a oven at 37ºC. Fixed cells were incubated with 0.057% (w/v) SRB dissolved in 1% of acetic acid for 1h at 37ºC. The unbound dye was carefully removed with 1% acetic acid solution and microplates were dried in an oven at 37ºC. Staining was solubilized with the addition of 10 mM Tris solution, pH=10, under orbital shaking until complete dissociation (≈15 min). The optical density of the solution was determined at 530 nm on a microplate reader (VictorX3, PerkinElmer) at 25ºC.

4.6.2 Metabolic inhibitors

The impacts of several metabolic inhibitors on cell proliferation were tested with three different concentrations (Chapter 7). These inhibitors were dissolved in an appropriate solvent and 10 μL were added to each well, to a final volume of 510 μL. To the control condition, 10 μL of solvent was added. The employed inhibitors and respective solvents are described in the Table 4.2.

Table 4.2 - Compounds tested in cell proliferation assays. This table shows the inhibitor name, common abbreviation, purchase reference, purity grade, target enzyme and solvent employed. PBS was used to buffer acidic inhibitor solutions. DMK and DMA are analogues of α-ketoglutarate and aspartate, respectively.

Compound	Abbr.	Sigma Ref.	Purity	Target	Solvent
Bromopyruvic acid	3-BrPA	16490	97%	HK	Water
Iodoacetatic acid	IA	I2512	98%	GAPDH	Water
Oxamate	-	O2751	98%	LDH	Water
Dichloroacetic acid	DCA	347795	98%	PDK	Water
Epigallocatechin gallate	EGCG	E4268	80%	GLDH	Water
O-(Carboxymethyl)hydroxylamine hemihydrochloride	AOA	C13408	98%	ALT/AST	Water
Dehydroepiandrosterone	DHEA	D4000	99%	G6PDH	Methanol
Dimethyl α-ketoglutarate	DMK	349631	96%	-	Water
L-Aspartic acid dimethyl ester hydrochloride	DMA	456233	97%	-	Water

4.7 Adenine nucleotide quantification

Quantification of intracellular adenine nucleotide content was performed by High Performance Liquid Chromatography (HPLC). Cells were extracted with a perchloric acid extraction procedure (see Section 4.3).

Extracts were thawed at room temperature prior to injection. With a microsyringe (Hamilton), 25 μL were injected into the loop. The device was a Beckman System Gold (Beckman Coulter) composed by a programmable UV detector (Module 166) and a programmable solvent binary pump (Module 126). The HPLC column was a LiChroCART 125-4, LiChrospher 100RP-18, 5 μm (MercK). Samples were eluted with a

100 mM phosphate buffer in 1.2% methanol, pH=6.5, at a flow rate of 1.1 mL/min and detected at 254 nm. Adenosine triphosphate (ATP), adenine diphosphate (ADP) and adenine monophosphate (AMP) were quantified and normalized for protein content. Energy charge was calculated according the following equation (Atkinson et al. 1979):

$$Energy\ Charge = \frac{[\mathrm{ATP}] + \frac{1}{2}[\mathrm{ADP}]}{[\mathrm{ATP}] + [\mathrm{ADP}] + [\mathrm{AMP}]}$$

4.8 Vital epifluorescence microscopy

For fluorescence microscopy experiments, cells were seeded at a density of 1×10^5 cells/well in 6-well plates with a glass coverslip at the bottom of each well. Cells were allowed to attach for 24h in RPMI medium without phenol-red. Thirty minutes before microscopic analysis, cells were incubated (in dark conditions) with the fluorescent probes. A PBS solution with a mixture of tetramethylrhodamine methyl ester (TMRM), Mitotracker Green and Hoescht 33342 (all from Invitrogen) were added, to a final concentration of 100 nM, 20 nM and 5 μg/mL, respectively. Hoescht dyes the nuclei, Mitotracker Green all mitochondria and TMRM the polarized mitochondria.

The glass coverslips containing the cells were transferred to custom-made microscope slides with a round spacer, which allowed keeping the cells in contact with ≈200 μL of culture media. Cells were observed in a Nikon Eclipse TE2000U epifluorescence microscope equipped with a monochromatic camera and 4 channels, bright field, blue, green and red. Camera and image processing were operated with NIS-Elements software. At least 3 different fields of view were captured for each slide, with a 60x magnification. As a negative control for TMRM fluorescence, a shot of FCCP was given to the cells to promote mitochondrial depolarization. For quantification of fluorescence overlap, ImageJ 1.46 with Mitophagy macro was used (Zhu et al. 2011).

4.9 Oxygen consumption

Whilst most of the assayed mitochondrial performance parameters are relative to isolated mitochondria, a growing number of studies use permeabilized or intact cells. Oxygen consumption experiments were performed in a classical Clark-type electrode (YSI 5331, Yellow Springs Instruments). The oxygen probe is composed by a cathode (platinum) and an anode (silver), which are physically separated from the media with a O_2 permeable Teflon membrane (YSI 5775, Yellow Springs Instruments). O_2 is reduced to H_2O by the electrode, generating an electric potential which is converted by an oxygen control system (YSI 5300) and plotted in a BD12 dual channel flatbed recorder (Kipp & Zonen). This current will be proportional to the O_2 concentration in the media. The electrode was calibrated with 37ºC air-saturated water, O_2 scale set to 150% at 1 V with a register speed of 10mm/min. All experiments were conducted on a 37ºC thermostatic, 1 mL water-jacketed glass chamber connected to an immersion thermostat pump, under constant magnetic stirring.

Cells were trypsinized, counted and 5×10^6 cells were resuspended in 200 μL of RPMI medium. Electrode signal was stabilized with aerated 800 μL RMPI and the cell suspension was transferred to the chamber. Chamber was closed and basal consumption rate was measured. Measurements took 2-3 min each, enough to draw a tangent line. Cells were treated consecutively with oligomycin (2 μg/mL), carbonyl cyanide 4-(trifluoromethoxy)phenylhydrazone (FCCP; 10 μM) and potassium cyanide (KCN; 1 mM). Injections of inhibitors were performed with a microsyringe. Calculated concentration of water-dissolved O_2, at 37ºC and 1013.25 hPa was 210.48 μmol/L and consumption rates were measures in rates of nmol O/min/1×10^6 cells.

Mitochondrial function was assessed according using previously defined parameters (Brand et al. 2011). Cell respiration without any inhibitor is considered the basal consumption rate. By inhibiting ATP synthase (complex V) with oligomycin, respiration rate diminishes, reflecting the ATP turnover ($ATP\ turnover = basal - oligomycin$). The ratio between oligomycin treated and basal rates represent the coupling efficiency, in other words, how much of the basal O_2 consumption is dedicated

to ATP synthesis ($coupling\ efficiency = oligomycin/basal$). The addition of an ionophore such as FCCP will dissipate the mitochondrial chemiosmotic gradient and uncouples the ETC function from ATP production, thereby boosting O_2 consumption to a peak. KCN is an inhibitor of cytochrome C oxidase (complex IV) and at 1 mM is enough to inhibit virtually all mitochondrial O_2 consumption. The difference between cyanide inhibition and FCCP stimulation is defined as maximal respiratory capacity ($maximal\ respiratory\ capacity = FCCP - KCN$) and the difference between FCCP peak and basal respiration rates is the spare respiratory capacity ($spare\ respiratory\ capacity = FCCP - basal$). This spare respiratory capacity reflects how close mitochondrial metabolism is to its bioenergetic limit. Finally, the difference between oligomycin treatment and full inhibition by KCN reveals the proton leak (oligomycin-insensitive respiration), which may indicate damaged mitochondria if increased ($proton\ leak = oligomycin - KCN$).

4.10 Silencing experiments

For transient silencing experiments, small interfering RNAs (siRNAs) with a lipid-based transfection reagent were employed. A non-targeting siRNA (D-001810-01), a pool of 4 siRNAs targeting IDH1 (MU-008294-00) and a pool of 4 siRNAs targeting IDH2 (MU-004013-00) were purchased from Dharmacon (GE Healthcare). siRNAs were prepared according to instructions with RNAse free water (B-003000-WB, Invitrogen) and siRNA buffer (B-002000-UB, Invitrogen). All cell culture material used in siRNA manipulation was DNAse/RNAse free.

Concentrations of siRNAs and transfection reagent (T-2002-03, Dharmacon) were tested and optimized. Cells were seeded at 1×10^6 in 60 mm Petri dishes and allowed to adhere for 24h. At a confluency of ≈80%, media was changed for OPTI-MEM reduced serum medium (11058-021, Invitrogen) and cells were incubated with the siRNA-transfection reagent complex for 24h. After 24h media was removed and labelled RPMI medium was added. After 48h cells were extracted (see Section 4.3)

4.11 NMR experiments

Through the use of nuclear magnetic resonance (NMR) techniques, a comprehensive analysis of cell metabolism can be achieved by measuring intermediary or end products of certain metabolic pathways. In this work three main NMR experiments were performed: one-dimensional ^{1}H, ^{2}H and ^{13}C NMR spectra. For that purpose, cells were grown in different media formulation containing NMR sensitive labelled substrates (see Section 4.2). Media aliquots and cell extracts were collected (see Section 4.3) for NMR analysis.

To analyze the extracellular kinetics of substrate consumption and metabolite buildup, aliquots of 200 μL of media were collected at different time points and frozen until analysis. Prior to NMR spectra acquisition, samples were thawed and to 160 μL of sample were added 40 μL of phosphate buffer (200 mM in 99.9% $^{2}H_2O$, pD=7.0), containing 10 mM fumarate that was used as standard (F8509, Sigma-Aldrich). The solution was loaded into 3 mm NMR grade tubes (Norell) and experiments were run on a VNMRS 600 MHz (Agilent) spectrometer equipped with a high-field switchable PFG indirect detection 1H-{X} 3 mm probe. Typical ^{1}H spectra acquisition parameters included a 3s acquisition time, defining a 7200 Hz spectral width, a 30º radiofrequency observe pulse and an interpulse delay of 10s (delay=4.5s, water saturation=2.5s, acquisition time=3s), to allow full relaxation. To achieve adequate signal to noise a total of 64 scans were averaged.

The aqueous extracts were lyophilized (see section 4.3) and prior to analysis were dissolved in 160 μL $^{2}H_2O$ plus 40 μL of phosphate buffer (200 mM in 99.9% $^{2}H_2O$, pD=7.0), containing 10 mM fumarate that was used as standard. ^{1}H and ^{13}C NMR spectra were run on a VNMRS 600 MHz (Agilent) spectrometer equipped with a high-field switchable PFG broadband X-{1H} 3 mm probe. Typical ^{1}H spectra acquisition parameters included a 3s acquisition time, defining a 7200 Hz spectral width, a 30º radiofrequency observe pulse and an interpulse delay of 10 s (delay=4.5s, water saturation=2.5s, acquisition time=3s), to allow full relaxation. To achieve adequate signal to noise a total of 128 scans were averaged. For proton-decoupled ^{13}C NMR spectra,

typical acquisition parameters included an acquisition time of 2.5s, defining a 35 KHz spectral width, a 45º radiofrequency observe pulse and between 9000 and 25000 scans to ensure adequate signal to noise ratios for isotopomer analysis.

The organic extracts were also lyophilized and prior to analysis samples were dissolved in 525 μL chloroform, 25 μL of a 99.03% ^{1}H/0.97% ^{2}H pyrazine solution, used as internal standard (P56003, 340456, Sigma-Aldrich) and 50 μL of hexafluorobenzene (H8706, Sigma-Aldrich), used for fluorine lock. Samples were loaded into 5 mm NMR grade tubes (Norell) and experiments performed on a 500 MHz Avance III HD (Bruker) spectrometer equipped with a gradient SE-X 2H-{1H} 5 mm probe. Typical ^{1}H spectra acquisition parameters included a 3s acquisition time, defining a 6000 Hz spectral width, a 30º radiofrequency observe pulse and an interpulse delay of 4s (delay=1s, acquisition time=3s), to allow full relaxation. To achieve adequate signal to noise a total of 128 scans were averaged. For proton-decoupled ^{2}H NMR spectra, typical acquisition parameters included an acquisition time of 3s, defining a 920 Hz spectral width, a 90º radiofrequency observe pulse and between 9000 and 25000 scans to ensure adequate signal to noise ratios for deuterium enrichment analysis.

All spectra were processed with NUTSPro™ (Acorn), with baseline correction. Before Fourier transform, the free induction decays (FID) were multiplied by a 0.2-0.5 Hz lorentzian (^{1}H NMR spectra) or a 1.0 Hz lorentzian (^{13}C/^{2}H spectra). For quantification, a polynomial fit baseline correction was applied and a line fitting command was executed with multiple iterations and individual line optimizations, until a good fit was achieved. Fumarate (singlet at 6.5 ppm) or pyrazine (singlet at 8.6 ppm) were used as standards for quantification purposes.

4.11.1 Metabolic profiling by ^{1}H

^{1}H NMR spectra provide information about several metabolites detectable (present in extracellular medium or cell extracts) in one single spectrum. During a pathologic development, dysfunctional processes cause an intracellular homeostatic imbalance relatively to a healthy condition. This imbalance may generate a downstream

deregulation of metabolic pathways, which can be detected and characterized by metabolic profiling.

This analysis is referred as Metabonomics, where different metabolic profiles are correlated with specific metabolic conditions, arising from pathological or non-pathological insults (Villaseñor et al. 2014; Martin et al. 2010). Large metabolic-related datasets (such as NMR or MS) can be interpreted by comparing the overall metabolic profile between conditions. For that purpose, multivariate analysis is employed to reveal the most significant variables (such as principal component analysis, PCA) and predictive mathematical models can be generated.

In this work, multivariate analysis was employed on ^{1}H NMR data for metabolic profile comparison between cell lines (see section 4.12). Moreover, culture media glucose consumption and lactate secretion were analyzed at different time points by ^{1}H NMR spectra. These fast and simple procedures allow a broad characterization of cell metabolism.

4.11.2 Isotopomer Analysis

For more detailed information about carbon intermediary metabolism, cells were incubated with ^{13}C labelled substrates. ^{13}C is a non-ionizing stable isotope tracer with a natural abundance of ~1.1%, which allows a non-invasive measurement of intracellular metabolism. Although the sensitivity of NMR techniques is much lower comparatively to MS techniques, NMR allows the quantification of fractional enrichments as well as positional isotopic labelling due to magnetic spin-spin interaction between adjacent labelled molecules. The ^{13}C labelling position inside a given molecule will generate isotope isomers, hence isotopomers (Malloy et al. 1990; Jeffrey et al. 1991; London 1988).

Combined ^{1}H and ^{13}C NMR experiments provide a significant amount of information about intermediary metabolism, and two main metabolites were chosen to perform the isotopomer analysis: lactate and glutamate. As discussed in the General Introduction (see Chapter 2), by providing ^{13}C labelled glucose, lactate and glutamate

may appear with multiple ^{13}C carbon labelling. Multiple labelled species will exhibit spin-spin coupling (homonuclear or heteronuclear, Table 4.3), which has been thoroughly described (Carvalho et al. 1999; Lloyd et al. 2004).

The couplings give rise to multiplets and allow distinguishing single and multiple labelled molecules in ^{13}C spectra. With this approach, quantitative measurements of metabolic fluxes can be assessed (Malloy et al. 1990; Jeffrey et al. 1991; Carvalho et al. 2001).

Table 4.3 – Coupling constants for glutamate and lactate.

	Glutamate		Lactate	
	Coupling (Hz)		Coupling (Hz)	
One bond	$^{1}J_{C1-C2}$	53.3	$^{1}J_{C1-C2}$	55.0
	$^{1}J_{C2-C3}$	34.8	$^{1}J_{C2-C3}$	37.0
	$^{1}J_{C3-C4}$	34.5	$^{1}J_{H-C2}$	146
	$^{1}J_{C4-C5}$	51.3	$^{1}J_{H-C3}$	128
Multiple bond	$^{2}J_{C1-C3}$	~1	$^{2}J_{C1-C3}$	~2
	$^{2}J_{C3-C5}$	~1	$^{2}J_{H-C1}$	3.5
	$^{2}J_{C2-C4}$	~1	$^{2}J_{H-C2}$	4.2
	$^{3}J_{C1-C4}$	2.3	$^{2}J_{H-C3}$	3.5
	$^{3}J_{C2-C5}$	3.3	$^{3}J_{H-H}$	7.0
			$^{3}J_{H-C1}$	4.2

Cells consuming [1,6-$^{13}C_2$]glucose will generate [3-^{13}C]pyruvate, which can either generate [3-^{13}C]lactate via LDH or [4-^{13}C]glutamate through TCA cycle. Although pyruvate cycling and TCA cycle turnover fluxes may generate more metabolite isotopomers, the previously mentioned enrichments are proportional to the flux in each pathway. Glycolysis-derived lactate is always labelled at C3 while all glycolysis-derived AcCoA will always label glutamate C4. Therefore, the ratio $TCA\ coupling = \frac{glutamate\ C4}{lactate\ C3}$ allows establishing the coupling between glycolysis and TCA cycle, which is increased with the higher oxidation of pyruvate by the TCA cycle or decreased by the reduction of pyruvate into lactate prompted by LDH. The same rationale can be applied to [U-^{13}C]glucose.

The second parameter that may be assessed is the TCA cycle turnover. Considering labelling with [U-^{13}C]glucose, on the first turn of TCA cycle, [4,5-$^{13}C_2$]glutamate is generated. However, with the consecutive turns in TCA cycle, this will originate multiple labelled species in the C4 of glutamate. Given the different couplings constants between glutamate carbons 4 and 5 ($^1J_{C4C5}$) and glutamate carbons 4 and 3 ($^1J_{C3C4}$), Table 4.3, the [4,5-$^{13}C_2$]glutamate isotopomer appears as a doublet (C4D45) while the [3,4,5-$^{13}C_3$]glutamate appears as a doublet of doublets (or pseudoquartet, C4Q). Considering that all labelling entering TCA cycle labels glutamate C4 and glutamate C3 labelling is only generated by posterior turnover, at a steady state, $Turnover = \frac{glutamate\ C4Q}{glutamate\ C4D45}$. A decreased ratio reflects a low turnover of the TCA cycle. When employing [1,6-$^{13}C_2$]glucose, the underlying principle is the same but since [4-^{13}C]glutamate generates a singlet (C4S) and [3,4-$^{13}C_2$]glutamate generates a doublet (C4D34), the equation should be $Turnover = \frac{glutamate\ C4D34}{glutamate\ C4S}$.

A third parameter is anaplerosis. Anaplerosis reflects the replenishment of TCA cycle intermediates. Considering the previous analysis for TCA cycle isotopomers, if all glutamate molecules labelled at C4 undergo consecutive turns in the TCA cycle, at a steady state, all glutamate molecules will eventually be labelled at both C3 and C4. However, anaplerotic fluxes will hinder (or improve) this ratio at the glutamate C3 labelling. If pyruvate cycling (see Chapter 2) is highly active, pyruvate may enter TCA cycle through pyruvate carboxylase (PC) in the form of labelled oxaloacetate. This anaplerotic labelled substrates may heighten glutamate C3 labelling. On the other hand, the inflow of unlabelled substrates in the TCA cycle, such as glutamine (from the culture media) will dilute the labelling at glutamate C3. Therefore, $Anaplerosis = 1 - \frac{glutamate\ C3}{glutamate\ C4}$, where a value close to zero indicates low anaplerotic levels.

A final indirect parameter is the redox status and can be calculated from either ^{1}H or ^{13}C spectra. Lactic fermentation produces lactate with the oxidation of a NADH molecule in order to regenerate NAD^+ to supply glycolysis. Imbalances in NADH levels may redirect pyruvate for alanine production by ALT. Considering the levels of labelled alanine as a reflection of intracellular labelled pyruvate concentrations, the ratio

$Redox = \frac{lactate}{alanine}$ is an indirect measurement of cytosolic redox (Nunes et al. 2011). Increased lactate levels reflect an increase in NADH/NAD^+ ratio, therefore reduced cytosolic conditions.

4.11.3 Deuterium experiments

Whilst ^{13}C labelling provides information about metabolism at the glycolysis and TCA cycle, ^{2}H labelling may provide information about DNL. By providing $^{2}H_2O$ in the cell culture media, many reactions involving H_2O may incorporate ^{2}H molecules by exchange with ^{1}H. ACLY, the enzyme responsible for the synthesis of cytosolic AcCoA pools, convert mitochondrial citrate into oxaloacetate and requires hydrolysis of ATP. This hydrolysis may incorporate a ^{2}H molecule in the C2 of AcCoA (methyl group). Furthermore, several reactions in glycolysis may also incorporate ^{2}H into pyruvate molecules (Silva et al. 2011).

If this ^{2}H labelled AcCoA molecule enters DNL as the initiating molecule for a fatty acid synthesis, that same methyl group (C2) will be the terminal methyl group of the fatty acid (Figure 4.1). Moreover, several other hydrogens may incorporate ^{2}H molecules, in stereospecific reactions. Considering a newly synthesized palmitate molecule, all hydrogen (or deuterium) of odd-numbered carbons are derived from NADPH while even-numbered carbons possess 7 hydrogen (or deuterium) that are derived from malonyl-CoA (and therefore AcCoA) and the other 7 that are directly derived from water (Murphy 2006; Silva et al. 2011). This will also generate an intense ^{2}H labelling at the methylenic signal.

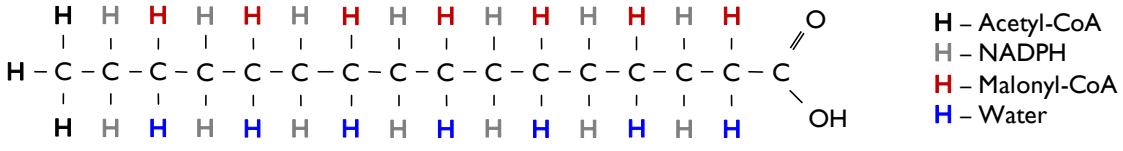

Figure 4.1 - Origin of hydrogen molecules in newly synthesized palmitate molecule. The hydrogen sources are stereospecific. In black are the hydrogens derived the first AcCoA molecules and in red from malonyl-CoA (and therefore AcCoA). In blue are the hydrogen directly derived from water. In grey, all in even-numbered carbons, are the NADPH derived hydrogen. Adapted from Murphy 2006.

Once extracted the lipid fraction and with the use of a double non-deuterated/deuterated standard, pyrazine in our experimental setup, we were able to correlate ^{1}H and ^{2}H NMR spectra. Note that the natural abundance of ^{2}H was accounted in the calculations for the pyrazine standard (0.0156%). Since the methyl group of fatty acids is an isolated peak at around 0.9 ppm, both unlabelled and labelled contributions can be measured. With this elegant approach, a simple ratio: $DNL = \frac{labelled\ methyl\ group}{total\ methyl\ group} \times \frac{100}{enrichment(\%)}$, normalized for the ^{2}H culture media enrichment (20% in this work) reflects the DNL rate during the incubation period.

4.12 Statistical analysis

4.12.1 Statistical software

All data rearrangements and necessary calculations or normalizations were performed in Excel (Microsoft Office, 2007). All statistical analyses were conducted using GraphPad Prism 6.01 (GraphPad Inc.) or Statistical Package for Social Sciences 17.1 (SPSS). Graphics are represented with mean with standard error mean (SEM) bars while written result descriptions are represented with mean and standard deviation (SD).

4.12.2 Normality and homoscedasticity

All data was tested for normality with the Kolmogorov-Smirnov in both GraphPad or SPSS. For homogeneity of variance analysis, F test was used for Student's t-test and Bartlett's test for all other analysis in GraphPad. In SPSS, the homoscedasticity was analyzed with the Levene test.

When dataset exhibited a normal distribution and homogeneity of variance, statistical parametric tests were applied. However, in datasets with a deviation of homoscedasticity, variance would be considered as homogeneous if comparisons were performed between groups with equal sample sizes. Moreover, in ANOVA procedures, normal distribution was not strictly necessary to perform the test, given the skewness

and kurtosis parameters were not excessively altered. Both violations are described and still allow a robust application of parametric tests (Zar 1999). Under any other circumstances, if normality or homoscedasticity tests were negative, the corresponding non-parametric tests were applied. In specific contexts with $n>6$ groups and using SPSS boxplot, outliers tagged as strong outliers were removed.

4.12.3 Statistical tests

For comparison of means between two groups, a Student's t-test was applied, with a Welch correction if the dataset lacked homogeneity of variances. If a normal distribution was absent, the corresponding non-parametric test was applied, the Mann-Whitney test.

On comparisons between three or more groups a one-way ANOVA was applied with a Tukey post-test. The equivalent non-parametric applied was the Kruskall-Wallis with a Dunn's post-test. For comparisons between three or more groups in time (or concentration) dependent experiments, a two-way ANOVA was applied, with Sidak post-test for multiple comparisons or Dunnet post-test for comparison with a control condition.

Multivariate analysis was performed on NMR data. A principal component analysis was applied in Spearman correlation matrix with a Varimax rotation of the matrix. The principal components selected had eigenvalues>1.

All statistical tests were employed for a significance value of α=0.05 (one symbol for $p<0.05$, two symbol for $p<0.01$ and three symbols for $p<0.001$). Throughout this work, the data are usually presented with transformations for ease of comprehension. However, all statistical tests were performed prior to transformation, only normalization or other required calculations were performed (Lew 2007a; Lew 2007b).

4.12.4 Mathematical models

Two models were applied on this work, linear regression and a nonlinear 4 parameter logistic (4PL) regression. Linear regression models were fitted without constraints in GraphPad. The general equation ($y = mx + b$) for each fit are shown with the slope (m), coordinate at the origin (b) and goodness of fit (r^2). For comparing slopes, a one-way ANOVA was performed.

The nonlinear 4PL was calculated with 4 parameters, minimum (min), maximum (max), slope and inflection point as shown by the following equation: $y = \frac{Min-Max}{1+\left(\frac{x}{\text{Inflection}}\right)^{\text{Slope}}} + Max$. These models were fitted without constraints and r^2 and 95% prediction bands were presented.

Chapter 5
Metabolic Characterization of Lung Cancer Cell Lines by Isotopomer Analysis

5.1 Introduction

One of the major remodeling occurring in cancer is the alteration of metabolic fluxes, generally towards aerobic glycolysis and increased anabolic pathways. However, these fluxes are far from being quantitatively analyzed and this Chapter will focus on the metabolic characterization of three human cell lines. The non-cancerous cell line is an embryonic lung fibroblast line (MRC-5 cell line) and the cancerous cell lines are derived from non-small cell lung carcinoma (A549 and H1299 cell lines). These cancer cell lines have been described to have a switch towards aerobic glycolysis through the expression of PKM2 (Christofk et al. 2008).

As described in the Chapter 1, most of the cancers present an increased aerobic glycolysis due to a large remodeling in cancer signaling and metabolism. However, this does not apply to all cancer types and there are some exceptions, which utilize TCA cycle and oxidative phosphorylation as their main energetic source (Zu et al. 2004). So, in

order to understand the underlying mechanisms of cancer metabolism, the metabolic performance of these cell lines must be evaluated.

Through the use of NMR sensitive labelled substrates supplemented as tracers, isotopomer analysis and NMR techniques allow a qualitative and quantitative assessment of metabolism (Tavares et al. 2015; Szyperski et al. 1996; Jeffrey et al. 1991; Malloy et al. 1990). The work will initiate with exploratory ^{1}H NMR experiments from cellular extracts of cells grown in regular culture media at different time-points in order to search for differences in the overall metabolic profile. Multivariate analysis will be the method of choice for the integration and recognition of metabolic patterns in the different cell lines.

Following these experiments, labelled substrates will be supplemented to the media, in order to apply isotopomer analysis methodologies. For the assessment of glycolytic and TCA cycle fluxes, [U-^{13}C]glucose will be supplied to the cells. Media aliquots and cell extracts will be analyzed using ^{1}H and ^{13}C NMR experiments. For the isotopomer analysis of DNL, organic cellular extracts grown in media reconstituted with 20% $^{2}H_2O$ will be analyzed by ^{1}H and ^{2}H NMR experiments.

Despite being a relatively descriptive experimental Chapter, few studies focus on the intermediary metabolism of cancer, measuring only end-reactions such as lactate production or oxygen consumption. Moreover, pathways such as DNL and PPP are most of the times neglected, and although their estimated fluxes are much lower than glycolysis and TCA cycle, their impact on cancer development may be important. Unfortunately, due to time availability constraints, PPP will not be assessed by isotopomer analysis in this work but will be matter of discussion on Chapter 7.

This Chapter aims for a metabolic profiling of each cell line. Combined with the metabolic profiling, a quantification of glycolytic, TCA cycle and DNL fluxes should be achieved, the data should be rationalized and integrated as a model and compared between each cell line.

The suggested hypothesis is that cancerous cell lines have a distinct metabolic profile from the non-cancerous cell lines towards a more glycolytic phenotype. A

secondary hypothesis rises from the fact that both cancerous cells are derived from non-small lung cancer; therefore it may exhibit similar profiles.

5.2 Results

5.2.1 Metabonomics of lung cells

Cells are composed by several classes of molecules, ranging from small to large molecules, hydrophilic to hydrophobic (or amphipathic). Considering that the majority of the metabolites are water soluble small molecules, aqueous cellular extracts can provide a fair amount of information about cellular metabolism. The Figure 5.1 depicts representative ^{1}H NMR spectra of aqueous cell extracts of each cell line, referenced and normalized for a fumarate standard (singlet at 6.5 ppm). The cells were grown under normal conditions (humidified 37 ºC with 5% CO_2) with regular RPMI media containing 10 mM glucose and 10% FBS. Cells were then collected and extracted at 8h, 24h and 48h to analyze the buildup of metabolites. Assuming that the relaxation delay in NMR experiments is set to allow a full relaxation of all proton nuclei in each of the small molecules, the area of a particular metabolite will be directly correlated with their concentration and number of equivalent nuclei. However, these spectra representations at different hours are not normalized for protein content and quantitative comparisons should be taken with care while qualitative comparisons can be readily applied.

Analyzing the Figure 5.1, cell lines have a notorious buildup of metabolites, especially from 24h to 48h. The metabolic profile of H1299 cell line (dark grey) is somewhat similar to the MRC-5 cell line (black), however it is more complex, namely at the 2.5-3.0 ppm region. At 1.31 ppm appears the highest signal in these expansions, a doublet arising from the ^{1}H signal of lactate methyl group with a $^{3}J_{HH}$=7.0 Hz. All cell lines exhibit increasing amounts of lactate over time. To the left of this peak, at 1.47 ppm there is another doublet with a $^{3}J_{HH}$=7.3 Hz, belonging to the methyl group of alanine. This aminoacid is almost undetectable in the A549 cell line (light grey) when compared with the other two cell lines. Another striking difference is the singlet at 3.21 ppm, arising from the $N(CH_3)_3$ group of choline, which clearly does follow a buildup trend in

the MRC-5 cell line. Other choline derivates such as phosphocholine (PCho) and glycerophosphocholine (GPCho) are also visible next to choline (3.20-3.25 ppm). The rest of the spectra show some differences in the overall amounts of glutamate, glutamine and other aminoacids.

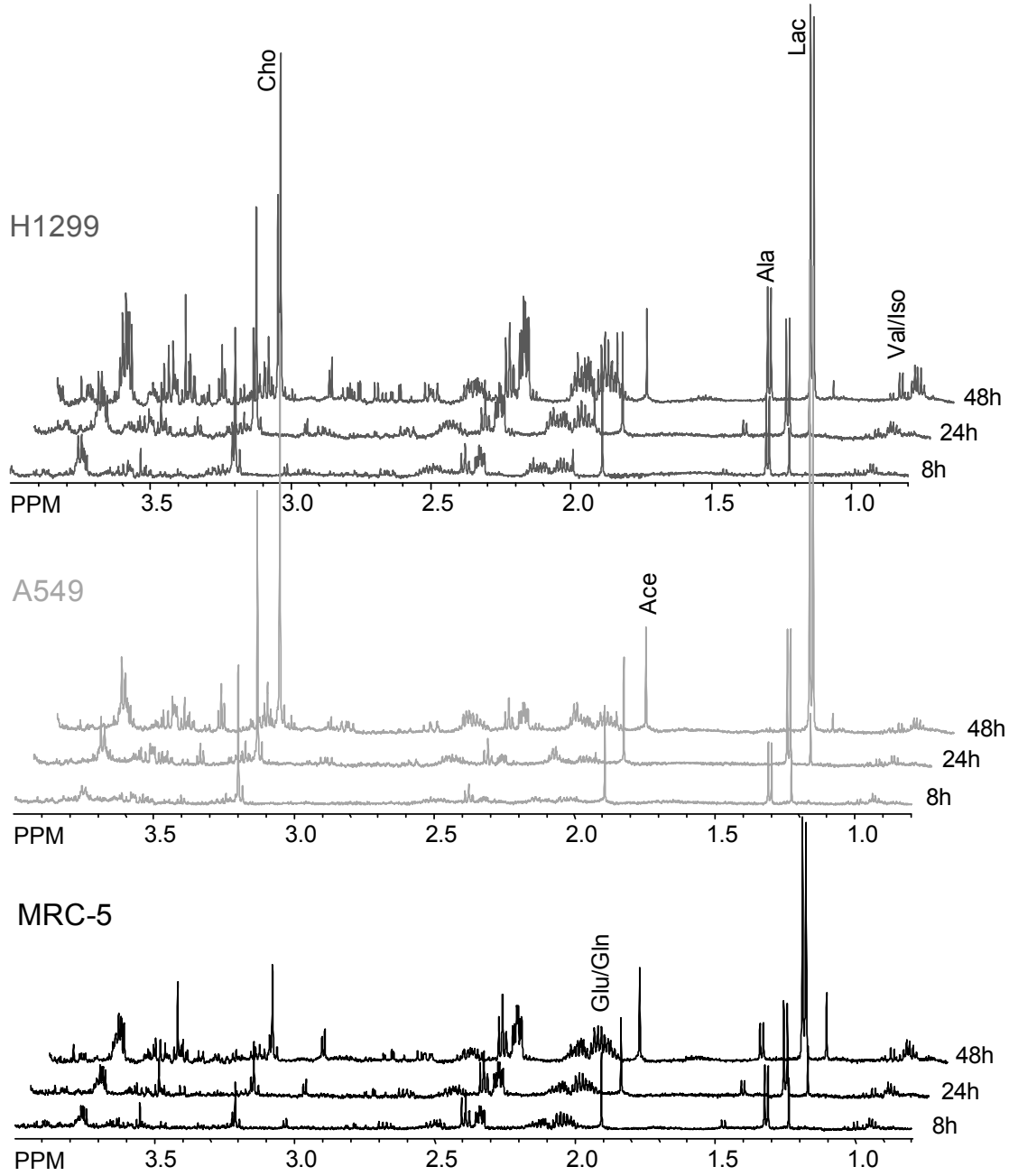

Figure 5.1 - ^{1}H NMR spectra of aqueous cell extracts at 8h, 24h and 48h. This panel depicts representative 0.75-4.0 ppm region of ^{1}H NMR spectra of each cell line, extracted at different time-points. The overall metabolic profile is clearly distinct between each cell line. MRC-5 cell line (black) and H1299 cell line (dark grey) possess a more complex profile than A549 cell line (light grey). Also, cancer cells produce and accumulate higher levels of choline over time when compared to the non-cancerous cell line. Another interesting difference is the near absence of alanine in the A549 cell line. (Ace) acetate; (Ala) alanine; (Cho) choline; (Glu/Gln) glutamate/glutamine; (Lac) lactate; (Val/Iso) valine/isoleucine.

Since each cell line is inherently different, data must be normalized for protein content (or number of cells), something that graphic display, such as in Figure 5.1, does not allow. From here on, all spectral data will be analyzed in quantitative terms, which allow the exact determination of concentrations, protein content normalization, and employment of statistical analysis for comparison between cell lines.

Since extracts at 8h, 24h and 48h provided enough cell mass to acquire NMR spectra with sufficient signal/noise, these were used for the first measurements. The metabolically relevant molecules previously referred were quantified throughout the time lapse. In Figure 5.2, lactate, alanine and choline were quantified in terms of mM/mg protein/hour, allowing the estimation of a production rate in each cell line, represented by different connecting lines.

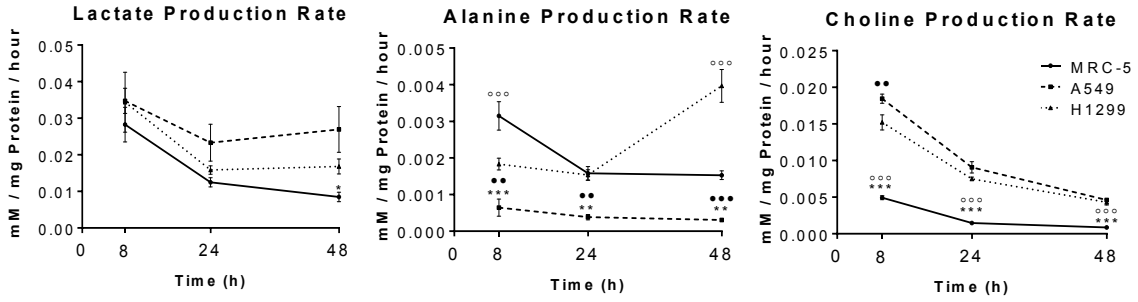

Figure 5.2 - Intracellular levels of metabolites quantified from aqueous cellular extracts. Lactate, alanine and choline levels were quantified from ^{1}H NMR spectra and are expressed in terms of mM/mg protein/hour. Lactate production is significantly lower ($p<0.05$) at 48h for the MRC-5 cell line when compared to the A549. Alanine production is significantly lower in the A549 cell line while H1299 exhibit a significantly increased production rate at 48h ($p<0.001$). Choline production rate is significantly lower for MRC-5 line at all time points ($p<0.001$).
Error bars represent SEM, n=6. A two-way ANOVA was applied with a Tukey post test. * $p<0.05$ between MRC-5 and A549; o $p<0.05$ between MRC-5 and H1299; • $p<0.05$ between A549 and H1299.

Lactate production rate (Figure 5.2) is increased at 8h and lowers at 24h for all cell lines. However, at 48h, the lactate production rate on the non cancerous cell line MRC-5 (8.5±3.2 μM/mg protein/h), represented in a full line, is significantly lower ($p<0.05$) than A549 cell line (26.9±15.3 μM/mg protein/h), represented in a dashed line.

Alanine production rate (Figure 5.2), as suspected by previous sheer observation of the spectra, is significantly lower at all time points ($p<0.05$, $p<0.001$) for the A549 cell line (0.31±0.06 μM/mg protein/h at 48h). The MRC-5 cell line has an initial response

with a significantly higher production ($p<0.001$; 3.15±0.95 μM/mg protein/h) than the H1299 cell line (1.83±0.39 μM/mg protein/h). However, MRC-5 cell line decreases the production rate at 24h and stabilizes (1.53±0.29 μM/mg protein/h at 48h) while H1299 cell line boosts alanine production achieving a significantly higher production rate at 48h ($p<0.001$; 3.97±1.10 μM/mg protein/h).

Finally, the choline production rate (Figure 5.2) is significantly lower for all time points on the non-cancerous MRC-5 cell line ($p<0.001$; 0.87±0.15 μM/mg protein/h). Moreover, at 8h, A549 cell line has a significantly higher production rate ($p<0.05$; 18.5±1.5μM/mg protein/h) than the H1299 cell line (15.2±2.5μM/mg protein/h). Nevertheless, all cell lines exhibit a decreased production over time.

Multivariate analysis

These previous concentrations were calculated with a line fitting algorithm, delivering precise and robust area integration but require a time-consuming processing. With the development and refinement of statistical software, new data analysis methods are becoming available. One of the methods that are applied to large datasets (mostly NMR and MS data) is multivariate analysis. This analysis greatly reduces the complexity of the data and is a faster processing method. Providing that spectra are pH buffered, well referenced, baseline corrected and normalized to a standard, it only requires peak height integration. Furthermore, either full spectra or just selected spectral regions can be used for analysis.

A PCA analysis was applied to a Spearman correlation matrix of 18 samples vs. 6 variables from the spectral data at 48h of previous experiments. The six areas of interest were calculated by integral display function on NutsPro (Acorn). Each section included the peaks corresponding to acetate, alanine, aspartate, glutamine, glutamate/glutamine and lactate. The spectra were baseline corrected, normalized to fumarate (external standard) and normalized for protein content.

In the Figure 5.3 are shown the loadings plot and the scores plot from the PCA analysis. Two principal components were selected: principal component 1 (PC1) with an eigenvalue=3.4 explain 56.8% of the total variance; principal component 2 (PC2) with an

eigenvalue=1.5 reflects 24.8% of the total variance. The plotted components PC1 and PC2 depict an accumulated variance of 81.6%. Each point in the scores plot represents an individual NMR spectral region and the axis represents each principal component. PC1 is strongly positively correlated with glutamate/glutamine, aspartate and alanine while PC2 is positively correlated with lactate and negatively correlated with alanine. Each point on the scores plot represents an individual sample (n=6), with MRC-5 cell line shown in black, A549 cell line in blue and H1299 cell line in red. The plotting is based on the score obtained by each sample at the loadings plot. A clear separation of each cell line is visible in the loadings plot, with fairly low internal dispersion. However, MRC-5 and H1299 cell lines share similar metabolic profiles with close groups. H1299 cell line scores higher in the PC1, which reflects higher levels of glutamate/glutamine than H1299 cell line. But the clearest distinction is between A549 cell line and MRC-5/H1299 cell lines, where A549 cell line score higher in the PC2, indicating higher levels of lactate and lower alanine than the other cell lines. MRC-5 cell line oppositely has lower levels of lactate and higher alanine.

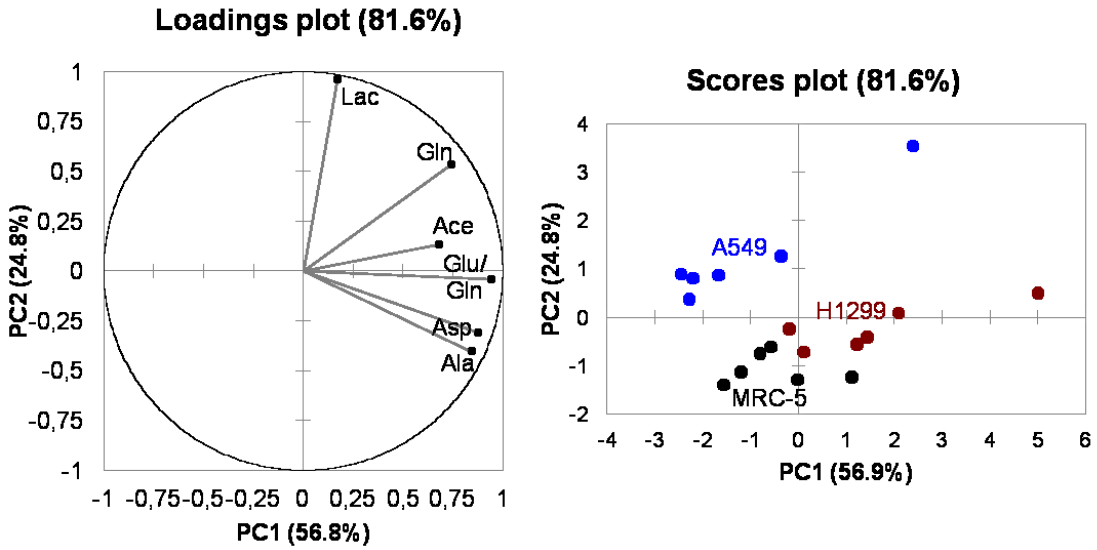

Figure 5.3 - Metabolic profiling by multivariate analysis of ^{1}H NMR data from aqueous cell extracts at 48h. Six spectral zones were processed by integral quantification, corresponding to the metabolites lactate (Lac), acetate (Ace), glutamine (Gln), glutamate/glutamine (Glu/Gln), aspartate (Asp) and alanine (Ala). Each sample obtains a score based on the loadings plot and is individually represented as a dot on the scores plot. Six samples of MRC-5 (black), A549 (blue) and H1299 (red) are plotted, with a clear separation of groups and low dispersion. This allows a broad metabolic profiling, where A549 present higher levels of lactate and lower alanine, contrarily to MRC-5 and H1299. Also, H1299 seem to have higher levels of glutamate and glutamine than MRC-5. MRC-5 seem to possess a somewhat similar metabolic profile while A549 is clearly distinct, pointing towards a glycolytic phenotype.
Principal Component Analysis was applied on a Spearman correlation matrix of 18 samples x 6 variables, exhibiting a combined variance of 81.6% for the principal components 1 and 2, both with an eigenvalue>1.

5.2.2 Isotopomer analysis

The data from unlabelled NMR experiments allow a descriptive characterization and quantification of certain metabolites but lacks intermediary metabolism information, which can be provided by ^{13}C tracers. Given that ^{12}C is insensitive in NMR and the only ^{13}C labelling present in the unlabelled culture media arises from natural abundance (1.1%), cells must be supplied with ^{13}C enriched tracers. By providing [U-^{13}C]glucose to the cells, besides ^{1}H NMR data, supplemental information can be acquired from ^{13}C spectra. Furthermore, by consuming [U-^{13}C]glucose, we are able to pinpoint the source of labelled carbon skeleton of several metabolites back to glucose and quantify metabolic intermediates. Cells were grown in 10 mM [U-^{13}C]glucose supplemented RPMI medium and aqueous extracts were collected at 48h, with aliquots of media collected at different time points.

Extracellular footprint

To initiate the tracer studies we will focus on the extracellular buildup of metabolic end-products. A sample of the [U-^{13}C]glucose supplemented media was collected throughout the experiment at different time points (0h, 2h, 4h, 8h, 24h and 48h) and ^{1}H NMR experiments acquired. Several metabolites present in the media can be identified, from aminoacids to glucose and even unlabelled molecules can be distinguished from their ^{13}C labelled homologue, such as lactate. While unlabelled lactate shows up as a doublet at 1.31 ppm, labelled lactate, as shown in Figure 5.4, appears as a multiplet of 12 peaks, divided into satellites of 6 peaks each. This multiplet

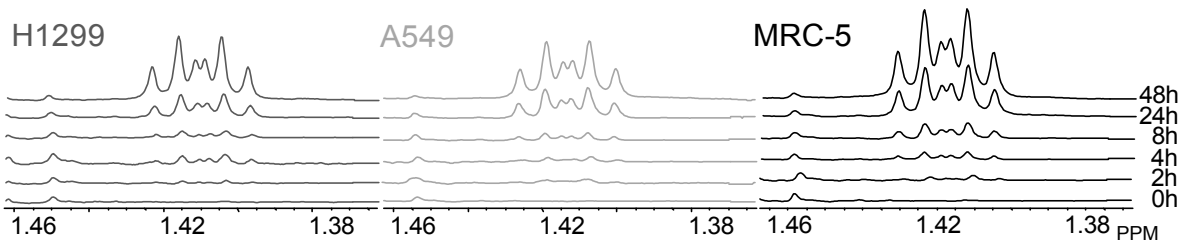

Figure 5.4 – Expansions of ^{1}H NMR spectra depicting one satellite of [U-^{13}C]lactate from the culture media. The signal is composed of 12 peaks, divided into two satellites of 6 each, arising from homonuclear ($^{3}J_{HH}$) and heteronuclear ($^{2}J_{HC}$ and $^{3}J_{HC}$) coupling. Cells were grown in RPMI with 10 mM [U-^{13}C]glucose and aliquots were collected at 0h, 2h, 4h, 8h, 24h and 48h for lactate buildup measurements.

structure is due to the occurrence of both homonuclear ($^3J_{HH}$=7.0 Hz) and heteronuclear scalar-scalar couplings ($^1J_{HC}$=128 Hz, $^2J_{HC}$~4.2 Hz and $^3J_{HC}$~4.2 Hz). In the Figure 5.4 the buildup of labelled lactate is clearly visible, absent at 0h and increasing through time.

The signals from lactate, glucose and some aminoacids were measured and are presented in the Table 5.1 in terms of mM at each time point. Unlabelled lactate has a relatively steady concentration while labelled lactate increases through time, up to 5.43± 0.76 mM in the MRC-5 cell line. Labelled glucose is consumed, reaching the lowest media concentration at 48h also in the MRC-5 cell line (4.82±0.77 mM). The aminoacids valine and isoleucine concentrations are also diminished over time, with lower levels again in the MRC-5 cell line.

Table 5.1 – Quantification of metabolites present in the culture media at different time points. Measurements performed on the ^{1}H NMR spectra of aliquots of RPMI containing 10 mM [U-^{13}C]glucose, collected throughout the experiment. Unlabelled lactate is derived from the FBS while [U-^{13}C]lactate derives from [U-^{13}C]glucose metabolism. Mean and standard deviation (SD) for n=6 are represented.

		Concentration (mM)									
Cell line	Time (h)	Unlabelled Lactate		Labelled Lactate		Labelled Glucose		Valine		Isoleucine	
		Mean	SD	Mean	SD	Mean	SD	Mean	SD	Mean	SD
MRC-5	0	1,67	0,17	0,00	0,00	9,78	1,07	0,17	0,01	0,33	0,03
	2	1,55	0,04	0,16	0,08	7,87	1,56	0,15	0,01	0,29	0,01
	4	1,66	0,20	0,36	0,05	8,92	0,79	0,16	0,02	0,32	0,04
	8	1,62	0,15	0,76	0,12	7,97	1,13	0,16	0,02	0,30	0,03
	24	1,62	0,06	2,49	0,25	7,08	0,56	0,14	0,01	0,26	0,02
	48	1,73	0,12	5,43	0,76	4,82	0,77	0,12	0,01	0,22	0,01
A549	0	1,68	0,15	0,00	0,00	9,55	0,68	0,16	0,02	0,33	0,03
	2	1,51	0,09	0,11	0,08	8,52	0,47	0,16	0,02	0,32	0,02
	4	1,60	0,11	0,25	0,08	8,38	0,65	0,16	0,01	0,32	0,03
	8	1,56	0,10	0,37	0,06	8,41	0,74	0,16	0,01	0,31	0,02
	24	1,59	0,13	1,39	0,25	8,67	0,84	0,15	0,01	0,30	0,02
	48	1,71	0,15	4,11	0,51	6,95	0,73	0,14	0,02	0,28	0,02
H1299	0	1,60	0,08	0,00	0,00	9,16	0,53	0,18	0,01	0,33	0,02
	2	1,60	0,13	0,14	0,05	8,60	0,56	0,17	0,02	0,32	0,03
	4	1,63	0,07	0,27	0,14	8,76	0,42	0,17	0,02	0,32	0,02
	8	1,56	0,08	0,33	0,10	8,92	0,63	0,17	0,02	0,32	0,03
	24	1,54	0,05	1,34	0,44	7,65	0,68	0,15	0,02	0,29	0,02
	48	1,59	0,13	3,67	0,72	6,39	0,71	0,14	0,03	0,27	0,03

The levels of labelled lactate were plotted as a function of time to understand how the concentration of secreted lactate varies over time (Figure 5.5). All three cell lines have a linear buildup of labelled lactate and fit a non-constrained linear regression with an r^2>0.92 (equations relative to each line are exhibited in the Figure 5.5). Since the

linear regressions fitted the data in very good models, the slopes of each regression were statistically analyzed to compare the labelled lactate secretion rate.

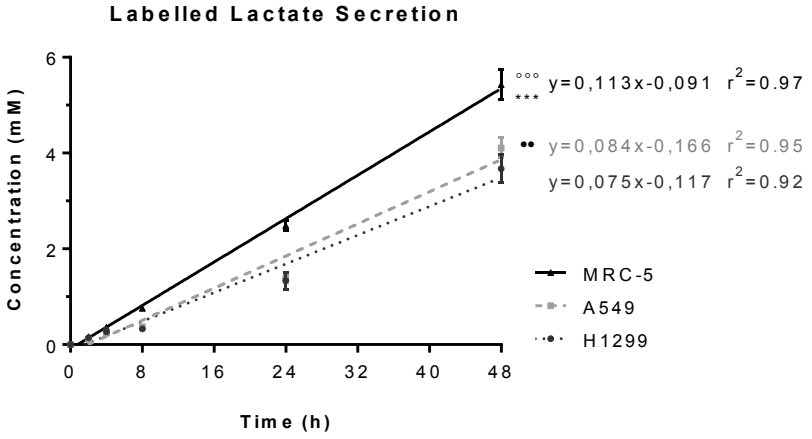

Figure 5.5 - Extracellular lactate buildup. [U-^{13}C]lactate measured from the aliquots of culture media by ^{1}H NMR experiments. A linear regression was fitted for the three cell lines and the respective equations (y=mx+b) are shown. All three cell lines fit the linear model with an elevated r^2 value. During the time of the experiment, MRC-5 (black) secretes significantly more labeled lactate than both cancer cells ($p<0.001$). The A549 line (dashed, light grey) also exported significantly more labeled lactate than the H1299 (dotted, dark grey) ($p<0.01$).
Error bars represent SEM, n=6. A linear regression model was fitted and a one-way ANOVA was applied with a Tukey post test. * $p<0.05$ between MRC-5 and A549; o $p<0.05$ between MRC-5 and H1299; • $p<0.05$ between A549 and H1299.

The MRC-5 cell line (black) has a significantly higher secretion rate ($p<0.001$) than both cancerous cell lines. However, the A549 cell line (dashed, light grey) also exports significantly higher levels of labelled lactate ($p<0.01$) than the H1299 cell line (dotted, dark grey).

These data can already suggest the fermentative state of each cell line but to have a more reliable picture we must also rely on the glucose consumption rates (Table 5.2). Considering that one molecule of [U-^{13}C]glucose can originate two [U-^{13}C]lactate molecules through glycolysis, followed by lactic acid fermentation, the number of expected lactate equivalents is twice the consumed glucose concentration, as depicted in the Table 5.2. By calculating a ratio between the secreted labelled lactate and the theoretical lactate production considering a full oxidation of glucose molecules, we can derive a fermentation rate. This fermentation rate reflects the coupling between glucose

consumption and lactate production, and seems higher in the cancerous cells, although it does not reach statistical significance (p=0.087).

Table 5.2 – Theoretical lactic acid fermentation rate. During the 48h time lapse, culture media [U-^{13}C]glucose consumption (ΔGlucose) and [U-^{13}C]lactate secretion can be measured using ^{1}H NMR spectra. Each glucose molecule is cleaved into two lactate molecules, therefore generating the double in lactate equivalents. A ratio between secreted labelled lactate and theoretical lactate equivalents may provide a broad assessment of the fermentation rate. Even though A549 line has the highest rate of fermentation and MRC-5 the lowest, the differences are not statistically significant.
Mean and standard deviation (SD) for n=6 are represented. A one-way ANOVA was applied on the Fermentation Rate dataset, with p=0.087.

	Concentration (mM)							
	ΔGlucose		Lactate equivalents (2x ΔGlucose)		Labelled lactate		Fermentation rate (Lac/Lac equi.)	
Cell line	Mean	SD	Mean	SD	Mean	SD	Mean	SD
MRC-5	4,96	0,81	9,92	1,62	5,43	0,76	0,56	0,10
A549	2,60	1,03	5,20	2,05	4,11	0,51	0,87	0,27
H1299	2,77	0,95	5,55	1,90	3,67	0,72	0,72	0,25

Intracellular metabolism by ^{1}H NMR experiments

The information obtained from the culture media is limited to secreted end-products of metabolism or substrate consumption. To dig further into the intermediary metabolism we must analyze the aqueous cellular extracts. The cells that were grown in 10 mM [U-^{13}C]glucose were extracted at 48h and analyzed by both ^{1}H and ^{13}C NMR experiments.

The ^{1}H NMR experiments of cell extracts with labelled glucose are somewhat similar to the previous unlabelled spectra from metabonomics analysis. However, these extracts show ^{12}C and ^{13}C metabolites, providing vital information about their origin (Figure 5.6). Due to the heteronuclear coupling, metabolites containing ^{1}H and ^{13}C will have their signal divided into multiplets, such as the case of lactate, alanine and acetate, identified in the Figure 5.6. [U-^{13}C]alanine generates a doublet of sextets similar to the [U-^{13}C]lactate. Unlabelled acetate appears as a singlet at 1.9 ppm from the methyl group while [U-^{13}C]acetate shows as doublet of doublets arising from the heteronuclear scalar-scalar ($^{1}J_{HC}$ and $^{2}J_{HC}$) couplings. The intracellular lactate, acetate and choline levels are lower in the MRC-5 cell line. The alanine remains nearly absent in the A549 cell line, which also has lower levels of creatine/phosphocreatine and the overall aminoacid pool appears diminished.

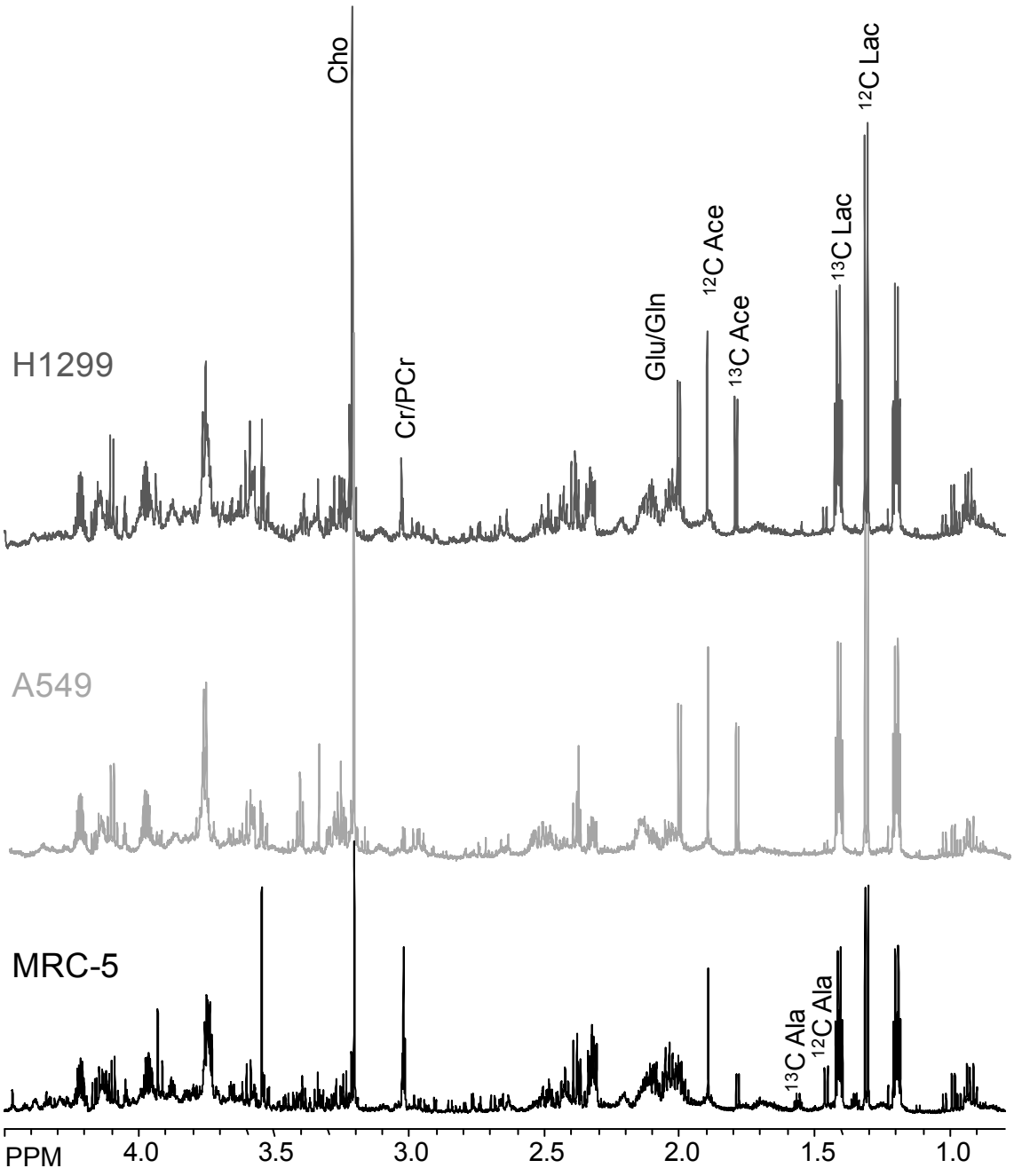

Figure 5.6.– Representative ^{1}H NMR spectra of aqueous cell extracts cultured in RPMI media supplemented with 10 mM of [U-^{13}C]glucose, during 48h. The metabolic profile for the three cell lines is shown for comparison in the region of 0.75-4.50 ppm. ^{12}C substrates can be distinguished from the ^{13}C labelled counterparts, showing up as satellites. (Ace) acetate; (Ala) alanine; (Cho) choline; (Cr/Pcr) creatine/phosphocreatine; (Glu/Gln) glutamate/glutamine; (Lac) lactate.

The spectra were quantified and the more relevant metabolites were analyzed in terms of mM/mg protein. The first was lactate, with both labelled and unlabelled forms quantified (Figure 5.7). The total lactate concentration is significantly higher ($p<0.01$) in the A549 cell line (2.28±0.57 mM/mg protein) when compared to the MRC-5 cell line (1.25±0.41 mM/mg protein). The H1299 cell line lactate concentration (1.71±0.44

mM/mg protein) sets between both cell lines but the difference does not reach statistical significance.

Alanine concentration is significantly increased ($p<0.001$) on the MRC-5 cell line (0.12±0.01 mM/mg protein) when compared to the cancerous cell lines (Figure 5.7). H1299 cell line alanine levels (0.04±0.01 mM/mg protein) are also significantly increased ($p<0.01$) relatively to the A549 cell line (0.02±0.004 mM/mg protein). Interestingly, the labelled alanine contribution on the cancerous cells is undetectable.

A ratio between lactate and alanine may provide an indirect measure of cytosolic redox and this ratio is significantly higher ($p<0.001$) on the A549 cell line (139.0±24.4) relatively to MRC-5 and H1299 cell lines (Figure 5.7). The H1299 cell line (42.6±19.7) also has a higher ratio when compared to MRC-5 cell line (10.5±4.3).

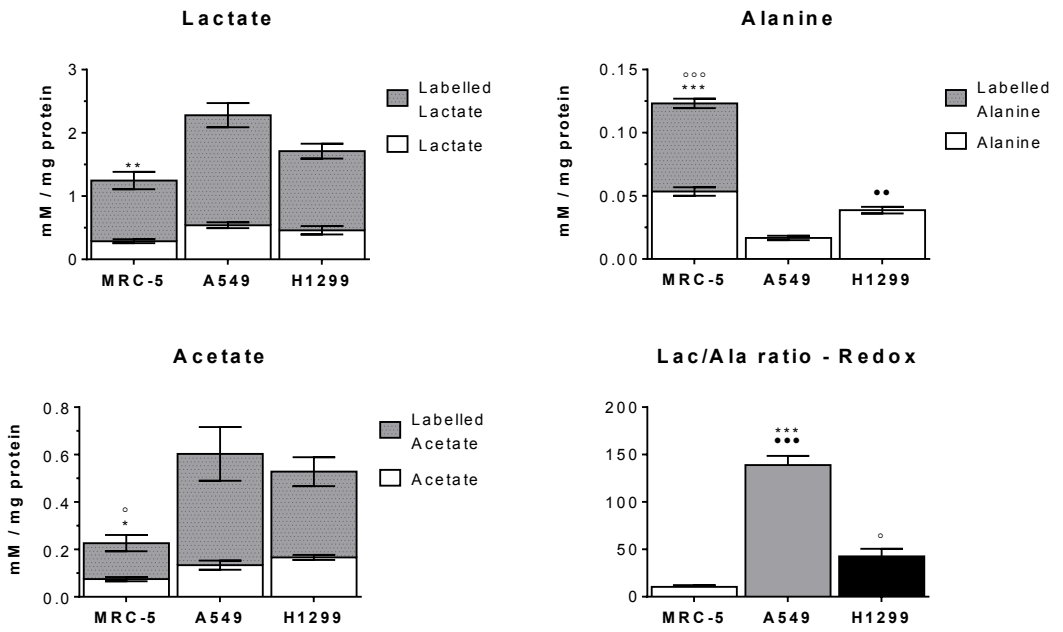

Figure 5.7 - Intracellular levels of lactate, alanine and acetate quantified from aqueous cellular extracts cultured with 10 mM [U-^{13}C]glucose during 48h. Concentrations were quantified from ^{1}H NMR spectra and are expressed in terms of mM/mg protein. Lactate concentration is significantly lower ($p<0.01$) in the MRC-5 cell line when compared to the A549 cell line. Alanine concentration is significantly higher ($p<0.001$) in the MRC-5 cell line when compared to cancerous lines. The H1299 cell line also has a significantly higher concentration ($p<0.01$) when compared to the A549 cell line. Furthermore, MRC-5 cell line is the only exhibiting detectable amounts of ^{13}C labelled alanine. Acetate concentration is also significantly lower ($p<0.05$) for the MRC-5 cell line when compared with the cancer cell lines. Lactate/alanine ratio, an indirect measure of intracellular redox, is significantly higher ($p<0.001$) in A549 and H1299 ($p<0.05$) cell lines relatively to MRC-5 cell line.
Error bars represent SEM, n=6. When possible, a one-way ANOVA was applied with a Tukey post test. * $p<0.05$ between MRC-5 and A549; o $p<0.05$ between MRC-5 and H1299; • $p<0.05$ between A549 and H1299.

Acetate concentration (Figure 5.7) is significantly increased ($p<0.05$) in both cancer cell lines (0.60±0.32 mM/mg protein for A549 cell line; 0.53±0.17 mM/mg protein for H1299 cell line) relatively to the MRC-5 cell line (0.15±0.08 mM/mg protein).

Intracellular metabolism by ^{13}C NMR experiments

To complement the previous information, ^{13}C NMR spectra of the same extracts provide important clues about the intermediary metabolism. By analyzing the glutamate labelling at the C4 and C3, we are able to measure quantitatively some TCA cycle parameters.

In the Figure 5.8 are shown representative ^{13}C spectra of each cell line and expansions of the glutamate C4 and C3 resonances. Analyzing the glutamate C4 expansion, the peaks are originated by the following isotopomers: [4-^{13}C]glutamate generates a singlet (C4S) at 34.2 ppm; [4,5-$^{13}C_2$]glutamate generates a doublet (C4D45) due to the $^1J_{C4C5}$=51.3 Hz; and [3,4,5-$^{13}C_3$]glutamate generates a doublet of doublets (C4Q) due to the $^1J_{C4C5}$ and $^1J_{C3C4}$=34.5 Hz, but also an unresolved, multiple bond, $^2J_{C3C5}\approx1$ Hz. All three cell lines exhibit a C4S, C4D45 and C4Q (represented in the Figure 5.8 as S, D, Q), but the ratio between the doublet and quartet is different in each cell line.

The glutamate C3 is also formed by several peaks: a singlet (C3S) at around 27.8 ppm, formed from [3-^{13}C]glutamate; a doublet from [3,4-$^{13}C_2$]glutamate due to $^1J_{C3C4}$; and a triplet due to [2,3,4-$^{13}C_3$]glutamate. Since $^1J_{C2C3}$=34.8 Hz and $^1J_{C3C4}$=34.5 Hz are very similar, it is not a true triplet but rather an unresolved center peak. However, in the spectra they are mainly composed by unresolved peaks and is nearly absent on the A549 cell line.

The methyl group of labelled lactate shows up as a small singlet at around 20.9 ppm and as a doublet from $^1J_{C2C3}$=36.9 Hz. By simply analyzing the spectra in Figure 5.8, the amounts seem similar between the cell lines. However, labelled glucose levels are increased in the MRC-5 and H1299 cell lines (showing up at around 92.8 and 96.6 ppm). Another dissimilar result is the alanine concentration, which is essentially undetectable in both cancerous cell lines (around 17.0 ppm).

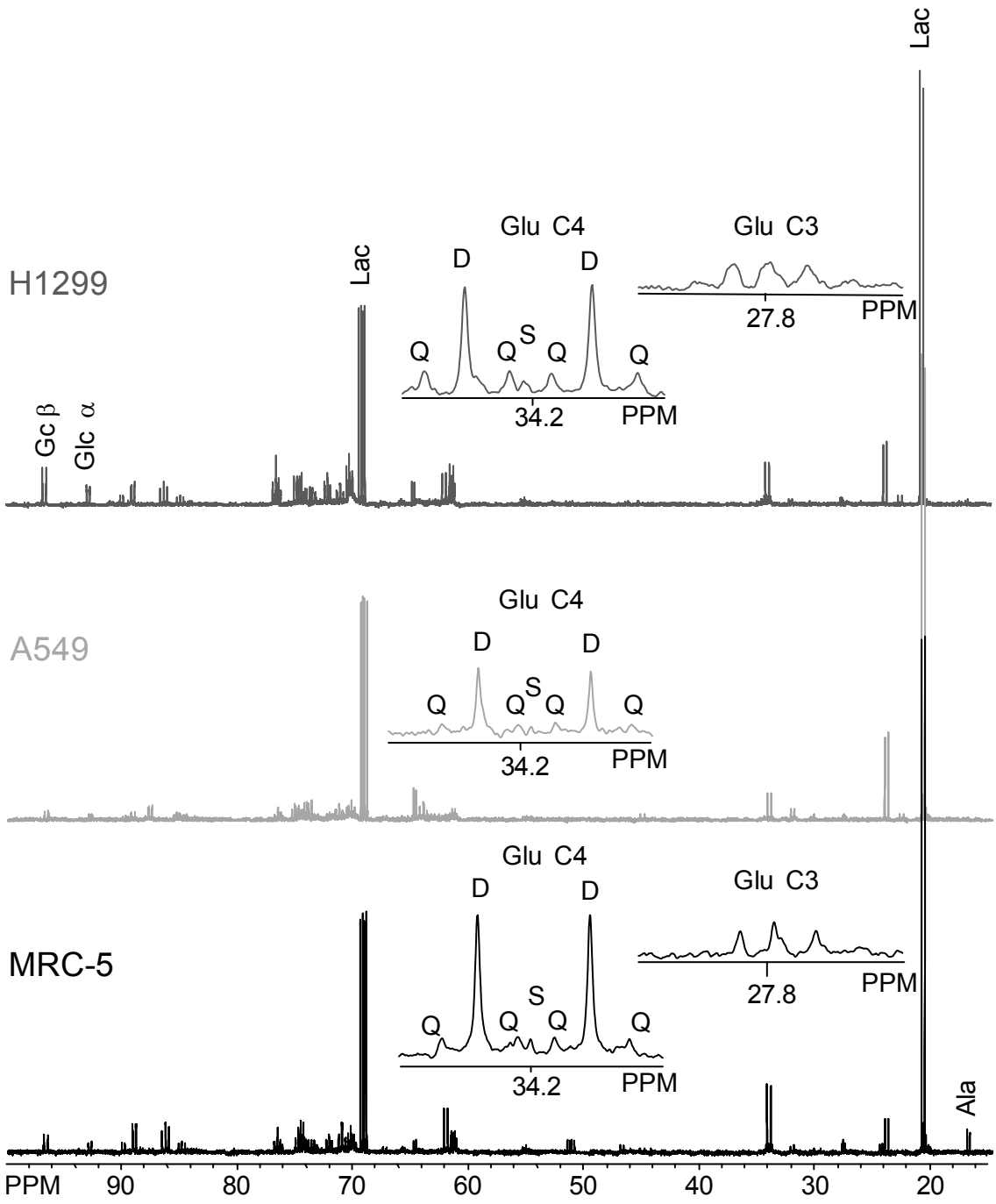

Figure 5.8 - Representative ^{13}C NMR spectra of aqueous cell extracts cultured with 10 mM [U-^{13}C]glucose during 48h. The metabolic profile for the three cell lines is shown for comparison in the region of 15-100 ppm. Labelled metabolites are shown, with expansions of glutamate C4 and C3. Isotopomers are shown as multiplets (doublets or quartets). (Ala) alanine; (Glc) glucose; (Glu) glutamate; (Lac) lactate.

The ^{13}C spectra of cell extracts were quantified and metabolic parameters were calculated through isotopomer analysis (as described in the Materials and Methods, Chapter 4) and the results are exhibited on Figure 5.9.

Briefly describing, TCA coupling is a ratio between the amount of labelling on glutamate C4 isotopomers and [U-^{13}C]lactate (GluC4F/LacC3F). This TCA coupling is significantly lower for the A549 cell line (0.066±0.020) when compared with MRC-5 ($p<0.01$; 0.257±0.092) or H1299 cell lines ($p<0.001$; 0.320±0.090).

Turnover is presented as the ratio between [3,4,5-$^{13}C_3$]glutamate and [4,5-$^{13}C_2$]glutamate (C4Q/C4D45). The H1299 cell line has a significantly higher turnover (0.634±0.148) than the A549 cell line ($p<0.01$; 0.350±0.103) and the MRC-5 ($p<0.001$; 0.301±0.068) cell lines.

Finally, anaplerosis is the difference to the unity of a ratio between the amount of labelling on glutamate C3 and glutamate C4 (1-(GluC3/GluC4)). On this parameter, the H1299 cell line has a significantly lower value (0.590±0.035) than the MRC-5 ($p<0.05$; 0.682±0.022) and the A549 cell line ($p<0.05$; 0.720±0.068) cell lines.

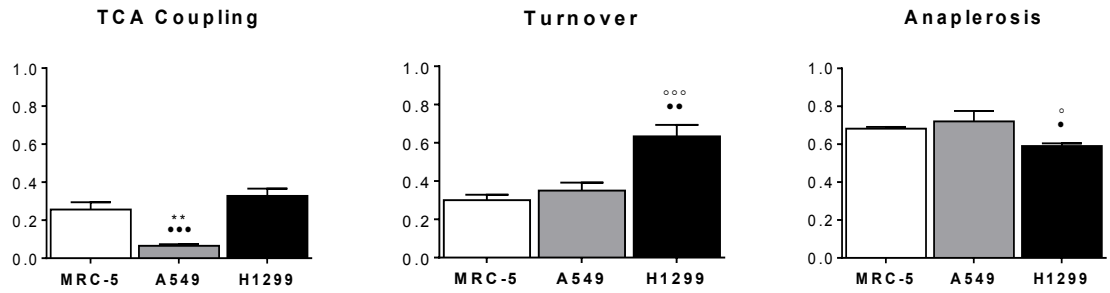

Figure 5.9 – Metabolic parameters quantified from ^{13}C NMR spectra of aqueous cell extracts cultured with 10 mM [U-^{13}C]glucose during 48h. Glucose consumption coupled to TCA cycle (glutamate C4/lactate) is significantly lower in the A549 line ($p<0.01$ vs MRC-5, $p<0.001$ vs H1299), implicating a higher glycolytic rate for this cell line. Turnover (glutamate C4Q/glutamate C4D34) is significantly increased in the H1299 cell line when compared to the other cell lines ($p<0.001$ vs MRC-5, $p<0.01$ vs A549). Anaplerosis (1-glutamate C3/glutamate C4), on the other hand, is significantly decreased in the H1299 cell line ($p<0.05$).
Error bars represent SEM, n=6. When possible, a one-way ANOVA was applied with a Tukey post test. * $p<0.05$ between MRC-5 and A549; o $p<0.05$ between MRC-5 and H1299; • $p<0.05$ between A549 and H1299.

5.2.3 Metabolic enzymatic expression

The activity of the metabolic pathways is dependent of intricate functional enzymatic machinery. Since metabolic enzymes expression is usually highly regulated, the protein content of some key enzymes was assessed by western blot techniques.

In Figure 5.10 we can observe that most of the glycolytic enzymes analyzed (HKI, GAPDH, PKM1+2, PKM2 and LDHA) have similar expressions in the three cell lines. The only significant difference is on the HKII expression, which is lower on the A549 cell line ($p<0.01$) when compared to the H1299 cell line.

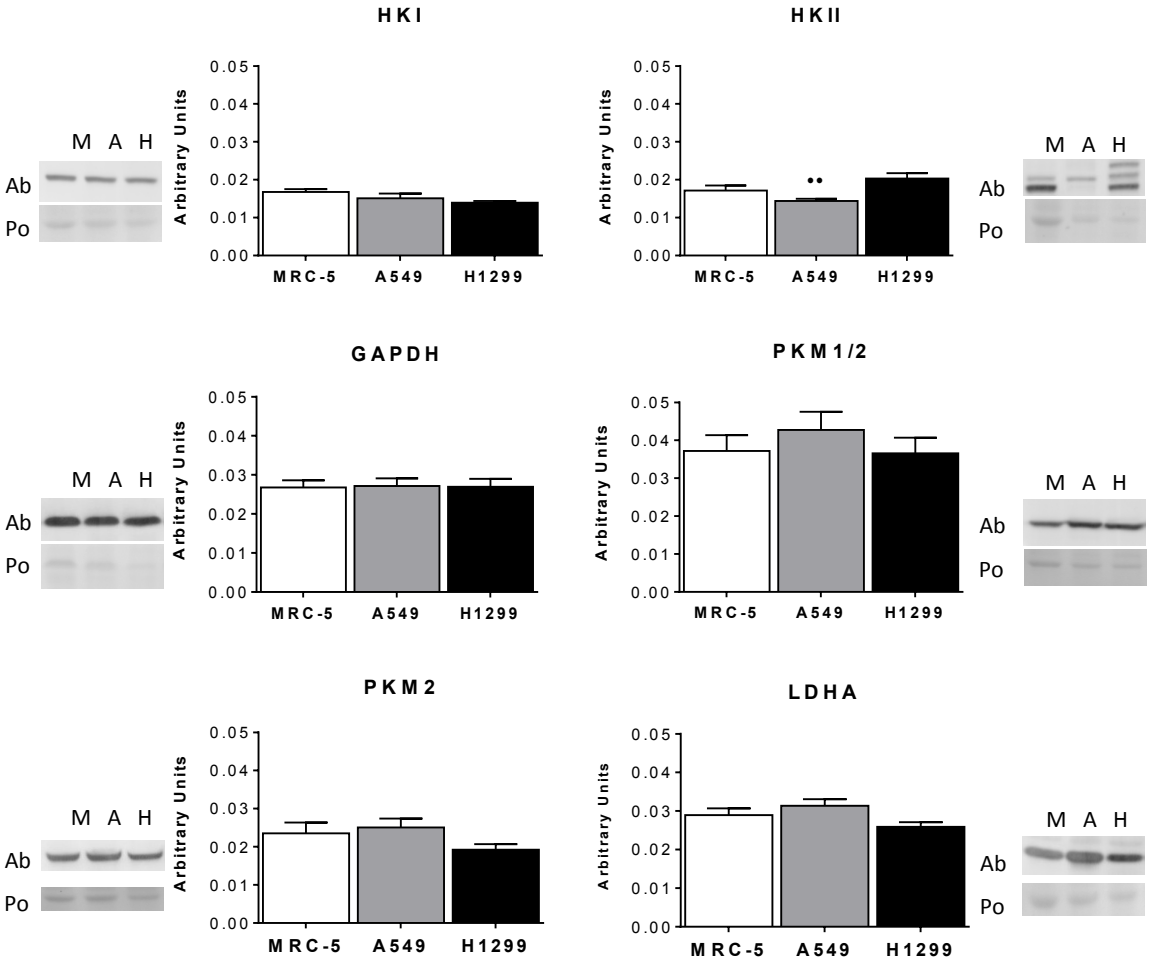

Figure 5.10 – Western blot quantification of glycolytic enzymes. All analyzed enzymes have similar expression levels, except HKII, which is significantly lower ($p<0.01$) for A549 when compared with H1299 cell line. (HKI, HKII) Hexokinase I and II, 102 kDa; (GAPDH) glyceraldehyde-3-phosphate dehydrogenase, 37 kDa; (PKM1/2, PKM2) pyruvate kinase muscle isoform I+2 and I, 60 kDa; (LDHA) lactate dehydrogenase A, 37 kDa; (Ab) antibody; (Po) Ponceau S.
Error bars represent SEM. n=12 for HKII, PKM1/2; n=8 for HKI, GAPDH, PKM2, LDHA. When possible, a one-way ANOVA was applied with a Tukey post test. • $p<0.05$ between A549 and H1299.

Besides glycolytic enzymes, PDH and PDK expression were also assessed by western blot, since PDH complex is a major gateway for shuttling pyruvate in the form of AcCoA into the TCA cycle (Figure 5.11). PDH expression is significantly increased in MRC-

5 cell line relatively to A549 and H1299 ($p<0.05$; $p<0.001$) cell lines, while PDK is similar in all cell lines.

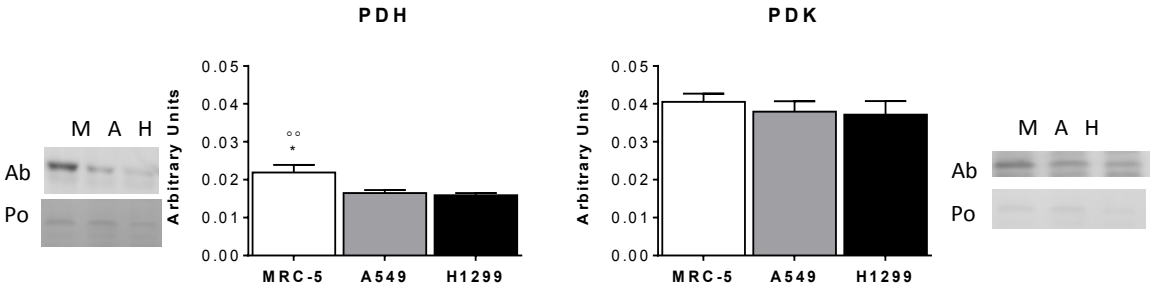

Figure 5.11 - Western blot quantification of PDH, 43 kDa and PDK, 47 kDa. While PDK presents similar protein content, PDH is significantly increased on the MRC-5 when compared to both cancer cell lines ($p<0.05$; $p<0.01$).
Error bars represent SEM. n=12 for PDH and n=4 for PDK. When possible, a one-way ANOVA was applied with a Tukey post test. * $p<0.05$ between MRC-5 and A549; o $p<0.05$ between MRC-5 and H1299.

5.2.4 Lipid metabolism by ^{1}H and ^{2}H NMR experiments

Carbon labelled substrates may elucidate glucose metabolism but in order to follow the lipid synthesis, more specifically the DNL, we must apply a different strategy. To collect the lipids and fatty acids we must perform organic extractions instead of aqueous and deliver a different tracer, ^{2}H. The biosynthesis of lipids allows the incorporation of ^{2}H stereospecifically in the methylene chain while the terminal methyl hydrogen atoms are always derived from AcCoA (see Materials and Methods, Chapter 4). For these experiments cells were grown in a media reconstituted with 20% of deuterated water and cells were extracted at 48h.

In the Figure 5.12 we can observe both ^{1}H and ^{2}H NMR spectra of the organic extracts. An external pyrazine standard was added and the total lipid amount can be assessed by the measurement of the terminal methyl group. All cell lines present similar amounts or unlabelled lipids but the incorporation of deuterium in both methyl and methylene groups is diminished on the non-cancerous cell line.

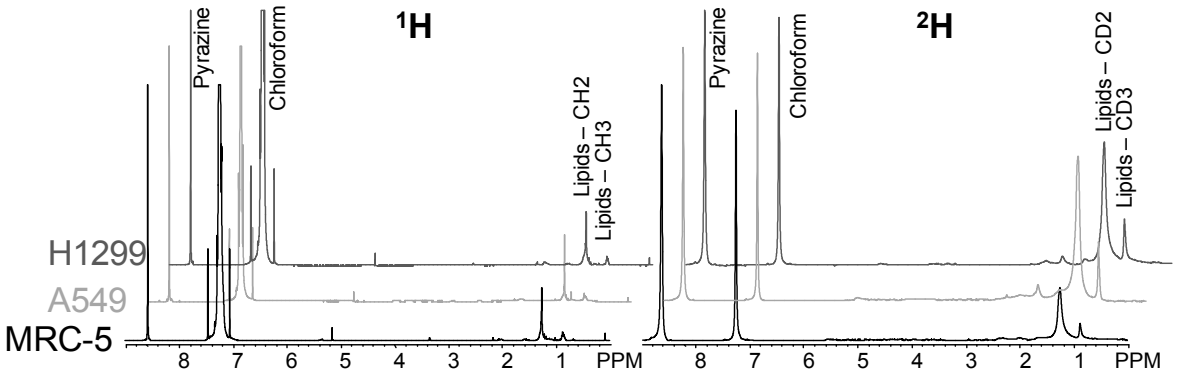

Figure 5.12 – Representative ^{1}H and ^{2}H spectra of organic cellular extracts cultured with 20% $^{2}H_2O$. Expansion of the region 0.0-9.0 ppm of each cell line for comparison. A pyrazine standard was used for reference and total lipids can be identified as two broad peaks, one relative to the terminal methyl group and another from the aliphatic chain. To the left are shown the unlabelled lipids (^{1}H) and to the right the lipids with incorporated ^{2}H.

To interpret these data we must perform tandem measurements in ^{1}H and ^{2}H NMR spectra in order to compare the DNL rate. Total lipid content will be proportional to the sum of unlabelled methyl and labelled methyl terminal groups from fatty acids, shown in Figure 5.12 and quantified in the Figure 5.13. The A549 cell line has higher levels of total lipid content but the difference is not significant (p=0.12).

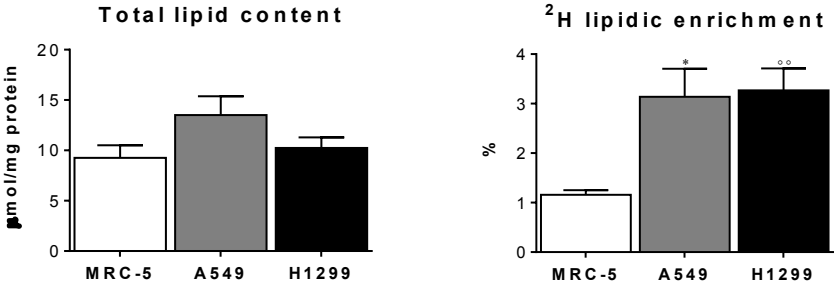

Figure 5.13 – Total lipid content (from methyl group) and terminal methyl ^{2}H enrichment ratio of fatty acids. On the total lipid content, the majority is derived from unlabelled while the fractional labelled lipids are a very small contribution, expressed in terms of μmol/mg protein. Even though A549 cell line has a higher lipid content, the differences were not statistically significant (p=0.12). However, the ^{2}H enrichment is significantly higher for the cancer cells A549 ($p<0.05$) and H1299 ($p<0.001$) when compared to the non-cancerous cell line MRC-5.
Error bars represent SEM, n=6. One-way ANOVA was applied with a Tukey post test. * $p<0.05$ between MRC-5 and A549; o $p<0.05$ between MRC-5 and H1299.

The ^{2}H enrichment (Figure 5.13) is a normalized ratio of the labelled methyl contribution and the total methyl content, providing a measure of DNL. Considering this, both A549 ($p<0.05$; 3.14 ± 1.39) and H1299 ($p<0.05$; 3.27 ± 1.08) cell lines exhibit a significantly higher DNL rate than MRC-5 cell line (1.16 ± 0.23).

5.3 Discussion

Considering the aspects referred in the Chapter 1 and particularly the Warburg effect, a comprehensive interpretation of the metabolic remodeling occurring in cancer cells will be discussed. This Chapter 5 focused mainly on the metabolic characterization of lung cancer cell lines by NMR techniques and isotopomer analysis.

The metabonomics data revealed different metabolic profiles for each cell line. ^{1}H NMR spectra of unlabelled extracts from cells collected at different time points (Figure 5.1) present a clear increase of metabolites at 48h due to exponential growth of cell lines and consequent increase of total metabolite pools. The MRC-5 non-cancerous cell line exhibits a lower lactate production than A549 cell line and overall lower choline production rates (Figure 5.2). An increase in both lactate and choline levels by the A549 cell line are potential biomarkers of an increased PI3K/Akt/mTOR pathway in glioblastoma cell lines (Al-Saffar et al. 2014). This signaling pathway is responsible for the stabilization of HIF-1α, one of the major contributors for the Warburg effect establishment (Semenza 2010). If in the brain, choline may provide the neurotransmitter acetylcholine (ACho), it is also a precursor of phosphocholine (PCho) and a breakdown product of phosphatidylcholine (PtdCho). PCho and PtdCho are components of cell membranes, responsible for maintaining structural integrity and PtdCho may also act as a second-messenger in signaling pathways. Due to the rapid cell proliferation in cancer cells, membrane synthesis is largely required and choline compounds are incremented in several types of cancers, including breast, ovarian, prostate or lung (Trousil et al. 2014; Podo et al. 2011; Shah et al. 2010). Increased choline levels could result from either increased PtdCho degradation or increased choline uptake (Trousil et al. 2014; Müller et al. 2009). Furthermore, increased expression of choline kinase α (ChoKα), the enzyme

that catalyzes the phosphorylation of choline into PCho, is a marker for aggressiveness in several types of cancer, including lung cancer (Granata et al. 2014; Ramírez de Molina et al. 2007; Shah et al. 2010). Therefore, the increase of choline in both cancer cell lines is not surprising. Alanine production, on the other hand, is relatively low for the A549 cell line at all time points (Figure 5.2). Alanine transaminase (ALT) is one of the main intracellular alanine pool regulators, by converting pyruvate into alanine. Therefore, alanine levels will be highly dependent of the size of pyruvate pools and consequently lactate pools, in a redox dependent balance, where a reduced cytosol shifts the conversion towards lactate for NAD^+ regeneration (Nunes et al. 2011; Williamson et al. 1967; Costa et al. 2009). Considering that lactate production is increased in A549 cell line, the pools of pyruvate may be diverted for the lactate dehydrogenase (LDH) catalyzed reaction instead of the ALT conversion. Although it is possible that ALT may have an altered expression or function, to the best of our knowledge no reference is made in literature concerning deficiencies of ALT for this cancer cell line. The H1299 cell line exhibits an increased alanine production at 48h, which may be inversely interpreted, due to a decreased lactate production related with a more oxidized cytosol.

The multivariate analysis of ^1H NMR spectra from cell extracts at 48h (Figure 5.3) by principal component analysis (PCA) shows a separation between each cell line. However, a clear gap separates the A549 cell line from the other two cell lines, due to higher scores for lactate concentration and lower alanine and aspartate. Aspartate levels are also regulated by aspartate transaminase (AST), which converts oxaloacetate into aspartate. This is especially relevant in the malate-aspartate shuttle, which allows the transport of $NADH/H^+$ reductive equivalents to the mitochondrial matrix for oxidation in ETC. This malate-aspartate shuttle, in cancer cells, is responsible for shuttling up to 20-80% of the total reducing equivalents generated in the glycolysis, which may account for up to one third of the ATP generated by the ETC (Greenhouse et al. 1977; Thornburg et al. 2008). Therefore, it is expectable that cancer cells with a more active mitochondrial metabolism exhibit higher levels of malate/oxaloacetate and aspartate when compared with more glycolytic cancer cells. Also, by recycling the NAD^+ in the ETC, cells are able to maintain a better redox homeostasis under elevated glycolytic rates. Although metabonomics are still a relatively recent field of research (Nicholson et al. 1999), which

requires robust mathematical and computational approaches, these metabolic data analysis are concordant with the previously discussed metabolites and provides a fast and reliable exploratory approach.

^{13}C NMR experiments allow quantifying metabolism of [U-^{13}C]glucose molecules. Since the natural abundance of ^{13}C in biological compounds is low (~1.1%), the probability of multilabelled species originating from natural abundance is very low (1.1%x1.1%=0.012%), being under most circumstances its contribution disregarded. Therefore, the vast majority of multilabelled end-products are derived from cell metabolism during the incubation period. Extracellular medium from labelled glucose experiments (Figure 5.5) exhibited a linear buildup of lactate with a rather good fit. All cell lines exhibit a significantly different slope, with the MRC-5 non-cancerous cell line possessing the highest rate of lactate secretion. This linearity shows that during the incubation period there were no substrate shortage, otherwise, lactate production would cease and started to be consumed (Kennedy et al. 2013; Abrantes et al. 2014). The coupling between glucose consumption and lactate production given by the fermentation rate is similar for all cell lines (Table 5.2).

Quantification of ^{1}H NMR spectra of cellular extracts (Figure 5.7 - Intracellular levels of lactate, alanine and acetate quantified from aqueous cellular extracts cultured with 10 mM [U-13C]glucose during 48h. Concentrations were quantified from ^{1H} NMR spectra and are expressed in terms of mM/mg protein. Lactate concentration is significantly lower ($p<0.01$) in the MRC-5 cell line when compared to the A549 cell line. Alanine concentration is significantly higher ($p<0.001$) in the MRC-5 cell line when compared to cancerous lines. The H1299 cell line also has a significantly higher concentration ($p<0.01$) when compared to the A549 cell line. Furthermore, MRC-5 cell line is the only exhibiting detectable amounts of ^{13C} labelled alanine. Acetate concentration is also significantly lower ($p<0.05$) for the MRC-5 cell line when compared with the cancer cell lines. Lactate/alanine ratio, an indirect measure of intracellular redox, is significantly higher ($p<0.001$) in A549 and H1299 ($p<0.05$) cell lines relatively to MRC-5 cell line.) shows an increased lactate concentration on the A549 cell line relatively to the non cancerous cell line, in agreement with previous data from unlabelled spectra. The largest proportion of lactate is derived from labelled glucose while unlabelled lactate may be generated from other unlabelled substrates present in the culture media or FBS. Alanine concentration, on the other hand, harbors new information. The MRC-5 cell line is the only cell line with labelled alanine, with a proportion of nearly 1:1 to unlabelled

alanine. Moreover, the total amount of alanine on MRC-5 is substantially higher when compared with cancerous cells. Interestingly, none of the cancerous cell lines exhibit traceable amounts of labelled alanine. Considering the function of ALT as a major regulator of alanine levels, these results imply that in cancer cells, labelled pyruvate arising from glycolytic degradation of labelled glucose is completely redirected for fermentation (supported by the large amounts of labelled lactate) or eventual oxidation at the TCA cycle through pyruvate dehydrogenase (PDH) complex. This phenomenon may be due to cytosolic redox status and/or intracellular compartmentalization of metabolic pathways. An increased glycolytic flux generates a surplus of $NADH/H^+$, which must be recycled back to NAD^+ to continuously supply glycolytic reactions. This is mostly done by fermentation at the LDH or oxidation at ETC. Considering that the Warburg effect is characterized by a lower TCA cycle and ETC activity, LDHA overexpression is a relatively common feature in cancer cells (as discussed in Chapter 1), most of the NAD^+ recycling is performed by lactic fermentation. Compartmentalization greatly aids this aspect. Hexokinase II (HKII) and LDH bound to mitochondria, together with other enzymatic megacomplexes perform an efficient chain reaction from beginning to end (Pastorino et al. 2002; Van Hall 2000). The conjunction of these two factors may explain the absence of significant levels of labeled alanine in cancer cells. In fact, the lactate/alanine ratio is, as previously pointed, an indirect measure of cytosolic redox status and both cancer cell lines have a significantly higher (especially A549 cell line) ratio than the MRC-5 cell line, supporting the notion of an increased pyruvate directed towards fermentation. Acetate levels are also significantly higher in both cancer cell lines. Considering that a large proportion of acetate is labelled, it is derived from labelled glucose. Pyruvate entering mitochondria through PDH forms AcCoA. Acetyl-CoA synthetase converts AcCoA into acetate with a production of an ATP molecule, in a reversible reaction. The isoform 2 of Acetyl-CoA synthetase (ACSS2) has been shown to have an important role in cancer cell survival, acting as a metabolic buffer. Under stress or hypoxia ACSS2 may provide ATP as a fast anaerobic energetic source, secreting acetate. Alternatively, ACSS2 could convert acetate back to AcCoA for biosynthethic purposes (Jones et al. 1993; Schug et al. 2015; Yun et al. 2009), prompting proliferation. Furthermore, this enzyme along with ATP citrate lyase (ACLY), is one of the major

suppliers of cytosolic AcCoA, which is required for *de novo* lipogenesis (DNL), which is heightened in these cancer cells (discussed below).

Completing this data with the ^{13}C isotopomer analysis (Figure 5.9), the TCA coupling is significantly decreased in the A549 cell line. The MRC-5 and the H1299 cell lines have similar TCA couplings. This is in agreement with metabonomics data, where the A549 cell line had a distinct metabolic profile from MRC-5 and H1299 cell lines, being the latter more similar to each other. Since the ratio reflects the amount of carbon skeletons directed for TCA or fermentation, A549 is clearly the most glycolytic and the other two cell lines more oxidative. Nevertheless, the TCA coupling is fairly low for all cell lines. The turnover ratio came as a surprise, since the H1299 cell line possess the highest turnover ratio. Due to the strong glycolytic flux exhibited in the previous experiments it was reasonable to envision that A549 cell line would exhibit a low TCA cycle turnover, fulfilling the characteristics of a 'typical' Warburg phenotype. However, the MRC-5 as a non-cancerous cell line would be expected to have an increased TCA activity. Instead, the MRC-5 cell line attains the same turnover rate of the strongly glycolytic cancer cell line (A549). The MRC-5 cell line was collected from a human fetus at 14 week gestation and still harbors embryonic-like characteristics, which result in bioenergetic metabolic resemblances with cancer cell lines (Bellance et al. 2009). Nonetheless, all cell lines show TCA cycle activity and H1299 succeed at maintaining substantial glycolytic and oxidative profiles. Finally, the anaplerosis is significantly lower in the H1299 cell line comparatively to the other cell lines. However, the high levels of anaplerosis registered in all cell lines are consistent with an increased recruitment of unlabelled substrates from the culture media, such as glutamine, occurring in cancer cells (Le et al. 2012). Due to a mixture of labelled and unlabelled anaplerotic sources present in culture media, this parameter should be considered as semi-quantitative.

The expression of several metabolic related enzymes was analyzed by Western blotting (Figure 5.10). While HKI levels were similar in all cell lines, the HKII levels were decreased in the A549 cell line. As analyzed previously, this cell line possesses the most glycolytic phenotype and HKII is a major contributor for such phenotype. However, the protein loaded on Western blots was from whole extracted cells. It is plausible that the A549 cell line possesses an increased mitochondrial bound fraction of HKII, which

improves the overall activity of the enzyme (Pastorino et al. 2002; John et al. 2011). Glyceraldehyde-3-phosphate dehydrogenase (GAPDH), which is frequently employed as a housekeeping protein, LDHA and pyruvate kinase muscle isozymes 1 and 2 (PKM1/2) levels were also similar between cell lines. Interestingly, PKM2 is similar between all cell lines. The PKM1 is the somatic isoform and PKM2 the embryonic isoform, which has been described has being overexpressed in cancer (Christofk et al. 2008). This shift is a major contributor for the Warburg establishment (see Chapter 1) and is similar between the MRC-5 and the cancer cell lines. This also supports the idea that the MRC-5 cell line still possesses embryonic metabolism characteristics.

Regarding the mitochondrial metabolism (Figure 5.11), the PDH complex expression is significantly increased in the MRC-5 cell line. However, both MRC-5 and H1299 cell lines have an increased TCA coupling. Pyruvate dehydrogenase kinase (PDK) phosphorylates and inhibits PDH complex activity, but the levels of this enzyme are similar in all cell lines. This difference may be explained by differential activities in the cell lines or different regulatory effects by pyruvate dehydrogenase phosphatase (PDP), not analyzed in this study.

The final experiment in this Chapter focused on the characterization of the DNL by ^{2}H enrichment, through a straightforward and relatively new methodological approach (Delgado et al. 2009). As described in the Chapter 4, by comparing the enrichment of the lipid methyl groups with the total lipid content, a quantification of the DNL is possible. Even though the total lipid content was similar in all cell lines (Figure 5.13), the ^{2}H enrichment was approximately three times higher in the cancer cells. This is in agreement with an increased need for biosynthesis of membranes or upregulation of enzymes involved in the pathway during proliferation (Scaglia et al. 2014; Daniels et al. 2014; Menendez et al. 2007). Furthermore, the heightened acetate production may be providing additional AcCoA sources for DNL through the discussed ACSS2 and the increase in choline compounds may be helping maintain the structural integrity of newly formed membranes. Also, the reductive carboxylation operated by isocitrate dehydrogenase (IDH) could also be providing AcCoA, which will be analyzed in the next Chapter (Mullen et al. 2012).

5.4 Conclusion

The lung cancer cell lines exhibited distinct metabolic profiles, as observed through the NMR experiments performed. The A549 cell line is the most glycolytic with low TCA cycle coupling and turnover while H1299 cell line maintains a glycolytic and oxidative profile simultaneously. MRC-5 cell line seems to present metabolic embryonic characteristics, such as the expression of PKM2 and a considerably glycolytic phenotype. Both cancer cell lines exhibit an increased DNL.

Chapter 6
Mitochondrial Function and Reductive Carboxylation

6.1 Introduction

Data collected from the previous Chapter point out to changes in several mitochondrial related metabolic parameters. The coupling between glycolysis and TCA cycle is altered and even TCA cycle turnover and anaplerosis differ between cell lines. As considered in the General Introduction, the deregulation of cellular bioenergetics is in fact a hallmark of cancer. However, this deregulation may arise from a remodeling of glycolytic enzymes, a dysfunctional mitochondrial network, or both.

In order to better understand the metabolic rearrangements occurring in these cells, this Chapter will focus into the mitochondrial function and energetic output. The first parameter to be evaluated was mitochondrial membrane potential through fluorescence microscopy techniques to understand the degree of active mitochondrial network. Then, we looked into the oxidative phosphorylation status by measuring O_2 consumption in a Clark electrode and the response to treatment with classic mitochondrial poisons. Also, the energetic charge of the cells was measured by HPLC techniques for adenine nucleotides quantification. These data were related with the previous isotopomer analysis studies.

With mitochondrial function assessed, we performed silencing studies of the TCA cycle enzyme, IDH. This enzyme converts isocitrate into α-ketoglutarate but it also may operate a reductive carboxylation, converting α-ketoglutarate into isocitrate (see Chapter 1). This reductive carboxylation may provide AcCoA for biosynthetic purposes and favor cancerous growth. With the use of siRNAs we attempted the silencing of the cytosolic IDH1, the mitochondrial IDH2 and both. On these studies we applied isotopomer analysis to better understand the role of this particular enzyme in the tumor metabolism. In these experiments, cell culture media was prepared with 20% $^{2}H_2O$ and supplemented with 10 mM [1,6-$^{13}C_2$]glucose.

This Chapter aims for an integration of mitochondrial function with the metabolic profile. In an attempt to better understand metabolic switches occurring in cancer, the impact generated by IDH1 and IDH2 silencing is analyzed in terms of glycolytic, TCA and DNL fluxes.

The hypotheses are that cancerous cell lines still have an active mitochondrial network despite their altered metabolism. A second hypothesis is that reductive carboxylation through IDH may act as an important supplier of anaplerotic substrates for biosynthetic purposes in cells with active mitochondria.

6.2 Results

6.2.1 Mitochondrial membrane potential

Active and healthy mitochondria are capable of maintaining the membrane potential. In order to assess the mitochondrial membrane potential we performed vital fluorescence microscopy. Three vital fluorescent probes were used (Figure 6.1), each one in a different channel: Hoescht dye the nuclei, in the blue channel; Mitotracker Green dye all mitochondria, in the green channel; TMRM dyes polarized mitochondria only, in the red channel. The merge is a composed imaged of all three probes.

As shown in Figure 6.1, the MRC-5 cell line fibroblast cells are larger, present a fusiform shape and have a well defined mitochondrial network, evenly spread across the cytosol (Mitotracker Green). On the other hand, the cancer cells, A549 cell line exhibited heavily condensed mitochondrial network surrounding the nucleus, with smaller and fragmented mitochondria. The H1299 cell line has a mixed mitochondrial profile with smaller and densely packed mitochondria around the nucleus and larger filamentous mitochondria closer to the cell membrane.

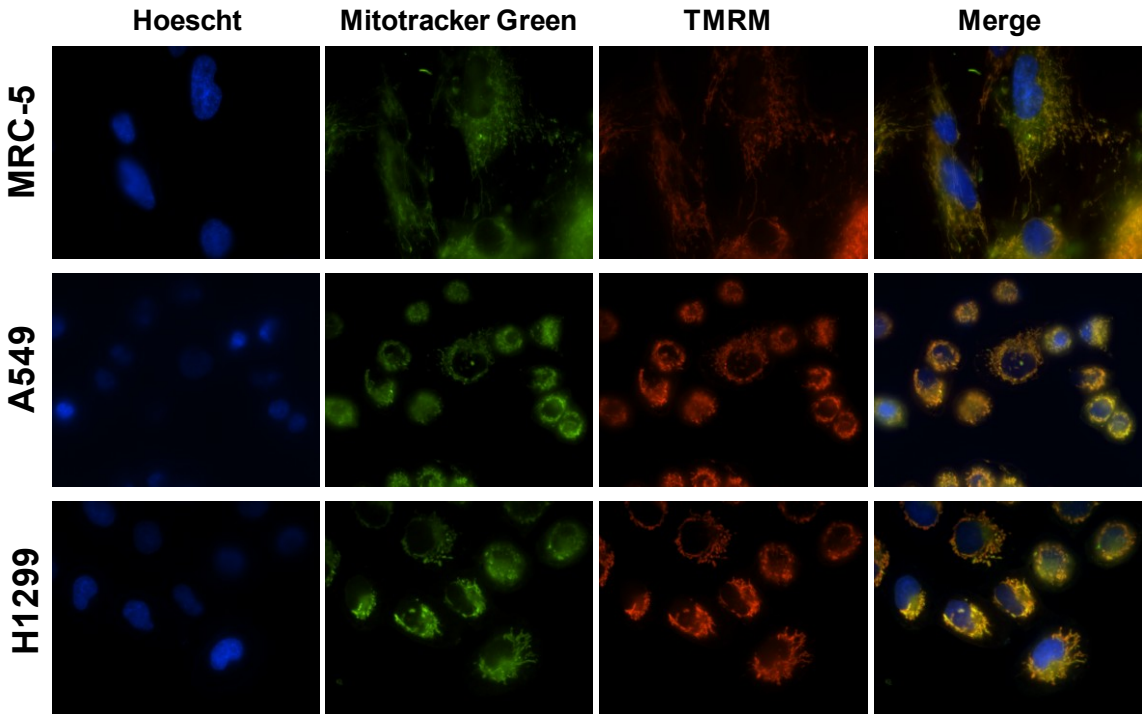

Figure 6.1 – Vital fluorescence microscopy with Hoescht, Mitotracker Green and TMRM. Cells were grown on a glass cover and incubated with a cocktail containing the three probes prior to analysis. Cells were kept in RPMI without phenol red during the process of acquisition. 60x magnification. Hoescht (nuclei). Mitotracker Green (mitochondria); TMRM (polarized mitochondria).

Upon visual analysis of the microscopy images, there are no clear differences between the amount of polarized mitochondria in all cell lines, exhibiting a high degree of overlap between TMRM and Mitotracker Green (showing up as yellow in the merge composed image, Figure 6.1). To understand if there were subpopulations of quiescent mitochondria, the fluorescence signal of both TMRM and Mitotracker Green was quantified and co-localization studies were performed (Figure 6.2). The overlap signaling

is presented in the form of a correlation between both probes. This correlation is slightly superior for the cancer cell lines but the differences are not statistically significant.

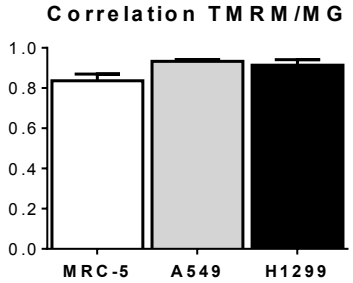

Figure 6.2 – TMRM and Mitotracker Green co-localization presented as a correlation coefficient. Data quantified from microscopy images with magnification of 60x. The overlap of TMRM and Mitotracker Green is greater than 90% for cancer cells. There are no statistically significant differences between cell lines.
Error bars represent SEM, n=3, measured from at least three different fields of view per n. A Kruskall-Wallis test was applied, with p=0.37.

6.2.2 Oxygen consumption and ATP production

In the previous Chapter the metabolic fluxes were analyzed, drawing some considerations about TCA cycle function, but the oxidative phosphorylation performance was not evaluated. Being mitochondria in these cells capable of maintaining their polarization, it is possible that an active ETC may be supplying energy in the form of ATP. We analyzed the O_2 consumption and ATP production to enlighten the oxidative phosphorylation and energetic status.

Oxygen consumption

For oxygen consumption studies, non-permeabilized intact cells were used on a classical Clark type electrode. O_2 consumption was measured in the basal state and cells were sequentially treated with mitochondrial poisons to better define the ETC activity.

The basal oxygen consumption (Figure 6.3) is significantly higher for the H1299 cell line (2.24±0.48 nmol O/min/1×10^6 cell) relatively to MRC-5 ($p<0.01$; 1.60±0.33 nmol O/min/1×10^6 cell) and A549 cell lines ($p<0.01$; 1.24±0.30 nmol O/min/1x10^6 cell).

In comparison with the basal state, oligomycin treatment significantly diminished the O_2 consumption in all cell lines ($p<0.01$ for MRC-5; $p<0.001$ for A549 and H1299 cell lines; not signaled in the graphic). However, oligomycin treated O_2 consumption rates are similar between all cell lines (Figure 6.3). This diminished rate reflects the coupling between O_2 consumption and ATP turnover since oligomycin is an inhibitor of ATP synthase (complex V). The variation can be seen in the cell respiratory function graphic of Figure 6.3 as ATP turnover (light grey). Given that the H1299 cell line possesses a higher basal consumption rate, it suffers a significantly higher drop (1.81±0.38 nmol O/min/1×10^6 cell) comparatively to MRC-5 ($p<0.01$; 1.20±0.37 nmol O/min/1×10^6 cell) or A549 ($p<0.001$; 0.95±0.26 nmol O/min/1×10^6 cell) cell lines. Another calculated parameter is the coupling efficiency, also in Figure 6.3, which is a ratio between the ATP turnover and the basal rate. This parameter is similar in all cell lines and does not reach statistical significance.

The addition of FCCP dissipates the chemiosmotic gradient and uncouples the ETC function from ATP production, thereby achieving a maximal respiratory capacity (Figure 6.3). Relatively to the basal consumption rate, FCCP treatment increase significantly the O_2 consumption in all cell lines ($p<0.01$ for MRC-5 cell line; $p<0.001$ for A549 and H1299 cell lines; not signaled in the graphic). Between cell lines, the H1299 reaches a significantly higher value (5.98±1.65 nmol O/min/1×10^6 cell) when compared with MRC-5 ($p<0.01$; 3.14±0.58 nmol O/min/1×10^6 cell) or A549 ($p<0.001$; 2.14±0.47 nmol O/min/1×10^6 cell). The difference between the maximal respiratory capacity and the basal consumption rate is the spare respiratory capacity. This parameter (shown in white on cell respiratory function graphic) is significantly increased ($p<0.001$) in the H1299 cell line (3.74±1.42 nmol O/min/1×10^6 cell) in comparison with the MRC-5 (1.54±0.41 nmol O/min/1×10^6 cell) or A549 cell lines (0.90±0.26 nmol O/min/1×10^6 cell). The final addition of KCN fully inhibited the respiration in all cell lines.

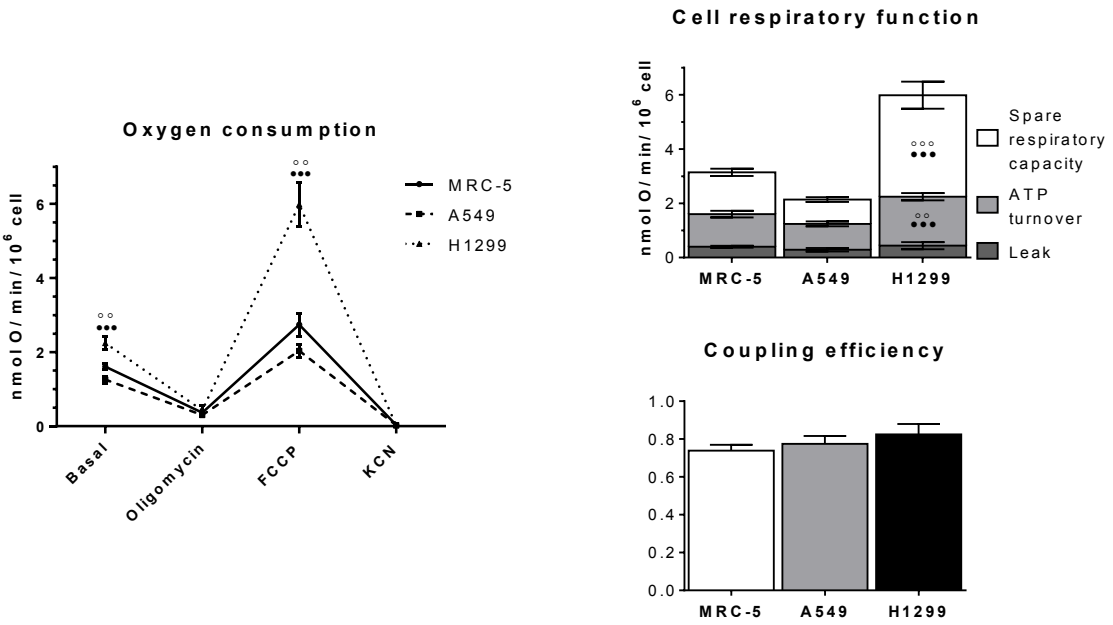

Figure 6.3 – Cell respiratory function. Oxygen consumption of each cell line at the basal state and treated with oligomycin, FCCP and KCN. The H1299 cell line exhibits a higher basal oxygen consumption rate and maximal respiratory capacity (FCCP) than both A549 and MRC-5 cell lines ($p<0.001$; $p<0.01$). The cell respiratory function was assessed by several parameters: proton leak, ATP turnover and spare respiratory reserve. Both ATP turnover and spare respiratory capacity are significantly increased in the H1299 cell line when compared with MRC-5 or A549 cell lines. The coupling efficiency between oxygen with ATP synthesis is similar between all cell lines.
Error bars represent SEM, n=9 MRC-5, A549; n=8 H1299. When possible, a one-way ANOVA was applied with a Tukey post test. * $p<0.05$ between MRC-5 and A549; o $p<0.05$ between MRC-5 and H1299; • $p<0.05$ between A549 and H1299.

Energetic status

The total adenine nucleotide concentrations of cell extracts were also measured to correlate with the oxygen consumption data and assess the energetic status of each cell line.

In Figure 6.4 both ATP/ADP and energy charge ratios of cellular extracts are shown. The commonly described ATP/ADP ratio is significantly increased ($p<0.05$) in the H1299 (18.37 ± 1.58) cell line by comparison with MRC-5 (15.15 ± 1.95) cell line. However, the energy charge ratio, which accounts for ATP, ADP and AMP pools and ranges from 0 to 1, is similar in all cell lines, scoring a value higher than 0.95.

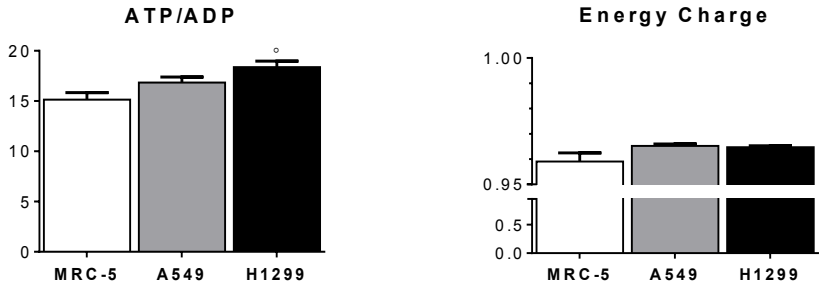

Figure 6.4 – Energetic status presented in the form of ATP/ADP ratio and energy charge. The ATP/ADP ratio is significantly increased in the H1299 cell line when compared to MRC-5 ($p<0.05$) cell line. However, the energy charge ratio is higher than 0.95 for all cell lines and the differences are not statistically significant.
Error bars represent SEM, $n\geq6$. A Kruskall-Wallis was applied with a Dunn's post test. o $p<0.05$ between MRC-5 and H1299.

6.2.3 Expression of mitochondrial related proteins

The expression of some mitochondrial proteins related with mitochondrial function was also assessed by western blotting. In Figure 6.5 are shown the expression levels of subunits of each ETC complex and proteins from different mitochondrial localization.

All ETC complexes have a significantly higher expression in the H1299 cell line when compared to MRC-5 cell line. Between cancerous cell lines, there are significant differences only in complexes I and V, with H1299 cell line exhibiting significantly higher expression levels (Figure 6.5).

The mitochondrial structural membrane integrity (Figure 6.5) was assessed by a cocktail of antibodies targeting proteins in different mitochondrial locations. All cells have similar expression profiles except for porin 1/2 in the outer membrane and cytochrome C in the intermembranar space. The porin 1/2 is significantly increased on the H1299 cell line relatively to MRC-5 ($p<0.05$) cell line. Cytochrome C is significantly increased in the H1299 cell line comparatively to the other cell lines ($p<0.05$).

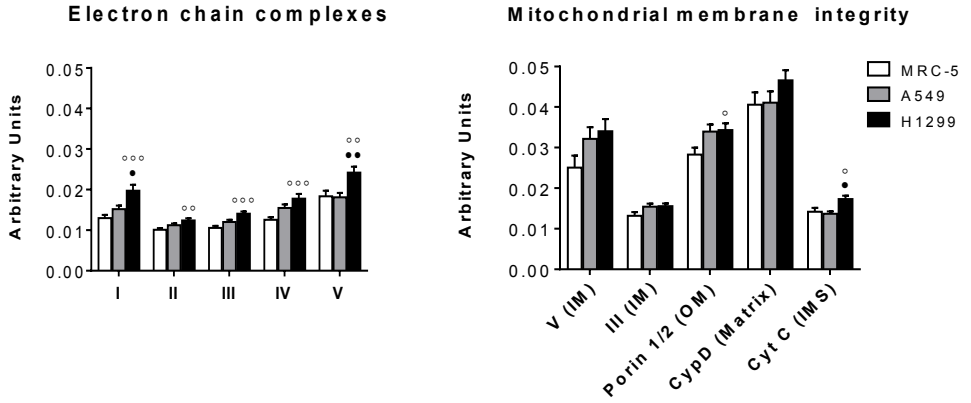

Figure 6.5 – Western blot quantification of mitochondrial proteins. All analyzed electron chain complex subunits have increased expression on the H1299 cell line when compared to the MRC-5 cell line. The H1299 cell line also has significantly higher expression of the complex I and V relatively to A549 cell line. On the mitochondrial membrane integrity, proteins from different mitochondrial localizations were analyzed. All cell lines have similar profiles except for porin 1/2 and CytC. Porin 1/2 is significantly higher on the H1299 cell line in comparison with MRC-5 ($p<0.05$) cell line. CytC is significantly increased on the H1299 cell lines in comparison with both A549 and MRC-5 ($p<0.05$) cell lines. (I) Complex I, 20 kDa; (II) Complex II, 30 kDa; (III) Complex III, 47 kDa; (IV) Complex IV, 39 kDa; (V) Complex V, 53 kDa; (V (IM)), Complex V, 55 kDa; (III (IM)), Complex III, 49 kDa; Porin 1/2, 29 kDa; (CypD), Cyclophilin D, 21 kDa; (CytC), cytochrome C, 12 kDa; (IM) inner membrane; (OM) outer membrane; (IMS) intermembranar space.
Error bars represent SEM (n=12). When possible, a one-way ANOVA was applied with a Tukey post test. * $p<0.05$ between MRC-5 and A549; o $p<0.05$ between MRC-5 and H1299; • $p<0.05$ between A549 and H1299.

Considering the ETC generation of ROS in the form of superoxide anion, the expression of superoxide dismutase (SOD) was also assessed for both cytosolic SOD1 and mitochondrial SOD2 (Figure 6.6). The SOD1 expression levels were similar in all cell lines while SOD2 were significantly decreased in the A549 cell line relatively to MRC-5 ($p<0.01$) and H1299 ($p<0.001$) cell lines.

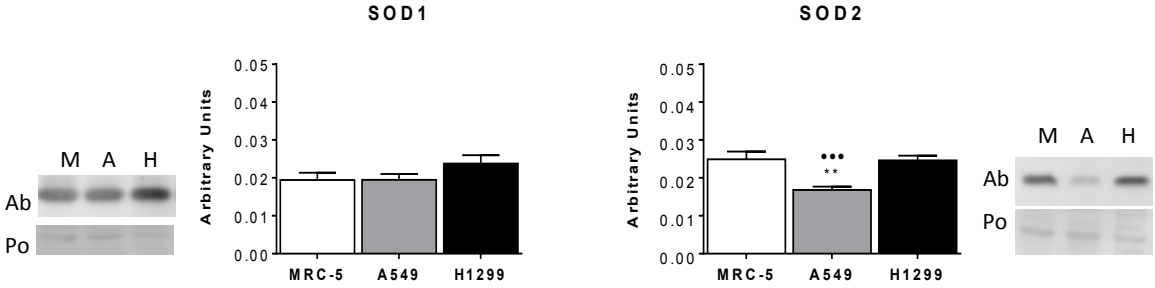

Figure 6.6 – Superoxide dismutase expression levels. Both cytosolic and mitochondrial isoforms expression were quantified by western blotting. While the cytosolic SOD1, 25 kDa, expression is similar in all cell lines, the mitochondrial SOD2, 25 kDa, was significantly lower in the A549 cell line comparatively to both MRC-5 ($p<0.01$) and H1299 ($p<0.001$) cell lines.
Error bars represent SEM. n=12 SOD1, n=8 SOD2. When possible, a one-way ANOVA was applied with a Tukey post test. o $p<0.05$ between MRC-5 and H1299; • $p<0.05$ between A549 and H1299.

6.2.4 Silencing of isocitrate dehydrogenase

The TCA cycle occurring in mitochondria may act as an oxidative pathway for ATP synthesis through the coupled oxidative phosphorylation or may simply provide several anabolic precursors for cellular proliferation. Recently, the reductive carboxylation operated by IDH has been suggested to favor carcinogenic metabolism (see Chapter 1). By converting α-ketoglutarate into isocitrate, the reversible reaction of aconitase on the TCA cycle may provide citrate. This citrate pool may be converted (by ACLY) into AcCoA, becoming available for DNL or other processes. Therefore, aminoacids such as glutamate or glutamine may be used through this pathway as anabolic sources. To evaluate the metabolic impact of the IDH we performed a transient silencing (siRNA transfection) of two isoforms, the cytosolic IDH1 and the mitochondrial IDH2, and both simultaneously. Metabolic effects were assessed using stable isotopic tracers and NMR isotopomer analysis.

During these experiments, some adjustments had to be performed. The first was that the use of MRC-5 cell line had to be abolished in these experiments. The fibroblast cell line, usually more sensitive to manipulation than A549 and H1299 cell lines, did not survive upon transfection. Several transfection protocols were attempted, with different transfection agents and different concentrations, but the adherent cell line always detached and perished. Another issue was the amount of transfected cells for NMR experiments. Since transfection protocols are less efficient in large pools of cells, the final amount of extracted cells in silencing experiments was at least ten times lower than the amount of cells extracted on the experiments performed on Chapter 5. Considering the elevated financial costs of these experiments (and optimization procedures) in terms of reagents, the experimental number had to be reduced. So, both ^{13}C and ^{2}H tracer experiments were performed simultaneously. This approach harbors an additional problem, the coupling between tracers will cause a further splitting of the NMR signal. To circumvent this issue, heightened by the low amount of transfected cells, [1,6-$^{13}C_2$]glucose was used instead of the [U-^{13}C]glucose, providing a better signal/noise ratio.

Metabolic alterations by ^{1}H NMR experiments

Cells were transfected with siRNAs for IDH and grown in 20% $^{2}H_2O$ RPMI media supplemented with 10 mM [1,6-$^{13}C_2$]glucose. At 48h cells were extracted for NMR experiments. The ^{1}H NMR spectra for both A549 and H1299 cell lines extracts for the non-targeting siRNA (NT), IDH1, IDH2 and IDH1+2 are presented in Figure 6.7.

The [1,6-$^{13}C_2$]glucose, through glycolysis and LDH will generate [3-^{13}C]lactate. The unlabeled lactate is a doublet at 1.31 ppm due to the $^{3}J_{HH}$=7.0 Hz. The [3-^{13}C]lactate is a doublet of doublets (instead of doublet of sextets previously analyzed, Chapter 5) due to the additional heteronuclear coupling with C3 ($^{1}J_{HC}$=128 Hz). There is also a small effect due to ^{2}H coupling ($^{1}J_{HD}$ or $^{3}J_{HD}$) and an isotopic shift, moving ^{1}H resonances upfield.

Both A549 an H1299 cell lines present an overall similar ^{1}H NMR spectrum between the non-targeting siRNA and the silenced condition (Figure 6.7). The clearest difference on the A549 cell line is the higher levels of labelled lactate when both IDH1+2 are silenced. The H1299 cell line also shows a similar metabolic profile with the non-targeted condition, however, the alanine levels are diminished in IDH1 and IDH1+2 silencing experiments.

The spectra were quantified and data is presented in Figure 6.8. Labelled lactate levels are significantly increased in the IDH1+2 silencing of A549 cell line (3.02±0.75 mM/mg protein) relatively to control (1.75±0.38 mM/mg protein). However the total amount of lactate (unlabelled plus labelled) is similar in all experiments. On the H1299 cell line, only the unlabelled lactate is significantly increased in the IDH1+2 transfection (0.76±0.04 mM/mg protein) relatively to control (0.64±0.06 mM/mg protein), but again, the total amount of lactate remains similar.

Alanine concentration (Figure 6.8) is ten-fold lower on A549 cell line relatively to H1299 cell line. However, in the A549 cell line, the amount of labelled alanine is significantly reduced in all transfections (17.36±7.44 μM/mg protein for IDH1; 18.80±11.33 μM/mg protein for IDH2; 16.69±2.66 μM/mg protein for IDH1+2) relatively to control (34.61±6.38 μM/mg protein). Furthermore, the total amount of alanine is significantly reduced in the IDH1+2 experiment (43.71±9.80 μM/mg protein) in

comparison with the control (63.88±5.98 μM/mg protein). Analyzing the H1299 cell line, the labelled alanine concentration is significantly decreased in IDH2 (0.32±0.08 mM/mg protein) and IDH1+2 (0.30±0.05 mM/mg protein) relatively to control (0.53±0.12 mM/mg protein). Also, the total alanine amount is significantly reduced in both IDH2 silencing experiments (0.42±0.09 mM/mg protein for IDH2; 0.41±0.08 mM/mg protein for IDH1+2) relatively to control (0.67±0.15 mM/mg protein).

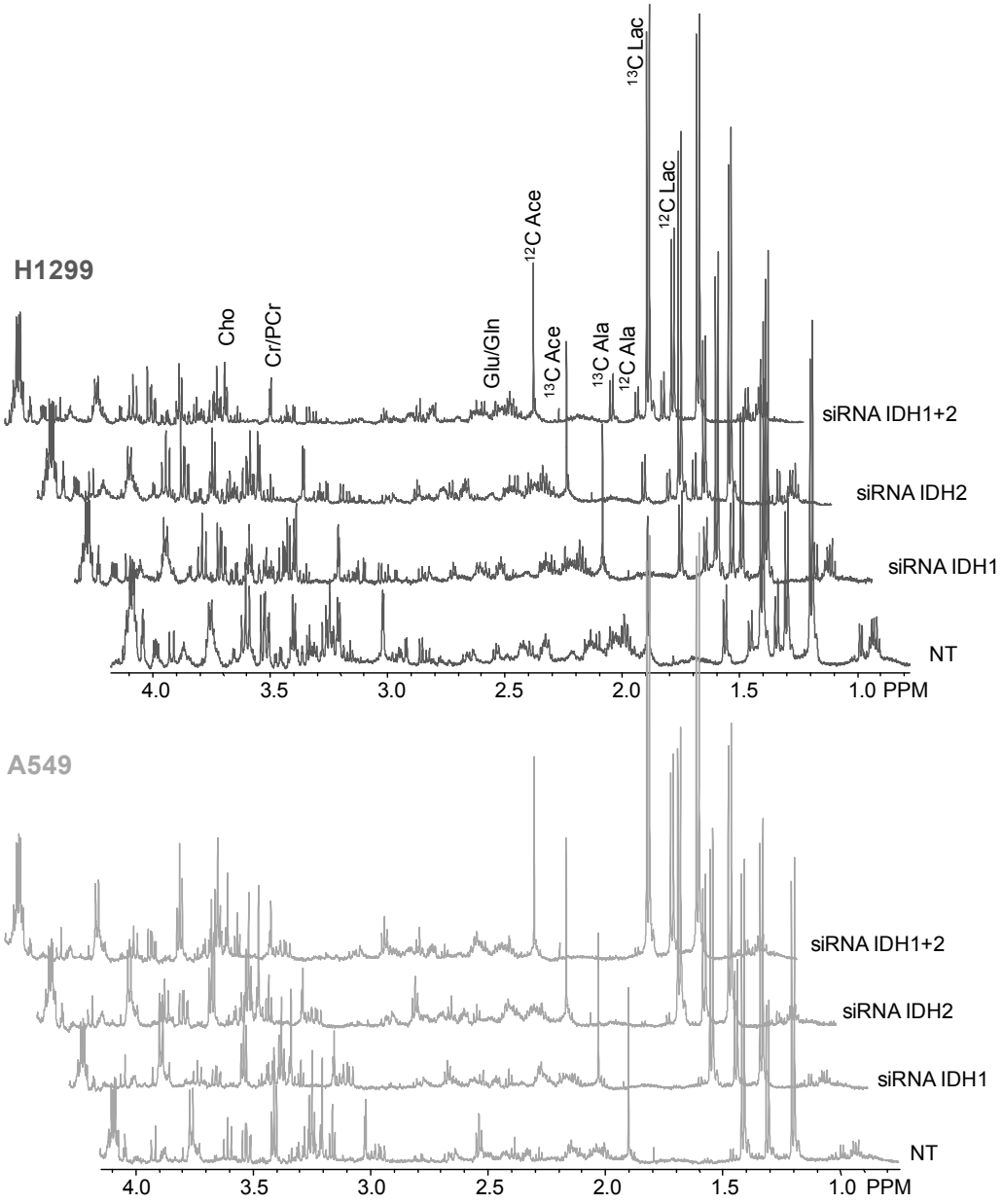

Figure 6.7 - Representative ^{1}H NMR spectra of aqueous cell extracts of transfected cells grown in 20% $^{2}H_2O$ and 10 mM [1,6-$^{13}C_2$]glucose. Expansions from 0.75-4.15 ppm region. For each cell line are shown for comparison the non-targeting siRNA (NT), IDH1, IDH2 and IDH1+2. On the A549 cell line the metabolic profile is similar in all conditions, with exception for the siRNA IDH1+2 which has an increased labelled lactate amount. On the H1299 cell line the alanine levels seem to be diminished on the IDH2 and IDH1+2 silencing experiments. (Ace) acetate; (Ala) alanine; (Cho) choline; (Cr/Pcr) creatine/phosphocreatine; (Glu/Gln) glutamate/glutamine; (Lac) lactate.

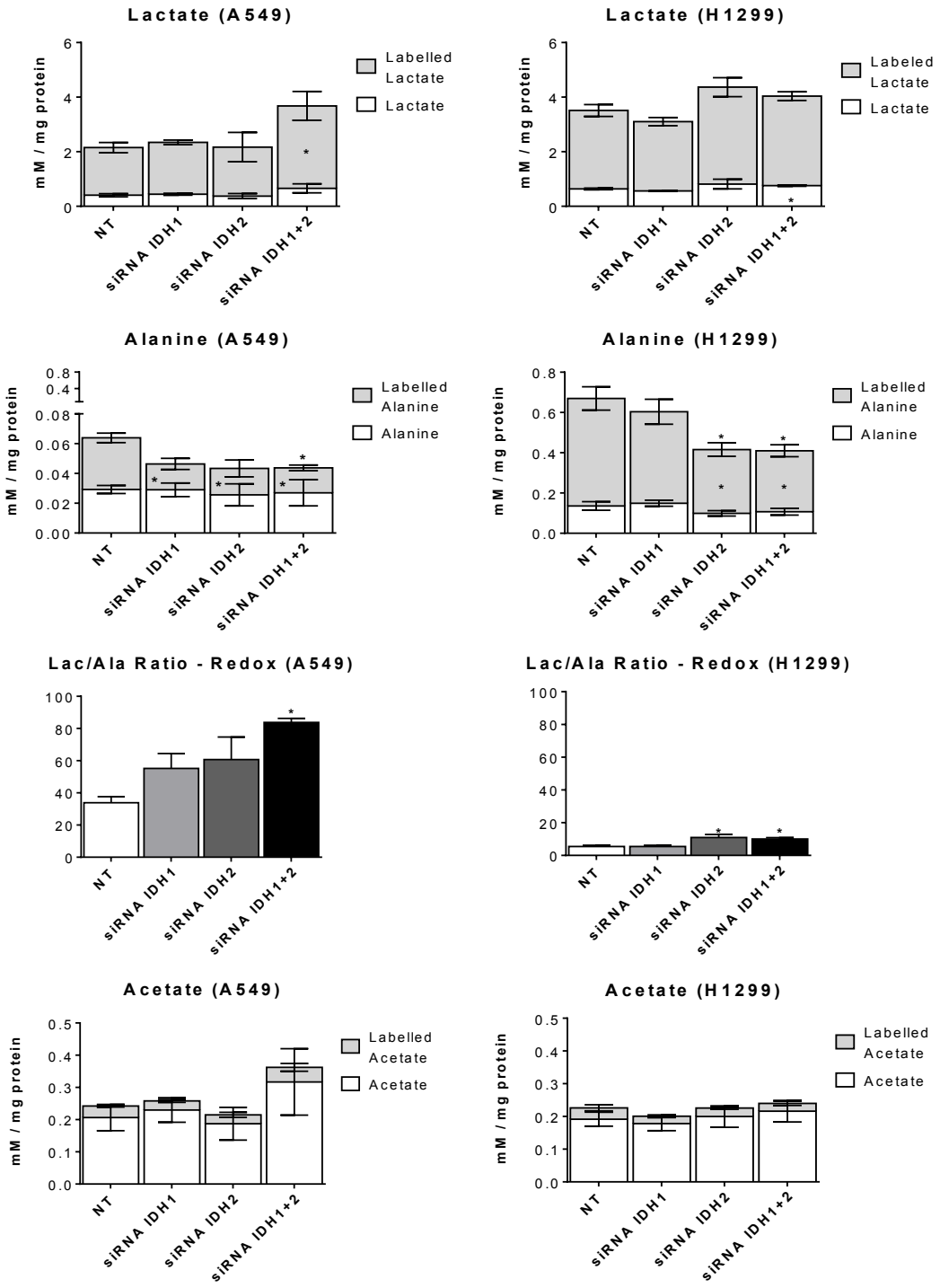

Figure 6.8 – Quantification of metabolites from the ^{1}H NMR spectra of transfected cells. To the left, the A549 cell line and to the right the H1299 cell line. The labelled lactate concentration is significantly higher in the silenced IDH1+2 of A549 cell line while the H1299 exhibits a significantly increase of unlabelled lactate in the IDH1+2 silencing. Labelled alanine concentration is significantly reduced in the IDH1, IDH2 and IDH1+2 treatments and total alanine is also significantly reduced in the IDH1+2. The H1299 cell line has a significantly lower labelled alanine and total alanine levels in the IDH2 and IDH1+2 experiments. The Lactate/Alanine (Lac/Ala) ratio is significantly higher on the IDH1+2 silencing of A549 cell line and on IDH1 and IDH1+2 silencing of H1299 cell line. Acetate levels are similar in both cell lines.

Error bars represent SEM, $4 \geq n \geq 2$. A Student t-test was applied in all comparisons. * $p<0.05$ relatively to NT (non-targeting siRNA).

The lactate/alanine ratio is significantly increased in the IDH1+2 of A549 cell line (83.76±3.57) relatively to control (33.84±7.58). On the H1299 cell line, lactate/alanine ratios increased both for IDH2 (10.97±3.73) and IDH1+2 silencing (10.03±1.45), when compared to the control (5.46±1.54).

The acetate levels are similar between all conditions in both cell lines.

Metabolic alterations by ^{13}C NMR experiments

The analysis ^{13}C spectra from the extracts allow the characterization of intermediary metabolic parameters.

In the Figure 6.9 are shown representative ^{13}C spectra of each cell line for comparison. The expansions show the glutamate C4, C3 and glutamine C4 resonances. The glutamate C4 resonance is composed by a singlet (C4S) at around 34.2 ppm due to [4-^{13}C]glutamate while [3,4-$^{13}C_2$]glutamate gives rise to a doublet (C4D34) due to the $^{1}J_{C3C4}$=34.5 Hz. The coupling between ^{13}C and ^{2}H causes further signal splitting, showing up as unresolved peaks at higher field (lower ppm). Both cell lines exhibit a C4S and C4D (represented as S and D), but it is more intense in the H1299 cell line.

The glutamate C3 is also more visible in the H1299 cell line and presents the same signal profile of the glutamate C3 analyzed on the previous Chapter. It is formed by a singlet (C3S) at around 27.8 ppm from [3-^{13}C]glutamate, a doublet (C3D34) from [3,4-$^{13}C_2$]glutamate and a triplet (T) due to [2,3,4-$^{13}C_3$]glutamate. Again, there are no notorious differences in the NMR spectra of transfected cells (Figure 6.9).

A clear difference between cell lines is the higher levels of labelled glutamine on the A549 cell line. Glutamine C4 is increased, especially in the IDH1 silencing of A549 cell line. The NMR signal is similar to glutamate C4, with a C4S and a C4D34.

The methyl group of labelled lactate shows up as a large singlet at 20.9 ppm due to [3-^{13}C]lactate. Since it is a strong signal, the coupling between ^{13}C and ^{2}H is clearly visible to the left of the singlet. Another singlet shows at lower ppm derived from the deuterium isotopic effect and a triplet upfield due to $^{1}J_{CD}$=19.5 Hz. Also, a smaller

contribution from multiple deuterated species is (barely) visible in some samples (Figure 6.9).

The labelled alanine has a signal around 17.0 ppm, analogous to lactate, and is present in higher concentration on the H1299 cell line. Moreover, the labelled alanine levels appear diminished in IDH2 and IDH1+2 transfections of H1299 cell line. Spectra were quantified and calculated metabolic parameters are exhibited in Figure 6.10.

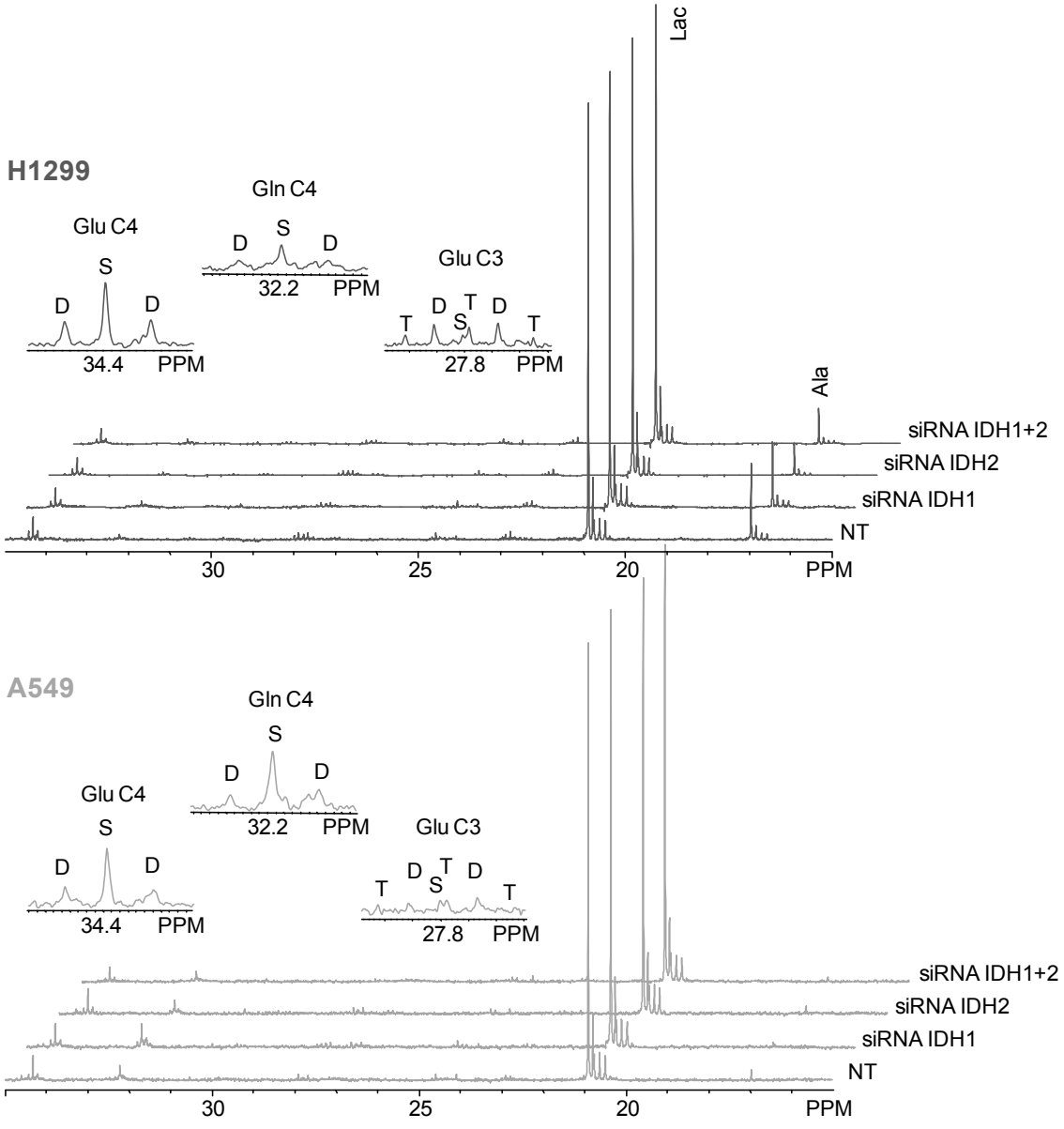

Figure 6.9 – Representative ^{13}C NMR spectra of aqueous cell extracts of transfected cells grown in 20% $^{2}H_2O$ and 10 mM [1,6-$^{13}C_2$]glucose. Expansions of glutamate and glutamine are shown above each set of spectra. The extracts are shown for comparison between the non-targeting siRNA (NT), IDH1, IDH2 and IDH1+2. On the A549 cell line the metabolic profile is similar in all conditions, with exception for the siRNA IDH1 which has an increased glutamine C4 labelling. The H1299 cell line shows diminished levels of labelled alanine on the IDH2 and IDH1+2 silencing experiments. (Ala) alanine; (Glu) glutamate; (Gln) glutamine; (Lac) lactate; (S) singlet; (D) doublet; (T) triplet.

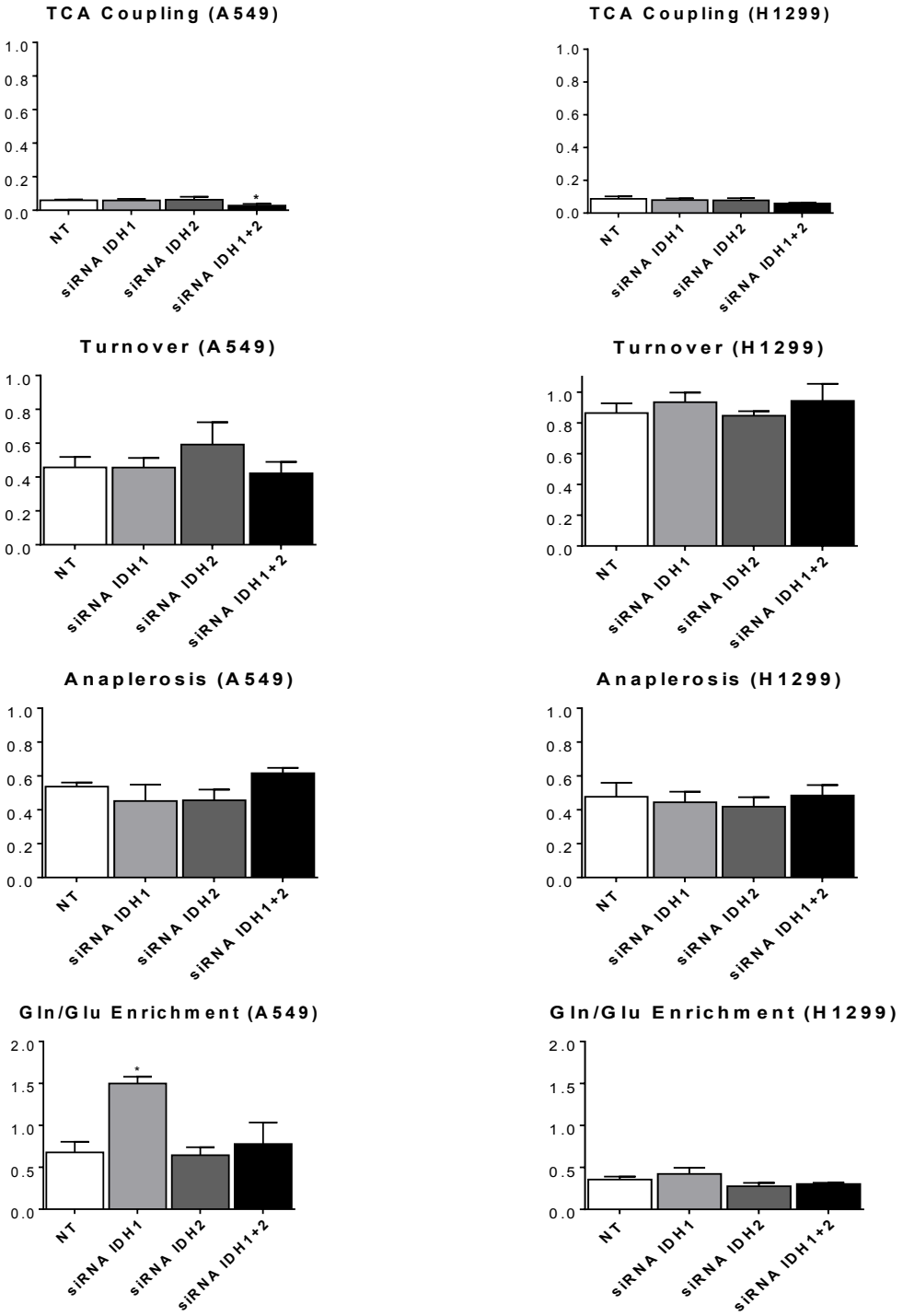

Figure 6.10 – Metabolic parameters quantified from ^{13}C NMR spectra of aqueous cell extracts extracts from cells cultured with 20% $^{2}H_2O$ and 10 mM [1,6-$^{13}C_2$]glucose for 48h. The A549 cell line data are presented to the left and H1299 to the right. Glucose consumption coupled to TCA cycle (glutamate C4/lactate) is significantly lower in the A549 cell line siRNA IDH1+2 experiment. The H1299 cell line has similar values between in all conditions. TCA turnover and anaplerosis are similar in both cell lines and in all conditions. The enrichment of glutamine relatively to glutamate pools are significantly increased in the IDH1 silencing of A549 cell line. The H1299 cell line shows no differences in this ratio.

Error bars represent SEM, $4 \geq n \geq 2$. A Student t-test was applied in all comparisons. * $p<0.05$ relatively to NT (non-targeting siRNA).

The spectra were quantified and the calculated metabolic parameters are present in Figure 6.10 (exhibited in the previous page). The TCA coupling reflects the association between TCA and glycolytic fluxes and is significantly decreased in the A549 IDH1+2 transfected cell line (3.77±0.84 %) relatively to control (5.97±0.84 %). On the H1299 cell line there are no significant differences.

The turnover is a ratio between [3,4-$^{13}C_2$]glutamate and [3-^{13}C]glutamate (C4D34/C4S) and provides a measure of the TCA cycle activity. This parameter is higher in the H1299 cell line but in each cell line there are no significant differences between transfections.

The anaplerosis also exhibits similar results in all experiments in both cell lines.

Considering the large amounts of labelled glutamine exhibited on the A549 cell line spectra, glutamine C4 labelling was quantified and is exhibited as a ratio between glutamine and glutamate pools (Figure 6.10). The ratio is significantly increased in the A549 IDH1 transfected cells (1.50±0.16) when compared with control (0.68±0.25).

Impact on *de novo* lipogenesis by ^{1}H and ^{2}H NMR experiments

To analyze the impact of IDH silencing on DNL, organic extracts were collected for ^{1}H and ^{2}H NMR experiments. Representative NMR spectra are shown in Figure 6.11 for each silencing experiment.

In both cell lines there are no clear differences between the transfected cells and control experiment. The methyl and methylene groups are visible in both spectra. In fact, due to the employment of combined ^{13}C and ^{2}H, an isotopic effect occurs in the ^{2}H NMR spectra. Analyzing the deuterated methyl group of lipids, we are able to define a singlet and a doublet. On the ^{2}H NMR spectra, the singlet at around 0.89 ppm is derived from deuterated methyl groups of fatty acids. The doublet is slightly dislocated upfield due to the deuterium isotopic effect, and is generated by a heteronuclear $^{1}J_{DC}$=19.5 Hz arising from ^{13}C-enriched pools of AcCoA.

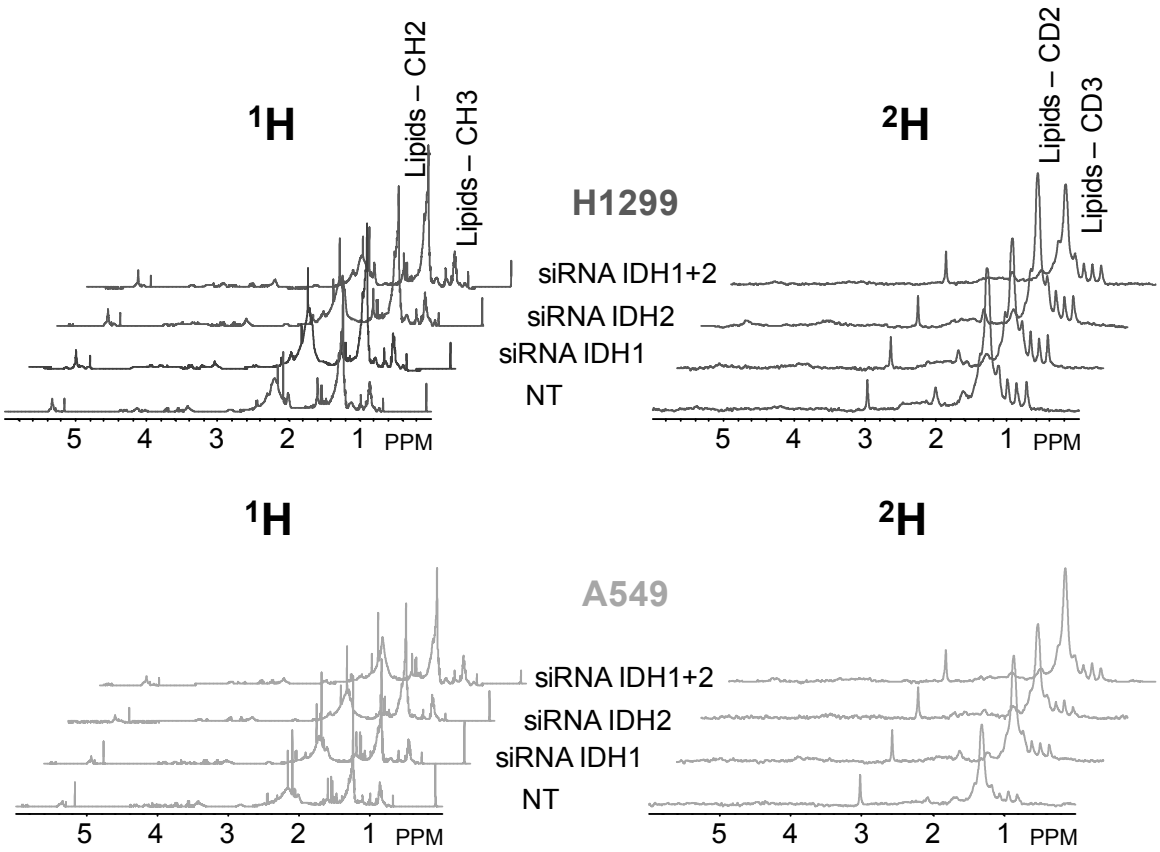

Figure 6.11 - Representative ^{1}H and ^{2}H NMR spectra of organic cellular extracts cultured with 10 mM [1,6-$^{13}C_2$]glucose and 20% $^{2}H_2O$. On the left are shown the ^{1}H NMR spectra and on the right the corresponding ^{2}H NMR spectra, with an expansion of the region 0.0-6.0 ppm. Pyrazine was used as internal standard and lipids can be identified as two broad peaks, one relative to the terminal methyl group and another from the aliphatic chain. Upon visual inspection of extracts, no clear differences appear between the different experiments and control (NT).

The quantification of the terminal methyl group in both spectra allows the quantification of DNL rates, shown in Figure 6.12. The amount of terminal methyl group is proportional to the amount of lipids. The labelled fraction is much smaller than the unlabelled. In the A549 cell line, the unlabelled lipid fraction of siRNA IDH1+2 transfected cells is significantly increased (1.48±0.42 μmol/mg protein) relatively to control (0.90±0.07 μmol/mg protein). This increase translates into a total methyl content significant increase (1.52±0.43 μmol/mg protein) in comparison to control (0.93±0.07 μmol/mg protein). The ^{2}H enriched fraction of A549 siRNA IDH1 transfected cells (0.036±0.006 μmol/mg protein) are significantly increased relatively to control (0.026±0.005 μmol/mg protein). On the H1299 cell line, all experiments are similar with

the exception of siRNA IDH1+2, where the ^{2}H enriched fraction (0.033±0.001 μmol/mg protein) is significantly lower than control (0.049±0.006 μmol/mg protein).

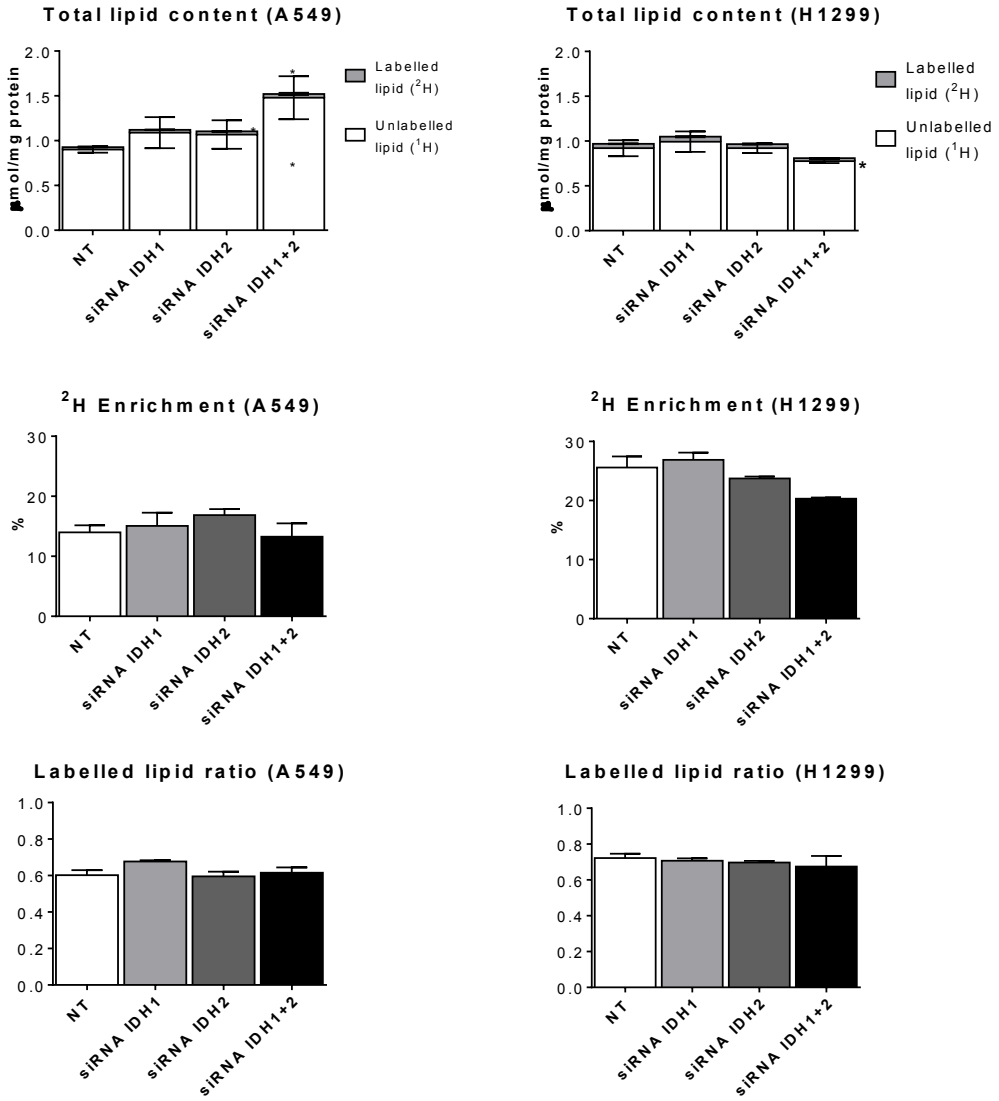

Figure 6.12 – Total lipid content, lipid ^{2}H enrichment ratio, and ^{13}C labelled lipid ratio (from terminal methyl group). Total lipid content is mostly derived from unlabelled sources while the fractional ^{2}H labelled lipids are a very small contribution on the top on the column, expressed in terms of μmol/mg protein. The A549 cell line has a significantly higher lipid content on the IDH1+2 cells, due to a significantly increased fraction of unlabelled lipids. Also, the IDH2 transfected cells have significantly higher levels of ^{2}H enriched lipids. The H1299 cell line has similar values in all transcfections, with the exception of IDH1+2 silencing, which have a significantly diminished ^{2}H fractional labelling. Despite these differences, the ^{2}H enrichment, a measure of DNL rates, is similar between transfection and control in both cell lines. The ^{13}C labelled lipid allows a characterization of the carbon source of newly synthesized fatty acids. Both cell lines have a ^{13}C labelled fraction of ≈60% or higher, but without significant differences between transfections.
Error bars represent SEM, 4≥n≥2. A Student t-test was applied in all comparisons. * p<0.05 relatively to NT (non-targeting siRNA).

Despite the previous differences, the ratio between labelled and total methyl groups, reflecting the ^{2}H enrichment, is similar between all silencing experiments and control (Figure 6.12). However, the H1299 cell line possesses higher enrichment values relatively to the A549 cell line.

Also, the ^{13}C labelled lipid ratio, a ratio between CD3 doublet and total CD3, does not show any differences between treatments. This reflects the ratio of ^{13}C labelled carbon incorporated into newly synthesized fatty acids, which achieves the value of 60.2±5.5 % for A549 cell line and 72.2±4.2 % for H1299 cell lines on the control experiments (NT).

6.3 Discussion

This Chapter has focused on mitochondrial metabolic performance and its relation with the isotopomer analysis previously made. Moreover, the impact of TCA cycle anaplerosis through reductive carboxylation prompted by IDH was assessed by silencing experiments and isotopomer analysis.

In the previous Chapter, TCA cycle parameters calculated by ^{13}C NMR experiments, namely the TCA coupling and turnover were different among cell lines. This could be due to dysfunctional mitochondria, hence the mitochondrial network and membrane potential status was analyzed through vital fluorescence microscopy (Figure 6.1). The MRC-5 cells are larger than the cancer cells, exhibiting a typical fusiform structure, a spread mitochondrial network and interconnected elongated mitochondria. The A549 cell line, on the other hand, possesses a heavily packed mitochondrial network, with small and fragmented mitochondria. The H1299 cell line has a mixed mitochondrial network profile, with small, heavily packed mitochondria near the nucleus and more disperse and elongated mitochondria in the outer regions of the cell. In fact, the mitochondrial structural change from elongated to round mitochondria has been described as an adaptation to energy substrates (Hackenbrock 1968). Under a higher respiratory activity, mitochondria adopt a more elongated form with larger intercristae spaces while in glycolytic cells with low O_2 consumption they appear smaller,

fragmented and with an expanded matrix (Rossignol et al. 2004; Hackenbrock 1968). These data correlates with the data from TCA coupling where both MRC-5 and H1299 cell lines exhibit a higher TCA coupling, therefore a higher TCA cycle activity and more elongated mitochondria. The fluorescence overlap between TMRM and Mitotracker Green is approximately 90% for all cell lines, showing that mitochondria are viable and functional (Figure 6.2). This data supports the notion that the differential TCA cycle activities in these cells are due to metabolic pathway remodeling and not to a mitochondrial failure. Several types of cancer cell lines, including A549 cell line, exhibit a mitochondrial membrane hyperpolarization, which results in an increased therapeutic and apoptosis resistance (Bonnet et al. 2007).

To better understand the mitochondrial membrane potential and TCA cycle activity, the oxidative phosphorylation was assessed through the O_2 consumption on intact cell lines (Figure 6.3). The basal O_2 consumption rate is significantly higher on the H1299 cell line relatively to the other cell lines. This data is in agreement with the TCA cycle turnover measured in the previous Chapter, where the H1299 cell line exhibited the highest rate. A higher turnover will generate more reducing equivalents, which can be oxidized in the ETC with the respective O_2 consumption. With the inhibition of ETC complexes with mitochondrial poisons or uncoupling ATP production from O_2 consumption, several respiratory parameters were calculated. By injecting oligomycin, the ATP synthase (complex V) is inhibited, causing a diminished O_2 consumption. The difference from this inhibited state to the basal rate reflects the ATP turnover and H1299 exhibited a higher ATP turnover comparatively to the other cell lines. In other terms, the O_2 amount used for ATP synthesis is higher on this cell line. However, the ATP coupling is similar for all cell lines. This ratio is a more trustworthy parameter for the assessment of O_2 consumption coupled ATP production since it is the fraction of basal O_2 consumption allocated to ATP synthesis, therefore, internally normalized (Brand et al. 2011). The obtained values for the coupling efficiency are high (>0.7) in all cell lines, reflecting a good mitochondrial and ETC function. This data is in agreement with the mitochondrial membrane potential, where all cell lines exhibited large pools of polarized mitochondria. The FCCP treatment uncouples the O_2 consumption from the chemiosmotic gradient, therefore achieving a maximal respiration, and the difference to

the basal state is the spare respiratory capacity. This spare respiratory capacity is higher in the H1299 cell line relatively to the other cell lines, which indicate that the H1299 cell line is operating farthest from their bioenergetic limit (Brand et al. 2011). In the event of stress stimuli, where an increased demand of ATP is required, the H1299 cell line exhibits a larger buffer zone relatively to MRC-5 and A549 cell lines, which are working closer to their limit capacity (Sriskanthadevan et al. 2015). KCN inhibited completely the respiration at the complex IV and the difference to the oligomycin treatment is relative to the proton leak. This parameter exhibits low values for all cell lines, which indicate good membrane structural integrity and allow the maintenance of a high mitochondrial membrane potential.

The adenine nucleotide concentration was also assessed by HPLC (Figure 6.4). While the ATP/ADP ratio is higher in the H1299, the energy charge is similar between all cell lines. Given that through HPLC we were able to quantify AMP levels, the energy charge is a more robust ratio than just ATP/ADP ratio since it accounts for all nucleotide contributions (Atkinson et al. 1967). The energy charge is higher than 0.95 for all cell lines, implying that the energetic supply in these cancer cells is not limiting. In fact, some authors consider that ATP is not a limiting factor and the Warburg effect is not mainly focused on energetic demands but rather on biosynthetic purposes for rapid cell proliferation (Vander Heiden et al. 2009; Locasale et al. 2010).

The expression of mitochondrial enzymes was assessed by Western blotting (Figure 6.5). All ETC complexes expression levels were higher in the H1299 cell line relatively to the MRC-5 cell line. The low expression levels of ETC complexes together with the low TCA cycle turnover on the MRC-5 cell line explains why both MRC-5 and H1299 cell lines have similar TCA couplings but different basal O_2 consumption. The A549 cell line has a decreased complex I and V expression relatively to the H1299 cell line. The complex I catalyzes the transfer of two electrons from NADH to ubiquinone with the translocation of 4 protons and is a major site of reactive oxygen species (ROS) production. A lower expression together with a lower TCA coupling may result in reduced generation of ROS, providing protection against apoptosis (Hirst et al. 2008). Also, mildly dysfunctional complex I may aid the establishment of the Warburg effect, however this mechanism is still not consensual (Iommarini et al. 2013; Calabrese et al.

2013). Nevertheless, the O_2 consumption data and show that the three cell lines have ETC activity and similar ATP coupling efficiencies despite different expression profiles. However, the higher spare respiratory capacity exhibited by the H1299 cell line can in fact be explained by the higher expression levels of the ETC complexes.

The mitochondrial membrane integrity possesses a cocktail of mitochondrial proteins from different localizations in the mitochondria (Figure 6.5). The cytochrome C (Cyt C) expression is higher on the H1299 cell line. Since all complexes were increased in the H1299 cell line, Cyt C expression is expectedly increased since it is a critical electron transporter between complex III and IV. Porin 1/2 expression is also significantly increased in the H1299 cell line relatively to the MRC-5 cell line. This antibody targets the voltage-dependent anion channel (VDAC) and an increase of VDAC expression in the outer membrane sensitizes the cells to apoptosis. VDAC, Cyt C and ROS generation are known triggers of apoptosis, which is consistent with H1299 cell line higher O_2 consumption and TCA cycle turnover rates (Sharaf El Dein et al. 2012; Vega-Naredo et al. 2014). Nevertheless, all membrane integrity markers are present and with several similar values, suggesting good membrane integrity, in agreement with the proton leak and mitochondrial membrane potential analyzed previously.

Finally, the superoxide dismutase (SOD) expression was also assessed (Figure 6.6). While cytosolic isoform SOD1 expression is similar between all cell lines, mitochondrial isoform SOD2 expression is lower in the A549 cell line. Considering the small and fragmented mitochondrial network in the A549 cell line, SOD2 reduced expression can be a response to such remodeling. The reverse applies to the MRC-5 and H1299 cell lines, which exhibit more elongated mitochondria and a higher TCA coupling.

The isotopomer analysis on the Chapter 5 suggested high anaplerotic rates. A plausible anaplerotic route was through a TCA cycle enzyme, the isocitrate dehydrogenase (IDH). As discussed in the Chapter 1, this enzyme has three isoforms, two mitochondrial (IDH2 and IDH3) and one cytosolic (IDH1). Adipocytes and cancer cells under hypoxia or with defective mitochondria have been shown to catalyze a reductive carboxylation through IDH, generating isocitrate from α-ketoglutarate (Yoo et al. 2008; Mullen et al. 2012; Metallo et al. 2012). By performing the reverse reaction, cells can

obtain AcCoA from glutaminolysis, providing carbon skeletons for aminoacid, nucleotide or lipid synthesis (See Chapter 1). We set out to clarify the impact of this reversible enzymatic process on carbon metabolism and *de novo* lipogenesis (DNL). These experiments required a few adjustments and optimizations and the MRC-5 cell line had to be removed from the experiment due to toxicity related with the lipid-based transfection reagent. The experiments were performed on both cancer cell lines and four silencing condition were assessed, the non-targeting (NT) siRNA as a control, the IDH1 siRNA, the siRNA IDH2 and both siRNA1+2. All experiments were compared with the siRNA NT.

The ^{1}H spectra were quantified (Figure 6.8) and several metabolites were measured. The labelled and unlabelled lactate was the first to be analyzed. Only A549 siRNA IDH1+2 transfected cells showed higher labelled lactate levels while siRNA IDH1 and siRNA IDH2 lactate levels remained similar. Nonetheless, the total amount of lactate was not significantly altered in none of the experiments, only a rearrangement of the labelled and unlabelled fractions occurred at the siRNA1+2 transfected cells (similar on H1299, discussed below). The silencing of just one isoform does not alter significantly the glycolytic flux, implying that either IDH1 or IDH2 are capable of individually overcome the suppression of the counterpart, acting probably as a redundant mechanism, even though these have different genetic, tissue and subcellular localizations (Lee et al. 2002; Macdonald et al. 2013). When both isoforms are silenced, the A549 cell line labelled lactate levels is altered.

The labelled alanine levels, on the other hand, are diminished in all siRNA IDH1/ IDH2/ IDH1+2 transfections of the A549 cell line (Figure 6.8). However, only the siRNA IDH1+2 transfection exhibits total lower alanine content. While the decrease in siRNA IDH1+2 transfection may be explained by the shift of alanine towards the generation of labelled lactate seen in the previous analysis, siRNA IDH1 and IDH2 do not exhibit altered labelled lactate levels. Since IDH1 and IDH2 reactions have a coupled conversion of $NADP^{+}$/NADPH, one might envision the deregulation of redox homeostasis and antioxidant defenses upon silencing of these enzymes. One main non-enzymatic defense is the glutathione (GSH) which is oxidized to glutathione disulfide (GSSG) and requires NADPH for the regeneration of the GSH and IDH1 was described as essential for

maintaining a reduced pool of GSH (Lee et al. 2002). In fact, the redox status provided by the lactate/alanine ratio (an indirect measure of redox, discussed in the previous Chapter) is altered in the siRNA IDH1+2 transfection. However, the alteration on the alanine levels by individual siRNA IDH1 or siRNA IDH2 transfections in not sufficient to achieve statistical significance. The acetate levels do not vary significantly between transfections, although siRNA IDH1+2 have a rather large error.

The H1299 siRNA IDH1+2 transfection exhibited higher levels on the unlabelled lactate fraction, certainly due the degradation of unlabelled sources. On this cell line, only the siRNA IDH2 and siRNA IDH1+2 transfections lowered the labelled alanine fraction and total alanine content. The cytosolic IDH1 silencing does not affect alanine levels as described for the A549 cell line. The cytosolic redox by the lactate/alanine ratio is significantly increased in the siRNA IDH2 and IDHI+2 transfections of the H1299 cell line. Even though IDH2 is located in the mitochondria, the reducing equivalents may cross mitochondrial membrane through the malate-aspartate shuttle and alter the cytosolic redox. Furthermore, the reductive carboxylation by IDH is regulated by nicotinamide nucleotide transhydrogenases (NNT), which convert the NADH into NADPH and vice-versa (Gameiro et al. 2013a). This supports the notion of a redox regulatory effect by IDH. However, the sources of $NADP^+$/NADPH and the mechanisms of redox balance operated by IDH are still a matter of debate (Smolková et al. 2012). The acetate levels on the H1299 cell line are similar between all transfections.

Analyzing the ^{13}C spectra and further metabolic information (Figure 6.10) we can observe that the TCA coupling is very low for both cell lines, with most of the carbon skeletons being directed towards lactic fermentation. However, the siRNA IDH1+2 transfection of A549 cell line exhibits a lower TCA coupling relatively to control, in agreement with the previously discussed labelled lactate increase in the ^1H spectra. However the turnover and anaplerosis do not exhibit any differences between transfections or cell lines. However there is an intriguing result at the glutamine/glutamate enrichment. The A549 siRNA IDH1 transfected cells possess a higher labelled glutamine fraction. This may indicate that cytosolic IDH1 may be regulating glutamine synthetase activity. Although this association is not clear, in a study in rat liver about alcohol consumption, both IDH1 and glutamine synthetase (GS) were

clustered together in the proteomics analysis, suggesting a direct regulation of IDH1 on GS (Aroor et al. 2012). Moreover, is it plausible that the reductive carboxylation operated by IDH1 may help regulate the pools of cytosolic α-ketoglutarate, therefore modulating the availability of glutamate has a substrate for GS. However this effect is not observed in A549 siRNA IDH1+2 transfected cells suggesting that this effect may be dependent on the intracellular redox status. Also, in several cell lines, the severe knockdown of cytosolic IDH1 resulted in non viable cells, suggesting that IDH1 plays an important cytosolic function (Macdonald et al. 2013). The possibility of a futile cycle between glutamate and glutamine in the liver was already proposed (Desmoulin et al. 1985) and could act has a sensor of glutamine/glutamate pools or possibly as an ammonia level regulator. Nonetheless, this hypothesis requires further research.

The ^{2}H experiments revealed the metabolic data about DNL (Figure 6.12). The total lipid content measured from the methyl resonance was increased in the siRNA IDH1+2, due to a higher unlabelled fraction. This implies that silencing of IDH1+2 causes an increase of lipid content as a response to an altered cytosolic redox, seen at the ^{1}H experiments. The A549 siRNA IDH2 and the H1299 siRNA IDH1+2 exhibit an increased labelled lipid fraction. However the ^{2}H enrichment is not altered in any condition or cell line. Also, given the mixture of ^{13}C and ^{2}H labelling, we are able to compare the AcCoA carbon skeleton sources in the methyl group resonance due to the coupling between the nuclei. Although there are no differences among groups in the ^{13}C labelled lipid ratio, we can point out that the majority of the carbon sources employed in DNL (>60% approximately) is derived from labelled glucose, under our experimental conditions.

Although IDH is a metabolically interesting enzyme, the major focus of IDH research in the recent years is the relationship with mutant IDH and cancer (such as gliomas). Even though IDH1 is a potential diagnostic and prognostic biomarker in non-small cancer, the same type of cancer of our cancer cell lines, the literature does not describe any mutated IDH isoform for A549 or H1299 cell lines (Tan et al. 2012). Considering that the reductive carboxylation only occurs in large scale under specific settings such as hypoxia or defective mitochondria, we believe that in the A549 and H1299 cell lines, the reductive carboxylation accounts for only a small contribution (Mullen et al. 2012; Metallo et al. 2012). This is based on the fact that the ^{13}C

metabolism on the silenced IDH experiments did not exhibited large differences but rather a redox alteration. The same is applied to ^{2}H experiments, where no clear differences were observed at the ^{2}H lipid enrichment and the major carbon source of DNL is glucose-derived AcCoA. Additionally, considering that mitochondria in these cells are functional, as analyzed in this Chapter, we cannot conclude that, in this experimental setup, the mitochondria are defective and employ large reductive carboxylation rates. Unfortunately, the A549 siRNA1+2 (^{1}H and ^{13}C experiments) and the H1299 siRNA1+2 (^{2}H experiments) groups have a low experimental number (n=2) due to extraction procedure problems and the author safeguards the possibility of erroneous data interpretations in these specific datasets.

6.4 Conclusion

All cell lines have a good energetic charge and exhibit active and functional mitochondria with intact membranes and capable of maintaining polarization. The H1299 cell line exhibits a higher basal O_2 consumption and a higher spare respiratory capacity due to a higher expression of all ETC complexes. However, the ATP coupling efficiency is similar in all cell lines despite their differential O_2 consumption and metabolic profiles.

Both IDH1 and IDH2 are involved in redox homeostasis of the lung cancer cell lines and IDH1 may have a regulatory effect on the glutamine pools. The reductive carboxylation operated by these enzymes does not play a significant role on anaplerosis or DNL in these cells, under normoxic conditions.

Chapter 7
Cellular Proliferation under Substrate Modulation and Metabolic Inhibitions

7.1 Introduction

As seen in the General Introduction, cancerous carbon metabolism possesses evident plasticity, allowing the recruitment of different types of substrates for anabolic purposes. This final Chapter will focus on substrate affinity and metabolic modulation by key-enzyme inhibitors in an attempt to decipher the connection between glycolytic and mitochondrial metabolism. This interplay may be important for the detection of metabolic relevant targets, unraveled in this chapter by specific pathway inhibition. Certainly, the improvement of co-adjuvant therapies will, in the future, increase success rates in cancer treatment.

The studied cells present heterogeneous metabolic profiles as seen by the previous metabolic characterization, with functional and active mitochondria. Their sensitivity to different inhibitors was assessed by cell proliferation assays. First, cell proliferation studies were applied with different media formulations to analyze the

substrate dependency of each cell line. The media was reconstituted without glucose, with galactose instead of glucose and without glutamine.

The following experiments involve the use of metabolic inhibitors, some of them already in clinical trials and used as co-adjuvant therapy. Most of the inhibitors employed are small molecules referenced in the General Introduction and the main focus will be the inhibition of glycolysis, TCA cycle, PPP and transaminases. These experiments are performed in regular culture media and three different concentrations are tested for each cell line.

This Chapter aims at a characterization of substrate affinity for each cell line through the modulation of substrates and pathway inhibition. In parallel, the effects of drugs in cancer proliferation will be analyzed as potential chemotherapeutic agents and their efficiency correlated with metabolic data.

The hypothesis is that each metabolic profile confers sensitivity to a different set of metabolic inhibitors and substrate media composition. Also, glutamine metabolism (and transaminases) inhibition must play an important role in cancer cell proliferation and has to be tackled towards better definition of substrate relevance in cell proliferation.

7.2 Results

7.2.1 Growth curve

To initiate the studies, a normal growth curve was performed with regular RPMI culture media, 10 % FBS, 10 mM glucose. The assay performed for measuring cell proliferation is the SRB assay.

In the Figure 7.1 the growth for each cell line is plotted as absorbance (from data collected from SRB assay) as a function of time. The data was fitted with a non-linear 4 parameter logistic regression, with an r^2=0.944 for MRC-5 (full line) cell line, r^2=0.984 for A549 (dashed line) cell line and r^2=0.987 for H1299 (dotted line) cell line. Above and

below each regression are the 95% prediction bands represented as small dotted lines. The H1299 cell line is the fastest growing cell, closely followed by A549 cell line, while the non-cancerous cell line MRC-5 is the slowest. Regression parameters show that during the exponential phase of growth, the slope is significantly lower for MRC-5 cell line ($p<0.05$; 2.90 ± 0.45) when compared with both cancer cell lines (4.34 ± 0.37 for A549; 4.24 ± 0.26 for H1299). For the following studies, a shorter timeline was selected, 120h for substrates studies and 96h for inhibition experiments to avoid over-confluency bias.

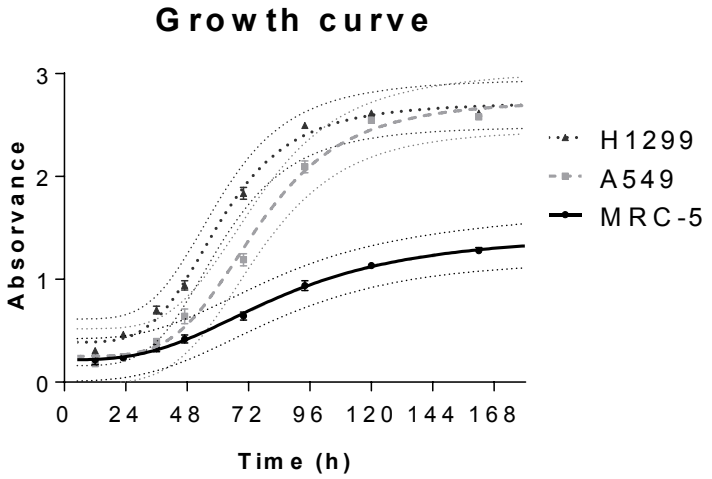

Figure 7.1 – Growth curve for each cell line. Cells were seeded and proliferation was assessed by the SRB assay over 160h. The H1299 cell line has the fastest growth rate, while MRC-5 cell line is the slowest.
Error bars represent SEM, n=7. Data was fitted with a 4 parameter logistic non-linear curve and 95% prediction bands are exhibited in doted lines above and below fit.

7.2.2 Substrate preference

To understand the substrate preferences for cell proliferation, several conditions were tested by modulating the substrate availability in the culture media. The proliferation assays are exibited on the Figure 7.2. Four media formulations were prepared: the control media is regular RPMI with 10 mM glucose and 1.85 mM of glutamine (+Glc +Gln, white); media without glucose (-Glc +Gln, light grey); media with 10 mM of galactose instead of glucose (-Glc +Gal +Gln, dark grey); and media without glutamine (+Glc –Gln, black).

The MRC-5 cell line proliferation is significantly decreased at 96h in glutamine deprived media to values close to 25% of normal proliferative rates ($p<0.001$). The removal of glucose or substitution for galactose does not significantly impair proliferation on these cells.

The A549 cell line proliferation is significantly lower on the glutamine deprived medium at 72h ($p<0.05$) and reaches a rate of 14% relatively to control at 120h. In fact, A549 cell line is the most affected by glutamine deprivation. The galactose supplementation is also deleterious for proliferation, with a reduction of 48% at 96h ($p<0.01$). Glucose removal only causes a significant reduction of cell proliferation at 120h ($p<0.05$).

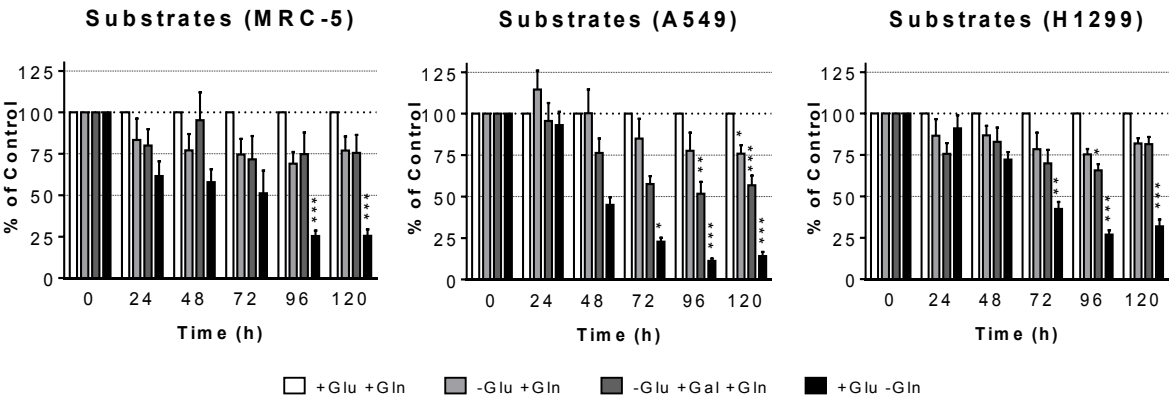

Figure 7.2 – Cell proliferation under different media formulations. Different media formulations were tested, regular medium (+Glc +Gln), without glucose (-Glc +Gln), with galactose instead of glucose (-Glu +Gal +Gln) and without glutamine (+Glc –Gln). The MRC-5 cell line is the least affected, with a significant reduction of cell proliferation at the final time points for media without glutamine. The A549 is the most affected by the removal of glutamine, while supplementation with galactose and glucose shortage is also deleterious to cell proliferation. The H1299 cell line is also affected by glutamine removal and galactose supplementation, however, glucose removal does not cause a significant reduction of cell proliferation.
Error bar represent SEM, n=7. A two-way ANOVA was applied with a Dunnet post-test for comparison with control. * $p<0.05$ to control (+Glc +Gln).

Proliferation of H1299 cell line is significantly reduced on the glutamine deprived medium at 72h ($p<0.01$) and reaches a 32% rate comparatively to control at 120h ($p<0.001$). Cell proliferation at 96h with galactose supplementation is significantly reduced ($p<0.05$) but recovers at 120h. The medium without glucose (-Glc +Gln) does not significantly alter cell proliferation in these cells.

Considering the glutamine effects on all cell lines, a rescue experiment was attempted (Figure 7.3) with a supplementation of 1.85 mM of asparagine (-Glc +Asn, light grey) or simply ammonia (-Glc +NH_4^+, dark grey) to glutamine deprived medium. A shorter time frame was selected for these experiments, to avoid depletion of culture media nutrients and autophagy mechanisms that might be occurring at 120h.

None of the selected substitutions, asparagine or ammonia was able to rescue the decreased cell proliferation caused by glutamine deprivation. Only supplementation with ammonia (dark grey) seems to delay the effects of glutamine deprivation for 24h in all cell lines.

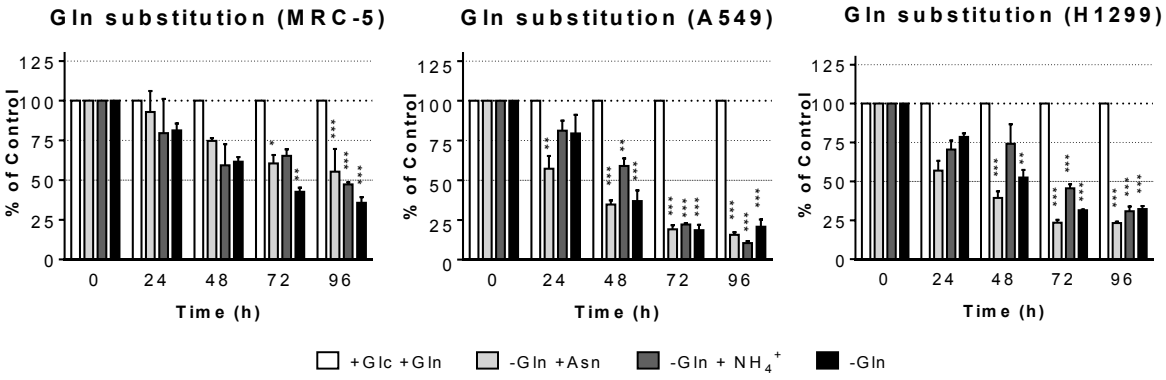

Figure 7.3 – Cell proliferation rescue with glutamine substitutes. Cells were grown 96h in media without glutamine (-Gln), media without glutamine and supplemented with asparagine (-Gln +Asn) and media without glutamine but supplemented with ammonia (NH_4^+). The control is regular media (+Glc, +Gln). None of the exhibited substitutes were able to efficiently rescue cell proliferation of glutamine deprived medium.
Error bars represent SEM, n=4 (3 for NH_4^+). A two-way ANOVA was applied with a Dunnet post-test for comparison with control. * $p<0.05$ to control (+Glc +Gln)

7.2.3 Inhibition studies

For the inhibition studies, regular RPMI medium was used. For each experiment was performed a control for all time points, with the respective vehicle. All experiments are compared to the control (presented as dotted line at 100% mark). All inhibitors were tested in three concentrations and at six time points (0h, 8h, 24h, 48h, 72h, and 96h).

Hexokinase

3-Bomopyruvate (3-BrPA) is an alkylating agent already in clinical trials and is described as an inhibitor of HK, the first enzyme in glycolysis, which converts glucose into glucose-6-phosphate with the consumption of an ATP molecule. The Figure 7.4 shows the results from HK inhibition on cell proliferation.

The MRC-5 and A549 cell lines have decreased proliferation rates at 72h with 50 μM, showing a decrease to 54% ($p<0.001$) on the MRC-5 cell line and 83% ($p<0.001$) on the A549 cell line. The H1299 cell line, on the other hand, at 48h with 50 μM shows significantly reduced proliferation rates ($p<0.001$) of 56% relatively to control. Moreover, the 25 μM concentration was enough to significantly diminish proliferation at 96h ($p<0.001$) for the H1299 cell line.

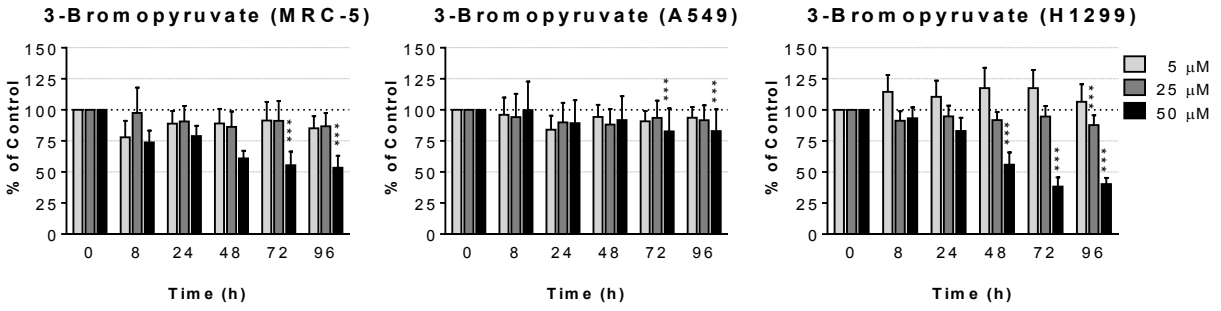

Figure 7.4 - Cell proliferation of each cell line with 3-bromopyruvate treatments. Three concentrations were assayed, 5, 25 and 50 μM. 3-Bromopyruvate is a known inhibitor of hexokinase. This inhibitor affected MRC-5 and A549 cell lines similarly at the concentration of 50 μM, while for H1299 cell line the decrease in proliferation happened sooner and also at lower concentrations.
Error bars represent SEM, n=8. A two-way ANOVA was applied with a Dunnet post-test for comparison with control. * $p<0.05$ to control.

Glyceraldehyde-3-phosphate dehydrogenase

Iodoacetate (IA) is another alkylating agent, which has been described as an inhibitor of GAPDH, a housekeeping protein that also participates in glycolysis (converting glyceradehyde-3-phosphate into 1,3-biphosphoglycerate), among other regulatory mechanisms (discussed in General Introduction).

The Figure 7.5 exhibits the inhibitory effects of iodoacetate. The inhibitor is extremely potent and at 10 μM decreases cell proliferation in all cell lines. While MRC-5 cell line presents a 17% proliferation rate relative to control at 96h ($p<0.01$), the A549 and H1299 cell lines exhibit 8% and 7%, respectively ($p<0.001$). However, the H1299 cell line is the most sensitive to the inhibition, which causes a diminished rate as early as 8h after treatment. Moreover, at 1 μM the effects are already visible at 96h ($p<0.001$).

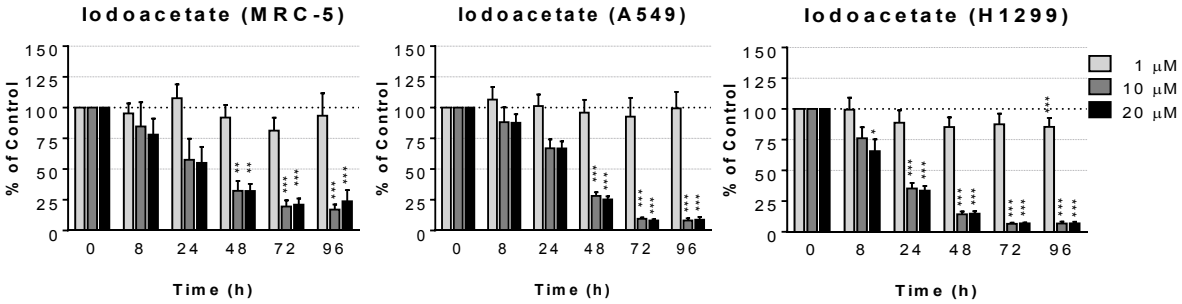

Figure 7.5 - Cell proliferation of each cell line with iodoacetate treatment. Three concentrations were assayed, 1, 10 and 20 μM. Iodoacetate is a known inhibitor of glyceraldehyde-3-phosphate dehydrogenase. This inhibitor affected MRC-5 and A549 cell lines similarly. The H1299 cell line at 8h after treatment already shows a decrease in proliferation, earlier than the other cell lines.
Error bars represent SEM, n=8. A two-way ANOVA was applied with a Dunnet post-test for comparison with control. * $p<0.05$ to control.

Lactate dehydrogenase

Lactate dehydrogenase converts pyruvate to lactate with coupled oxidation of a NADH molecule, regenerating NAD^+. This enzyme is competitively inhibited by oxamate, an analog of pyruvate.

The Figure 7.6 shows the cell proliferation effects of such inhibition. The concentrations for achieving a significant decrease in proliferation rates are higher than the previous inhibitors. For the selected range up to 4 mM, only MRC-5 and H1299 cell lines showed decreased rates. The MRC-5 cell line at 72h with 4 mM has a decrease of 38% ($p<0.001$) and even at 96h with 2 mM a significant reduction is shown. The H1299 cell line proliferation is decreased at 4 mM from 48h. The A549 cell line shows no differences under any treatments.

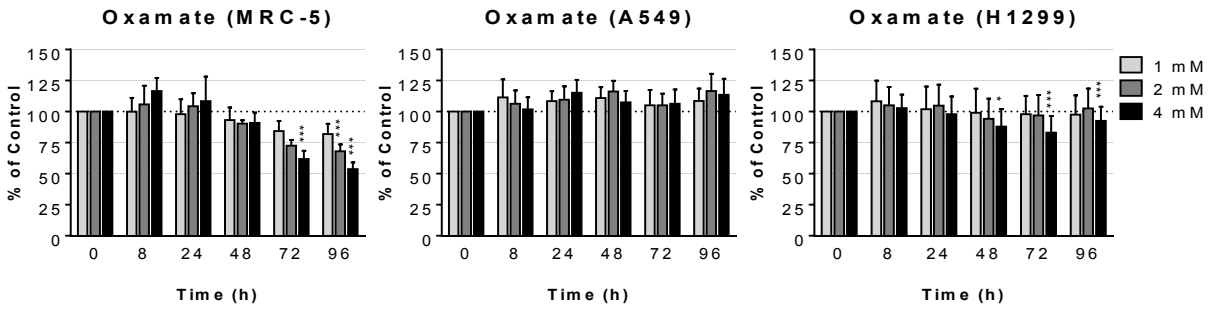

Figure 7.6 - Cell proliferation of each cell line with oxamate treatment. Three concentrations were assayed, 1, 2 and 4 mM. Iodoacetate is a known inhibitor of lactate dehydrogenase. This inhibitor diminished cell proliferation on the MRC-5 and H1299 cell lines, while A549 was essentially unaffected.
Error bars represent SEM, n=8. A two-way ANOVA was applied with a Dunnet post-test for comparison with control. * p<0.05 to control.

Pyruvate dehydrogenase kinase

Dichloroacetate (DCA) is an inhibitor of PDK. PDK inhibits the PDH complex. By inhibiting PDK, PDH remains non-inhibited, prompting the conversion of pyruvate to AcCoA in mitochondria and therefore promoting TCA cycle activity.

DCA demonstrates anti-proliferative effects (p<0.001) at 10 mM for all cell lines (Figure 7.7). However, the A549 cell line is the most sensitive to this inhibitor, by significantly decreasing the proliferation rate at 72h, 24h earlier than MRC-5 and H1299 cell lines. Additionally, with 5 mM at 96h the A549 cell line also has a decreased proliferation (p<0.001) to 74% of control rate.

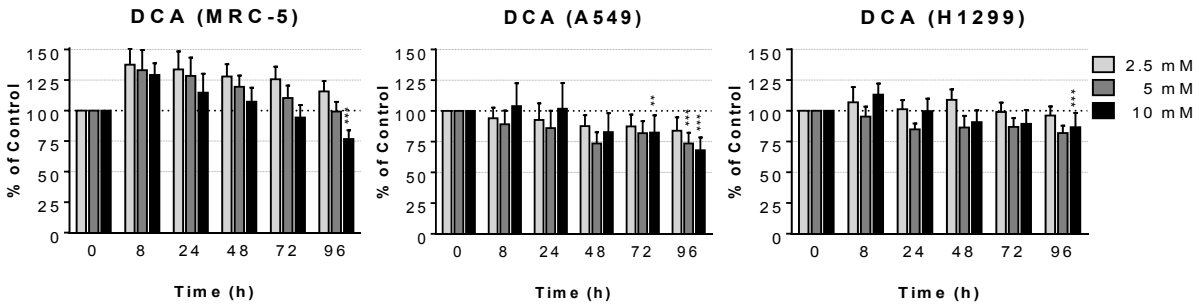

Figure 7.7 - Cell proliferation of each cell line with dichloroacetate (DCA) treatment. Three concentrations were assayed, 2.5, 5 and 10 mM. DCA is a known inhibitor of pyruvate dehydrogenase kinase. This inhibitor showed a higher decrease in cell proliferation on the A549 cell line, at early time points and lower concentrations. The H1299 and MRC-5 cell lines have similar responses, only for the highest concentration at the final time point.
Error bars represent SEM, n=8. A two-way ANOVA was applied with a Dunnet post-test for comparison with control. * p<0.05 to control.

Glutamate dehydrogenase

Glutamate dehydrogenase (GLDH) is responsible for the conversion of glutamate to α-ketoglutarate with a reduction of a $NAD(P)^+$ molecule, and vice-versa. This reaction allows the recruitment of glutamate and glutamine pools for TCA cycle replenishment. Epigallocatechin gallate (EGCG) is a described inhibitor of GLDH (Li et al. 2006).

In Figure 7.8 are shown the effects of EGCG on cell proliferation. All concentrations tested (1, 10 and 25 μM) cause a significant decrease in MRC-5 cell line proliferation at 96h. Nevertheless, the earliest significant decrease ($p<0.001$) happens at 72h with 25 μM, to 61% of control rate. On the H1299 cell line, at 48h with 25 μM, the cell proliferation is significantly reduced ($p<0.001$) to 59% of control proliferation rate. At 72h with 10 μM, H1299 cell line exhibits a significant decrease, but recovers at 120h. On the contrary, the A549 cell line shows no significant differences between treatment and control experiments.

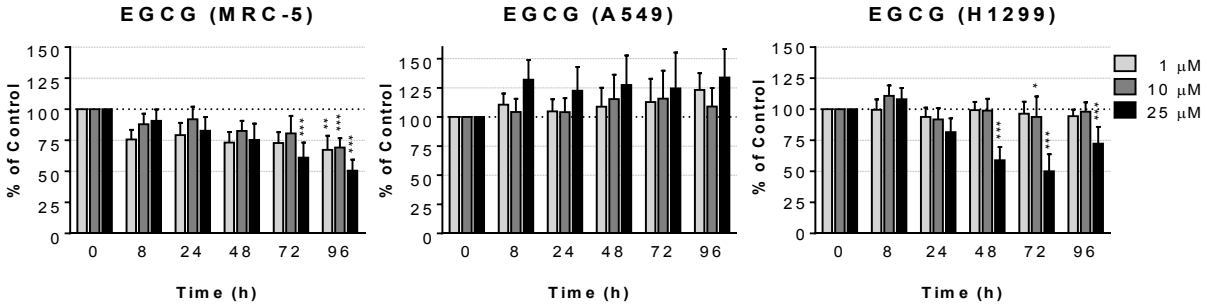

Figure 7.8 - Cell proliferation of each cell line with epigallocatechin gallate (EGCG) treatment. Three concentrations were assayed, 1, 10 and 25 μM. EGCG is a known inhibitor of glutamate dehydrogenase. This inhibitor diminished cell proliferation on the MRC-5 and H1299 cell lines, while A549 was essentially unaffected.
Error bars represent SEM, n=8. A two-way ANOVA was applied with a Dunnet post-test for comparison with control. * $p<0.05$ to control.

By inhibiting this enzyme, the cell is deprived of a main anaplerotic source. To understand if, in fact, the anti-proliferative effects are due to the lack of α-ketoglutarate, a rescue experiment was performed. The higher concentration of EGCG was selected and a medium supplementation with membrane permeable 2 mM dimethyl α-ketoglutarate (DMK).

As shown in Figure 7.9, EGCG inhibition with DMK supplementation (black) improves the proliferation rates to normal levels on the H1299 cell line (48h and 72h).

The MRC-5 and A549 cell lines shown a slight improvement with DMK supplementation (at 96h) but it is not enough to reach normal proliferation levels.

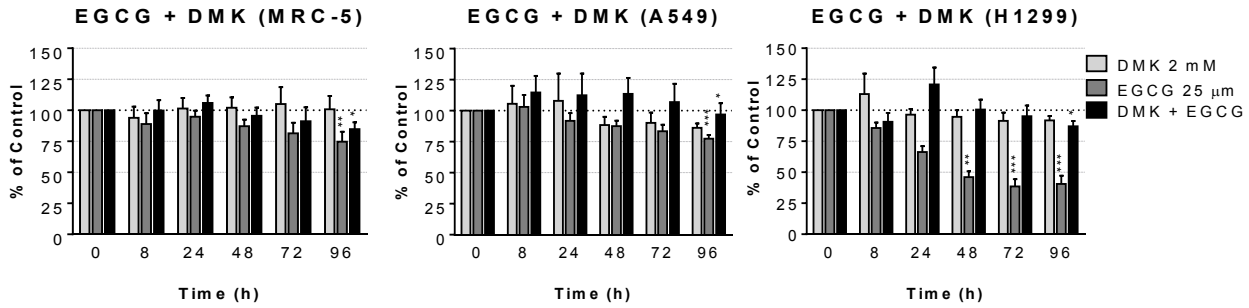

Figure 7.9 - Cell proliferation rescue from epigallocatechin gallate (EGCG) inhibition with dimethyl α-ketoglutarate (DMK). Cells were treated with 25 μM EGCG and DMK, a α-ketoglutarate membrane permeable analog, supplemented to media. The DMK was able to revert inhibition effects to normal proliferation values on the H1299 cell line. The MRC-5 and A549 cell lines exhibit an improved cell proliferation but values are not reverted to control levels.
Error bars represent SEM, n=8. A two-way ANOVA was applied with a Dunnet post-test for comparison with control. * p<0.05 to control.

Transaminases

Transaminases operate the reversible conversion of pools of non-essential aminoacids and their respective ketoacids. Two widely studied transaminases are the ALT and AST (see Chapter 2). Aminooxyacetic acid (AOA) is a non-specific inhibitor of transaminases and the Figure 7.10 shows the proliferation assays for this inhibitor.

The MRC-5 cell line is the least affected by the inhibition of transaminases, with a significant decrease of proliferation ($p<0.001$) at 72h with 400 μM, to a rate of 62%. The A549 cell line exhibits the most severe effect, with significantly decreased proliferation at 24h for 400 μM ($p<0.05$) and 48h for 200 μM ($p<0.001$). The H1299 cell line proliferation is also inhibited by the 400 μM and 200 μM ($p<0.001$) but at 48h and 72h, respectively.

Both ALT and AST are important for a regular function of the cell but given that AST operates a metabolically relevant bypass inside the TCA cycle, a rescue experiment was performed with supplementation of 2 mM dimethyl aspartate (DMA), a membrane permeable analog of aspartate (Figure 7.11).

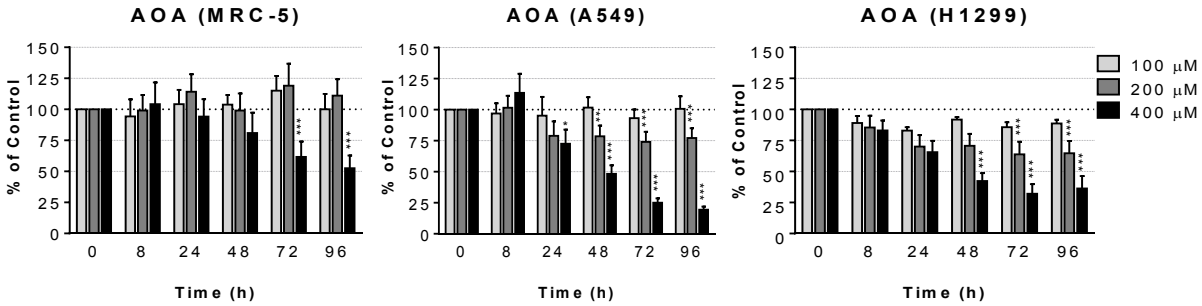

Figure 7.10 - Cell proliferation of each cell line with aminooxyacetic acid (AOA) treatment. Three concentrations were assayed, 100, 200 and 400 μM. AOA is a known inhibitor of transaminases. This inhibitor diminished cell proliferation in all cell lines, but at lower concentrations and earlier time points in the cancerous cell lines, especially the A549 cell line.
Error bars represent SEM, n=8. A two-way ANOVA was applied with a Dunnet post-test for comparison with control. * p<0.05 to control.

The MRC-5 cell line proliferation was rescued to normal values with the addition of DMA to the AOA inhibitor. The A549 cell line exhibited an improvement from 40% to 62% at 48h and the H1299 cell line from 47% to 62% at 48h. However, the rescued cell proliferation is still significantly lower than control (p<0.001) for both cancer cell lines.

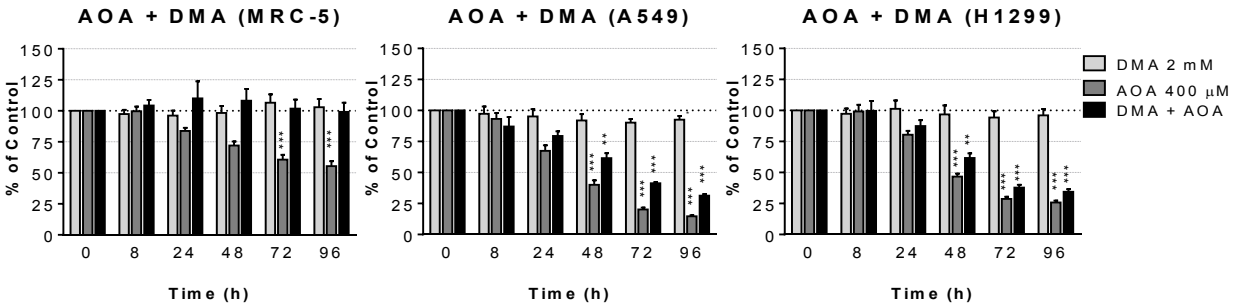

Figure 7.11 - Cell proliferation rescue from aminooxyacetic acid (AOA) inhibition with dimethyl aspartate (DMA). Cells were treated with 400 μM AOA and DMA, an aspartate membrane permeable analog, supplemented to media. The DMA was able to revert inhibition effects in MRC-5 cell line, attaining normal proliferation values. The A549 and H1299 cell lines exhibited a slightly improved cell proliferation but values are far from control levels.
Error bars represent SEM, n=8. A two-way ANOVA was applied with a Dunnet post-test for comparison with control. * p<0.05 to control.

Glucose-6-phosphate dehydrogenase

The final inhibitor to be tested is dehydroepiandrosterone (DHEA), an inhibitor of G6PDH, the first and rate-limiting step of PPP.

In Figure 7.12 the proliferation assays are shown. The MRC-5 cell line is the least affected by the inhibition of PPP, with a significant decrease at 96h with 100 μM, to 73% of control. A different scenario is found on cancer cell lines, with an earlier decrease of cell proliferation and also at lower concentrations (25 μM at 96h). The A549 cell line proliferation is significantly reduced ($p<0.05$) at 72h with 50 μM while H1299 cell line is significantly reduced ($p<0.001$) at 72h for 100 μM.

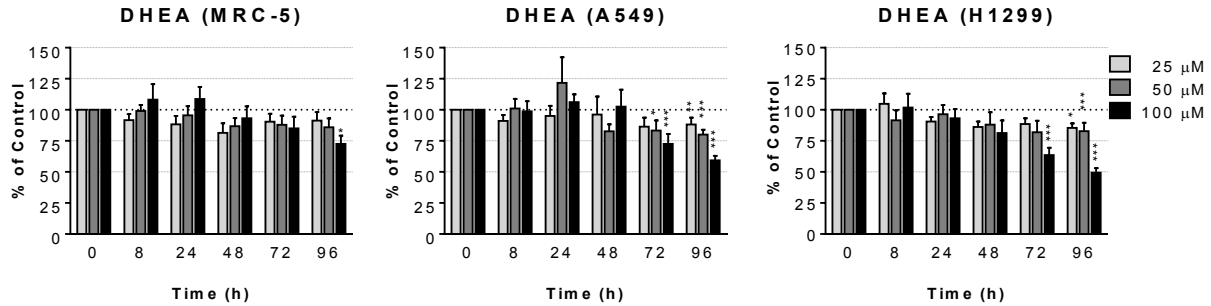

Figure 7.12 - Cell proliferation of each cell line with dehydroepiandrosterone (DHEA) treatment. Three concentrations were assayed, 25, 50 and 100 μM. DHEA is a known inhibitor of glucose-6-phosphate dehydrogenase. This inhibitor diminished cell proliferation in all cell lines, but at lower concentrations and earlier time points for the cancerous cell lines, especially A549 cell line.
Error bars represent SEM, n=8. A two-way ANOVA was applied with a Dunnet post-test for comparison with control. * $p<0.05$ to control.

7.3 Discussion

This final Chapter focused also on metabolism but through a toxicological approach, with the inhibition of several key-enzymes with small molecule inhibitors, described in Chapter I.

The studies were initiated with a definition of a growth curve for each cell line with regular RPMI media (Figure 7.1). The growth fits a 4 parameter logistic non-linear curve with very good r^2 values. Given that these cells are adherent in monolayer, the maximum plateau is due to a complete confluency at the multiwell. However, the cancer cells are smaller in size relatively to MRC-5 cell line, as seen by the microscopy experiments, so they grow up to larger numbers in the same surface area. Relatively to

the growth rates, cancer cells clearly outgrow the MRC-5 cell line, which in fact is a defining characteristic of cancer, the uncontrolled growth.

Considering the metabolic remodeling occurring in cancer and the discussed need of anabolic precursors to satisfy the fast proliferative needs, culture media was reconstituted with different formulations to assess substrate preference in these cells (Figure 7.2). A regular media with glutamate and glutamine was used as control at every time point. Amazingly, the removal of glucose (10 mM) only decreased the A549 cell line proliferation at the final time point while MRC-5 and H1299 remain unaffected. Since A549 cell line exhibits the most glycolytic phenotype, as seen in the previous Chapters, it was expected that it would be the most sensitive to glucose removal. However, the literature refers a faster decrease in cancer cell proliferation under glucose-deprivation conditions (Priebe et al. 2011; Wu et al. 2012). One plausible explanation may be due to the fact that the FBS was not dialyzed, therefore containing small amounts of glucose, lactate and other aminoacids, delaying the effects of nutrient deprivation.

The media with galactose and glutamine has been described to force mitochondrial metabolism through glutaminolysis (Rossignol et al. 2004; Vega-Naredo et al. 2014). This effect was especially deleterious to the A549 cell line proliferation. By forcing aerobic metabolism, there is an increased O_2 consumption, accompanied by a mitochondrial remodeling from fragmented to elongated, sensitizing the cells to ROS and apoptosis (Rossignol et al. 2004; Vega-Naredo et al. 2014). The MRC-5 and H1299 cell lines, which already exhibited a higher TCA cycle coupling and elongated mitochondria with interconnected mitochondrial network (Chapters 5 and 6), are insensitive to this media modification. Yet, the H1299 had a small decrease in cell proliferation at 96h but returned to normal values at the final time point.

The last media formulation contained glucose but was deprived of glutamine. With this media, all cell lines exhibited a decreased proliferation rate, earlier in the cancer cells. This data reveals that these cell lines require glutamine to support fast proliferation rates. The deprivation of glutamine has been linked to an increased apoptosis and a diminished cell proliferation an viability (Zhang et al. 2014).

Given this specific requirement for glutamine, an attempt was made to understand if other aminoacid could substitute the missing glutamine or if simply ammonia supplementation could be enough to rescue proliferation (Figure 7.3). Glutamine was substituted by asparagine, which is implied in the regulation of apoptosis in glutamine-deprived condition and rescue the viability in glutamine deprived cells (Zhang et al. 2014). However, cell proliferation did not improve in any cell line with supplemented asparagine. Even though ammonia delayed the effects of glutamine deprivation for 24h on the MRC-5 and H1299 cell line, none of these substitutes effectively rescued cell proliferation. Therefore, glutamine is an essential substrate for fast cell proliferation. Although reductive carboxylation is not a very active pathway in this experimental design, glutamine may still be providing energy by oxidation at the TCA and substrate for nucleotide biosynthesis, as discussed in Chapter 1 (Yang et al. 2014b; Wise et al. 2008; DeBerardinis et al. 2007).

In the final part of the work focused on bridging metabolic performance with differential treatment sensitivities. Several small molecule inhibitors were tested, targeting different enzymes and metabolic pathways.

HKII bound to mitochondria is correlated with a glycolytic phenotype and evading apoptosis (Pastorino et al. 2002). 3-BrPA is an HK inhibitor and was able to decrease cell proliferation in all three cell lines, but at lower concentrations for the H1299 cell line (Figure 7.4). Consistent results are described for similar concentrations in both A549 and H1299 cell lines. The inhibition generates a reduction of HK expression and dissociation of HKII from mitochondria, resulting in increased apoptosis (Zhang et al. 2012; Chen et al. 2009). The H1299 cell line possesses an increased mitochondrial activity and is subject to a higher oxidative stress. By dislodging the mitochondrial bound HKII due to 3-BrPA action, cells become more sensitive to apoptosis (Chen et al. 2009; Zhang et al. 2012). Also, this cell line exhibited higher cytochrome C expression, a major regulator of the apoptotic cascade. Intriguingly, the A549 cell line (in our study, is the most glycolytic) is the least affected by this inhibition. However the work, with the same cell lines and 3-BrPA, also reported a quick depletion in ATP levels for H1299 cell line but not for the A549 cell line (Zhang et al. 2012).

As discussed in Chapter I, GAPDH is a major regulatory enzyme and is considered a housekeeping enzyme. However, the expression of GAPDH has been found upregulated in lung cancers (Tokunaga et al. 1987). IA is an alkylating agent such as 3-BrPA, and even though it has an increased specificity for GAPDH, it may also target G6PDH or LDH (Schmidt et al. 2009). The inhibition of GAPDH by IA (Figure 7.5) revealed a drastic reduction of proliferation at 10 μM, in all cell lines, shutting down glycolysis in agreement with published data (Schmidt et al. 2009). This decrease in cell proliferation is surely related with glycolytic metabolism control, but given the multitask nature of GAPDH we cannot rule out the interference with other relevant cellular mechanisms (see Chapter 1).

LDH converts pyruvate into lactate with oxidation of a NAD^+ molecule and oxamate is a known competitive inhibitor of this enzyme. The MRC-5 and H1299 cell lines have a decreased proliferation while the A549, the most glycolytic cell line does not show any decrease, even at the highest oxamate concentration (Figure 7.6). Since the A549 cell line relies more on glycolysis, it would be expected that the inhibition of LDH would be more deleterious, as it is a critical mechanism for NAD^+ recycling. However, in a study with A549 cell line oxamate inhibition, only with 20 mM of oxamate the LDH activity was reduced and a half maximal inhibitory concentration (IC_{50}) ≈58 mM was calculated, which is exceedingly higher than the 4 mM applied on our experiments (Yang et al. 2014a). The authors suggested that these cells are resistant to oxamate treatment due to a cell cycle arrest in G_0/G_1 phase and the onset of autophagic protective mechanisms. Nonetheless, H1299 and MRC-5 cell lines were sensitive to inhibition, probably due to a redox imbalance and increased ROS production (Zhao et al. 2015).

The DCA is an inhibitor of PDK, which in turn will allow the PDH to remain non-inhibited. This step is crucial to promote TCA cycle coupling, by converting pyruvate to AcCoA. All cell lines were affected by the upregulation of PDH activity, however the A549 cell line shows a decrease in cell proliferation even at the lower DCA concentration (Figure 7.7). By promoting TCA cycle activity, an increased generation of ROS and O_2 consumption initiate apoptotic mechanisms (Bonnet et al. 2007; Shavit et al. 2015). These results are in agreement with the substrate preference experiments with galactose. When the A549 cell line is forced to employ mitochondrial metabolism, it

must perform a large mitochondrial remodeling, sensitizing the cell to apoptosis (Vega-Naredo et al. 2014).

GLDH converts glutamate to α-ketoglutarate in reversible reactions, establishing a bridge between the two pools and EGCG is an inhibitor of this enzyme. Upon treatment with EGCG, both MRC-5 and H1299 cell lines decreased their proliferation, while A549 cell line was not affected (Figure 7.8). To confirm if these effects were due to lack of α-ketoglutarate, a membrane permeable analog of α-ketoglutarate, DMK, was supplied at 2 mM (Figure 7.9). In this experiment, the supplementation of DMK with the EGCG resulted in an improvement of cell proliferation in all cell lines. However, only H1299 cell line was rescued to control values. This experiment is different for the A549 cell line, which shows a decreased cell proliferation that was not exhibited before and even for the MRC-5 cell line there is an altered sensitivity to EGCG. This may be due to experimental error. Also, the purchased EGCG had only 80% purity grade and the stock concentrations of EGCG employed in both experiments were not the same. Taken together could explain such a variability in this data. Nonetheless, EGCG effects have been described for A549 and H1299, referring that the A549 cell line is less sensitive to EGCG than H1299 cell line (Li et al. 2010; Sakamoto et al. 2013). The same work showed that EGCG induce ROS formation and apoptosis since the effects were attenuated by the addition of antioxidants (Li et al. 2010). Considering that the H1299 cell line exhibited higher TCA coupling and turnover, higher expression of cytochrome C and voltage-dependent anion channel (previous Chapter) it is likely to be more sensitive to EGCG ROS-induced apoptosis. The A549 cell line, on the other hand, has a more glycolytic phenotype with a low TCA turnover, being thus less sensitive to GLDH inhibition and ROS production. Also, on the H1299 cell line, glutamate is certainly an important oxidative and/or anaplerotic source for sustaining fast cell proliferation rates, hypothesis supported by the rescue operated by DMK

AST converts aspartate and α-ketoglutarate into oxaloacetate and glutamate in a reversible reaction. This is a parallel reaction to GLDH and is also involved in the malate-aspartate shuttle. The transaminases were inhibited by AOA, a non specific inhibitor of transaminases (Carvalho et al. 2001). The inhibition resulted in a decreased cell proliferation for the cancer cell lines at a lower concentration than for the MRC-5 cell

line (Figure 7.10). To understand if AST plays an important role in cell proliferation, dimethyl aspartate (DMA) was supplemented to the cells for a rescue experiment. In this rescue experiment, all cells improved their proliferation but only MRC-5 was rescued to control levels (Figure 7.11). This reflects the cancer needs for anabolic precursors, since aspartate is a precursor for asparagine, arginine and nucleotides (Thornburg et al. 2008; DeBerardinis et al. 2007).

Finally, the pentose phosphate pathway was inhibited at the G6PDH with DHEA. Again, cancer cells are the most affected by the inhibition of the first step of PPP (Figure 7.12). This also reflects the anabolic process remodeling occurring in cancer cells, as described in Chapter 1. An inhibition of PPP at the oxidative phase will cause a decrease in nucleotide precursors and NADPH sources, useful for anabolic processes, such as DNL or redox homeostasis such as GSH recycling (Boros et al. 1997; Shibuya et al. 2015; Yang et al. 2013c).

On the Figure 7.13 is shown a schematic representation of the inhibitory data collected in this Chapter. Large arrows represent strong inhibitory effects and thin arrows represent mild inhibitory effects. We can appreciate that none of the cell lines have equal responses, which could be interpreted has a reflection of the quite distinct metabolic profiles.

The MRC-5 and H1299 cell lines are paired in the inhibition of GLDH, PDK and LDH, reflecting an altered sensitivity to ROS generation and/or redox status, relatively to the A549 cell line. GLDH allows the recruitment of glutamine-derived pools for oxidative or anabolic purposes while PDH upregulation promotes a higher TCA cycle turnover and O_2 consumption (Bonnet et al. 2007). The LDH is a major regulator of NADH/NAD^+ pools, and therefore inhibition of this enzyme will also cause a redox imbalance and increased pools of pyruvate. This excess pyruvate pool require handling, either it is converted to alanine or is directed to TCA cycle towards its oxidation and subsequent regeneration of NAD^+ by oxidative phosphorylation activity. Interestingly, these inhibitors affect differently the cell lines with similar TCA couplings.

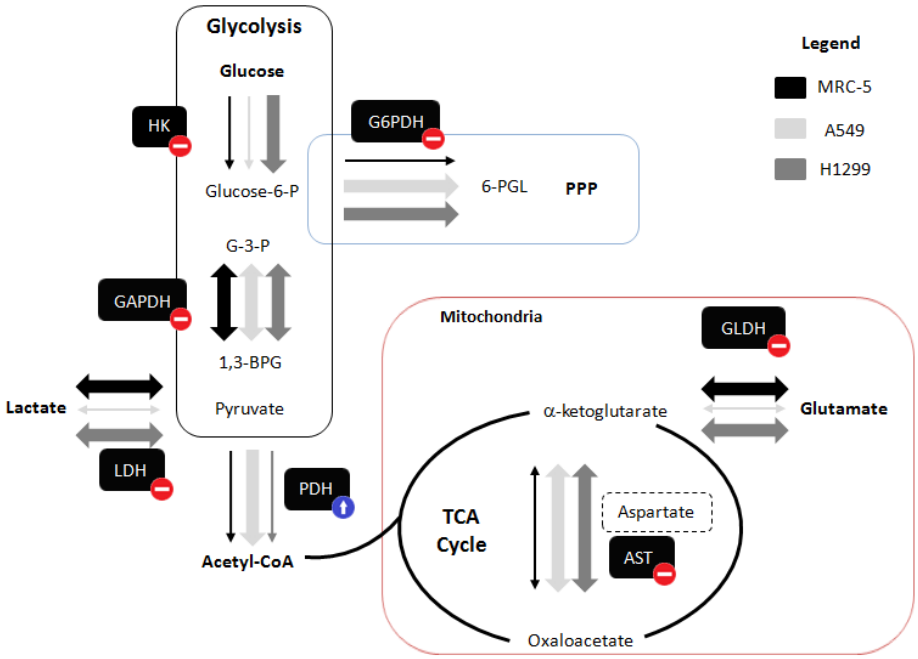

Figure 7.13 - Schematics of metabolic inhibitions. Large arrows represent strong inhibitory effects while thin arrows represent mild/absent inhibitory effects on cell proliferation. (HK) hexokinase; (GAPDH) gliceraldehyde-3-phosphate dehydrogenase; (LDH) lactate dehydrogenase; (PDH) pyruvate dehydrogenase; (GLDH) glutamate dehydrogenase; (AST) aspartate transaminase; (G6PDH) glucose-6-phosphate dehydrogenase; (Glucose-6-P) glucose-6-phosphate; (G-3-P) glyceraldehyde-3-phosphate; (1,3-BFG) 1,3-bisphosphoglycerate; (6-PGL) 6-phosphogluconolactone; (PPP) pentose phosphate pathway.

At a closer look, there are also three strong inhibitory effects in common between the A549 and H1299 cancer cell lines. These are the inhibition of GAPDH, G6PDH and AST, which are related with anabolic precursor synthesis and redox homeostasis. The G6PDH, is a rate-limiting enzyme in the PPP and the inhibition of this enzyme will block the production of NADPH and ribose molecules for nucleotide synthesis, essential for fast proliferation rates (Boros et al. 1997). The GAPDH regulates the pools of glyceraldehyde-3-phospate and may reroute the glycolytic flux towards PPP, acting as an important homeostatic regulator (Ralser et al. 2007). The AST is also required for the maintenance of a malate-aspartate shuttle in the mitochondria and for non-essential aminoacid and nucleotide biosynthesis (DeBerardinis et al. 2007). Since MRC-5 present slower proliferative rates, their need for anabolic precursors is expectedly lower, and therefore, is less sensitive to the inhibition of this pathways. This is in agreement with the discussed need for anabolic sources in rapidly dividing cells, as seen in Chapter 1.

7.4 Conclusion

Under glutamine deprivation conditions, all cell lines exhibit a notorious decrease in cell proliferation while glucose deprivation was not so deleterious.

The overall effects caused by metabolic inhibitors allowed distinguishing the cancer cell lines from the non cancerous cell line. Upon mitochondrial metabolism disturbances, cells with higher TCA coupling reacted differently relatively to a less TCA coupled cell line. The cancer cell lines show an increased sensitivity upon inhibition of G6PDH and AST, which may lead to a decreased production of reducing equivalents and/or anabolic precursors to sustain fast proliferative rates.

Part III

Conclusion

Chapter 8
Final Conclusion

8.1 Conclusion

Lung cancer is a major health problem throughout the world, with rising incidence numbers, especially in the developing countries (Cancer Research UK 2014). Unfortunately, treatment for this disease has an expected 5-year survival rate of 17% even under adequate treatments (DeSantis et al. 2014). In the last three decades, some cancers such as prostate or breast cancer improved their 5-year survival rate to up 20% while lung cancer did not improved more than 10% (May 2014). In order to achieve better treatment outcomes, actual therapies require considerable improvements or new strategies must be designed. For either, a deep comprehension of the alterations occurring in cancer is required, from genetic to metabolic. As discussed in the Chapter 1, the cancer onset is described by a major metabolic remodeling. This work focused on the lung cancer metabolism characterization as a tool to define new targets of antitumorigenic activity.

The work proposed the measurement of major metabolic fluxes such as glycolysis, TCA cycle and *de novo* lipogenesis (DNL). These fluxes were successfully quantified either by ^{13}C or ^{2}H methods. To our knowledge, we successfully implemented a new ^{2}H enrichment method for DNL assessment for the first time in cancer research. These results showed the occurrence of metabolic heterogeneity between the two

selected cancer cell lines. One cell line exhibited a relatively active TCA cycle (H1299) and the other showed a more glycolytic phenotype. Nonetheless, both exhibited an increased DNL rate.

On the second part of the work several mitochondrial related parameters were measured. Also, the influence of reductive carboxylation mediated by isocitrate dehydrogenase (IDH) in the lipogenic activity was assessed. The cancer cell lines exhibited polarized and active mitochondria despite different TCA turnover and O_2 consumption rates. The reductive carboxylation mediated by IDH did not contributed significantly to DNL. However, IDH is involved in redox homeostasis and IDH1 may have a regulatory effect on glutamine pools.

The final part of the work bridges the connection between metabolic fluxes and cell proliferation, through the modulation of cell culture substrates and the use of metabolic inhibitors. The presence of glutamine is critical to support rapid cell proliferation in all cell lines. Cancer cells were more sensitive to the inhibition of glucose-6-phosphate dehydrogenase and aspartate transaminase, reflecting an increased need of anabolic precursors and reducing equivalents for cell proliferation.

One of the major goals in therapeutics and drug research is to find targets, within certain pathology, that are distinguishable from healthy conditions. Cancer is characterized by certain common features such as the Warburg effect but is also defined by heterogeneous microenvironments and different genetic predispositions. In this study, with two non-small lung cancer cell lines, we have two distinct metabolic profiles, reminding that heterogeneity is in fact a major problem towards achieving a common solution that fits all cases. Nonetheless, with this metabolic approach, some common pathways between cancer cells emerged, even with significantly altered carbon metabolism. Given the cancer cell lines requirements for anabolic precursors, reducing equivalents and increased DNL, these may be regarded as putative targets for therapy in lung cancer.

In conclusion, the present work presents new findings in lung cancer metabolism and establishes a connection between metabolism and plausible therapeutic targets. However, the IDH role in cancer remains to be clarified, in particular the connection between IDH1 and glutamine pools.

8.2 Future perspectives

Although this work characterized and elucidated several metabolic aspects and mechanism occurring in lung cancer cell lines, some new questions were raised or remained unclear. Therefore, the author suggests a few future experiments.

One question is relatively to the IDH1 and the role of this enzyme in cancer. The levels of labelled glutamine generated by IDH1 silencing in the Chapter 6 suggest a regulation of glutamine pools by IDH1. However, this mechanism is not described and our data could not explain anything further. The IDH1 has been associated with cytosolic but also peroxisomal localizations, which reinforces the hypothesis of a regulatory function for IDH1. However, all these mechanisms are still poorly described and require further research.

Although carbon metabolism and DNL were analyzed in these cells, one important pathway that remained to be clarified was the pentose phosphate pathway. Given the effects caused by the inhibition of glucose-6-phosphate dehydrogenase on cancer cell proliferation (Chapter 7) it would be interesting to analyze the fluxes on this pathway. This raises another question on which method to employ for such measurement. For that purpose, it would be interesting to validate, in cancer cells, a protocol described in our laboratory in erythrocytes, employing NMR stable isotope tracers, namely [2-^{13}C]glucose. Although the technique has some limitations, it would provide an invaluable tool for quantifying PPP using NMR techniques.

Since DCA promotes the TCA coupling by converting pyruvate to AcCoA, an interesting experiment would be to follow the alterations by isotopomer analysis in

cancer metabolism under treatment with this drug. Although there are already some studies with stable isotopes and hyperpolarized ^{13}C, few characterized all the metabolic parameters that were employed in this work. Also, more inhibition studies could be performed using fatty acid synthetase or PPP inhibitors, or even combined treatments with different inhibitors.

Bibliography

Abrantes, A M, L C Tavares, S Pires, J Casalta-Lopes, C Mendes, M Simões, M M Grazina, R A Carvalho, M F Botelho. 2014. "Metabolic Effects of Hypoxia in Colorectal Cancer by (13) C NMR Isotopomer Analysis." *BioMed Research International* 2014 (January). doi:10.1155/2014/759791.

Adam, J, M Yang, C Bauerschmidt, M Kitagawa, L O'Flaherty, P Maheswaran, G Özkan, et al. 2013. "A Role for Cytosolic Fumarate Hydratase in Urea Cycle Metabolism and Renal Neoplasia." *Cell Reports* 3 (5): 1440–48. doi:10.1016/j.celrep.2013.04.006.

Adamo, A F, D E Haft. 1965. "An Alternate Pathway of Alpha-Ketoglutarate Catabolism in the Isolated, Perfused Rat Liver. I. Studies with DL-Glutamate-2 and -5-14C." *The Journal of Biological Chemistry* 240 (2): 613–17.

Al-Saffar, N M S, L V Marshall, L E Jackson, G Balarajah, T R Eykyn, A Agliano, P A Clarke, et al. 2014. "Lactate and Choline Metabolites Detected In Vitro by Nuclear Magnetic Resonance Spectroscopy Are Potential Metabolic Biomarkers for PI3K Inhibition in Pediatric Glioblastoma." *PLoS ONE* 9 (8): e103835. doi:10.1371/journal.pone.0103835.

Ameer, F, L Scandiuzzi, S Hasnain, H Kalbacher, N Zaidi. 2014. "De Novo Lipogenesis in Health and Disease." *Metabolism: Clinical and Experimental* 63 (7): 895–902. doi:10.1016/j.metabol.2014.04.003.

American Cancer Society. 2014. "Cancer Facts & Figures 2014." *American Cancer Society*.

Araújo Jr, R F, G A Lira, J A Vilaça, H G Guedes, M C A Leitão, H F Lucena, and C C O Ramos. 2014. "Prognostic and Diagnostic Implications of MMP-2, MMP-9, and VEGF-A Expressions in Colorectal Cancer." *Pathology, Research and Practice*, October. doi:10.1016/j.prp.2014.09.007.

Aroor, A R, R J Lowery, R J Restrepo, B P Mooney, S D Shukla. 2012. "A Proteomic Analysis of Liver after Ethanol Binge in Chronically Ethanol Treated Rats." *Proteome Science*. doi:10.1186/1477-5956-10-29.

Atkinson, D E, G M Walton. 1967. "Adenosine Triphosphate Conservation in Metabolic Regulation. Rat Liver Citrate Cleavage Enzyme." *Journal of Biological Chemistry* 242: 3239–41.

Atkinson, D E, A G Chapman. 1979. "The Adenylate Energy Charge in the Study of Enzymes in Vitro." *Methods in Enzymology* 55 (January): 229–35. doi:10.1016/0076-6879(79)55027-7.

Baysal, B E, R E Ferrell, J E Willett-Brozick, E C Lawrence, D Myssiorek, A Bosch, A van der Mey, et al. 2000. "Mutations in SDHD, a Mitochondrial Complex II Gene, in Hereditary Paraganglioma." *Science (New York, N.Y.)* 287 (5454): 848–51.

Bellance, N, G Benard, F Furt, H Begueret, K Smolková, E Passerieux, J P Delage, J M Baste, P Moreau, R Rossignol. 2009. "Bioenergetics of Lung Tumors: Alteration of Mitochondrial

Biogenesis and Respiratory Capacity." *The International Journal of Biochemistry & Cell Biology* 41 (12): 2566–77. doi:10.1016/j.biocel.2009.08.012.

Bender, E. 2014a. "Developing World: Global Warning." *Nature* 509 (7502): S64–65. doi:10.1038/509S64a.

Bender, E. 2014b. "Epidemiology: The Dominant Malignancy." *Nature* 513 (7517): S2–3. doi:10.1038/513S2a.

Bensaad, K, A Tsuruta, M A Selak, M N C Vidal, K Nakano, R Bartrons, E Gottlieb, K H Vousden. 2006. "TIGAR, a p53-Inducible Regulator of Glycolysis and Apoptosis." *Cell* 126 (1): 107–20. doi:10.1016/j.cell.2006.05.036.

Beuster, G, K Zarse, C Kaleta, R Thierbach, M Kiehntopf, P Steinberg, S Schuster, M Ristow. 2011. "Inhibition of Alanine Aminotransferase in Silico and in Vivo Promotes Mitochondrial Metabolism to Impair Malignant Growth." *The Journal of Biological Chemistry* 286 (25): 22323–30. doi:10.1074/jbc.M110.205229.

Bieging, K T, S S Mello, L D Attardi. 2014. "Unravelling Mechanisms of p53-Mediated Tumour Suppression." *Nature Reviews. Cancer* 14 (5): 359–70. doi:10.1038/nrc3711.

Bonnet, S, S L Archer, J Allalunis-Turner, A Haromy, C Beaulieu, R Thompson, C T Lee, et al. 2007. "A Mitochondria-K+ Channel Axis Is Suppressed in Cancer and Its Normalization Promotes Apoptosis and Inhibits Cancer Growth." *Cancer Cell* 11 (1): 37–51. doi:10.1016/j.ccr.2006.10.020.

Bonuccelli, G, A Tsirigos, D Whitaker-Menezes, S Pavlides, R G Pestell, B Chiavarina, P G Frank, et al. 2010. "Ketones and Lactate 'fuel' Tumor Growth and Metastasis: Evidence That Epithelial Cancer Cells Use Oxidative Mitochondrial Metabolism." *Cell Cycle* 9 (17): 3506–14. doi:10.4161/cc.9.17.12731.

Boros, L G, J Puigjaner, M Cascante, W N Lee, J L Brandes, S Bassilian, F I Yusuf, et al. 1997. "Oxythiamine and Dehydroepiandrosterone Inhibit the Nonoxidative Synthesis of Ribose and Tumor Cell Proliferation." *Cancer Research* 57 (19): 4242–48.

Brand, M D, D G Nicholls. 2011. "Assessing Mitochondrial Dysfunction in Cells." *The Biochemical Journal* 435: 297–312. doi:10.1042/BJ20110162.

Calabrese, C, L Iommarini, I Kurelac, M A Calvaruso, M Capristo, P Lollini, P Nanni, et al. 2013. "Respiratory Complex I Is Essential to Induce a Warburg Profile in Mitochondria-Defective Tumor Cells." *Cancer & Metabolism* 1: 11. doi:10.1186/2049-3002-1-11.

Cancer Research UK. 2014. "World Cancer Factsheet." Vol. 2012.

Cardaci, S, M R Ciriolo. 2012. "TCA Cycle Defects and Cancer: When Metabolism Tunes Redox State." *International Journal of Cell Biology* 2012 (January): 161837. doi:10.1155/2012/161837.

Carvalho, R A, P Zhao, C B Wiegers, F M Jeffrey, C R Malloy, A D Sherry. 2001. "TCA Cycle Kinetics in the Rat Heart by Analysis of (13)C Isotopomers Using Indirect (1)H." *American Journal of Physiology. Heart and Circulatory Physiology* 281 (3): H1413–21.

Carvalho, R A, E E Babcock, F M Jeffrey, A D Sherry, C R Malloy. 1999. “Multiple Bond 13C-13C Spin-Spin Coupling Provides Complementary Information in a 13C NMR Isotopomer Analysis of Glutamate.” *Magnetic Resonance in Medicine : Official Journal of the Society of Magnetic Resonance in Medicine / Society of Magnetic Resonance in Medicine* 42 (1): 197–200.

Cerella, C, M Dicato, M Diederich. 2014. “Modulatory Roles of Glycolytic Enzymes in Cell Death.” *Biochemical Pharmacology* 92 (1): 22–30. doi:10.1016/j.bcp.2014.07.005.

Cerfolio, R J, A S. Bryant. 2013. “Quality of Life after Pulmonary Resections.” *Thoracic Surgery Clinics*. doi:10.1016/j.thorsurg.2013.05.004.

Chance, E M, S H Seeholzer, K Kobayashi, J R Williamson. 1983. “Mathematical Analysis of Isotope Labeling in the Citric Acid Cycle with Applications to 13C NMR Studies in Perfused Rat Hearts.” *The Journal of Biological Chemistry* 258 (22): 13785–94.

Chen, J-Q, J Russo. 2012. “Dysregulation of Glucose Transport, Glycolysis, TCA Cycle and Glutaminolysis by Oncogenes and Tumor Suppressors in Cancer Cells.” *Biochimica et Biophysica Acta* 1826 (2): 370–84. doi:10.1016/j.bbcan.2012.06.004.

Chen, L, T Liu, J Zhou, Y Wang, X Wang, W Di, S Zhang. 2014. “Citrate Synthase Expression Affects Tumor Phenotype and Drug Resistance in Human Ovarian Carcinoma.” *PloS One* 9 (12): 1–19. doi:10.1371/journal.pone.0115708.

Chen, Z, H Zhang, W Lu, P Huang. 2009. “Role of Mitochondria-Associated Hexokinase II in Cancer Cell Death Induced by 3-Bromopyruvate.” *Biochimica et Biophysica Acta* 1787 (5): 553–60. doi:10.1016/j.bbabio.2009.03.003.

Cheung, E C, R L Ludwig, K H Vousden. 2012. “Mitochondrial Localization of TIGAR under Hypoxia Stimulates HK2 and Lowers ROS and Cell Death.” *Proceedings of the National Academy of Sciences of the United States of America* 109 (50): 20491–96. doi:10.1073/pnas.1206530109.

Christofk, H R, M G Vander Heiden, M H Harris, A Ramanathan, R E Gerszten, R Wei, M D Fleming, S L Schreiber, L C Cantley. 2008. “The M2 Splice Isoform of Pyruvate Kinase Is Important for Cancer Metabolism and Tumour Growth.” *Nature* 452 (7184): 230–33. doi:10.1038/nature06734.

Cline, G W, K F Petersen, M Krssak, J Shen, R S Hundal, Z Trajanoski, S Inzucchi, A Dresner, D L Rothman, G I Shulman. 1999. “Impaired Glucose Transport as a Cause of Decreased Insulin-Stimulated Muscle Glycogen Synthesis in Type 2 Diabetes.” *The New England Journal of Medicine* 341 (4): 240–46. doi:10.1056/NEJM199907223410404.

Cogliano, V J, R Baan, K Straif, Y Grosse, B Lauby-Secretan, F El Ghissassi, V Bouvard, et al. 2011. “Preventable Exposures Associated with Human Cancers.” *Journal of the National Cancer Institute* 103 (24): 1827–39. doi:10.1093/jnci/djr483.

Cohen, A L, S L Holmen, H Colman. 2013. “IDH1 and IDH2 Mutations in Gliomas.” *Current Neurology and Neuroscience Reports* 13 (5): 345. doi:10.1007/s11910-013-0345-4.

Colell, A, J-E Ricci, S Tait, S Milasta, U Maurer, L Bouchier-Hayes, P Fitzgerald, et al. 2007. "GAPDH and Autophagy Preserve Survival after Apoptotic Cytochrome c Release in the Absence of Caspase Activation." *Cell* 129 (5): 983–97. doi:10.1016/j.cell.2007.03.045.

Costa, V M, R S, L C Tavares, R Vitorino, F Amado, F Carvalho, M L Bastos, M Carvalho, R A Carvalho, F Remião. 2009. "Adrenaline and Reactive Oxygen Species Elicit Proteome and Energetic Metabolism Modifications in Freshly Isolated Rat Cardiomyocytes." *Toxicology* 260 (1-3): 84–96. doi:10.1016/j.tox.2009.03.012.

Cuezva, J M, G Chen, A M Alonso, A Isidoro, D E Misek, S M Hanash, D G Beer. 2004. "The Bioenergetic Signature of Lung Adenocarcinomas Is a Molecular Marker of Cancer Diagnosis and Prognosis." *Carcinogenesis* 25 (7): 1157–63. doi:10.1093/carcin/bgh113.

Dang, L, D W White, S Gross, B D Bennett, M A Bittinger, E M Driggers, V R Fantin, et al. 2009. "Cancer-Associated IDH1 Mutations Produce 2-Hydroxyglutarate." *Nature* 462 (7274): 739–44. doi:10.1038/nature08617.

Dang, C V. 2012. "Links between Metabolism and Cancer." *Genes & Development* 26 (9): 877–90. doi:10.1101/gad.189365.112.

Dang, C V, M Hamaker, P Sun, A Le, P Gao. 2011. "Therapeutic Targeting of Cancer Cell Metabolism." *Journal of Molecular Medicine (Berlin, Germany)* 89 (3): 205–12. doi:10.1007/s00109-011-0730-x.

Dani, J A, D J K Balfour. 2011. "Historical and Current Perspective on Tobacco Use and Nicotine Addiction." *Trends in Neurosciences* 34 (7): 383–92. doi:10.1016/j.tins.2011.05.001.

Daniels, V W, K Smans, I Royaux, M Chypre, J V Swinnen, N Zaidi. 2014. "Cancer Cells Differentially Activate and Thrive on De Novo Lipid Synthesis Pathways in a Low-Lipid Environment." *PLoS ONE* 9 (9): 13–19. doi:10.1371/journal.pone.0106913.

DeBerardinis, R J, T Cheng. 2010. "Q's next: The Diverse Functions of Glutamine in Metabolism, Cell Biology and Cancer." *Oncogene* 29 (3): 313–24. doi:10.1038/onc.2009.358.

DeBerardinis, R J, A Mancuso, E Daikhin, I Nissim, M Yudkoff, S Wehrli, C B Thompson. 2007. "Beyond Aerobic Glycolysis: Transformed Cells Can Engage in Glutamine Metabolism That Exceeds the Requirement for Protein and Nucleotide Synthesis." *Proceedings of the National Academy of Sciences of the United States of America* 104 (49): 19345–50. doi:10.1073/pnas.0709747104.

Delgado, T C, D Pinheiro, M Caldeira, M M Castro, C F Geraldes, P López-Larrubia, S Cerdán, J G Jones. 2009. "Sources of Hepatic Triglyceride Accumulation during High-Fat Feeding in the Healthy Rat." *NMR in Biomedicine* 22 (November 2008): 310–17. doi:10.1002/nbm.1327.

Delgado, T C, M M Castro, C F Geraldes, J G Jones. 2004. "Quantitation of Erythrocyte Pentose Pathway Flux with [2-13C]glucose and 1H NMR Analysis of the Lactate Methyl Signal." *Magnetic Resonance in Medicine : Official Journal of the Society of Magnetic Resonance in Medicine / Society of Magnetic Resonance in Medicine* 51 (6): 1283–86. doi:10.1002/mrm.20096.

Demarse, N A, S Ponnusamy, E K Spicer, E Apohan, J E Baatz, B Ogretmen, C Davies. 2009. “Direct Binding of Glyceraldehyde 3-Phosphate Dehydrogenase to Telomeric DNA Protects Telomeres against Chemotherapy-Induced Rapid Degradation.” *Journal of Molecular Biology* 394 (4): 789–803. doi:10.1016/j.jmb.2009.09.062.

DeSantis, C E, C C Lin, A B Mariotto, R L Siegel, K D Stein, J L Kramer, R Alteri, A S Robbins, A Jemal. 2014. “Cancer Treatment and Survivorship Statistics, 2014.” *CA: A Cancer Journal for Clinicians* 64 (4): 252–71. doi:10.3322/caac.21235.

Desmoulin, F, P Canioni, P J Cozzone. 1985. “Glutamate-Glutamine Metabolism in the Perfused Rat Liver.” *FEBS Letters*. doi:10.1016/0014-5793(85)80734-1.

Dettmer, K, N Nürnberger, H Kaspar, M Gruber, M F Almstetter, P J Oefner. 2011. “Metabolite Extraction from Adherently Growing Mammalian Cells for Metabolomics Studies: Optimization of Harvesting and Extraction Protocols.” *Analytical and Bioanalytical Chemistry* 399 (3): 1127–39. doi:10.1007/s00216-010-4425-x.

Downward, J. 2009. “Cancer: A Tumour Gene’s Fatal Flaws.” *Nature* 462 (7269): 44–45. doi:10.1038/462044a.

Drogat, B, M Bouchecareilh, S North, C Petibois, G Déléris, E Chevet, A Bikfalvi, M Moenner. 2007. “Acute L-Glutamine Deprivation Compromises VEGF-α Upregulation in A549/8 Human Carcinoma Cells.” *Journal of Cellular Physiology* 212 (2): 463–72. doi:10.1002/jcp.21044.

Dusick, J R, T C Glenn, W N Paul Lee, P M Vespa, D F Kelly, S M Lee, D Hovda, N A Martin. 2007. “Increased Pentose Phosphate Pathway Flux after Clinical Traumatic Brain Injury: A [1,2-13C2]glucose Labeling Study in Humans.” *Journal of Cerebral Blood Flow and Metabolism : Official Journal of the International Society of Cerebral Blood Flow and Metabolism* 27 (9): 1593–1602. doi:10.1038/sj.jcbfm.9600458.

Ehrke, E, C Arend, R Dringen. 2014. “3-Bromopyruvate Inhibits Glycolysis, Depletes Cellular Glutathione, and Compromises the Viability of Cultured Primary Rat Astrocytes.” *Journal of Neuroscience Research* (September). doi:10.1002/jnr.23474.

Elhammali, A, J E Ippolito, L Collins, J Crowley, J Marasa, D Piwnica-Worms. 2014. “A High-Throughput Fluorimetric Assay for 2-Hydroxyglutarate Identifies Zaprinast as a Glutaminase Inhibitor.” *Cancer Discovery* 4 (7): 828–39. doi:10.1158/2159-8290.CD-13-0572.

Emadi, A, S Ah Jun, T Tsukamoto, A T Fathi, M D Minden, C V Dang. 2014. “Inhibition of Glutaminase Selectively Suppresses the Growth of Primary Acute Myeloid Leukemia Cells with IDH Mutations.” *Experimental Hematology* 42 (4): 247–51. doi:10.1016/j.exphem.2013.12.001.

Fan, T W M, A N Lane, R M Higashi, M A Farag, H Gao, M Bousamra, D M Miller. 2009. “Altered Regulation of Metabolic Pathways in Human Lung Cancer Discerned by (13)C Stable Isotope-Resolved Metabolomics (SIRM).” *Molecular Cancer* 8 (January): 41. doi:10.1186/1476-4598-8-41.

Fantin, V R, J St-Pierre, P Leder. 2006. “Attenuation of LDH-A Expression Uncovers a Link between Glycolysis, Mitochondrial Physiology, and Tumor Maintenance.” *Cancer Cell* 9 (6): 425–34. doi:10.1016/j.ccr.2006.04.023.

Filipp, F V. 2013. “Cancer Metabolism Meets Systems Biology: Pyruvate Kinase Isoform PKM2 Is a Metabolic Master Regulator.” *Journal of Carcinogenesis* 12 (January): 14. doi:10.4103/1477-3163.115423.

Flavin, R, S Peluso, P L Nguyen, M Loda. 2010. “Fatty Acid Synthase as a Potential Therapeutic Target in Cancer.” *Future Oncology (London, England)* 6 (4): 551–62.

Flügel, D, A Görlach, T Kietzmann. 2012. “GSK-3β Regulates Cell Growth, Migration, and Angiogenesis via Fbw7 and USP28-Dependent Degradation of HIF-1α.” *Blood* 119 (5): 1292–1301. doi:10.1182/blood-2011-08-375014.

Fogal, V, I Babic, Y Chao, S Pastorino, R Mukthavaram, P Jiang, Y-J Cho, et al. 2014. “Mitochondrial p32 Is Upregulated in Myc Expressing Brain Cancers and Mediates Glutamine Addiction.” *Oncotarget*, November.

Frezza, C, L Zheng, O Folger, K N Rajagopalan, E D MacKenzie, L Jerby, M Micaroni, et al. 2011. “Haem Oxygenase Is Synthetically Lethal with the Tumour Suppressor Fumarate Hydratase.” *Nature* 477 (7363): 225–28. doi:10.1038/nature10363.

Fuchs, Y, Hermann Steller. 2011. “Programmed Cell Death in Animal Development and Disease.” *Cell* 147 (4): 742–58. doi:10.1016/j.cell.2011.10.033.

Galina, A. 2014. “Mitochondria: 3-Bromopyruvate vs. Mitochondria? A Small Molecule That Attacks Tumors by Targeting Their Bioenergetic Diversity.” *The International Journal of Biochemistry & Cell Biology* 54 (September): 266–71. doi:10.1016/j.biocel.2014.05.013.

Gallagher, S R. 2012. “One-Dimensional SDS Gel Electrophoresis of Proteins.” *Current Protocols in Molecular Biology* Chapter 10 (January): Unit 10.2A. doi:10.1002/0471142727.mb1002as97.

Gallagher, S R, S E Winston, S A Fuller, J G R Hurrell. 2008. *Immunoblotting and Immunodetection. Current Protocols in Immunology*. Vol. Chapter 8. doi:10.1002/0471142735.im0810s83.

Gameiro, P A, L A Laviolette, J K Kelleher, O Iliopoulos, G Stephanopoulos. 2013a. “Cofactor Balance by Nicotinamide Nucleotide Transhydrogenase (NNT) Coordinates Reductive Carboxylation and Glucose Catabolism in the Tricarboxylic Acid (TCA) Cycle.” *The Journal of Biological Chemistry* 288 (18): 12967–77. doi:10.1074/jbc.M112.396796.

Gameiro, P A, J Yang, A M Metelo, R Pérez-Carro, R Baker, Z Wang, A Arreola, et al. 2013b. “In Vivo HIF-Mediated Reductive Carboxylation Is Regulated by Citrate Levels and Sensitizes VHL-Deficient Cells to Glutamine Deprivation.” *Cell Metabolism* 17 (3): 372–85. doi:10.1016/j.cmet.2013.02.002.

Ganapathy-Kanniappan, S, J-F H Geschwind. 2013. “Tumor Glycolysis as a Target for Cancer Therapy: Progress and Prospects.” *Molecular Cancer* 12 (January): 152. doi:10.1186/1476-4598-12-152.

Ganapathy-Kanniappan, S, R Kunjithapatham, M S Torbenson, P P Rao, K A Carson, M Buijs, M Vali, J-F H Geschwind. 2012. “Human Hepatocellular Carcinoma in a Mouse Model: Assessment of Tumor Response to Percutaneous Ablation by Using Glyceraldehyde-3-Phosphate Dehydrogenase Antagonists.” *Radiology* 262 (3): 834–45. doi:10.1148/radiol.11111569.

Gao, P, I Tchernyshyov, T-C Chang, Y-S Lee, K Kita, T Ochi, K I Zeller, et al. 2009. “C-Myc Suppression of miR-23a/b Enhances Mitochondrial Glutaminase Expression and Glutamine Metabolism.” *Nature* 458 (7239): 762–65. doi:10.1038/nature07823.

Gaude, E, C Frezza. 2014. “Defects in Mitochondrial Metabolism and Cancer.” *Cancer & Metabolism* 2 (1): 10. doi:10.1186/2049-3002-2-10.

Girgis, H, O Masui, N Ma White, A Scorilas, F Rotondo, A Seivwright, M Gabril, et al. 2014. “Lactate Dehydrogenase A Is a Potential Prognostic Marker in Clear Cell Renal Cell Carcinoma.” *Molecular Cancer* 13 (1): 101. doi:10.1186/1476-4598-13-101.

Granata, A, R Nicoletti, V Tinaglia, L De Cecco, M E Pisanu, A Ricci, F Podo, et al. 2014. “Choline Kinase-Alpha by Regulating Cell Aggressiveness and Drug Sensitivity Is a Potential Druggable Target for Ovarian Cancer.” *British Journal of Cancer* 110 (2). Nature Publishing Group: 330–40. doi:10.1038/bjc.2013.729.

Green, D R, J E Chipuk. 2006. “p53 and Metabolism: Inside the TIGAR.” *Cell* 126 (1): 30–32. doi:10.1016/j.cell.2006.06.032.

Greenhouse, W V V, L Lehninger. 1977. “Magnitude of Malate-Aspartate Reduced Nicotinamide Adenine Dinucleotide Shuttle Activity in Intact Respiring Tumor Cells.” *Cancer Research* 37 (November): 4173–81.

Griffith, F. 1928. “The Significance of Pneumococcal Types.” *The Journal of Hygiene* 27 (2): 113–59.

Guo, C, S Liu, M-Z Sun. 2013. “Novel Insight into the Role of GAPDH Playing in Tumor.” *Clinical & Translational Oncology : Official Publication of the Federation of Spanish Oncology Societies and of the National Cancer Institute of Mexico* 15 (3): 167–72. doi:10.1007/s12094-012-0924-x.

Guo, W, Y Zhang, T Chen, Y Wang, J Xue, Y Zhang, W Xiao, X Mo, Y Lu. 2011. “Efficacy of RNAi Targeting of Pyruvate Kinase M2 Combined with Cisplatin in a Lung Cancer Model.” *Journal of Cancer Research and Clinical Oncology* 137 (1): 65–72. doi:10.1007/s00432-010-0860-5.

Hackenbrock, C R. 1968. “Chemical and Physical Fixation of Isolated Mitochondria in Low-Energy and High-Energy States.” *Proceedings of the National Academy of Sciences of the United States of America* 61: 598–605. doi:10.1073/pnas.61.2.598.

Hajdu, S I. 2011a. “A Note from History: Landmarks in History of Cancer, Part 1.” *Cancer* 117 (5): 1097–1102. doi:10.1002/cncr.25553.

Hajdu, S I. 2011b. “A Note from History: Landmarks in History of Cancer, Part 2.” *Cancer* 117 (12): 2811–20. doi:10.1002/cncr.25825.

Hajdu, S I. 2012a. “A Note from History: Landmarks in History of Cancer, Part 3.” *Cancer* 118 (4): 1155–68. doi:10.1002/cncr.26320.

Hajdu, S I. 2012b. “A Note from History: Landmarks in History of Cancer, Part 4.” *Cancer* 118 (20): 4914–28. doi:10.1002/cncr.27509.

Hajdu, S I, F Darvishian. 2013a. “A Note from History: Landmarks in History of Cancer, Part 5.” *Cancer* 119 (8): 1450–66. doi:10.1002/cncr.27889.

Hajdu, S I, M Vadmal. 2013b. “A Note from History: Landmarks in History of Cancer, Part 6.” *Cancer* 119 (23): 4058–82. doi:10.1002/cncr.28319.

Hanahan, D, R A Weinberg. 2000. “The Hallmarks of Cancer.” *Cell* 100 (1): 57–70.

Hanahan, D, R A Weinberg. 2011. “Hallmarks of Cancer: The next Generation.” *Cell* 144 (5): 646–74. doi:10.1016/j.cell.2011.02.013.

Hao, H-X, O Khalimonchuk, M Schraders, N Dephoure, J-P Bayley, H Kunst, P Devilee, et al. 2009. “SDH5, a Gene Required for Flavination of Succinate Dehydrogenase, Is Mutated in Paraganglioma.” *Science (New York, N.Y.)* 325 (5944): 1139–42. doi:10.1126/science.1175689.

He, P, T Takeuchi, E Yano. 2013. “An Overview of the China National Tobacco Corporation and State Tobacco Monopoly Administration.” *Environmental Health and Preventive Medicine* 18 (1): 85–90. doi:10.1007/s12199-012-0288-4.

Hensley, C T, A T Wasti, R J DeBerardinis. 2013. “Glutamine and Cancer: Cell Biology, Physiology, and Clinical Opportunities.” *The Journal of Clinical Investigation* 123 (9): 3678–84. doi:10.1172/JCI69600.

Hirst, J, M S King, K R Pryde. 2008. “The Production of Reactive Oxygen Species by Complex I.” *Biochemical Society Transactions* 36: 976–80. doi:10.1042/BST0360976.

Hitosugi, T, S Kang, M G Vander Heiden, T-W Chung, S Elf, K Lythgoe, S Dong, et al. 2009. “Tyrosine Phosphorylation Inhibits PKM2 to Promote the Warburg Effect and Tumor Growth.” *Science Signaling* 2 (97): ra73. doi:10.1126/scisignal.2000431.

Holohan, B, W E Wright, J W Shay. 2014. “Cell Biology of Disease: Telomeropathies: An Emerging Spectrum Disorder.” *The Journal of Cell Biology* 205 (3): 289–99. doi:10.1083/jcb.201401012.

Hsu, P P, D M Sabatini. 2008. “Cancer Cell Metabolism: Warburg and Beyond.” *Cell* 134 (5): 703–7. doi:10.1016/j.cell.2008.08.021.

Hu, S, A Balakrishnan, R A Bok, B Anderton, P E Z Larson, S J Nelson, J Kurhanewicz, D B Vigneron, A Goga. 2011. “13C-Pyruvate Imaging Reveals Alterations in Glycolysis That Precede c-Myc-Induced Tumor Formation and Regression.” *Cell Metabolism* 14 (1): 131–42. doi:10.1016/j.cmet.2011.04.012.

Huebner, R J, G J Todaro. 1969. “Oncogenes of RNA Tumor Viruses as Determinants of Cancer.” *Proceedings of the National Academy of Sciences of the United States of America* 64 (3): 1087–94.

Hulsewé, K W E, R R W J van der Hulst, G Ramsay, C L H van Berlo, N E P Deutz, P B Soeters. 2003. “Pulmonary Glutamine Production: Effects of Sepsis and Pulmonary Infiltrates.” *Intensive Care Medicine* 29 (10): 1833–36. doi:10.1007/s00134-003-1909-6.

Icard, P, and H Lincet. 2012. “A Global View of the Biochemical Pathways Involved in the Regulation of the Metabolism of Cancer Cells.” *Biochimica et Biophysica Acta* 1826 (2): 423–33. doi:10.1016/j.bbcan.2012.07.001.

Ihrlund, L S, E Hernlund, O Khan, M C Shoshan. 2008. “3-Bromopyruvate as Inhibitor of Tumour Cell Energy Metabolism and Chemopotentiator of Platinum Drugs.” *Molecular Oncology* 2 (1): 94–101. doi:10.1016/j.molonc.2008.01.003.

Iommarini, L, M A Calvaruso, I Kurelac, G Gasparre, A M Porcelli. 2013. “Complex I Impairment in Mitochondrial Diseases and Cancer: Parallel Roads Leading to Different Outcomes.” *The International Journal of Biochemistry & Cell Biology* 45 (1): 47–63. doi:10.1016/j.biocel.2012.05.016.

Isaacs, J S, Y J Jung, D R Mole, S Lee, C Torres-Cabala, Y-L Chung, M Merino, et al. 2005. “HIF Overexpression Correlates with Biallelic Loss of Fumarate Hydratase in Renal Cancer: Novel Role of Fumarate in Regulation of HIF Stability.” *Cancer Cell* 8 (2): 143–53. doi:10.1016/j.ccr.2005.06.017.

Jeffrey, F M, A Rajagopal, C R Malloy, A D Sherry. 1991. “13C-NMR: A Simple yet Comprehensive Method for Analysis of Intermediary Metabolism.” *Trends in Biochemical Sciences* 16: 5–10. doi:10.1016/0968-0004(91)90004-F.

Jha, M K, K Suk. 2013. “Pyruvate Dehydrogenase Kinase as a Potential Therapeutic Target for Malignant Gliomas.” *Brain Tumor Research and Treatment* 1 (2): 57–63. doi:10.14791/btrt.2013.1.2.57.

Jiang, Peng, Wenjing Du, and Mian Wu. 2014. “Regulation of the Pentose Phosphate Pathway in Cancer.” *Protein & Cell* 5 (8): 592–602. doi:10.1007/s13238-014-0082-8.

John, S, J N Weiss, B Ribalet. 2011. “Subcellular Localization of Hexokinases I and II Directs the Metabolic Fate of Glucose.” *PloS One* 6 (3): e17674. doi:10.1371/journal.pone.0017674.

Jonas, S K, C Benedetto, A Flatman, R H Hammond, L Micheletti, C Riley, P A Riley, D J Spargo, M Zonca, T F Slater. 1992. “Increased Activity of 6-Phosphogluconate Dehydrogenase and Glucose-6-Phosphate Dehydrogenase in Purified Cell Suspensions and Single Cells from the Uterine Cervix in Cervical Intraepithelial Neoplasia.” *British Journal of Cancer* 66 (1): 185–91.

Jones, J G, A D Sherry, F M Jeffrey, C J Storey, C R Malloy. 1993. “Sources of Acetyl-CoA Entering the Tricarboxylic Acid Cycle as Determined by Analysis of Succinate 13C Isotopomers.” *Biochemistry* 32: 12240–44.

Jose, C, N Bellance, R Rossignol. 2011. “Choosing between Glycolysis and Oxidative Phosphorylation: A Tumor’s Dilemma?” *Biochimica et Biophysica Acta* 1807 (6): 552–61. doi:10.1016/j.bbabio.2010.10.012.

Kaelin, W G. 2009. “SDH5 Mutations and Familial Paraganglioma: Somewhere Warburg Is Smiling.” *Cancer Cell* 16 (3): 180–82. doi:10.1016/j.ccr.2009.08.013.

Kankotia, S, P W Stacpoole. 2014. “Dichloroacetate and Cancer: New Home for an Orphan Drug?” *Biochimica et Biophysica Acta* 1846 (2): 617–29. doi:10.1016/j.bbcan.2014.08.005.

Kayser, G, W Sienel, B Kubitz, D Mattern, E Stickeler, B Passlick, M Werner, A Z Hausen. 2011. “Poor Outcome in Primary Non-Small Cell Lung Cancers Is Predicted by Transketolase TKTL1 Expression.” *Pathology* 43 (7): 719–24. doi:10.1097/PAT.0b013e32834c352b.

Kennedy, K M, P M Scarbrough, A Ribeiro, R Richardson, H Yuan, P Sonveaux, C D Landon, et al. 2013. “Catabolism of Exogenous Lactate Reveals It as a Legitimate Metabolic Substrate in Breast Cancer.” *PLoS ONE* 8 (9). doi:10.1371/journal.pone.0075154.

Kim, J-W, I Tchernyshyov, G L Semenza, C V Dang. 2006. “HIF-1-Mediated Expression of Pyruvate Dehydrogenase Kinase: A Metabolic Switch Required for Cellular Adaptation to Hypoxia.” *Cell Metabolism* 3 (3): 177–85. doi:10.1016/j.cmet.2006.02.002.

Knox, W E, M L Horowitz, G H Friedell. 1969. “The Proportionality of Glutaminase Content to Growth Rate and Morphology of Rat Neoplasms.” *Cancer Research* 29 (3): 669–80.

Ko, Y H, B L Smith, Y Wang, M G Pomper, D A Rini, M S Torbenson, J Hullihen, P L Pedersen. 2004. “Advanced Cancers: Eradication in All Cases Using 3-Bromopyruvate Therapy to Deplete ATP.” *Biochemical and Biophysical Research Communications* 324 (1): 269–75. doi:10.1016/j.bbrc.2004.09.047.

Ko, Y H, P L Pedersen, J F Geschwind. 2001. “Glucose Catabolism in the Rabbit VX2 Tumor Model for Liver Cancer: Characterization and Targeting Hexokinase.” *Cancer Letters* 173 (1): 83–91. doi:10.1016/S0304-3835(01)00667-X.

Koivunen, P, S Lee, C G Duncan, G Lopez, G Lu, S Ramkissoon, J A Losman, et al. 2012. “Transformation by the (R)-Enantiomer of 2-Hydroxyglutarate Linked to EGLN Activation.” *Nature* 483 (7390): 484–88. doi:10.1038/nature10898.

Kroemer, G, J Pouyssegur. 2008. “Tumor Cell Metabolism: Cancer’s Achilles' Heel.” *Cancer Cell* 13 (6): 472–82. doi:10.1016/j.ccr.2008.05.005.

Le, A, C R Cooper, A M Gouw, R Dinavahi, A Maitra, L M Deck, R E Royer, D L Vander Jagt, G L Semenza, C V Dang. 2010. “Inhibition of Lactate Dehydrogenase A Induces Oxidative Stress and Inhibits Tumor Progression.” *Proceedings of the National Academy of Sciences of the United States of America* 107 (5): 2037–42. doi:10.1073/pnas.0914433107.

Le, A, A N Lane, M Hamaker, S Bose, A Gouw, J Barbi, T Tsukamoto, et al. 2012. “Glucose-Independent Glutamine Metabolism via TCA Cycling for Proliferation and Survival in B Cells.” *Cell Metabolism* 15 (1): 110–21. doi:10.1016/j.cmet.2011.12.009.

Lee, S M, H J Koh, D C Park, B J Song, T L Huh, J W Park. 2002. “Cytosolic NADP+-Dependent Isocitrate Dehydrogenase Status Modulates Oxidative Damage to Cells.” *Free Radical Biology and Medicine* 32 (11): 1185–96. doi:10.1016/S0891-5849(02)00815-8.

Leite, T C, R G Coelho, D Silva, W S Coelho, M M Marinho-Carvalho, M Sola-Penna. 2011. “Lactate Downregulates the Glycolytic Enzymes Hexokinase and Phosphofructokinase in Diverse Tissues from Mice.” *FEBS Letters* 585 (1). Federation of European Biochemical Societies: 92–98. doi:10.1016/j.febslet.2010.11.009.

Leonardi, R, C Subramanian, S Jackowski, C O Rock. 2012. “Cancer-Associated Isocitrate Dehydrogenase Mutations Inactivate NADPH-Dependent Reductive Carboxylation.” *The Journal of Biological Chemistry* 287 (18): 14615–20. doi:10.1074/jbc.C112.353946.

Levesley, J, L Steele, C Taylor, P Sinha, S E Lawler. 2013. “ABT-263 Enhances Sensitivity to Metformin and 2-Deoxyglucose in Pediatric Glioma by Promoting Apoptotic Cell Death.” *PloS One* 8 (5): e64051. doi:10.1371/journal.pone.0064051.

Lew, M. 2007a. “Good Statistical Practice in Pharmacology. Problem 1.” *British Journal of Pharmacology* 152 (3): 295–98. doi:10.1038/sj.bjp.0707370.

Lew, M. 2007b. “Good Statistical Practice in Pharmacology. Problem 2.” *British Journal of Pharmacology* 152 (3): 299–303. doi:10.1038/sj.bjp.0707372.

Li, C, A Allen, J Kwagh, N M Doliba, W Qin, H Najafi, H W Collins, F M Matschinsky, C A Stanley, T J Smith. 2006. “Green Tea Polyphenols Modulate Insulin Secretion by Inhibiting Glutamate Dehydrogenase.” *Journal of Biological Chemistry* 281 (15): 10214–21. doi:10.1074/jbc.M512792200.

Li, D-M, Y-M Feng. 2011. “Signaling Mechanism of Cell Adhesion Molecules in Breast Cancer Metastasis: Potential Therapeutic Targets.” *Breast Cancer Research and Treatment* 128 (1): 7–21. doi:10.1007/s10549-011-1499-x.

Li, G X, Y K Chen, Z Hou, H Xiao, H Jin, G Lu, M J Lee, et al. 2010. “Pro-Oxidative Activities and Dose-Response Relationship of (-)-Epigallocatechin-3-Gallate in the Inhibition of Lung Cancer Cell Growth: A Comparative Study in Vivo and in Vitro.” *Carcinogenesis* 31 (5): 902–10. doi:10.1093/carcin/bgq039.

Lieser, E A T, G A Croghan, W K Nevala, M J Bradshaw, S N Markovic, A S Mansfield. 2013. “Up-Regulation of pro-Angiogenic Factors and Establishment of Tolerance in Malignant Pleural Effusions.” *Lung Cancer (Amsterdam, Netherlands)* 82 (1): 63–68. doi:10.1016/j.lungcan.2013.07.007.

Lincet, H, and P Icard. 2014. “How Do Glycolytic Enzymes Favour Cancer Cell Proliferation by Nonmetabolic Functions?” *Oncogene* 0 (August). Nature Publishing Group: 1–9. doi:10.1038/onc.2014.320.

Liu, H, D Huang, D L McArthur, L G Boros, N Nissen, A P Heaney. 2010. “Fructose Induces Transketolase Flux to Promote Pancreatic Cancer Growth.” *Cancer Research* 70 (15): 6368–76. doi:10.1158/0008-5472.CAN-09-4615.

Liu, Y. 2006. “Fatty Acid Oxidation Is a Dominant Bioenergetic Pathway in Prostate Cancer.” *Prostate Cancer and Prostatic Diseases* 9: 230–34. doi:10.1038/sj.pcan.4500879.

Lloyd, S G, H Zeng, P Wang, J C Chatham. 2004. “Lactate Isotopomer Analysis by 1H NMR Spectroscopy: Consideration of Long-Range Nuclear Spin-Spin Interactions.” *Magnetic Resonance in Medicine* 51: 1279–82. doi:10.1002/mrm.20075.

Locasale, J W, L C Cantley. 2010. “Altered Metabolism in Cancer.” *BMC Biology* 8 (January): 88. doi:10.1186/1741-7007-8-88.

London, R E. 1988. “13C Labeling in Studies of Metabolic Regulation.” *Progress in Nuclear Magnetic Resonance Spectroscopy*. doi:10.1016/0079-6565(88)80010-4.

Lyssiotis, C A, J Son, L C Cantley, A C Kimmelman. 2013. “Pancreatic Cancers Rely on a Novel Glutamine Metabolism Pathway to Maintain Redox Balance.” *Cell Cycle* 12 (13): 1987–88. doi:10.4161/cc.25307.

Macdonald, Michael J., Laura J. Brown, Melissa J. Longacre, Scott W. Stoker, and Mindy a. Kendrick. 2013. “Knockdown of Both Mitochondrial Isocitrate Dehydrogenase Enzymes in Pancreatic Beta Cells Inhibits Insulin Secretion.” *Biochimica et Biophysica Acta - General Subjects* 1830 (11). Elsevier B.V.: 5104–11. doi:10.1016/j.bbagen.2013.07.013.

Mainali, P, S Pant, A P Rodriguez, A Deshmukh, J L Mehta. 2014. “Tobacco and Cardiovascular Health.” *Cardiovascular Toxicology*, September. doi:10.1007/s12012-014-9280-0.

Malloy, C R, A D Sherry, F M Jeffrey. 1988. “Evaluation of Carbon Flux and Substrate Selection through Alternate Pathways Involving the Citric Acid Cycle of the Heart by 13C NMR Spectroscopy.” *The Journal of Biological Chemistry* 263 (15): 6964–71.

Malloy, C R, A D Sherry, F M Jeffrey. 1990. “Analysis of Tricarboxylic Acid Cycle of the Heart Using 13C Isotope Isomers.” *The American Journal of Physiology* 259 (3 Pt 2): H987–95.

Martin, F P J, N Sprenger, I Montoliu, S Rezzi, S Kochhar, J K Nicholson. 2010. “Dietary Modulation of Gut Functional Ecology Studied by Fecal Metabonomics.” *Journal of Proteome Research* 9: 5284–95. doi:10.1021/pr100554m.

Mason, G F, D L Rothman. 2004. “Basic Principles of Metabolic Modeling of NMR 13C Isotopic Turnover to Determine Rates of Brain Metabolism in Vivo.” *Metabolic Engineering* 6 (1): 75–84. doi:10.1016/j.ymben.2003.10.003.

May, M. 2014. “Statistics: Attacking an Epidemic.” *Nature* 509 (7502): S50–51. doi:10.1038/509S50a.

Maya-Mendoza, A, J Ostrakova, M Kosar, A Hall, P Duskova, M Mistrik, J M Merchut-Maya, et al. 2014. “Myc and Ras Oncogenes Engage Different Energy Metabolism Programs and Evoke Distinct Patterns of Oxidative and DNA Replication Stress.” *Molecular Oncology*, November: 1–16. doi:10.1016/j.molonc.2014.11.001.

Mazurek, S, C B Boschek, F Hugo, E Eigenbrodt. 2005. “Pyruvate Kinase Type M2 and Its Role in Tumor Growth and Spreading.” *Seminars in Cancer Biology* 15 (4): 300–308. doi:10.1016/j.semcancer.2005.04.009.

Menendez, J A, R Lupu. 2007. “Fatty Acid Synthase and the Lipogenic Phenotype in Cancer Pathogenesis.” *Nature Reviews. Cancer* 7 (October): 763–77. doi:10.1038/nrc2222.

Metallo, C M, P A Gameiro, E L Bell, K R Mattaini, J Yang, K Hiller, C M Jewell, et al. 2012. “Reductive Glutamine Metabolism by IDH1 Mediates Lipogenesis under Hypoxia.” *Nature* 481 (7381): 380–84. doi:10.1038/nature10602.

Miao, P, S Sheng, X Sun, J Liu, G Huang. 2013. “Lactate Dehydrogenase A in Cancer: A Promising Target for Diagnosis and Therapy.” *IUBMB Life* 65 (11): 904–10. doi:10.1002/iub.1216.

Micke, P, A Ostman. 2004. “Tumour-Stroma Interaction: Cancer-Associated Fibroblasts as Novel Targets in Anti-Cancer Therapy?” *Lung Cancer (Amsterdam, Netherlands)* 45 Suppl 2 (August): S163–75. doi:10.1016/j.lungcan.2004.07.977.

Minor, R K, D L Smith, A M Sossong, S Kaushik, S Poosala, E L Spangler, G S Roth, et al. 2010. “Chronic Ingestion of 2-Deoxy-D-Glucose Induces Cardiac Vacuolization and Increases Mortality in Rats.” *Toxicology and Applied Pharmacology* 243 (3): 332–39. doi:10.1016/j.taap.2009.11.025.

Mogi, A, K Koga, M Aoki, M Hamasaki, N Uesugi, A Iwasaki, T Shirakusa, K Tamura, and K Nabeshima. 2013. “Expression and Role of GLUT-1, MCT-1, and MCT-4 in Malignant Pleural Mesothelioma.” *Virchows Archiv : An International Journal of Pathology* 462 (1): 83–93. doi:10.1007/s00428-012-1344-6.

Moore, P S, Y Chang. 2010. “Why Do Viruses Cause Cancer? Highlights of the First Century of Human Tumour Virology.” *Nature Reviews. Cancer* 10 (12): 878–89. doi:10.1038/nrc2961.

Morin, A, E Letouzé, A-P Gimenez-Roqueplo, J Favier. 2014. “Oncometabolites-Driven Tumorigenesis: From Genetics to Targeted Therapy.” *International Journal of Cancer. Journal International Du Cancer* 135 (10): 2237–48. doi:10.1002/ijc.29080.

Mullen, A R, W W Wheaton, E S Jin, P-H Chen, L B Sullivan, T Cheng, Y Yang, W M Linehan, N S Chandel, R J DeBerardinis. 2012. “Reductive Carboxylation Supports Growth in Tumour Cells with Defective Mitochondria.” *Nature* 481 (7381): 385–88. doi:10.1038/nature10642.

Müller, S A, K Holzapfel, C Seidl, U Treiber, B J Krause, R Senekowitsch-Schmidtke. 2009. “Characterization of Choline Uptake in Prostate Cancer Cells Following Bicalutamide and Docetaxel Treatment.” *European Journal of Nuclear Medicine and Molecular Imaging* 36: 1434–42. doi:10.1007/s00259-009-1117-x.

Murphy, E J. 2006. “Stable Isotope Methods for the in Vivo Measurement of Lipogenesis and Triglyceride Metabolism.” *Journal of Animal Science* 84 Suppl (April): E94–104.

Navab, R, D Strumpf, B Bandarchi, C Zhu, M Pintilie, V R Ramnarine, E Ibrahimov, et al. 2011. “Prognostic Gene-Expression Signature of Carcinoma-Associated Fibroblasts in Non-Small Cell Lung Cancer.” *Proceedings of the National Academy of Sciences of the United States of America* 108 (17): 7160–65. doi:10.1073/pnas.1014506108.

Nederlof, R, O Eerbeek, M W Hollmann, R Southworth, C J Zuurbier. 2014. “Targeting Hexokinase II to Mitochondria to Modulate Energy Metabolism and Reduce Ischaemia-Reperfusion Injury in Heart.” *British Journal of Pharmacology* 171 (8): 2067–79. doi:10.1111/bph.12363.

Nelson, D E, D W Jarman, J Rehm, T K Greenfield, G Rey, W C Kerr, P Miller, K D Shield, Y Ye, T S Naimi. 2013. “Alcohol-Attributable Cancer Deaths and Years of Potential Life Lost in the United States.” *American Journal of Public Health* 103 (4): 641–48. doi:10.2105/AJPH.2012.301199.

Nelson, D E, A Lehninger, M Cox. 2005. *Lehninger Principles of Biochemistry*. *Biochemistry and Molecular Biology Education*. 4th Editio. Vol. 33. New York: W. H. Freeman.

Nicholls, C, A R Pinto, H Li, L Li, L Wang, R Simpson, J-P Liu. 2012. “Glyceraldehyde-3-Phosphate Dehydrogenase (GAPDH) Induces Cancer Cell Senescence by Interacting with Telomerase RNA Component.” *Proceedings of the National Academy of Sciences of the United States of America* 109 (33): 13308–13. doi:10.1073/pnas.1206672109.

Nicholson, J K, J C Lindon, E Holmes. 1999. “‘Metabonomics’: Understanding the Metabolic Responses of Living Systems to Pathophysiological Stimuli via Multivariate Statistical Analysis of Biological NMR Spectroscopic Data.” *Xenobiotica; the Fate of Foreign Compounds in Biological Systems* 29 (11): 1181–89. doi:10.1080/004982599238047.

Nieminen, A-L, S Qanungo, E A Schneider, B-H Jiang, F H Agani. 2005. “Mdm2 and HIF-1alpha Interaction in Tumor Cells during Hypoxia.” *Journal of Cellular Physiology* 204 (2): 364–69. doi:10.1002/jcp.20406.

Nunes, P M, J G Jones, A P Rolo, C M M Palmeira, R A Carvalho. 2011. “Ursodeoxycholic Acid Treatment of Hepatic Steatosis: A 13C NMR Metabolic Study.” *NMR in Biomedicine* 24 (December 2010): 1145–58. doi:10.1002/nbm.1672.

Obre, E, R Rossignol. 2014. “Emerging Concepts in Bioenergetics and Cancer Research: Metabolic Flexibility, Coupling, Symbiosis, Switch, Oxidative Tumors, Metabolic Remodeling, Signaling and Bioenergetic Therapy.” *The International Journal of Biochemistry & Cell Biology*, December. doi:10.1016/j.biocel.2014.12.008.

Oermann, E K, J Wu, K-L Guan,Y Xiong. 2012. “Alterations of Metabolic Genes and Metabolites in Cancer.” *Seminars in Cell & Developmental Biology* 23 (4). Elsevier Ltd: 370–80. doi:10.1016/j.semcdb.2012.01.013.

Oliveira, P F, M G Alves, L Rato, S Laurentino, J Silva, R Sá, A Barros, et al. 2012. “Effect of Insulin Deprivation on Metabolism and Metabolism-Associated Gene Transcript Levels of in Vitro Cultured Human Sertoli Cells.” *Biochimica et Biophysica Acta* 1820 (2): 84–89. doi:10.1016/j.bbagen.2011.11.006.

Pàez-Ribes, M, E Allen, J Hudock, T Takeda, H Okuyama, F Viñals, M Inoue, G Bergers, D Hanahan, O Casanovas. 2009. “Antiangiogenic Therapy Elicits Malignant Progression of Tumors to Increased Local Invasion and Distant Metastasis.” *Cancer Cell* 15 (3): 220–31. doi:10.1016/j.ccr.2009.01.027.

Pastorino, J G, N Shulga, J B Hoek. 2002. “Mitochondrial Binding of Hexokinase II Inhibits Bax-Induced Cytochrome c Release and Apoptosis.” *The Journal of Biological Chemistry* 277 (9): 7610–18. doi:10.1074/jbc.M109950200.

Patra, K C, N Hay. 2014. “The Pentose Phosphate Pathway and Cancer.” *Trends in Biochemical Sciences* 39 (8): 347–54. doi:10.1016/j.tibs.2014.06.005.

Pedersen, P L. 2007. “Warburg, Me and Hexokinase 2: Multiple Discoveries of Key Molecular Events Underlying One of Cancers’ Most Common Phenotypes, the ‘Warburg Effect’, I.e., Elevated Glycolysis in the Presence of Oxygen.” *Journal of Bioenergetics and Biomembranes* 39 (3): 211–22. doi:10.1007/s10863-007-9094-x.

Pedersen, P L. 2012. “3-Bromopyruvate (3BP) a Fast Acting, Promising, Powerful, Specific, and Effective ‘Small Molecule’ Anti-Cancer Agent Taken from Labside to Bedside: Introduction to a Special Issue.” *Journal of Bioenergetics and Biomembranes* 44 (1): 1–6. doi:10.1007/s10863-012-9425-4.

Pelicano, H, D S Martin, R-H Xu, P Huang. 2006. “Glycolysis Inhibition for Anticancer Treatment.” *Oncogene* 25 (34): 4633–46. doi:10.1038/sj.onc.1209597.

Pfeiffer, T, S Schuster, S Bonhoeffer. 2001. “Cooperation and Competition in the Evolution of ATP-Producing Pathways.” *Science (New York, N.Y.)* 292 (5516): 504–7. doi:10.1126/science.1058079.

Phelan, J J, F MacCarthy, R Feighery, N J O’Farrell, N Lynam-Lennon, B Doyle, D O’Toole, N Ravi, J V Reynolds, J O’Sullivan. 2014. “Differential Expression of Mitochondrial Energy Metabolism Profiles across the Metaplasia-Dysplasia-Adenocarcinoma Disease Sequence in Barrett’s Oesophagus.” *Cancer Letters* 354 (1): 122–31. doi:10.1016/j.canlet.2014.07.035.

Podo, F, S Canevari, R Canese, M E Pisanu, A Ricci, E Iorio. 2011. “MR Evaluation of Response to Targeted Treatment in Cancer Cells.” *NMR in Biomedicine* 24 (May 2010): 648–72. doi:10.1002/nbm.1658.

Pollard, P J, J J Brière, N A Alam, J Barwell, E Barclay, N C Wortham, T Hunt, et al. 2005. “Accumulation of Krebs Cycle Intermediates and over-Expression of HIF1alpha in Tumours Which Result from Germline FH and SDH Mutations.” *Human Molecular Genetics* 14 (15): 2231–39. doi:10.1093/hmg/ddi227.

Popovici-Muller, J, J O Saunders, F G Salituro, J M Travins, S Yan, F Zhao, S Gross, et al. 2012. “Discovery of the First Potent Inhibitors of Mutant IDH1 That Lower Tumor 2-HG in Vivo.” *ACS Medicinal Chemistry Letters* 3 (10): 850–55. doi:10.1021/ml300225h.

Preuss, J, A D Richardson, A Pinkerton, M Hedrick, E Sergienko, S Rahlfs, K Becker,L Bode. 2013. “Identification and Characterization of Novel Human Glucose-6-Phosphate Dehydrogenase Inhibitors.” *Journal of Biomolecular Screening* 18 (3): 286–97. doi:10.1177/1087057112462131.

Priebe, A, L Tan, H Wahl, A Kueck, G He, R Kwok, A Opipari, J R Liu. 2011. “Glucose Deprivation Activates AMPK and Induces Cell Death through Modulation of Akt in Ovarian Cancer Cells.” *Gynecologic Oncology* 122 (2): 389–95. doi:10.1016/j.ygyno.2011.04.024.

Proctor, R N. 2012. “The History of the Discovery of the Cigarette-Lung Cancer Link: Evidentiary Traditions, Corporate Denial, Global Toll.” *Tobacco Control* 21 (2): 87–91. doi:10.1136/tobaccocontrol-2011-050338.

Rakheja, D, S Konoplev, L J Medeiros, W Chen. 2012. “IDH Mutations in Acute Myeloid Leukemia.” *Human Pathology* 43 (10): 1541–51. doi:10.1016/j.humpath.2012.05.003.

Ralser, M, M M Wamelink, Al Kowald, B Gerisch, G Heeren, E Struys, E Klipp, et al. 2007. "Dynamic Rerouting of the Carbohydrate Flux Is Key to Counteracting Oxidative Stress." *Journal of Biology* 6 (4): 10. doi:10.1186/jbiol61.

Ramírez de Molina, A, J Sarmentero-Estrada, C Belda-Iniesta, M Tarón, V Ramírez de Molina, P Cejas, M Skrzypski, et al. 2007. "Expression of Choline Kinase Alpha to Predict Outcome in Patients with Early-Stage Non-Small-Cell Lung Cancer: A Retrospective Study." *The Lancet. Oncology* 8 (10): 889–97. doi:10.1016/S1470-2045(07)70279-6.

Rodríguez-Enríquez, S, L Carreño-Fuentes, J C Gallardo-Pérez, E Saavedra, H Quezada, A Vega, A Marín-Hernández, V Olín-Sandoval, M E Torres-Márquez, R Moreno-Sánchez. 2010. "Oxidative Phosphorylation Is Impaired by Prolonged Hypoxia in Breast and Possibly in Cervix Carcinoma." *The International Journal of Biochemistry & Cell Biology* 42 (10): 1744–51. doi:10.1016/j.biocel.2010.07.010.

Rohle, D, J Popovici-Muller, N Palaskas, S Turcan, C Grommes, C Campos, J Tsoi, et al. 2013. "An Inhibitor of Mutant IDH1 Delays Growth and Promotes Differentiation of Glioma Cells." *Science (New York, N.Y.)* 340 (6132): 626–30. doi:10.1126/science.1236062.

Rossignol, R, R Gilkerson, R Aggeler, K Yamagata, S J Remington, R Capaldi. 2004. "Energy Substrate Modulates Mitochondrial Structure and Oxidative Capacity in Cancer Cells." *Cancer Research* 64: 985–93. doi:10.1158/0008-5472.CAN-03-1101.

Roy, M, Y-H Luo, M Ye, J Liu. 2013. "Nonsmall Cell Lung Cancer Therapy: Insight into Multitargeted Small-Molecule Growth Factor Receptor Inhibitors." *BioMed Research International* 2013 (January): 964743. doi:10.1155/2013/964743.

Rysman, E, K Brusselmans, K Scheys, L Timmermans, R Derua, S Munck, P P Van Veldhoven, et al. 2010. "De Novo Lipogenesis Protects Cancer Cells from Free Radicals and Chemotherapeutics by Promoting Membrane Lipid Saturation." *Cancer Research* 70: 8117–26. doi:10.1158/0008-5472.CAN-09-3871.

Sakamoto, Y, N Terashita, T Muraguchi, T Fukusato, S Kubota. 2013. "Effects of Epigallocatechin-3-Gallate (EGCG) on A549 Lung Cancer Tumor Growth and Angiogenesis." *Bioscience, Biotechnology, and Biochemistry* 77 (9): 1799–1803. doi:10.1271/bbb.120882.

Samanta, D, D M Gilkes, P Chaturvedi, L Xiang, G L Semenza. 2014. "Hypoxia-Inducible Factors Are Required for Chemotherapy Resistance of Breast Cancer Stem Cells." *Proceedings of the National Academy of Sciences of the United States of America* 111 (50): E5429–38. doi:10.1073/pnas.1421438111.

Scaglia, N, S Tyekucheva, G Zadra, C Photopoulos, M Loda. 2014. "De Novo Fatty Acid Synthesis at the Mitotic Exit Is Required to Complete Cellular Division." *Cell Cycle* 13 (January 2015): 859–68. doi:10.4161/cc.27767.

Schmidt, M M, R Dringen. 2009. "Differential Effects of Iodoacetamide and Iodoacetate on Glycolysis and Glutathione Metabolism of Cultured Astrocytes." *Frontiers in Neuroenergetics* 1 (March): 1. doi:10.3389/neuro.14.001.2009.

Schug, Z T, B Peck, D T Jones, Q Zhang, S Grosskurth, I S Alam, L M Goodwin, et al. 2015. “Acetyl-CoA Synthetase 2 Promotes Acetate Utilization and Maintains Cancer Cell Growth under Metabolic Stress.” *Cancer Cell* 27 (1): 57–71. doi:10.1016/j.ccell.2014.12.002.

Seeley, R, T Stephens, P Tate. 2001. *Anatomia & Fisiologia*. Lusodidacta.

Selak, M A, S M Armour, E D MacKenzie, H Boulahbel, D G Watson, K D Mansfield, Y Pan, M C Simon, C B Thompson, E Gottlieb. 2005. “Succinate Links TCA Cycle Dysfunction to Oncogenesis by Inhibiting HIF-Alpha Prolyl Hydroxylase.” *Cancer Cell* 7 (1): 77–85. doi:10.1016/j.ccr.2004.11.022.

Semenza, G L. 2000. “Expression of Hypoxia-Inducible Factor 1: Mechanisms and Consequences.” *Biochemical Pharmacology* 59 (1): 47–53. doi:10.1016/S0006-2952(99)00292-0.

Semenza, G L. 2010. “HIF-1: Upstream and Downstream of Cancer Metabolism.” *Current Opinion in Genetics & Development* 20 (1): 51–56. doi:10.1016/j.gde.2009.10.009.

Semilia, M, J Hennenlotter, C Pavone, T Bischoff, U Kühs, G Gakis, J Bedke, A Stenzl, C Schwentner, T Todenhöfer. 2015. “Expression Patterns and Prognostic Role of Transketolase-like 1 in Muscle-Invasive Bladder Cancer.” *World Journal of Urology* 2 (January): 18. doi:10.1007/s00345-014-1473-4.

Shah, T, F Wildes, M F Penet, P T Winnard, K Glunde, D Artemov, E Ackerstaff, et al. 2010. “Choline Kinase Overexpression Increases Invasiveness and Drug Resistance of Human Breast Cancer Cells.” *NMR in Biomedicine* 23 (6): 633–42. doi:10.1002/nbm.1510.

Sharaf El Dein, O, C Gallerne, C Brenner, C Lemaire. 2012. “Increased Expression of VDAC1 Sensitizes Carcinoma Cells to Apoptosis Induced by DNA Cross-Linking Agents.” *Biochemical Pharmacology* 83 (9): 1172–82. doi:10.1016/j.bcp.2012.01.017.

Sharma, B K, R Srinivasan, S Kapil, B Singla, Y K Chawla, A C, N Saini, et al. 2013. “Angiogenic and Anti-Angiogenic Factor Gene Transcript Level Quantitation by Quantitative Real Time PCR in Patients with Hepatocellular Carcinoma.” *Molecular Biology Reports* 40 (10): 5843–52. doi:10.1007/s11033-013-2690-4.

Shavit, R, M Ilouze, T Feinberg, Y R Lawrence, Y Tzur, N Peled. 2015. “Mitochondrial Induction as a Potential Radio-Sensitizer in Lung Cancer Cells - a Short Report.” *Cellular Oncology*. doi:10.1007/s13402-014-0212-6.

Shi, Y, B M Pinto. 2014. “Human Lactate Dehydrogenase a Inhibitors: A Molecular Dynamics Investigation.” *PloS One* 9 (1): e86365. doi:10.1371/journal.pone.0086365.

Shibuya, N, K Inoue, G Tanaka, K Akimoto, K Kubota. 2015. “Augmented Pentose Phosphate Pathway Plays Critical Roles in Colorectal Carcinomas.” *Oncology*. doi:10.1159/000369905.

Shulman, R G, D L Rothman. 2001. “The ‘Glycogen Shunt’ in Exercising Muscle: A Role for Glycogen in Muscle Energetics and Fatigue.” *Proceedings of the National Academy of Sciences of the United States of America* 98 (2): 457–61. doi:10.1073/pnas.98.2.457.

Siegel, R, J Ma, Z Zou, A Jemal. 2014. “Cancer Statistics, 2014.” *CA: A Cancer Journal for Clinicians* 64 (1): 9–29. doi:10.3322/caac.21208.

Silva, A M, F Martins, J G Jones, Rui A Carvalho. 2011. “2H2O Incorporation into Hepatic Acetyl-CoA and de Novo Lipogenesis as Measured by Krebs Cycle-Mediated 2H-Enrichment of Glutamate and Glutamine.” *Magnetic Resonance in Medicine : Official Journal of the Society of Magnetic Resonance in Medicine / Society of Magnetic Resonance in Medicine* 66 (6): 1526–30. doi:10.1002/mrm.22955.

Smith, P K, R I Krohn, G T Hermanson, A K Mallia, F H Gartner, M D Provenzano, E K Fujimoto, N M Goeke, B J Olson, D C Klenk. 1985. “Measurement of Protein Using Bicinchoninic Acid.” *Analytical Biochemistry* 150 (1): 76–85. doi:10.1016/0003-2697(85)90442-7.

Smolková, K, P Ježek. 2012. “The Role of Mitochondrial NADPH-Dependent Isocitrate Dehydrogenase in Cancer Cells.” *International Journal of Cell Biology* 2012 (January): 273947. doi:10.1155/2012/273947.

Sobus, S L, G W Warren. 2014. “The Biologic Effects of Cigarette Smoke on Cancer Cells.” *Cancer* 120 (23): 3617–26. doi:10.1002/cncr.28904.

Soga, T. 2013. “Cancer Metabolism: Key Players in Metabolic Reprogramming.” *Cancer Science* 104 (3): 275–81. doi:10.1111/cas.12085.

Sotgia, F, D Whitaker-Menezes, U E Martinez-Outschoorn, N Flomenberg, R C Birbe, A K Witkiewicz, A Howell, N J Philp, R G Pestell, M P Lisanti. 2012. “Mitochondrial Metabolism in Cancer Metastasis: Visualizing Tumor Cell Mitochondria and the ‘Reverse Warburg Effect’ in Positive Lymph Node Tissue.” *Cell Cycle (Georgetown, Tex.)* 11 (7): 1445–54. doi:10.4161/cc.19841.

Soucek, L, J Whitfield, C P Martins, A J Finch, D J Murphy, N M Sodir, A N Karnezis, L B Swigart, S Nasi, G I Evan. 2008. “Modelling Myc Inhibition as a Cancer Therapy.” *Nature* 455 (7213): 679–83. doi:10.1038/nature07260.

Sriskanthadevan, S, D V Jeyaraju, T E Chung, S Prabha, W Xu, M Skrtic, B Jhas, et al. 2015. “AML Cells Have Low Spare Reserve Capacity in Their Respiratory Chain That Renders Them Susceptible to Oxidative Metabolic Stress.” *Blood*, January. doi:10.1182/blood-2014-08-594408.

Stincone, A, A Prigione, T Cramer, M M C Wamelink, K Campbell, E Cheung, V Olin-Sandoval, et al. 2014. “The Return of Metabolism: Biochemistry and Physiology of the Pentose Phosphate Pathway.” *Biological Reviews of the Cambridge Philosophical Society*, September. doi:10.1111/brv.12140.

Stratton, M R, P J Campbell, P A Futreal. 2009. “The Cancer Genome.” *Nature* 458 (7239). Nature Publishing Group: 719–24. doi:10.1038/nature07943.

Sullivan, E J, M Kurtoglu, R Brenneman, H Liu, T J Lampidis. 2014. “Targeting Cisplatin-Resistant Human Tumor Cells with Metabolic Inhibitors.” *Cancer Chemotherapy and Pharmacology* 73 (2): 417–27. doi:10.1007/s00280-013-2366-8.

Sun, L, S Shukair, T J Naik, F Moazed, H Ardehali. 2008. “Glucose Phosphorylation and Mitochondrial Binding Are Required for the Protective Effects of Hexokinases I and II.” *Molecular and Cellular Biology* 28 (3): 1007–17. doi:10.1128/MCB.00224-07.

Sutendra, G, A Kinnaird, P Dromparis, R Paulin, T H Stenson, A Haromy, K Hashimoto, N Zhang, E Flaim, E D Michelakis. 2014. “A Nuclear Pyruvate Dehydrogenase Complex Is Important for the Generation of Acetyl-CoA and Histone Acetylation.” *Cell* 158 (1): 84–97. doi:10.1016/j.cell.2014.04.046.

Szyperski, T, J E Bailey, K Wüthrich. 1996. “Detecting and Dissecting Metabolic Fluxes Using Biosynthetic Fractional 13C Labeling and Two-Dimensional NMR Spectroscopy.” *Trends in Biotechnology*. doi:10.1016/S0167-7799(96)10056-1.

Tan, F, Y Jiang, N Sun, Z Chen, Y Lv, K Shao, N Li, et al. 2012. “Identification of Isocitrate Dehydrogenase 1 as a Potential Diagnostic and Prognostic Biomarker for Non-Small Cell Lung Cancer by Proteomic Analysis.” *Molecular & Cellular Proteomics : MCP* 11 (2): M111.008821. doi:10.1074/mcp.M111.008821.

Tavares, L C, Ivana Jarak, F N Nogueira, P J Oliveira, R A Carvalho. 2015. “Metabolic Evaluations of Cancer Metabolism by NMR-Based Stable Isotope Tracer Methodologies.” *Eur J Clin Invest* 45 (1): 37–43. doi:10.1111/eci.12358.

Tavares-Valente, D, F Baltazar, R Moreira, O Queirós. 2013. “Cancer Cell Bioenergetics and pH Regulation Influence Breast Cancer Cell Resistance to Paclitaxel and Doxorubicin.” *Journal of Bioenergetics and Biomembranes* 45 (5): 467–75. doi:10.1007/s10863-013-9519-7.

Ternette, N, M Yang, M Laroyia, M Kitagawa, L O’Flaherty, K Wolhulter, K Igarashi, et al. 2013. “Inhibition of Mitochondrial Aconitase by Succination in Fumarate Hydratase Deficiency.” *Cell Reports* 3 (3): 689–700. doi:10.1016/j.celrep.2013.02.013.

Thornburg, J M, K K Nelson, B F Clem, A N Lane, S Arumugam, A Simmons, J W Eaton, S Telang, J Chesney. 2008. “Targeting Aspartate Aminotransferase in Breast Cancer.” *Breast Cancer Research : BCR* 10 (5): R84. doi:10.1186/bcr2154.

Tokunaga, K, Y Nakamura, K Sakata, K Fujimori, M Ohkubo, K Sawada, S Sakiyama. 1987. “Enhanced Expression of a Glyceraldehyde-3-Phosphate Dehydrogenase Gene in Human Lung Cancers.” *Cancer Research* 47: 5616–19.

Tomlinson, I P M, N A Alam, A J Rowan, E Barclay, E E M Jaeger, D Kelsell, I Leigh, et al. 2002. “Germline Mutations in FH Predispose to Dominantly Inherited Uterine Fibroids, Skin Leiomyomata and Papillary Renal Cell Cancer.” *Nature Genetics* 30 (4): 406–10. doi:10.1038/ng849.

Traverso, N, R Ricciarelli, M Nitti, B Marengo, A L Furfaro, M A Pronzato, U M Marinari, C Domenicotti. 2013. “Role of Glutathione in Cancer Progression and Chemoresistance.” *Oxidative Medicine and Cellular Longevity* 2013 (January): 972913. doi:10.1155/2013/972913.

Tristan, C, N Shahani, T W Sedlak, A Sawa. 2011. “The Diverse Functions of GAPDH: Views from Different Subcellular Compartments.” *Cellular Signalling* 23 (2): 317–23. doi:10.1016/j.cellsig.2010.08.003.

Trousil, S, P Lee, D J Pinato, J K Ellis, R Dina, E O Aboagye, H C Keun, R Sharma. 2014. “Alterations of Choline Phospholipid Metabolism in Endometrial Cancer Are Caused by Choline Kinase Alpha Overexpression and a Hyperactivated Deacylation Pathway.” *Cancer Research* 74: 6867–77. doi:10.1158/0008-5472.CAN-13-2409.

Tsouko, E, A S Khan, M A White, J J Han, Y Shi, F A Merchant, M A Sharpe, L Xin, and D E Frigo. 2014. “Regulation of the Pentose Phosphate Pathway by an Androgen Receptor-mTOR-Mediated Mechanism and Its Role in Prostate Cancer Cell Growth.” *Oncogenesis* 3 (5). Nature Publishing Group: e103. doi:10.1038/oncsis.2014.18.

Unwith, S, H Zhao, L Hennah, and D Ma. 2014. “The Potential Role of HIF on Tumour Progression and Dissemination.” *International Journal of Cancer. Journal International Du Cancer* 00 (April): 1–13. doi:10.1002/ijc.28889.

Van Hall, G. 2000. “Lactate as a Fuel for Mitochondrial Respiration.” In *Acta Physiologica Scandinavica*, 168:643–56. doi:10.1046/j.1365-201X.2000.00716.x.

Vander Heiden, M G, S Y Lunt, T L Dayton, B P Fiske, W J Israelsen, K R Mattaini, N I Vokes, et al. 2011. “Metabolic Pathway Alterations That Support Cell Proliferation.” *Cold Spring Harbor Symposia on Quantitative Biology* 76 (January): 325–34. doi:10.1101/sqb.2012.76.010900.

Vander Heiden, M G, L C Cantley, C B Thompson. 2009. “Understanding the Warburg Effect: The Metabolic Requirements of Cell Proliferation.” *Science (New York, N.Y.)* 324 (2009): 1029–33. doi:10.1126/science.1160809.

Vega-Naredo, I, R Loureiro, K A Mesquita, I A Barbosa, L C Tavares, A F Branco, J R Erickson, et al. 2014. “Mitochondrial Metabolism Directs Stemness and Differentiation in P19 Embryonal Carcinoma Stem Cells.” *Cell Death and Differentiation* 21 (10): 1560–74. doi:10.1038/cdd.2014.66.

Vestweber, D. 2014. “Cadherins in Tissue Architecture and Disease.” *Journal of Molecular Medicine (Berlin, Germany)*, December. doi:10.1007/s00109-014-1231-5.

Vichai, V, and K Kirtikara. 2006. “Sulforhodamine B Colorimetric Assay for Cytotoxicity Screening.” *Nature Protocols* 1 (3): 1112–16. doi:10.1038/nprot.2006.179.

Villaseñor, A, J M Kinross, J V Li, N Penney, R H Barton, J K Nicholson, A Darzi, C Barbas, E Holmes. 2014. “1H NMR Global Metabolic Phenotyping of Acute Pancreatitis in the Emergency Unit.” *Journal of Proteome Research* 13 (12): 5362–75. doi:10.1021/pr500161w.

Wang, J, X Zhang, D Ma, W-N P Lee, J Xiao, Y Zhao, V L Go, et al. 2013. “Inhibition of Transketolase by Oxythiamine Altered Dynamics of Protein Signals in Pancreatic Cancer Cells.” *Experimental Hematology & Oncology* 2 (1): 18. doi:10.1186/2162-3619-2-18.

Wang, J, W Yuan, Z Chen, S Wu, J Chen, J Ge, F Hou, Z Chen. 2012. “Overexpression of G6PD Is Associated with Poor Clinical Outcome in Gastric Cancer.” *Tumour Biology : The Journal of the International Society for Oncodevelopmental Biology and Medicine* 33 (1): 95–101. doi:10.1007/s13277-011-0251-9.

Warburg, O. 1956. “On Respiratory Impairment in Cancer Cells.” *Science (New York, N.Y.)* 124 (3215): 269–70.

Warburg, O, F Wind, E Negelein. 1927. “The Metabolism of Tumors in the Body.” *The Journal of General Physiology* 8 (6): 519–30.

Ward, P S, J Patel, D R Wise, O Abdel-Wahab, B D Bennett, H A Coller, J R Cross, et al. 2010. “The Common Feature of Leukemia-Associated IDH1 and IDH2 Mutations Is a Neomorphic Enzyme Activity Converting Alpha-Ketoglutarate to 2-Hydroxyglutarate.” *Cancer Cell* 17 (3): 225–34. doi:10.1016/j.ccr.2010.01.020.

Watson, J D, F H Crick. 1953. “Molecular Structure of Nucleic Acids; a Structure for Deoxyribose Nucleic Acid.” *Nature* 171 (4356): 737–38.

Weiss, R G, M D Stern, C P Albuquerque, K Vandegaer, V P Chacko, G Gerstenblith. 1995. “Consequences of Altered Aspartate Aminotransferase Activity on 13C-Glutamate Labelling by the Tricarboxylic Acid Cycle in Intact Rat Hearts.” *Biochimica et Biophysica Acta* 1243 (3): 543–48.

White, M C, D M Holman, J E Boehm, L A Peipins, M Grossman, S J Henley. 2014. “Age and Cancer Risk: A Potentially Modifiable Relationship.” *American Journal of Preventive Medicine* 46 (3 Suppl 1): S7–15. doi:10.1016/j.amepre.2013.10.029.

WHO. 2008. *World Cancer Report*. Edited by Peter Boyle and Bernard Levin. WHO Press. International Agency for Research on Cancer.

Wigfield, S M, S C Winter, A Giatromanolaki, J Taylor, M L Koukourakis, A L Harris. 2008. “PDK-1 Regulates Lactate Production in Hypoxia and Is Associated with Poor Prognosis in Head and Neck Squamous Cancer.” *British Journal of Cancer* 98 (12): 1975–84. doi:10.1038/sj.bjc.6604356.

Williamson, D H, P Lund, H A Krebs. 1967. “The Redox State of Free Nicotinamide-Adenine Dinucleotide in the Cytoplasm and Mitochondria of Rat Liver.” *The Biochemical Journal* 103: 514–27.

Wilson, J E. 2003. “Isozymes of Mammalian Hexokinase: Structure, Subcellular Localization and Metabolic Function.” *The Journal of Experimental Biology* 206 (Pt 12): 2049–57. doi:10.1242/jeb.00241.

Wise, D R, R J DeBerardinis, A Mancuso, N Sayed, X-Y Zhang, H K Pfeiffer, I Nissim, et al. 2008. “Myc Regulates a Transcriptional Program That Stimulates Mitochondrial Glutaminolysis and Leads to Glutamine Addiction.” *Proceedings of the National Academy of Sciences of the United States of America* 105 (48): 18782–87. doi:10.1073/pnas.0810199105.

Wolpert, L. 1995. “Evolution of the Cell Theory.” *Philosophical Transactions of the Royal Society of London. Series B, Biological Sciences* 349 (1329): 227–33. doi:10.1098/rstb.1995.0106.

Wong, C C-L, S L Au, A P-W Tse, I M-J Xu, R K-H Lai, D K-C Chiu, L L Wei, et al. 2014. “Switching of Pyruvate Kinase Isoform L to m2 Promotes Metabolic Reprogramming in Hepatocarcinogenesis.” *PloS One* 9 (12): e115036. doi:10.1371/journal.pone.0115036.

Wu, H, Z Li, P Yang, L Zhang, Y Fan, Z Li. 2014. “PKM2 Depletion Induces the Compensation of Glutaminolysis through B-Catenin/c-Myc Pathway in Tumor Cells.” *Cellular Signalling* 26 (11): 2397–2405. doi:10.1016/j.cellsig.2014.07.024.

Wu, H, Z Ding, D Hu, F Sun, C Dai, J Xie, X Hu. 2012. “Central Role of Lactic Acidosis in Cancer Cell Resistance to Glucose Deprivation-Induced Cell Death.” *Journal of Pathology* 227: 189–99. doi:10.1002/path.3978.

Wyld, L, R A Audisio, G J Poston. 2014. “The Evolution of Cancer Surgery and Future Perspectives.” *Nature Reviews. Clinical Oncology*, November. doi:10.1038/nrclinonc.2014.191.

Xu, R, H Pelicano, Y Zhou, J Carew, L Feng, K N Bhalla, M J Keating, P Huang. 2005. “Inhibition of Glycolysis in Cancer Cells: A Novel Strategy to Overcome Drug Resistance Associated with Mitochondrial Respiratory Defect and Hypoxia.” *Cancer Research* 65 (2): 613–21.

Xu, W, H Yang, Y Liu, Y Yang, P Wang, S Kim, S Ito, et al. 2011. “Oncometabolite 2-Hydroxyglutarate Is a Competitive Inhibitor of A-Ketoglutarate-Dependent Dioxygenases.” *Cancer Cell* 19 (1): 17–30. doi:10.1016/j.ccr.2010.12.014.

Yang, C, B Ko, C T Hensley, L Jiang, A T Wasti, J Kim, J Sudderth, et al. 2014b. “Glutamine Oxidation Maintains the TCA Cycle and Cell Survival during Impaired Mitochondrial Pyruvate Transport.” *Molecular Cell*. doi:10.1016/j.molcel.2014.09.025.

Yang, M, P J Pollard. 2013b. “Succinate: A New Epigenetic Hacker.” *Cancer Cell* 23 (6): 709–11. doi:10.1016/j.ccr.2013.05.015.

Yang, W, Z Lu. 2013a. “Nuclear PKM2 Regulates the Warburg Effect.” *Cell Cycle (Georgetown, Tex.)* 12 (19): 3154–58. doi:10.4161/cc.26182.

Yang, Y, D Su, L Zhao, D Zhang, J Xu, J Wan, S Fan, M Chen. 2014a. “Different Effects of LDH-A Inhibition by Oxamate in Non-Small Cell Lung Cancer Cells.” *Oncotarget* 5 (23): 11886–96.

Yang, Y, A N Lane, C J Ricketts, C Sourbier, M-H Wei, B Shuch, L Pike, et al. 2013c. “Metabolic Reprogramming for Producing Energy and Reducing Power in Fumarate Hydratase Null Cells from Hereditary Leiomyomatosis Renal Cell Carcinoma.” *PloS One* 8 (8): e72179. doi:10.1371/journal.pone.0072179.

Ye, J, J Fan, S Venneti, W Ying-Wooi, B Pawel, J Zhang, L Finley, et al. 2014. “Serine Catabolism Regulates Mitochondrial Redox Control during Hypoxia.” *Cancer Discovery* 4 (12). doi:10.1158/2159-8290.CD-14-0250.

Yeung, S J, J Pan, M-H Lee. 2008. “Roles of p53, MYC and HIF-1 in Regulating Glycolysis - the Seventh Hallmark of Cancer.” *Cellular and Molecular Life Sciences : CMLS* 65 (24): 3981–99. doi:10.1007/s00018-008-8224-x.

Yogev, O, O Yogev, E Singer, E Shaulian, M Goldberg, T D Fox, O Pines. 2010. “Fumarase: A Mitochondrial Metabolic Enzyme and a Cytosolic/nuclear Component of the DNA Damage Response.” *PLoS Biology* 8 (3): e1000328. doi:10.1371/journal.pbio.1000328.

Yoo, H, M R Antoniewicz, G Stephanopoulos, J K Kelleher. 2008. “Quantifying Reductive Carboxylation Flux of Glutamine to Lipid in a Brown Adipocyte Cell Line.” *The Journal of Biological Chemistry* 283 (30): 20621–27. doi:10.1074/jbc.M706494200.

Yoshida, S, A Honda, Y Matsuzaki, S Fukushima, N Tanaka, A Takagiwa, Y Fujimoto, H Miyazaki, G Salen. 2003. "Anti-Proliferative Action of Endogenous Dehydroepiandrosterone Metabolites on Human Cancer Cell Lines." *Steroids* 68 (1): 73–83. doi:10.1016/S0039-128X(02)00117-4.

Yun, M, S-H Bang, J W Kim, J Y Park, K S Kim, J D Lee. 2009. "The Importance of Acetyl Coenzyme A Synthetase for 11C-Acetate Uptake and Cell Survival in Hepatocellular Carcinoma." *Journal of Nuclear Medicine : Official Publication, Society of Nuclear Medicine* 50 (8): 1222–28. doi:10.2967/jnumed.109.062703.

Yuneva, M, N Zamboni, P Oefner, R Sachidanandam, Y Lazebnik. 2007. "Deficiency in Glutamine but Not Glucose Induces MYC-Dependent Apoptosis in Human Cells." *The Journal of Cell Biology* 178 (1): 93–105. doi:10.1083/jcb.200703099.

Zagorodna, O, S M Martin, D T Rutkowski, T Kuwana, D R Spitz,C Michael Knudson. 2012. "2-Deoxyglucose-Induced Toxicity Is Regulated by Bcl-2 Family Members and Is Enhanced by Antagonizing Bcl-2 in Lymphoma Cell Lines." *Oncogene* 31 (22): 2738–49. doi:10.1038/onc.2011.454.

Zaidi, N, L Lupien, N B Kuemmerle, W B Kinlaw, J V Swinnen, Karine Smans. 2013. "Lipogenesis and Lipolysis: The Pathways Exploited by the Cancer Cells to Acquire Fatty Acids." *Progress in Lipid Research* 52 (4): 585–89. doi:10.1016/j.plipres.2013.08.005.

Zar, J H. 1999. *Biostatistical Analysis*. 4th ed. NJ: Prentice Hall.

Zeng, L, A Morinibu, M Kobayashi, Y Zhu, X Wang, Y Goto, C J Yeom, et al. 2014. "Aberrant IDH3α Expression Promotes Malignant Tumor Growth by Inducing HIF-1-Mediated Metabolic Reprogramming and Angiogenesis." *Oncogene*, no. October (December). doi:10.1038/onc.2014.411.

Zhang, J, J Fan, S Venneti, J R Cross, T Takagi, B Bhinder, H Djaballah, et al. 2014. "Asparagine Plays a Critical Role in Regulating Cellular Adaptation to Glutamine Depletion." *Molecular Cell* 56 (2). doi:10.1016/j.molcel.2014.08.018.

Zhang, J, W S Ahn, P A Gameiro, M A Keibler, Z Zhang, G Stephanopoulos. 2014. "13C Isotope-Assisted Methods for Quantifying Glutamine Metabolism in Cancer Cells." *Methods in Enzymology* 542 (January): 369–89. doi:10.1016/B978-0-12-416618-9.00019-4.

Zhang, Q, J Pan, P E North, S Yang, R Lubet, Y Wang, M You. 2012. "Aerosolized 3-Bromopyruvate Inhibits Lung Tumorigenesis without Causing Liver Toxicity." *Cancer Prevention Research* 5: 717–25. doi:10.1158/1940-6207.CAPR-11-0338.

Zhang, Q, Y Zhang, P Zhang, Z Chao, F Xia, C Jiang, X Zhang, Z Jiang, H Liu. 2014. "Hexokinase II Inhibitor, 3-BrPA Induced Autophagy by Stimulating ROS Formation in Human Breast Cancer Cells." *Genes & Cancer* 5 (3-4): 100–112.

Zhao, Y, E B Butler, M Tan. 2013. "Targeting Cellular Metabolism to Improve Cancer Therapeutics." *Cell Death & Disease* 4 (3). doi:10.1038/cddis.2013.60.

Zhao, Z, F Han, S Yang, J Wu, W Zhan. 2015. “Oxamate-Mediated Inhibition of Lactate Dehydrogenase Induces Protective Autophagy in Gastric Cancer Cells: Involvement of the Akt–mTOR Signaling Pathway.” *Cancer Letters* 358 (1). doi:10.1016/j.canlet.2014.11.046.

Zhou, M, Y Zhao, Y Ding, H Liu, Z Liu, O Fodstad, A I Riker, et al. 2010. “Warburg Effect in Chemosensitivity: Targeting Lactate Dehydrogenase-A Re-Sensitizes Taxol-Resistant Cancer Cells to Taxol.” *Molecular Cancer* 9 (11): 33. doi:10.1186/1476-4598-9-33.

Zhu, J, R K Dagda, C T Chu. 2011. “Monitoring Mitophagy in Neuronal Cell Cultures.” *Methods in Molecular Biology* 793 (January): 325–39. doi:10.1007/978-1-61779-328-8_21.

Zu, X L, M Guppy. 2004. “Cancer Metabolism: Facts, Fantasy, and Fiction.” *Biochemical and Biophysical Research Communications* 313 (3): 459–65. doi:10.1016/j.bbrc.2003.11.136.